SOL-GEL NANOCRYSTALLINE CATALYTIC TITANIA POWDERS AND FUNCTIONAL COATINGS

THESIS SUBMITTED TO THE COCHIN UNIVERSITY OF SCIENCE AND TECHNOLOGY IN PARTIAL FULFILMENT OF THE REQUIREMENTS FOR THE DEGREE OF

DOCTOR OF PHILOSOPHY

IN CHEMISTRY

UNDER THE FACULTY OF SCIENCE

BY

SIBU C. P.

UNDER THE SUPERVISION OF

Dr. K. G. K. WARRIER

CERAMIC TECHNOLOGY DIVISION

REGIONAL RESEARCH LABORATORY (CSIR)

TRIVANDRUM – 695 019

KERALA, INDIA

JUNE 2004

Council of Scientific & Industrial Research
क्षेत्रीय अनुसंधान प्रयोगशाला, तिरुवनन्तपुरम् - 695 019
REGIONAL RESEARCH LABORATORY
Thiruvananthapuram - 695 019, INDIA
Phone : +91- 471- 2490674, 2515280 (O); Gram : CONSEARCH
Fax : +91- 471- 2491712, E-mail:warrier@csrrltrd.ren.nic.in

Dr. K. G. K. Warrier
Deputy Director
Head, Ceramic Technology Division

June, 2004

CERTIFICATE

This is to certify that the work embodied in the thesis entitled: **"Sol-Gel Nanocrystalline Catalytic Titania Powders and Functional Coatings"** has been carried out by **Mr. Sibu C. P.** under my supervision at the Ceramic Technology Division of the Regional Research Laboratory (CSIR), Trivandrum, and the same has not been submitted elsewhere for any other degree.

K. G. K. Warrier
(Thesis Supervisor)

CONTENTS

PREFACE

Nanostructured materials have seen an explosion of scientific and industrial interest over the last few decades. Nanostructured microstructures have been obtained for ceramic, metallic, polymer and composite materials. The different forms in which these materials find applications include dry powders, liquid dispersions, coatings and films, and bulk solids. Increased interest in nanomaterials is a result of the unique properties that can be obtained, and the exciting applications that result from these properties. Enhanced electrical, mechanical, magnetic and optical properties have been reported for these materials. Nanostructured materials possess microstructures, with characteristic dimension 1-100 nanometers.

Titanium oxide is well known for its application as a white pigment in paints, as filler in pigments and in ceramic glasses as opacifiers. More recently titanium oxide has also found applications in electronic ceramics as semiconductors, as catalyst and as photocatalysts. The photocatalytic applications of titania has been also investigated with respect to its capability in splitting of water molecules, in the treatment of industrial effluents and in the development of self-cleaning coatings and catalytic ceramic membranes. Sol-gel method has been reported to be an effective route for the synthesis of nanocrystalline titanium oxide powders and functional coatings. Further, use of various dopant oxides such as V_2O_5, Fe_2O_3 and CuO has found to improve the catalytic properties, as well as to influence the anatase to rutile transformation

temperature. Most of the applications of catalytic titanium oxide have been conducted in presence of particle suspensions and recently nano coatings of doped titanium oxide are being investigated. Such coatings are usually made by sol-gel route especially on glass substrates where the end use is projected as self-cleaning surfaces. The electrophilic nature of the catalytic titanium oxide is reported to be improved in presence of aluminium oxide. Earlier reports have shown that rare earth oxide doped nano titania could be successfully synthesized by sol-gel route starting from alkoxide hydrolysis or from titanyl salt.

In the present work, titania bulk powders as well as functional coatings were prepared by subjecting titanium tetraisopropoxide solution to a controlled hydrolysis-condensation process. The effect of doping (lanthana and/or ceria), co-dopants and chemical leaching is discussed in detail. The suitable precursor sols were used for the film fabrication on glass surfaces and their morphological analysis as well as optical characterizations was carried out and possible correlations were arrived with the sol synthesis procedure.

The thesis is divided into five chapters. Relevant references are given at the end of each chapter.

A general introduction to nanomaterials, nanocrystaline titania and sol-gel chemistry is presented in chapter 1. A brief literature review on sol-gel titania, catalytic/photocatalytic properties, A>R transformation, high surface area titania, titania coatings and /or films and the definition of the research problem is also provided in this chapter.

The second chapter describes the preparation methods and the characterization techniques employed. Nanosize titanium oxide with and without addition of dopants (lanthanum oxide cerium oxide and praseodymium oxide) was prepared by solution sol-gel method. Titanium tetraisopropoxide (Fluka, Switzerland) was used for the synthesis of titanium oxide. Lanthanum nitrate, and cerium nitrate (Indian Rare Earth Ltd., India) were used for doping. The sols were used for coating on the glass surfaces and the photoactivity as well as the morphological features of the coatings was studied.

The third chapter presents a detailed discussion on the physico-chemical characterization of the powder systems. The role of acetic acid and the dopants on the structural as well as the textural properties is also discussed in detail. The influence of dopants on the physico-chemical properties as well as their influence on photoactivity is also included. A detailed discussion on the high surface area mesoporous titania systems synthesized through a co-doping (pseudo-templating)-leaching process is also provided.

Chapter 4 discusses on the structural/functional coatings of different titania compositions. Optical and morphological characterizations of the coated films are provided and compared with the sol preparation process.

Chapter 5 includes the summary and general conclusion of the thesis.

It may be mentioned that all the chapters of the thesis are presented as continuation of the earlier chapter and therefore the tables and figures are numbered continuously.

ABBREVIATIONS

A	Anatase
A→R	Anatase to rutile
AFM	Atomic force microscopy
BET	Brunauer-Emmet-Teller
BF	Bright field
CB	Conduction band
DTA	Differential thermal analysis
EDS	Energy dispersive spectroscopy
FTIR	Fourier transform infrared
GLY	Glycerol
MB	Methylene blue
PEG	Poly(ethylene glycol)
R	Rutile
RE	Rare earth
RMS	Root mean square
SAED	Selected area electron diffraction
SLG	Soda-lime glass
SSA	Specific surface area
TC-1	1% CeO_2-doped TiO_2
TC-2	2% CeO_2-doped TiO_2
TC-3	3% CeO_2-doped TiO_2
TC-5	5% CeO_2-doped TiO_2

TC-GLY	0.5% Glycerol added 1% CeO_2-doped TiO_2
TCS	5% SiO_2-1% CeO_2 co-doped TiO_2
TEM	Transmission electron microscopy
TEOS	Tetraethylorthosilicate
TG	Thermogravimetry
TL-1	1% La_2O_3-doped TiO_2
TL-1 GLY0.5	0.5% Glycerol added 1% La_2O_3-doped TiO_2
TL-1PEG0.5	0.5% PEG added 1%La_2O_3 doped TiO_2
TL-1PEG1	1% PEG added 1%La_2O_3 doped TiO_2
TL-2	2% La_2O_3-doped TiO_2
TL-3	3% La_2O_3-doped TiO_2
TL-5	5% La_2O_3-doped TiO_2
TLA10	10% Al_2O_3-1% La_2O_3 co-doped TiO_2
TLS	5% SiO_2-1% La_2O_3 co-doped-TiO_2
TLSN	5% SiO_2-1% La_2O_3 co-doped-TiO_2 after leaching
TPD	Temperature programmed desorption
TS-1	1% SiO_2-doped TiO_2
TS-5	5% SiO_2-doped TiO_2
TS-5N	5% SiO_2-doped TiO_2 after leaching
TTIP	Titanium tetraisopropoxide
TU	Undoped TiO_2
VB	Valence band
XRD	X-ray diffraction

List of Tables

List of Figures

Chapter I

An Introduction to Nanomaterials, Sol-Gel Chemistry with Special Reference to Titania Based Systems and Catalytic / Photocatalytic / Functional Applications

1.1 An Overview on Nanomaterials

Nanostructured materials have seen an explosion of scientific and industrial interest over the last few years. [1] Nanostructured microstructures have been obtained for ceramic, metallic, diamond, semi conducting, polymer and composite materials. The different forms in which these materials may appear include dry powders, liquid dispersions, coatings, films and bulk solids.

Increased interest in nanomaterials is a result of the unique properties that can be obtained, and the exciting applications that result from these properties. [2] Enhanced electrical, mechanical, magnetic and optical properties have been reported for these materials.

Nanocrystalline materials are three-dimensional solids composed of nanometer sized grains, or crystallites (building blocks). [3] Because of their unique structure, which is characterized by ultrafine grains and a rather high density of crystal lattice defects, these materials have extraordinary

fundamental properties that could be exploited to make next-generation super strong metals, ductile ceramics and wear-free materials. Nanostructured materials have a microstructure, the characteristic length of which is on the order of a few (typically 1-100) nanometers [4] and therefore may be in or far away from thermodynamic equilibrium. Nanostructured materials consisting of nanometer-sized crystallites (e.g., of Au or NaCl) with different crystallographic orientations and/or chemical compositions are far away from thermodynamic equilibrium, while those synthesized by supramolecular chemistry follows thermodynamic equilibrium. The properties of nanomaterials deviate from those of single crystals (or coarse grained polycrystals) and/or glasses with the same average chemical composition. This deviation results from the reduced size and/or dimensionality of the nanometer sized crystallites as well as from the numerous interphases between adjacent crystallites. [5] The reduced size in the nanometric range also characterizes the material to transmit visible light considerably. This feature helps the nanomaterials to act as transparent envelopes over various substrates without affecting their aesthetic/original look. Besides, the extremely high surface to volume ratio possessed by the nanomaterials makes them highly energetic in terms of surface energy, which in turn let the surface to undergo suitable reactions to reduce its surface energy. This possibility can be exploited by using the nanomaterials in catalysis/photocatalysis.

1.2 *Titanium Dioxide*

Titanium oxide has been known for many years as a constituent of naturally occurring mineral ilmenite ($FeO.TiO_2$). Extraction of titanium oxide from the mineral is a chemical process followed through a sulphate route or a chloride route. [6] Many other processes such as plasma decomposition and direct reduction have also been reported. [7-10] Presently titanium oxide is well recognized as a valuable material with application as a white pigment in paints, [11-13] as filler in paper, [14] textiles and in rubber/plastics. [15] Applications of titania have further been extended to active as well as passive coatings for electro-optical, [16-18] optical, [19-21] electronic [22] and structural applications. [23] Titanium dioxide is used in heterogeneous catalysis, [24-26] as a photocatalyst, [27-32] in solar cells for the production of hydrogen and electric energy, [33-39] as gas [40-41] and/or bio sensor, [42] as a corrosion-protective coating, [43-48] as an optical coating, [49-54] in ceramics, and in electric devices such as varistors. [55] It is important in earth sciences, plays a role in the biocompatibility of bone implants, [56-58] is being discussed as a gate insulator for the new generation of MOSFETS [59] and as a spacer material in magnetic spin-valve systems, and finds applications in nanostructured form in Li-based batteries and electrochromic devices. [60-62]

Titanium oxide has attractive properties. It has a quite high refractive index (~2.4), [63] that favour in the field of passive optical coatings [19-21] and the wide band gap (~3.2 eV) combined with the high UV absorption could be exploited in the field of optically active coatings. [63] Its photoactive potential and photocatalytic activity are being exploited for practical applications such as

the photocleavage of water, [32,64-67] photocatalytic decomposition of organics, [68-82] and in anti-fogging as well as self-cleaning coatings. [83-85] Further, it finds use in microelectronics [86-87], wastewater purification, [88-89] inorganic membranes [90-95] and as catalyst support. [96] Titania is also a potential ceramic sensor element. [97]

Titania has been found to exist in three forms, anatase (tetragonal, D_{4h}^{19}-$I4_1/amd$, $a=b=3.782$ Å, $c=9.502$ Å), rutile (tetragonal, D_{4h}^{14}-$P4_2/mnm$, $a=b=4.584$ Å, $c=2.953$ Å [98] and brookite (rhombohedral, D_{2h}^{15}-Pbca, $a=5.436$ Å, $b=9.166$ Å, $c=5.135$ Å). [99] Anatase and rutile are in tetragonal structure and brookite is orthorhombic. In all the three TiO_2 structures, the stacking of the octahedra results in three-fold coordinated oxygen atoms. [100] Thermodynamically, rutile structure is the stable one. While the rutile and anatase structure have many similarities they also differ in a variety of ways. In both structures, Ti atoms (formally in a +4 oxidation state) are coordinated to six oxygen atoms (formally O^{2-}), and the O atoms are linked to three Ti atoms. The octahedron of anatase is somewhat more distorted than that of rutile. The mass density of the anatase phase is lower, and the band gap of anatase is somewhat wider, which affects the photocatalytic activity. [101-102] The nature of chemical bonds in the three titanium oxides studied through ab initio cluster model approach revealed that there is an increasing covalence in TiO, Ti_2O_3 and TiO_2. TiO can nearly be described as an ionic compound, and TiO_2 can nearly be described as covalent. [103]

Brookite has an orthorhombic crystal structure and spontaneously transforms to rutile at ~750°C. [104-105] Its mechanical properties are very similar to those of rutile, but it is the least common of the three phases and is rarely used commercially. In all the three crystalline forms each of Ti^{4+} ions are surrounded by an irregular octahedron of oxide ions; but the number of edges shared by the octahedron increases from two in rutile to three in brookite and to four in anatase. Both in rutile and anatase the six oxide ions that surround the Ti^{4+} ions can be grouped into two. The two oxygen atoms are farthest from Ti^{4+} and the other four oxide ions are relatively closer to Ti^{4+}. In rutile these distances are 2.01Å and 1.92Å respectively and in anatase they are 1.95Å and 1.91Å (Figure 1). In case of brookite the farthest oxide ions are the only ones, which are equidistant from Ti^{4+} ions. At room temperature titania exists in the anatase phase and at high temperature it exists as rutile. The anatase to rutile transformation is a metastable to thermodynamically stable phase transformation and therefore there is no unique phase transformation temperature as in the case of equilibrium reversible transformation. [106] Anatase transforms irreversibly and exothermically to rutile in the temperature range 600-800°C. [107]

Different crystalline forms of titania are provided in Figures 1a-c. Anatase has a tetragonal crystal structure in which the Ti-O octahedron shares four corners, as shown in Figure 1a. [108] Rutile has a crystal structure similar to that of anatase, with the exception that the octahedra share four edges instead of four corners. This leads to the formation of chains, which are subsequently

arranged in four-fold symmetry as shown in Figure 1b. A comparison of Figures 1 and 2 shows that the rutile structure is more densely packed than anatase. As a point of reference, the densities of the anatase and rutile phases are known to be 3.87 g/cm^3 and 4.24 g/cm^3 respectively. [15] Typical properties of the major two crystal forms of titania are provided in Table 1.

The current research trend to synthesize, characterize, and investigate nanomaterials is also being extended to titanium oxide. This material lends itself quite well to building tiny structures in all sorts of sizes and shapes. Such nano-TiO_2 is typically produced by sol-gel process, where a titanium alkoxide or halide ($TiCl_4$, TiF_4) is hydrolysed, often in presence of a template such as nano-spheres, nano-rods or anodic porous alumina, [109-113] but other techniques have been used as well. [7-10]

Titanium dioxide has attracted lot of interest from both theoretical [114-115] and practical point of view as an attractive material for metallic oxide semiconductors. [116-117] The choice of TiO_2 in the present work was based on its importance in environmental purification and treatment of water, since pollution of water and air is a major concern in the present world. [28,118] Therefore in the present thesis a systematic study of the synthesis and characterization of photoactive TiO_2 is presented and the study was extended by analyzing the effect of addition of dopants on the photoactivity of titania. Further, TiO_2 films were fabricated out of the various compositions prepared and the photoactivity of the films was analyzed. Finally, the preparation – property correlation is drawn with the help of available experimental results.

Table 1: Typical properties of TiO_2 [15]

Crystal form	**Anatase**	**Rutile**
Density (g/cm^3)	3.87	4.24
Hardness (moh)	5-6	6-7
Crystal structure	Tetragonal, Uniaxial, negative	Tetragonal, Uniaxial, positive
Compressibility coefficient (10^{-6} cm^2 Kg^{-1})	--	0.53 – 0.58
Melting point (°C)		
In Air	--	1830 ± 15
At higher % O_2	--	1879 ± 15
Specific heat (Cal $°C^{-1}$ g^{-1})	0.17	0.17
Dielectric constant	48	114

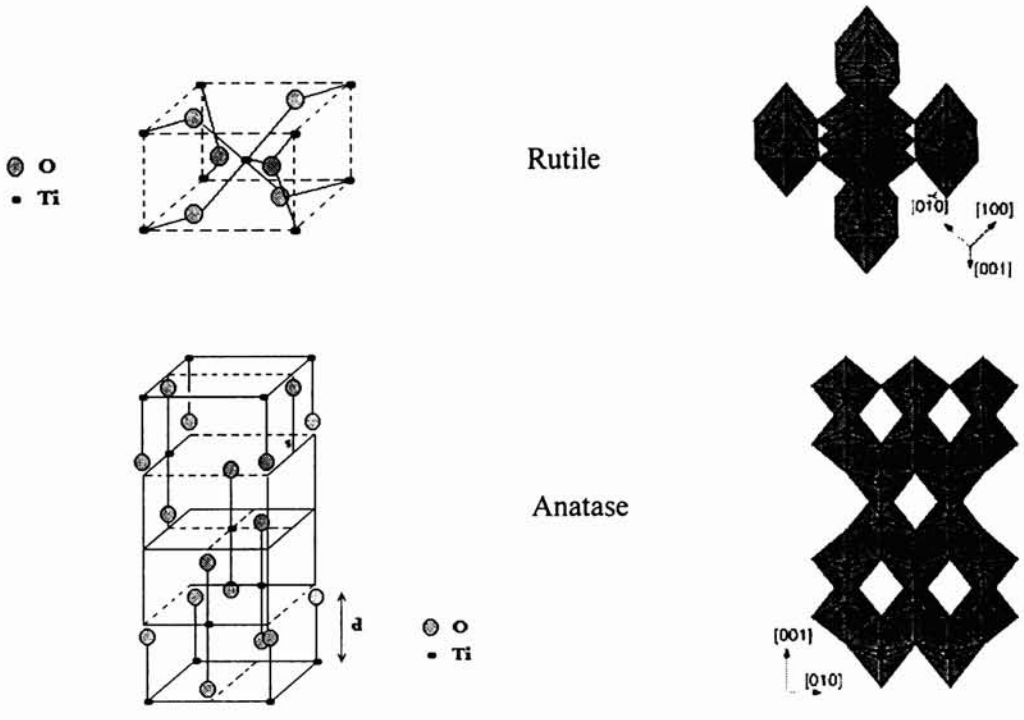

Figure 1a

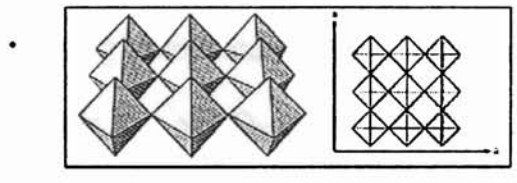

Anatase crystal

Figure 1b

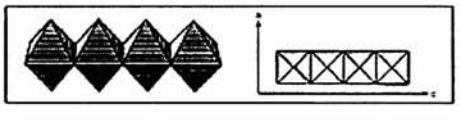

Rutile crystal

Figure 1c

Figure 1: Anatase and rutile unit cells and crystals

1.3 Nanocrystalline Titanium Oxide

Nano titania has got semiconductor properties owing to the band gap arrangement on clustering. [119-121] Fine TiO_2 semiconductor nanoparticles are ideal photocatalysts due to their chemical stability, non-toxicity and high photocatalytic reactivity. [122-125] The photocatalysis by titania semiconductors has received considerable attention and has been widely studied after the discovery by Honda and Fujishima in 1972, [27] with the final aim of efficiently converting solar light energy into useful chemical energy. [126-133] The effective utilization of clean, safe, and abundant solar energy will lead to promising solutions not only for energy issues due to the exhaustion of natural energy sources but also for the many problems caused by environmental pollution. TiO_2 semiconductor photocatalysts have the potential to oxidize a wide range of organic compounds, including chlorinated organic compounds, such as dioxins, into harmless compounds such as CO_2 and H_2O by irradiation with UV light. [67-74,77] High-purity titania powder catalysts are typically made in a flame process from titanium tetrachloride. [134] The shapes of the crystallites vary with preparation techniques and procedures. Typically, (1 0 1) and (1 0 0)/(0 1 0) surface planes are found, together with some (0 0 1). [135] Several theoretical studies have predicted the stability of different low-index anatase surfaces. [136-137] The (1 0 1) face is the thermodynamically most stable surface. [138-139] While it is difficult to obtain accurate values for surface energies with density functional theory (DFT) calculations, the relative surface energies are still meaningful. The calculated Wulff shape of an anatase crystal, based on these

numbers, compares well with the shape of naturally grown mineral samples. Interestingly, the average surface energy of an equilibrium-shaped anatase crystal is smaller than the one of rutile, [138-139] which might explain the fact that nanoscopic TiO_2 particles are more stable in the anatase phase. [138-139]

The most common procedures for preparing the titania powders have been based on the hydrolysis of acidic solutions of Ti(IV) salts, [110-112,140-142] or by gas-phase oxidation reaction of $TiCl_4$ at high temperatures. [143-144] Alternative methods like vapour-phase hydrolysis, [145] pyrolysis, [146] and sol-gel synthesis [147-150] of organic precursors (e.g. titanium tetraisopropoxide, TTIP), have been developed to synthesize titania nanoparticles with high purity. Sol-gel synthesis generally refers to a low-temperature method using chemical precursors that can produce ceramics and glasses with better purity and homogeneity [151-156] than high temperature conventional processes.

1.4 Sol-Gel Process In General

The sol-gel process is a versatile solution process for making ceramic and glass materials. In general, the sol-gel process involves the transition of a system from a liquid sol (mostly colloidal) into a solid gel phase. By applying the sol-gel process, it is possible to fabricate ceramic or glass materials in a wide variety of forms: ultrafine or spherical shaped powders, thin film coatings, [157-160] ceramic fibers, microporous inorganic membranes, [90-92,161]

monolithic ceramics and glasses, or extremely porous aerogel materials. An overview of the sol-gel process is presented in Figure 2.

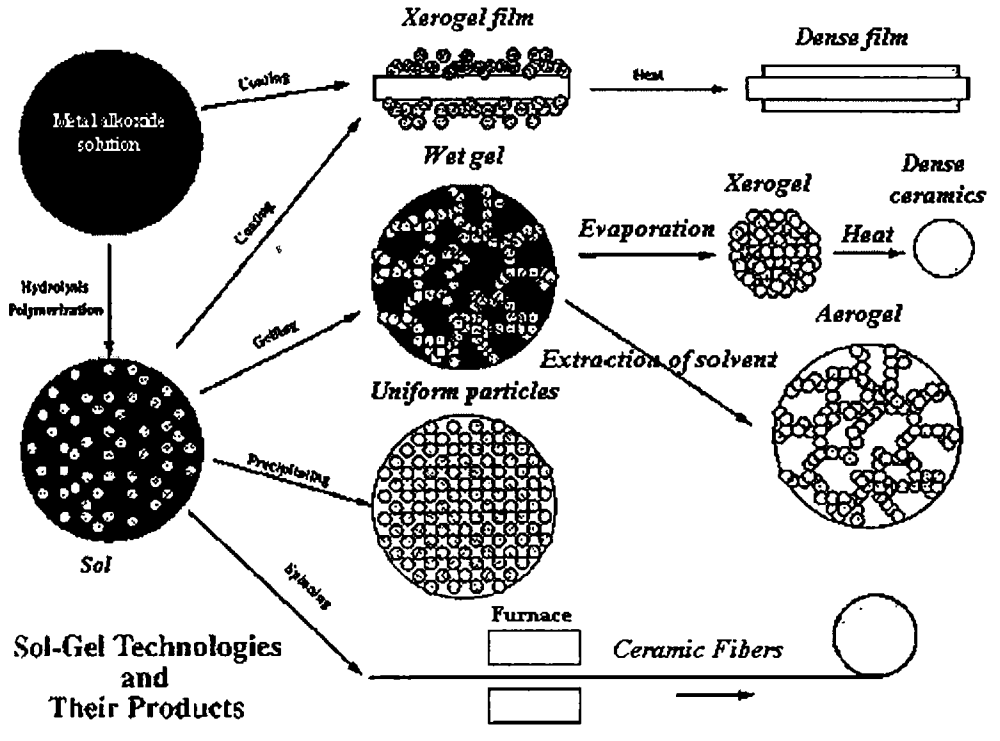

Figure 2: An overview of sol-gel process

The starting materials used in the preparation of the sol are usually inorganic metal salts or metal organic compounds such as metal alkoxides. [162-165] In a typical sol-gel process, the precursor is subjected to a series of controlled hydrolysis and polymerization reactions to form a colloidal suspension, or a sol. Further processing of the sol enables one to make ceramic materials in different forms. Thin films can be produced on a piece of substrate by spin coating or dip-coating. When the sol is cast into a mold, a wet gel will

form. With further drying and heat-treatment, the gel is converted into dense ceramic or glass articles. If the liquid in a wet gel is removed under supercritical condition, a highly porous and extremely low-density material called aerogel is obtained. [166-169] If the viscosity of the sol is adjusted to a proper viscosity range, ceramic fibers can be drawn from the sol. Ultrafine and uniform ceramic powders are formed by precipitation, spray pyrolysis, and/or emulsion techniques.

Therefore, the motivation behind selecting the sol-gel process is the higher purity and homogeneity of the product and the lower processing temperatures associated with the method compared to traditional glass melting or ceramic powder methods.

In the sol-gel synthesis, two simultaneous reactions – hydrolysis and polycondensation – take place when metal alkoxide reacts with water. These two reactions are sensitive to many experimental parameters such as water concentration, [170] pH, [171-174] type and amount of solvent, [175-176] reaction temperature, [177-183] and mixing conditions. Therefore, it is essential to understand the hydrolysis and condensation reactions in a sol-gel process since the structure of a gel is established at the time of gelation, drying, stabilization and densification all depend upon the gel structure. [184-186] The variables of major importance are temperature, nature and concentration of electrolyte (acid, base), nature of the solvent, and type of alkoxide precursor. [187] In fact many studies have reported the variation of the gelation time, viscosity, or

textural characteristics (e.g. specific surface area) of the gel as a function of experimental conditions. [188-191]

Most of the titanium oxide was prepared by hydrolysis reactions involving salts. [110-112,140-142] The need for finer particle size and well-defined compositional tolerance along with tailored surface properties lead to adaptation of sol-gel route. [192] The sol-gel process essentially is the hydrolysis of metal alkoxides by controlled addition of water in presence of alcohol due to the fact that the alcohol with its intermediate polarity makes the apolar alkoxide and polar water compatible. [193-194] Such hydrolysis produces essentially primary nanoparticles, which may aggregate on aging of the sol. [195] The pH and temperature also has considerable influence on the sol-gel system. Final drying and calcination of the gel produces the metal oxide. [196-198]

The parameters such as type of precursors, [199] pH of the system, ambient temperature, solvents, water/Ti mole ratio, solvent/Ti ratio, (stabilizer/chelating agent)/Ti ratio and electrolyte/Ti ratio [200] are need to be considered to obtain suitable nanometric building blocks. The influence of building blocks on the microstructure [201-202] and on the physical, chemical and the mechanical properties need to be understood to tailor the final product. [152,203] Apart from that, hydrolysis of precursors, [204-205] the commencement of condensation, its propagation, termination, the nature of polycondensation, effect of solvents on the process and effect of by-products on further reaction are very important parameters and many of these factors have been well studied by many

researchers. Suresh *et al* [206] showed that hydrolysis of titanium tetraisopropoxide at pH 4 resulted in a precursor having an anatase to rutile transformation temperature as high as ~ 800°C in place of the usual temperature of ~ 600°C. Trace of anatase phase was seen even at 800°C.

Kallala *et al* [207] identified the structure of inorganic polymers, produced as a result of hydrolysis of sol-gel precursors. The hydrolysis and condensation of titanium alkoxides such as ethoxide, propoxide, butoxide etc. could be selectively controlled by the inhibition of condensation through H^+ ions, which prevents precipitation and provided gelation. Depending on the presence of the inhibitor, the resultant gel could be transparent, turbid or opaque, based on which different properties for the resultant oxides could be obtained. Attempts for obtaining nanosize titanium oxide particles, titania-mixed oxide catalysts and titania for photocatalytic activity is widely investigated. As has been found in the various applications of titania, the characteristics required for the oxide are diverse, but specific to the end use. Since hydrolysis of titanium alkoxide and further condensation of the hydrolysed species can be controlled by manipulating the synthesis conditions, it has been possible to achieve the required oxide with reasonable success. Most of the preparative methods are modifications on the hydrolysis reactions of titanium alkoxides. [208-210] Titanium ethoxide, propoxide and butoxide are the usual starting alkoxides. The main approaches to synthesis have been the following:

1. Use of acid catalysts (HCl/HNO_3) on direct hydrolysis

2. Hydrolysis in presence of different alcohol-water ratios.
3. Hydrolysis in presence of chelating agents or intermediates.
4. Hydrolysis involving large polymeric molecules in the medium
5. Hydrolysis involving emulsion templating
6. Hydrolysis of titanium salts (aqueous processing) in place of alkoxides.

The hydrolysis of titanium alkoxides results in a polymeric gel or a particulate colloidal gel. Generally, for high surface area powders and membranes, particulate gels are the precursors. The initial step is the hydrolysis of the alkoxides. [147, 170, 177, 204] This is followed by peptization using acid or base, [211-216] which is responsible for the stabilization of sol. Shi *et al* [208] hydrolysed titanium alkoxide under slow and fast rates in presence of nitric acid and the particle size was observed. It was found that the slow hydrolysis resulted in a large particle size, ~57 nm, while the fast one has ~36 nm. Similarly, when started with titanium butoxide, and isopropoxide, the latter yielded a slow rate of hydrolysis but also a smaller particle size of ~19 nm. This is supposed to be due to the isopropoxide moiety sterically hindering the hydrolysis reaction. Hydrochloric acid catalyst has been widely used in the hydrolysis and peptization of titanium alkoxide for obtaining high surface area oxides often for catalyst applications. [175,217] Such processing route yielded finer crystallite size titania, which had an earlier anatase to rutile transformation temperature. Long aging of such gels, also, raised the anatase to rutile

transformation temperature. Ferreira *et al* [211] have had a detailed study on the peptization and the associated structural properties like phase assemblage and anatase to rutile transformation. A detailed study on the peptization of titanium isopropoxide solution using tetraethyl ammonium hydroxide and HCl has been carried out. They reported that peptization is efficient compared to the hydrolysis - peptization in terms of anatase to rutile transformation. The isopropanol derived as a by-product of hydrolysis was described as responsible for the destabilization of the colloidal particles, by enhancing their aggregation. Furthermore, they have suggested a higher ratio of HCl to Ti as responsible for the earlier rutile formation. Polycarboxylic acid was recently used as a peptising agent and the formation of nanoparticles of anatase during the anti-aggregation process was attributed to its chelation effect. [218] A few more reports on acid and base peptization have also been reported. [219]

Another factor influencing the particle size is the amount of hydrolysis water. Hydrolysis with low water content yields smaller grain size for titania and a lower anatase to rutile phase transformation temperature. However, contradicting results have also been reported by Barringer and Bowen (1982). [147] They showed that the average particle size of the titania powders decreased with increasing water concentration or decreasing alkoxide concentration. Heterogeneous mixture of oxides have been prepared based on titania and oxides such as silica, [220] zirconia, [128] alumina, [221-222] vanadia [223] and minor additives, either by preferentially hydrolysing one alkoxide in a salt solution or peptising suspension of precipitate to nanoparticles. Monophasic alumina-

titania [224] systems have been prepared by co-hydrolysis of mixed alkoxides, and a comparison with heterogeneous catalysts having similar diphasic counterparts indicated that the monophasic one had much larger efficiencies, and could be an excellent substitute for conventional aluminium trichloride - sulphuric acid systems.

Titanium oxide, synthesized in nanometer range shows excellent magnetic / ferromagnetic, [225] optical [19-21] and catalytic properties [226-227] due to their large surface to volume ratio as well as the quantum size effect [228-231] associated with them. The important challenges in nanotechnology are, therefore, the real control over its preparative parameters in order to arrive at suitable properties for specific end uses. Hydrolysis of two metal alkoxides needs separate control owing to the differing electropositivity of the metal atoms. [193] Titanium tetraisopropoxide (TTIP) is highly reactive compared to tetraethylorthosilicate, [193] which is also used as a dopant in the present system, and hence needs additional control against hydrolysis. Acetic acid is a suitable stabilizer, which effectively stabilizes the titanium tetraisopropoxide moiety by either modifying its coordination sphere to six or by ester formation. [232-236] However, silica sol was prepared without a chelating agent, but in presence of a solvent and by the controlled addition of water. Temperature has also been found to influence the hydrolysis - condensation process.

1.5 Effect of Solvents, Catalysts and Complexing Ligands

Depending on titanium resources and the final target, various solvents have been used to prepare nanometric TiO_2 particles, such as alcohols, [237-238] carboxylic acids [239] and water. [240-241] In most cases, some additional reagents have been used together with the solvent either as a peptizer (e.g., inorganic acids), [237] or as a stabilizer [242-244] in order to monitor hydrolysis and condensation reactions. The hydrolysis of titanium alkoxides is rather fast, and therefore, chelating agents are incorporated to control the rate of hydrolysis. Common chelating agents reported are acetyl acetone, [245] acetic acid, [246-251] tartaric acid, [252] and certain polymers such as polyvinyl acetate and polyvinyl alcohol. [253] The influence of ligands on the acceleration of crystallization as well as their effect on two component systems, prepared by sol-gel process, was recently reported by Nishide and Mizukami. [242-244] Use of chelating intermediates in the development of titania coatings have been reviewed recently, where acetyl acetone, acetic acid and diethanolamine were employed. [254-256] A complexing agent-assisted sol-gel process using an organic ligand as a modulator can tailor the crystal structure and optical properties of TiO_2 thin films. [257] Takahashi and Matsuoka reported that control of firing temperature, when diethanolamine is used as a ligand, forms pure anatase and rutile TiO_2 films. [254] Kato *et al* [238,258] reported that the anatase TiO_2 film with preferred orientation is formed when polyethylene glycol is used. Gotić *et al* [259] reported a hydroxypropyl cellulose (HPC) stabilized sol-gel preparation of nanosize TiO_2 particles. The particle size and pore distribution in membranes can be

controlled by using polyethylene glycol or glycerol [260] as a gelling agent or a surfactant that is adsorbed on the surface of primary nanoparticles. The use of surfactants [175,217,261] and templating agents [262-266] are attaining great importance in view of the demand for high surface area, meso / macroporous unsupported materials for energy applications. [267] Recently, mixed organic media has also been used for the synthesis of nanocrystalline anatase and rutile titania by Wang *et al.* [268]

The influence of ligands on the crystal structures and optical properties of TiO_2 was reported by Nishide and Mizukami. [242-244] The authors have also reported the complexing agent assisted sol-gel process for the preparation of TiO_2-SiO_2 (1: 1) films. Livage and coworkers have [233] studied the role of acetic acid on the molecular level modification of titanium alkoxide precursors. They observed the reproducibility of preparation of monolithic TiO_2 gels in presence of acetic acid, which not only acts as an acid catalyst but also as a ligand and changes the alkoxide precursor at a molecular level and thus modifying the whole hydrolysis condensation process. The bidentate acetate ligand formation by the replacement of OR groups directly bounded to the titanium are reported to be determined by infra-red experiments, which showed the arrangement of both chelating and bridging acetates leading to $Ti(OR)_x(Ac)_y$ oligomers. The reaction sequences investigated through infra-red experiments indicated the preferential removal of (OR) groups first and bridging acetates subsequently in the hydrolysis – condensation process, where the chelating acetates were

removed only upon heating above 200° C. Recently, Ivanova *et al* [269] studied the role of acetic acid on the thermal transformations of the sol-gel TiO_2-MnO system through FTIR technique. The other reports on the chelating agents include the work by Moriguchi *et al*, [270] in which they report the role of *n*-octadecylacetoacetate as an amphiphilic chelating agent in the two-dimensional sol-gel synthesis of ultrathin films of titania and zirconia, and that by Trung *et al.* [260] They have, recently, reported the effect of glycerol as a new stabilizer in aqueous and non-aqueous media on the preparation of pseudo-spherical TiO_2 nanoparticles of very small size ranging from 4 to 10 nm.

Polyethylene glycol (PEG) is an important gelling, dispersion and filming agent that has been employed many times to prepare the powders and coatings of nanocrystalline TiO_2. [271] Polyethylene glycol coordinates to a structure formed by the controlled hydrolysis and polycondensation reactions of titanium tetraisopropoxide chelated with diethanolamine. From the resulting chemically modified precursor solution, anatase coatings consisting of nanometer-sized pores and grains with diameters of ~30 nm and a preferred orientation along the c-axis were prepared on quartz-glass plates by a dip coating method. In contrast, anatase coatings consisting of submicrometer-sized pores and randomly orientated grains were prepared from the solution in which the poly(ethylene glycol) had been isolated. [272] There is another report on an improved sol-gel method using PEG as a multifunctional agent and

inorganic titanate as a precursor for preparing ultrafine and crystallized TiO_2 powders, without a high temperature calcination step. [273]

The effect of HCl and NH_4OH catalysts on the control of phase and pore structure was reported by Song *et al.* [274] According to them, the catalyst concentration has an immense effect on the porosity of powders. Titania powders prepared near the isoelectric point with low concentration of NH_4OH showed the highest textural properties and high degree of aggregation. The porosity consists of both intra-aggregate and inter-aggregate pores and the average pore diameter of the intra-aggregate pores decreased with increasing HCl concentration and increased with increasing NH_4OH concentration. So, in order to achieve the desirable properties, a variety of synthetic techniques are attempted, where each method highlights certain property. Simple hydrolysis of titanium alkoxide in presence of acid catalysts and controlled hydrolysis by involving stabilizing agents, which may form intermediate compounds on hydrolysis in presence of only water and alcohol, resulted in titanium oxide with different properties. Use of macromolecules in the hydrolysed sol has indicated the possibility of less agglomeration. Use of size specific emulsion droplets on which sol-particles can provide a coating and finally result in mesoporous / macroporous gels has been one of the recent findings. [194] Titania and silica based porous gel systems are also possible candidate materials as high efficiency bio and humidity sensors. [275] Report by Suresh *et al* [206] showed that hydrolysis of titanium isopropoxide at pH 4 adjusted by the addition of

dilute HNO_3 could produce a precursor having an A > R transformation temperature as high as ~ 800° C in place of the usual phase transformation temperature of ~ 600° C. Recently Bosc *et al* [171] proposed a simple route for the low temperature synthesis of mesoporous and nanocrystalline anatase thin films.

1.6 *Effect of Temperature*

Pratsinis and co-workers investigated the effect of hydrolysis temperature on the phase transformation and pore structure of titania in detail. [177] They observed a slight retardation in the phase transformation with increasing hydrolysis temperature, at a small initial water concentration. Recently, Zhang *et al* [179] reported the preparation of single-phase nanocrystalline anatase from amorphous titania. Their work addresses the effect of temperature on the tailoring of particle size of nanocrystalline titania.

Gotic et al [276] investigated the microstructure of TiO_2, synthesized by sol-gel procedure. The aim of their and some other group's research was to obtain nanosized TiO_2 with improved properties, which was used for development of photoanodes in dye-sensitized solar cells [37,277]. Liu *et al* [278] have proposed and improved sol-gel method for the preparation of ultrafine and crystallized titania powders. In addition, Venz *et al* [279] reported the physical properties of chemically modified titania hydrolysates. Again, recently the size-controlled TiO_2 nanoparticles were prepared by Chae *et al* [132] in order to use in

the field of optically transparent photocatalytic films. Recent reports also indicate various propositions in the synthesis of nano titania such as by Liu *et al*, [280] who proposes a photoassisted sol-gel route for the formation of an early rutile phase.

Bacsa and Grätzel (1996) [281] studied the effect of peptization on the phase transformation and found that the anatase-rutile phase transformation was critically dependent on the water / alkoxide molar ratio. [282] Vorkapic and Matsoukas (1998) [282] investigated the effect of temperature and alcohols on the size of the titania particles. Due to the various possibilities of sol-gel process in terms of the variety of products that can be achieved, this process is being used considerably in present days.

1.7 Anatase - Rutile Transformation

Anatase and rutile are the two polymorphs of titania at atmospheric pressure. [283-285] The room temperature phase is anatase and the high temperature phase is rutile. Anatase transforms irreversibly and exothermically to rutile in the range 400°C to 1200°C [286-287] depending on parameters such as the method of preparation, [216,288] grain size, [289] morphology, [290] degree of agglomeration, [291] nature of impurities [292-297] and reaction atmosphere. [298-299] At atmospheric pressure, the transformation is time and temperature dependent and is also a function of impurity concentration. The complexity of the transition is typically attributed to the reconstructing nature. The phase

transition is a nucleation-growth process and follows the first order rate law with activation energy of ~90 Kcal/mol. [300-305]

The anatase - rutile transformation involves an overall contraction of oxygen and a movement of ions so that a cooperative rearrangement of Ti^{4+} and O^{2-} occur. The transformation implies that two of the six Ti-O bonds of anatase structure break to form a rutile structure. [306] Removal of the oxygen ions, which generate lattice vacancies, accelerate the transformation and inhibit the formation of interstitial titanium. [307]

The impurities that have most pronounce inhibiting action are chloride, sulphate and fluoride ions whereas that accelerates the transformation includes alkaline earth and a few of the transition metal ions. [308] Those ions with valency greater than four reduce the oxygen vacancy concentration and will retard the reaction. [309-310]

The effect of reaction atmosphere shows that vacuum conditions and atmosphere of hydrogen, static air, flowing air, oxygen, argon, nitrogen and chlorine affect the phase transformation to different extents. Lida and Ozaki [311] as well as Shannon [312] found that the transformation rate in a hydrogen atmosphere is greater than in air and under vacuum decreasing as oxygen partial pressure increases. Oxygen vacancies are formed in hydrogen atmosphere whereas the interstitial Ti^{3+} ions are generated under vacuum. The rate constant of the transformation in hydrogen was 10 times larger than in air.

It has been reported that at 950°C the phase transformation in Ar/Cl_2 atmosphere is about 300 times faster than in air. [311] The accelerating effect of chlorine atmosphere on the anatase-rutile phase transformation involves two mechanisms that probably occur simultaneously - vapour mass transport and oxygen vacancy formation in which the first generate nucleation and growth in the bulk and the second provide pathways for the diffusion of ions. When the vapour transport is negligible, the primary mechanism is based on oxygen vacancies.

The effect of metal cations such as Li, Na, K, Mg, Ca, Sr, Ba, Al, Y, La, Er, Co, Ni, Cu and Zn on anatase - rutile transformation was studied earlier. [309] A linear relationship between phase transition temperature and ionic radius, for alkali and alkaline earth metals and group III elements are reported. Transition metals, which entered the matrix interstitially, gave a high transition temperature, whereas those dopants introduced substitutionally did not make any significant change in transition temperature. It was concluded that the oxidation state together with ionic radii of cations and type of sites occupied were the important parameters, which control phase transition temperature.

Depending on the ionic radius of dopant compared with radius of titanium, it can be introduced substitutionally or interstitially or if the size of the dopant is larger than oxygen, it could be intercalated into the matrix, producing a lattice deformation. [310] The dopants had no effect on the amorphous gel to anatase transformation temperature, but influenced the anatase - rutile transformation. If dopant ion size is less than that of titanium,

anatase phase will be stabilized to a higher temperature. Dopants bigger than oxygen ion produce large local deformation of lattice. Those dopant ions whose size falls in between titanium and oxygen stabilize the anatase phase. Those dopants near to oxygen size can stabilize the titania phase more. The enhancement or inhibiting effect of additives on anatase - rutile transformation depends on their ability to enter the TiO_2 lattice, thereby creating oxygen vacancies or interstitial Ti^{3+} ions. Oxides of Cu, Co, Ni, Mn and Fe mixed with anatase TiO_2 increases the transformation rate efficiently. Transition metals, which entered the matrix interstitially, gave a high transition temperature, whereas those dopants introduced substitutionally did not give a significant change in transition temperature.

The influence of impurities on the nucleation and growth of rutile from anatase was studied by Shannon and Pask. [313] They concluded that processes that create oxygen vacancies, such as the addition of acceptor dopants (ions with a lower valence than Ti^{4+}) and use of reducing atmospheres accelerate the anatase-rutile transformation. Conversely, processes that increase the concentration of titanium interstitials, such as the addition of donor dopants, inhibit the transformation. Shannon and Pask hypothesized that an increase in the concentration of oxygen vacancies reduces the strain energy that must be overcome before the rearrangement of the Ti-O octahedra can occur, and that cations with a valency less than that of titania (4^+) will increase the concentration of oxygen vacancies, due to the necessity for charge balance.

Depero *et al* [314] have studied the anatase - rutile transformation in TiO_2 powders and reported an increase of the crystallites and/or of the lattice perfection accompanied by the transformation on the basis of X-ray microstructural analysis. The studies were carried out on vanadia-treated TiO_2. The vanadia-treated surface layer was particularly distorted and apparently acted as a restraint to perfecting by thermal treatments. Only the transition to rutile was capable of overcoming that restraint by allowing crystallite growth at the expense of the smaller and distorted anatase crystallites.

Zhang and Banfield [315] observed that the synthesis of ultrafine titania resulted in anatase and/or brookite, which on coarsening transformed to rutile after reaching a certain particle size. Based on the inferred lower surface energy of nanocrystalline anatase, phase stability reversal is predicted at particle size under 13 nm and supported by coarsening and phase transformation experiments by Gribb and Banfield [302] as well as by Zhang and Banfield. [289] Once rutile was formed, it grew much faster than anatase. [306] They analyzed the phase stability of anatase and rutile thermodynamically to conclude that anatase became more stable than rutile for particle size <14 nm. Hwu *et al* [316] have reported on the dependence of anatase or rutile formation on the preparation method. Small particle size (<50 nm) anatase seemed more stable and transformed to rutile at ~973 K.

Zhang and Banfield [315] studied the phase transformation behavior of nanocrystalline aggregates during their growth in isothermal and isochronal

reactions by using XRD. They suggested that transformation sequence and thermodynamic phase stability depend on the initial particle sizes of anatase and brookite. They concluded that, for equally sized particles, for particle size <11 nm, anatase was thermodynamically stable, and for particle size between 11 nm and 35 nm, brookite was stable, and for particle size >35 nm, rutile was stable. They cautioned that, for real samples, the particle sizes of different phases were not equal, and this could alter the direction of the initial transformation. They concluded that the energetics of these polymorphs were sufficiently close that they could be reversed by small differences in surface energy.

Ye *et al* [317] studied the thermal behavior of nanocrystalline brookite by thermogravimetric analysis, differential thermal analysis, and diffraction. They observed a slow transition from brookite to anatase phase below 1053 K along with grain growth. Between 1053 K and 1123 K, they noticed rapid brookite to anatase and anatase to rutile phase transformations. Above 1123 K, they observed rapid grain growth of rutile, which became the dominant phase. They concluded that brookite couldn't transform directly to rutile but through anatase phase only. Kominami *et al* [318] observed that nanocrystals of brookite directly transformed to rutile above 973 K, in contrast to the observation by Ye *et al.*

Zhang *et al* [319] measured micro-Raman spectra of nano-sized TiO_2 powders prepared by vapour hydrolysis. They obtained amorphous TiO_2 at 533 K and predominantly anatase between 873-1173 K. The anatase-rutile

transformation temperature depended on particle size and was complete at ~1323 K. They noted that the phase transformation of amorphous TiO_2 is a two-step process; amorphous to anatase followed by anatase to rutile. They proposed that the rutile formation started at the surface and migrated into the bulk. They also noted that the brookite impurities as detected by Raman spectroscopy but not by XRD, were present on the anatase surface.

Zhang and Banfield [320-321] proposed that the mechanism of anatase-rutile phase transformation was temperature-dependent. They suggested that this transformation was dominated by interface nucleation below 873 K, by both interface and surface nucleation between 893-1273 K, and by bulk nucleation above 1273 K.

The anatase-rutile transformation depends on impurities, grain size, reaction atmosphere, and synthesis conditions. Zhang and Banfield reported that the anatase-rutile phase transformation occurred at higher temperature with the addition of Al_2O_3. [321] They attributed this to suppression of coarsening caused by surface diffusion. Okada *et al* [322] and Yoshinaka *et al* [323] found that the anatase-rutile phase transformation occurs at higher temperature with the addition of SiO_2. Ferreira and Yang [211] showed that synthesis conditions (chemicals/peptizing agents) affect the crystallinity and anatase-rutile phase transition temperature. Zaban *et al* [324] noted that the surface structure of TiO_2 is affected by the preparation conditions. Ahonen *et al* [325] studied the effect of gas atmospheres (nitrogen and air) and temperature on the crystal structure and

transition temperature. Zaban *et al* [324] noted that the surface structure of TiO_2 is affected by the preparation conditions. Ahonen *et al* [325] studied the effect of gas atmospheres (nitrogen and air) and temperature on the crystal structure and specific surface area. They observed that anatase synthesized in air transformed to rutile at 973 K, whereas anatase synthesized in nitrogen persisted to 1,173 K. Gouma and Mills [326] studied the anatase-rutile phase transformation in commercial TiO_2 powders with an average particle size of 100 nm. Using transmission and scanning electron microscopy, they concentrated on the structural evolution (shape and morphology) of the particles. They proposed that rutile plates are formed initially by a shear force and subsequent coarsening involved interactions between the transforming particles and surrounding anatase particles. Studies by Fransisco *et al* [327] and many others on the anatase to rutile phase transformation illustrate its technical importance in various application fields.

1.8 TiO_2 Films and Coatings

The films were prepared/attempted for chemical reactions since conventional powder catalyst suffered from disadvantages in stirring during the reaction and getting it separated after the reaction. [119,328] When the TiO_2 is used in the powder form, two major difficulties occur. First, ultrafine powders will agglomerate into larger particles, reducing the effective surface area for the

reaction resulting in an adverse effect on catalyst performance. Second, it is very difficult to recover TiO_2 powders from water when they are used in aqueous systems, leading to a potential difficulty in downstream separation. [119,328] The catalyst coated as thin film was found to be useful in overcoming these disadvantages. Also, industrial applications of TiO_2 thin films, as a basic unit of antibacterial ceramic tile or self-cleaning glass [85,329-330] look promising.

The coatings can also be used as passive solar control in architectural windows. [39] For solar control and prevention of superheating of buildings, absorbing glasses (coatings) could be used but a part of the absorbed energy succeeds in infiltrating the buildings by re-emission in the far infrared region. Using reflective coatings attains more efficient reduction of the entering solar radiation, which partially changes the colour characteristics of the transmitted light in the visible region of the spectra. In other words, there must be a decrease of the admitted light energy level, while keeping the colour characteristics of the natural light as good as possible. So, a spectral-neutral transmission is necessary, or if it is possible, a more horizontal spectral transmission curves in the visible spectral region from 0.4 to 0.8 μm need be achieved.

Even though lot of research has carried out in the area of TiO_2 thin films, various approaches are still being reported with respect to basic aspects such as deposition on glass substrates, [331-332] which emphasize the potentiality of the research on TiO_2 films and coatings. Different photocatalytic titania were

compared recently by Du *et al.* [129] Bosc *et al* [171] recently developed a simple route for the preparation of mesoporous and nanocrystalline anatase thin layers. The method consists of templating the acid hydrolysed titanium isopropoxide sol with the poly (ethylene oxide) – poly (propylene oxide) - poly (ethylene oxide) triblock copolymer.

1.9 TiO_2 Nano Catalysts

Traditionally, TiO_2 finds use in mixed vanadia / titania catalysts used for selective oxidation reactions. [333] The surface science of vanadium and vanadia/TiO_2 systems was addressed by several groups. [334-337]

In developing novel catalyst systems it is especially critical to develop a powder with the highest possible surface area, or, equivalently, the smallest possible particle size Non-crystalline TiO_2 powder can be easily obtained at treatment temperatures ≤ 300°C, [338] however, crystallized nanosized TiO_2, e.g. anatase phase, would have better catalysis activity. [339-342]

In the past two decades, considerable research has been reported in the synthesis and evaluation of catalytic property of titania based mixed oxides. These oxides have specific surface areas in the range 150-250 m^2/g. The various mixed oxides reported are with silica, [322,343-346] alumina, [347] lanthanum oxide, [348-349] cerium oxide [93,327,350] and vanadium oxide. [351-352] Fine metal particles also have been introduced.

One of the studies has been to see any preferential reactivity exists for anatase compared to rutile in reaction with alcohols. [353] The cation coordination environment is the same in anatase and rutile bulk structures where the role of oxygen vacancies (defect states) in titania [354] was investigated by water vapour adsorption and carbon monoxide oxidation. However, the rutile phase showed higher efficiency in the decomposition of H_2S gas than anatase [355] having similar surface areas. In order to keep the phase assemblage at the desired high temperatures, the anatase to rutile transformation temperature has to be controlled, and this is largely achieved, by introducing appropriate dopant oxides in the precursor gel. Benjaram *et al* [356] reported the catalytic property of V_2O_5/ La_2O_3-TiO_2 mixed oxide systems prepared by co-precipitation route. The anatase form of titania is believed to possess enhanced catalytic activity, probably due to its open structure compared to rutile and its high specific surface area. [303]

1.10 Effect of Dopants

Suitably modified titanium oxide has been reported to be efficient catalysts in chemical reactions. [32,357-360] A high anatase to rutile transition temperature [347,362] or otherwise high anatase phase stability is desirable for use of titania in photoreactions at elevated temperatures. The transition temperatures and hence, the transition from one crystalline form of TiO_2 to

another can be influenced by chemical doping [363-365] or alcohol washing (butanol). [366] The catalytic and photocatalytic properties are being investigated widely in the form of bulk powders, films and membranes. [94,367-371] Nanocrystalline titania was synthesized by chemical methods involving sol-gel approach. Titania undergoes phase transformation from the low temperature anatase phase to rutile, which is seen to extend to as high as 1000° C depending on the method of preparation and in presence of dopant oxides. [372-373] The role of a few dopant oxides such as Fe_2O_3, V_2O_5 and CuO [374-379] on the anatase to rutile transformation is well reported and certain correlation between the ionic radii of the dopants and anatase phase stability was drawn by Ferreira *et al.* [380] Anatase-rutile transformation is usually followed by XRD techniques, but impedance spectral analysis was also used to study the transformation. [381] Bjorkert *et al* [95] reported the influence of La_2O_3 as dopant on the phase development of Al_2O_3: TiO_2 ceramic membranes. In their work, lanthana was used to stabilize γ-alumina phase in Al_2O_3:TiO_2 composite ceramic compositions. $LaAl_2O_3$ phase is reported to form at the alumina surface, which stabilized the γ-alumina phase. There are reports on the effects of addition of metal ion dopants on the quantum efficiency of heterogeneous photocatalysis of titanium dioxide. [382-385] Also Lin *et al* [386] reported the effect of addition of Y_2O_3, La_2O_3 and CeO_2 on the photocatalytic activities of titania for the oxidation of acetone. A few other reports on lanthanum oxide doped titania include the work of Gopalan *et al* [349] and LeDuc *et al.* [387] The former reports the evolution of pore structure and anatase phase stability as a result of the

addition La_2O_3. The anatase phase is stable upto 650° C and this is explained by a possible monolayer coverage of lanthana over Titania. Report by LeDuc *et al* deals also with textural stability La_2O_3-doped Titania prepared by suspending a commercial titania catalyst in a solution of lanthanum nitrate. A doping level of 5 % La_2O_3 was recommended for long-term thermal stability upto 650° C. Recently, Francisco *et al* [327] have studied the effect of ceria on the inhibition of the anatase-rutile phase transformation in the CuO-TiO_2 system.

The high surface area TiO_2, which is a necessity for good catalysts, were also prepared by many researchers. Titanium oxides prepared via sol-gel method exhibit comparatively high surface areas and hence have an advantage over conventional materials for potential applications as catalysts, sorbents, or electrodes. [152,388] The rutile form of Titania, which has a lower surface area and high refractive index as well as high opacity is used for cosmetics and pigment applications. On the other hand, the anatase form of titania is believed to possess enhanced catalytic activity, compared to rutile. [121,257,389-390] However, a drastic reduction in surface area of titania is reported to occur on heating to higher temperatures. [106] It has been suggested that the enhanced sintering rate during the phase change from anatase to rutile is responsible for this drastic reduction in surface area. [106] Suitable doping can retard the rate of reduction in surface area at higher temperatures. Kumar *et al* [347] have earlier reported the effect of second phases such as yttria and lanthana on the textural properties of anatase phase. Kumar *et al* have also studied the pore structure stability of

ceria doped structured alumina. Ozawa *et al* [391] reported the thermal stability of γ-alumina modified with lanthanum or cerium. Koebrugge *et al* [350] reported the thermal-stability of nanostructured titania and titania ceria ceramic powders prepared by the sol-gel process. We have reported the influence of lanthana on the structural and textural properties of titania. Report by Kasuga *et al* [392] points toward a silica doping-and-subsequent leaching out to be a possible method to synthesize high surface area titania. However, the maximum surface area obtained by them was 150 m^2/g at 600°C. Further, Sang *et al* [393] reported the preparation of mesoporous titania by selective dissolving of titania-silica binary oxides. The material showed enhanced photoactivity compared to the untreated titania. High surface area obtained as a result of the treatment was reported to be major reason for the enhanced photoactivity. High surface area titania have also been synthesized by many methods by many researchers. [175,210,217]

1.11 Effect of Additives

Titania-silica sol-gel systems have been subjected to studies related to catalysis [394-396] in various chemical environments. In fact, addition of titania to a silica gel matrix had synergistic effects. The crystal sizes vary and spherical titania was dispersed in disc shaped silica matrix. The particle size was in the range 10-5 nm. The presence of Si-O-Ti bond has been identified. [397]

Titania-silica sol-gel systems exhibit significant changes in the surface acidities. [398] Certain results from temperature programmed desorption (TPD) and infra red spectral data indicated that the total acidity and relative acid strength of silica decreased as silica was introduced to titania. All the acid sites on pure titania were originally Lewis type whereas more than 80% on the mixed oxides were of Bronsted type. The enrichment in reactivity with respect to Brönsted acid was present in the titania in mixed oxide, while it is not present in pure titania. This should be due to the local charge imbalance associated with tetrahedrally coordinated silica, chemically mixing with octahedral titania matrix. On the other hand, in silica rich mixed oxides, titanium substituted isomorphously for Si in tetrahedral silica matrix, eliminating the local charge imbalance carrying Brönsted acidity. Evidence for the decrease for the Ti-O bond distances by incorporation of Si into mixed oxide was observed through EXAFS and thus disruption of usual octahedral coordination of pure titania. [399] This is also associated with formation of Ti-O-Si linkages in the mixed oxides. Diffuse reflectance UV-VIS spectroscopy (DRS) has been used to identify the presence of isolated Ti sites in titania-silica mixed oxides [400] which are understood to be the primary reason for the extraordinary catalytic activity of titania-silica mixed oxides. Further, it has also been shown that there should be a high Titania dispersion in the silica matrix, in addition to the site isolated Titania. The existence of Ti-O-Si bond in such titania-silica xerogels calcined in the range 400-800°C was also confirmed by infra red and Raman spectral data. [251,343] Hydrophilicity of titania

dispersed silica containing monomodal pore size distribution of about 0.7 nm has been accounted for the size selective epoxidation reactions of olefins. [220] In a matrix of silica, titanium oxide along with other oxides such as MoO_3 and WO_3 were also substituted in a sol-gel medium and enhanced catalytic properties were observed. The IR spectral data indicate Si-OH vibrations and MAS NMR data indicate that the molecular dispersion of the metal oxide takes place in xerogels. [401] These gels have a microporous nature with average pore diameter of 1.5 nm and specific surface area as high as 750 m^2/g. Recently, Warrier *et al* [344] reported on the effect of silica addition on the high temperature stabilization of pores compared to the undoped titania. The homogeneously distributed silica particles in titania matrix, prepared through sol-gel route, helped the matrix to retain its microporosity considerably even after tempering for 32 hours.

In order to achieve the high efficiency titania-silica catalysts, a variety of techniques are reported. The drying method was investigated with respect to TiO_2-SiO_2 catalyst system. [402] A comparative evaluation of drying of a titania-silica precursor sol under high temperature supercritical drying, low temperature supercritical drying and evaporative drying adopted for xerogels are reported. Low temperature supercritical drying was shown to be the most ideal. High epoxide selectivity is reported in titania-silica gels. Partial hydrolysis of Ti-O-Si bonds was observed which had a sort of correlation

between oxidation rate and Ti-O-Si connectivity, which is a characteristic of the Ti dispersion in silica. [403]

Alumina-titania systems are reported to be potential solid acid catalysts and a range of compositions with varying Al/Ti are synthesized as well as characterized. [404-407] These compounds have been found to have high specific surface areas and enhanced acidity than comparable mixed oxides. The strength and density of the acid sites have been found to be proportional to the Ti content. Effect of addition of other oxides such as WO_3 to alumina-titania was investigated. [408] The tungsten species is present largely as mono oxo wolframyl species and are strong Lewis acid sites. By absorption of water, the overall coordination of tungsten grows and it behaves as a strong Brönsted acid site. There appeared W-O- (Ti, Al) bonds without significant W-O-W bridges. Vanadium oxide has been loaded on to alumina-silica-titania composite oxide and the alumina rich or silica rich catalysts are found to have comparable properties. [336] In such catalysts, specific surface area appears to play a major role.

Vanadium-titanium oxide catalysts showed presence of Brönsted acid sites associated with $[V^{5+}]$ –OH surface sites [409] as was revealed by temperature programmed desorption study. Catalytic reduction of nitric oxide by ammonia over vanadia-titania mixed oxide catalysts has indicated that the concentration of Brönsted acid groups on the catalyst determines the efficiency. [410] Comparative studies of temperature programmed desorption between titania

and titania-vanadia mixed oxide catalysts for NO reduction [223] showed that the mixed oxides were more efficient. Further, mechanism of the vanadia-titania catalyst indicated a catalyst cycle that consisted of both acid and redox reactions involving surface V-OH (Brönsted acid sites) and VO species. [226] Many other mixed oxides with titanium oxide were prepared and tested for various catalytic reactions. Sol-gel mixtures of silica or zirconia with titania have shown enhanced catalytic property when compared to individual oxides. Other mixed oxides, which are less reported, but may be, potential candidates are, chromia-titania and ceria-titania. Chromia-titania was found to be efficient as selective catalytic reduction of NO by ammonia [379] and the Brönsted acid site bound ammonia enhances absorption of NO and is responsible for selective catalytic reduction of NO to NO_2. Chromium ion doped polycrystalline titania catalysts were further characterized [411] by FTIR and XPS. Two identical compositions prepared by co-precipitation and impregnation on analysis showed that irrespective of the method of preparation, there are two types of acid sites, Lewis and Brönsted. The latter is characteristic of chromium since pure titania does not show any Brönsted acid site. The one prepared by co-precipitation containing upto 2% Cr has given better results. Ruiz *et al* [40] reported that Cr-doped TiO_2 p-type semiconductor thin film could be used for gas sensor applications. Table 2 presents various titania compositions and the major chemical conversions reported for catalytic reactions.

Table 2: Titania aerogels and xerogels and various catalytic systems reported

Titania system	Reaction system	Reference
TiO_2	Gamma-Ray Destruction of EDTA	412
	Water vapour chemisorption and CO oxidation	354
TiO_2 Anatase & Rutile	Adsorption of alcohols	353
TiO_2-based oxide catalysts	Selective catalytic reduction of NO	413
WO_x/TiO_2	Adsorption of alcohols	414
Halogen Ions-Modified Al_2O_3, ZrO_2, and TiO_2 as Catalysts	Selective Catalytic Reduction (SCR) of NO with NH_3 at Low Temperature	415
V_2O_5/TiO_2 aerogel	Reduction of NO	416-418
V_2O_5/TiO_2 xerogel	Reduction of NO by NH_3	408-409
V_2O_5/TiO_2 and Cr_2O_3/TiO_2	Catalytic Removal of Nitrogen Oxides	419
Vanadium Oxide Incorporated into Mesoporous Titania	Catalytic Oxidation	420
Chromia/TiO_2	Reduction of NO by NH_3	379

$Al_2O_3/SiO_2/TiO_2/V_2O_5$	Reduction of NO by NH_3	225
TiO_2/SiO_2 aerogel	1-butene isomerisation	421
TiO_2/SiO_2 xerogel	Si-O-Ti bonds	397
	1-butene isomerisation	398
	Epoxidation olefins	400
$TiO_2/MoO_3/WO_3/SiO_2$	Oxidation hydrocarbon	401
Pd-TiO_2 aerogel	Hydrogenation	422
Pt-TiO_2 aerogel	Hydrogenation	423

1.12 TiO_2 Photocatalysts

The photoelectric and photochemical properties of TiO_2 are in the focus of active research for the last one-decade. The initial work by Fujishima and Honda [27] on the photolysis of water on TiO_2 electrodes without an external bias, and the thought that surface defect states may play a role in the decomposition of water into H_2 and O_2, has stimulated much of the early work on TiO_2. Unfortunately, TiO_2 has a low quantum yield for the photochemical conversion of solar energy. The use of colloidal suspensions with the addition of dye molecules has been shown to improve efficiency of solar cells, [35,36,424] and has moved TiO_2-based photoelectrochemical converters into the realm of economic competitiveness. [425] Another method to improve the quantum yield is the maninpulation of band gap, [119,426] which necessitates an active research and

the researchers all over the world are looking at it. The huge number of research papers getting published in this aspect shows its technological importance.

By far, the most actively pursued applied research on titania is its use for photo-assisted degradation of organic molecules. TiO_2 is a semiconductor and the electron-hole pair that is created upon irradiation with sunlight may

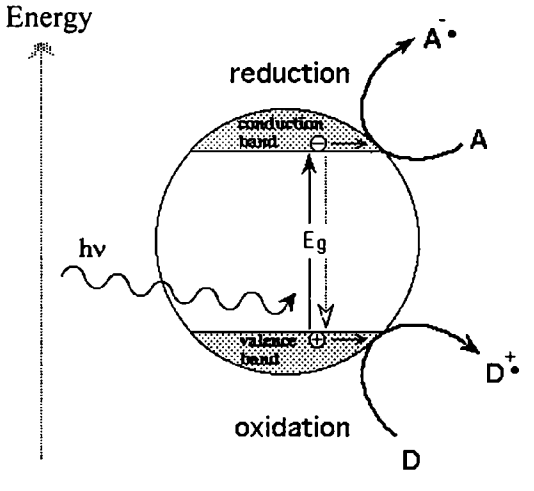

Figure 3: Energy scheme of a semiconductor particle in which an electron is excited by light absorption. Located now in the conduction band it is capable of reducing species A (in most cases just oxygen from air). When excited by absorbing a photon hν there remains a positive charge (defect electron or hole) in the valence band capable of oxidizing species D. In TiO_2 the oxidizing power of such a hole is very high.

separate and the resulting charge carriers might migrate to the surface where they react with adsorbed water and oxygen to produce radical species. [119] These attack any adsorbed organic molecule and can, ultimately, lead to complete

decomposition into CO_2 and H_2O. A schematic representation of photoassisted reaction is provided in Figure 3. The applications of this process range from purification of wastewaters; [89] disinfections based on the bactericidal properties of TiO_2 [85,329-330,427-430] (for example, in operating rooms in hospitals); use of self-cleaning coatings on car windshields, [431] to protective coatings of marble (for preservation of ancient Greek statues against environmental damage. [432] It was even shown that subcutaneous injection of TiO_2 slurry in rats, and subsequent near-UV illumination, could slow or halt the development of tumour cells. [29,433-435] Several review papers discuss the technical and scientific aspects of TiO_2 photocatalysis.. [436-439] An extensive review of the surface science aspects of TiO_2 photocatalysis has been given by Linsebigler *et al*, [120] and some of these more recent results are discussed.

Other oxides of similar behaviour are, ZnO, iron oxide, cadmium sulphide and ZnS. ZnO, which is also a reasonable substitute for titania, except for its property of undergoing incongruent dissolution resulting in formation of zinc hydroxide coating on the ZnO particles leading to slow catalyst inactivation. Among the photocatalysts, titania is believed to be the most promising material due to its superior photoreactivity, nontoxicity, long-term stability and low price. Titania crystallizes mostly in two polymorphic forms: anatase and rutile, whose band gaps are 3.23 and 3.02 eV, respectively (Figure 4). It is generally accepted that anatase titania is more efficient as photocatalyst than rutile titania. [257,389-390] Some researchers showed that catalysts with mixed

phases possessed a significantly higher catalytic activity than the pure anatase phase. [440] Degussa P-25, a standard industrial photocatalyst, which is composed of 70% anatase and 30% rutile, is a good example. [441] The main reason is ascribed to better charge carrier separation in the mixed phase. Ohtani *et al* [442] proposed that a high photocatalytic activity of titania can be achieved when two requirements are satisfied, namely, a large surface area to absorb substrates and high crystallinity to minimize the photoexcited electron-hole recombination rate. However, these requirements are in general conflict with each other, because the crystallinity increases with calcination temperature while the surface area decreases. Photoactivity of amorphous titania is negligible [443] compared to that of nanocrystalline anatase, which is greater than that of rutile. The activity of nanocrystalline rutile increases with decreasing particle size. [444]

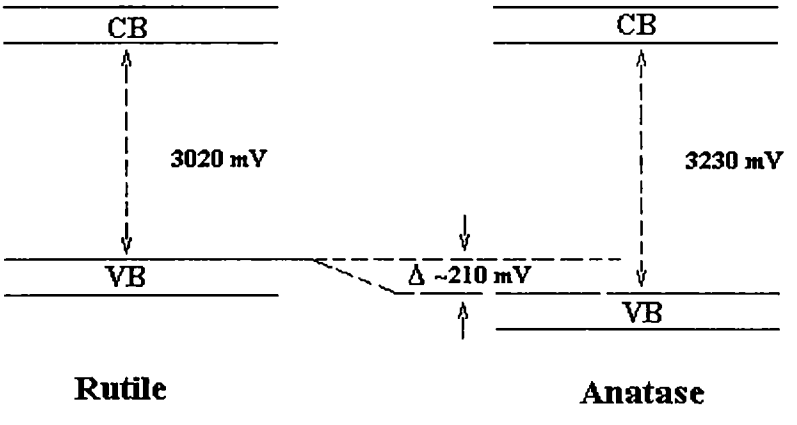

Figure 4: Schematic representation of band gaps of anatase and rutile

Conduction band edges of anatase and rutile are nearly at the same level of electron energy, whereas the edge of the valence band of anatase lays 140-

210 mV lower than rutile. Therefore the photoreduction power of anatase and rutile is equal but the oxidation power of anatase is significantly higher than rutile. This makes anatase attractive as species for photocatalytic oxidation reactions. In addition, its nature as a solid acid with adjustable surface properties and active H^+ and Ti^{4+} centers make anatase attractive for a wide range of organic reactions. E.g., the synthesis of α-pinen.

However, the band gap of titania, 3.2 eV is too large to absorb in the visible region, which contains the largest amount (~40%) of solar energy. Hence, efforts have been made to dope titania with impurities and introduce states in the band structure about 2 eV below the conduction band minimum of titania so that the band gap of resultant material would be optimum for the photo production of hydrogen. Doping of transition metals into TiO_2 has been tried. [357,445-448] However, doped materials suffer from thermal instability, increase in the number of carrier recombination centers and require expensive ion implantation facility. Also, it has been argued that creation of oxygen deficiency introduces localized oxygen vacancy states located at 0.75 to 1.18 eV below the conduction band minimum of TiO_2, so that the energy levels of the optically excited electrons are lower than the redox potential of the hydrogen evolution (H_2/H_2O) located just below the conduction band minimum of TiO_2 and that the electron mobility in the bulk region will be small because of the localization. [21]

Photocatalytic decomposition of trichloroethylene in water was investigated [449] in which anatase form was found to be better compared with rutile form. [257,389-390] Titania prepared by sol-gel route was porous, having high specific surface area of ~ 600 m^2/g containing anatase microcrystallites of the size of ~50 Å and was highly photoactive. [450] Chloroform was subjected to photo degradation in a medium containing suspended particles of titania. [451] Similarly, phenol photodecomposition has been reported using fine titanium oxide. [452] Photocatalytic reactions involving NO were conducted in presence of Titania. [453] Silica as support and titania as the active catalyst were tested for photoreactions and compared with the precursor characteristics. [454] Titania supported on alumina and silica was used for photocatalytic decomposition of salicylic acid and the titania-alumina system showed improved performance. [394] On analysis, it has been found that titania-silica consisted of matrix isolated titania quantum particles while the TiO_2-Al_2O_3 did not have such particles. Pt/Pd metal particle carrying Titania was also prepared and tested. Titania film containing well dispersed Au or Ag metal particles were prepared by sol-gel method, the effect of the dispersed metal particles on the photo-electrochemical properties of the titania electrodes has been reported. [455] The photo responsive formation of gold particles dispersed silica-titania composite gels was further investigated recently. [456] Photoreduction of such systems containing Au (III) ions yielded gold particles and this principle was used to produce micro patterns of gold particles on silica-titania films.

There are reports on the effects of addition of metal ion dopants on quantum efficiency of heterogeneous photocatalysis of titanium dioxide. [457-459] The enhanced photoactivity of titania doped by rare-earth oxides such as Europium, Praseodymium and Ytterbium oxides was recently reported by Ranjit *et al.* [460] The high activity of oxide /TiO_2 photocatalysts is attributed to the enhanced electron density imparted to titania surface by the dopant oxides. Table 3 presents various titania compositions and the major chemical conversions reported for photocatalytic reactions.

Table 3: TiO_2 compositions for photocatalysis.

Sample	**Reaction / remark**	**Reference**
TiO_2	Photocatalytic Transformation of 2,4,5-Trichlorophenol	461
Titanium Dioxide	Photocatalytic Oxidation of Cadmium-EDTA	462
TiO_2	Stearic Acid	463
TiO2	Degradation of Bisphenol A in Water	464
Titanium Oxide	Decomposition of NO	465
TiO_2 Thin Film	Microbial sterilisation	466
TiO_2 films	Trichloroethylene	467
TiO_2 Microsphere	Water and Wastewater Treatment	468

TiO_2 aerogel	Aquatic decontamination	450
TiO_2 suspension	Chloroform	451
TiO_2 in zeolite	Phenol	452
structure	Reactions of NO	453
TiO_2-WO_3	Energy storage in the gas phase	469
TiO_2-SiO_2	Oxidation of 2-Chloroethyl Ethyl Sulfide	470
TiO_2-SiO_2 Binary Oxides	Photocatalytic Epoxidation of Propene	471
Titanium Silicalite	Decomposition of Acetic Acid	472
Titanium Dioxide-Coated Surfaces	Photocatalytic Oxidation of Bacteria, Bacterial and Fungal Spores, and Model Biofilm Components to Carbon Dioxide	473
Silver-Coated TiO_2	Bactericidal Activities	474
TiO_2-Supported Gold Nanoclusters	Cryogenic CO Oxidation	475
Defective TiO_2 (110) Surfaces	DCOOD Decomposition	476
Cu-deposited TiO_2	Bactericidal Activity	477
Pt/TiO_2	CO Photooxidation	478
Au/Au (III)-TiO_2	Visible Photooxidation for Water	479

1.13 High Temperature Catalysts

Most of the applications of titania ceramics at high temperature require pure rutile phase, which is usually formed by heating the titanium salts above 600°C. However, with the expanding applications in the area of catalysts, photocatalysts, membranes and active humidity sensors, the need for obtaining anatase phase stable at elevated temperatures become significant. Earlier work indicates that even as a surface modifier for anatase titania pigments, alumina was used as a coating in order to improve gloss property as well as to prevent degradation. Recent identification of 'self-cleaning' surfaces by transparent anatase coatings on glass, ceramic tiles and bricks [480] necessitates the anatase phase to be retained at the processing temperature above 1000°C.

The anatase-rutile transformation temperatures are fairly dependent on the history of the sample. [308-309] Further, the low temperature densification in titania could be associated with the phase formation temperature. Early indicative reports on the incorporation of aluminum oxide, copper oxide, manganese oxide, iron oxide and zinc oxide postulated that the mechanism for modification of anatase-rutile transformation is related to oxygen vacancies on titania. This was also explained that the dispersion of alumina on titania stabilizes its surface and increases the apparent activation energy for the rutile

nucleation at titania-alumina interfaces. By using copper chloride as a dopant solution, a modified titania having nanocrystalline brookite stable at 400°C and having a narrow band gap than normal titania, could be produced through sol-gel route. [19] However, a detailed investigation using thermal analysis and XRD techniques on the role of alumina in increasing the anatase-rutile transformation indicate [481] that a metastable anatase solid solution containing alumina is formed at relatively low temperatures, and alumina is formed from exsolution process of the as formed anatase solid solution, in which rutile is formed at higher temperature. This argument is further supported by the fact that ∝-alumina is formed at as early as 900°C in presence of titania while the usual ∝-alumina formation is above 1100°C. The influence of addition of zirconia in the raising of transformation temperature of anatase to rutile is also reported. Since zirconia is not expected to involve in any oxygen vacancy change in Titania, the role of zirconia was identified to be due to incorporation of Zr ions into anatase lattice. The formation of a limited solid solution [482] of zirconia in anatase at low temperature increased the strain energy and thus leads to a higher anatase to rutile transformation temperature. An investigation on the effect of several cations of lanthanum, zinc, aluminum, potassium, sodium, calcium, barium and cobalt on the anatase-rutile transformation has been reported. [483] The dopants were introduced into the Titania gel in the form of nitrates, heat-treated in the range 350-1100°C and was characterized by wide angle X-ray diffraction (WAXS) and thermogravimetry. Depending on the ionic radius of the dopant compared with titanium, can be introduced

substitutionally or interstitially or if the size of dopant is larger than oxygen it could be intercalated into the matrix, producing a large lattice deformation. The conclusion of the study is while the dopants have no effect on the amorphous gel to anatase transformation temperature, the anatase-rutile transformation is influenced considerably. Anatase phase is stabilized to a higher temperature when the dopant ion size is less than that of titania. Similarly, dopants bigger than oxygen ion produce large local deformation of the lattice. Those dopant ions whose size is falling between titanium and oxygen will stabilize the anatase phase. Those dopants near to oxygen size can stabilize the titania phase more. Similarly there is a correlation between the anatase phase stabilization temperature and charge of the ion times the cation volume.

Lanthanum oxide was doped in Titania membrane precursors in order to study the thermal stability and it was seen that there was an increase of 150°C in the anatase to rutile transformation in the doped composition. [484] SnO_2, Al_2O_3, and Fe_2O_3 were doped in nanocrystalline Titania precursors and found that while SnO_2 and Fe_2O_3 decrease the transformation temperature, Al_2O_3 increased the same. However, the interesting fact is that these oxides were successful in controlling grain growth, which normally occurs in rutile as a result of the transformation. [152] As is known in the case of nanocrystalline materials, the grain growth can be regarded as coalescence of smaller neighbouring grains, where grain boundary motion is mainly involved, and the role of these dopant oxides would be to restrict the movement of these grain

boundaries thus lowering the grain growth. [485] The transformation kinetics in presence of Fe_2O_3 has been reported, [292] where Fe_2O_3-TiO_2 mixture was heated in air and in argon atmosphere to different temperatures and the phases formed were analyzed for using XRD techniques. As found in the earlier study, the Fe_2O_3 primarily decreases the anatase to rutile transformation temperature.

Platinum was incorporated in titania prepared through titanium butoxide and platinum acetyl acetonate. [486] Platinum promoted the formation of rutile probably through metal catalyzed dehydroxylation of anatase precursor or through the presence of PtO_2, which has the rutile structure, as an intermediate phase. Platinum atoms, however, did not go into crystalline structure of rutile. In another study, chromium (III) was incorporated in anatase titania catalyst in different concentrations and analysis of the cell parameters indicated that there is a stability limit for the system at ~1.4 atomic percentage. [487] Acceleration in the rate of anatase to rutile phase transition was also reported. Further, nanosize silver was incorporated in titania precursor gel and its effect of A>R transformation was investigated using impedance spectral measurements. The transformation was delayed in presence of silver. [381]

1.14 Definition of The Research Problem

Titanium dioxide is used in heterogeneous catalysis and as a photocatalyst for the decomposition of organics, in the treatment of industrial wastewater, for elimination of harmful bacteria and in the photocleavage of

water, in solar cells for the production of hydrogen and electric energy and in antifogging and self-cleaning coatings. Even though, lots of studies are reported on the synthesis and on various properties of titania, there exist many gaps in the understanding of the various parameters, which control the effectiveness of titania as photocatalysts. Further, methods of synthesis for nano crystalline titania and doped titania with general reference to effectiveness, to high temperature and on phase stability, reactivity and pore stability in bulk as well as in transparent nano coatings are still a very potential field of research. Sol-gel method is one of the most effective methods for synthesis of such active nano titania. The present study is an investigation into synthesis of nano size titania by sol-gel process involving an intermediate such as acetic acid, during hydrolysis-condensation reaction of titanium alkoxide. The role of acetic acid in modifying the hydrolysis-condensation reactions of titanium tetraisopropoxide in presence of dopants such as lanthana and/or ceria, which has been chosen based on the Hard and Soft Acids and Bases (HSAB) principle. Further, the HSAB principle helps in utilizing the heterodentating effect of acetate moiety to the fullest. Due to the specific reaction mechanism, the process is found to be repeatable, which is a concern in the sol-gel process.

Therefore, in the present work an attempt is made to

1. Study the synthesis of nanocrystalline titania and lanthanum and or cerium oxide doped titania through a modified polymeric sol-gel route.
2. Study the effect of acetic acid (stabilizing agent) and lanthanum and/or cerium (III) nitrate (dopant precursors) on the texturing of

nanocrystalline doped-titania and to correlate its chemical sequences with the structural and textural (surface area, porosity and pore volume) properties.

3. Modify the textural features by a co-doping-chemical leaching process, where silica was employed as the co-dopant.
4. Study the chemical interaction between titania and lanthana and/or ceria based on the HSAB principle.
5. Investigate the A>R transformation as well as photocatalytic efficiency in detail.
6. Fabrication and detailed morphological investigation of transparent, photoactive, self-cleaning, nanocrystalline titania coatings on glass surfaces.

Chapter II

Experimental and Characterization Techniques

2.1 Chemicals Used

1. Titanium tetraisopropoxide (Fluka, Switzerland, 99.99%)
2. Tetraethylorthosilicate (Fluka, Switzerland, 99.99%)
3. Alumina (A16SG, ACC-Alcoa, Kolkata, 99.9%)
4. Lanthanum Nitrate (IRE, India, 99.99%)
5. Cerium Nitrate (IRE, India, 99.99%)
6. Acetic Acid (S D Fine Chemicals, India)
7. Propan-2-ol AR (S D Fine Chemicals, India)
8. Sodium hydroxide LR (Qualigens India Ltd.)
9. Nitric Acid 69% GR (Merck, India)
10. Polyethylene glycol 300 LR (S D Fine Chemicals, India)
11. Glycerol AR (S D Fine Chemicals, India)
12. Methylene Blue (Qualigens India Ltd.)

2.2 Experimental Methods

2.2.1 Synthesis of Nanocrystalline Titania

In the present study nanocrystalline titania is prepared by a modified sol-gel technique. Acetic acid is used as stabilizing agent against hydrolysis. Acetic acid modifies the co-ordination sphere of titania and makes it more stable against hydrolysis. Further, dopants were added to the partially hydrolyzed titanium tetraisopropoxide solution as their respective nitrates.

2.2.1.1 Synthesis of Undoped TiO_2 Sol

Titanium tetraisopropoxide (TTIP) was used as received. Ti^{4+} moiety owing to its extremely high reactivity with water [193] requires a pre-stabilization against hydrolysis. Therefore glacial acetic acid was used as a stabilizing / catalyzing agent. Titanium isopropoxide stabilized with acetic acid usually follows a condensation pattern producing linear chains and enclosing small pores that result in high surface area. This is because the acid-catalyzed condensation is directed preferentially toward the ends rather than the middles of chains. [233-236] Synthesis started with the addition of titanium tetraisopropoxide (3.56g) to glacial acetic acid (7.16 ml). Glacial acetic acid modifies the coordination sphere of titanium [233-236] to a more stable state. Dropwise addition of 78.85 ml deionized water accomplished the hydrolysis under vigorous stirring conditions. The solution is then stirred for homogenization for a period of 3 h. After trial and error methods, the titanium tetraisopropoxide/acetic acid/water mole ratio was fixed as 1:10:350.

2.2.1.2 *Synthesis of La_2O_3-doped TiO_2 Sol*

Lanthanum nitrate hexahydrate [$La(No_3)_3.6H_2O$, 99.99%] was used as such. In a typical experiment for the preparation of 1% La_2O_3-doped TiO_2, stoichiometric quantity of lanthanum nitrate solution (0.53 ml) was added dropwise to the TiO_2 solution prepared as discussed in section 2.2.1.1 after 1h stirring. Stirring continued for 2 more hours to ensure the homogeneity of the mixture. Separately, 0.1, 0.5, 2.0, 5.0 and 10 wt. % LaO_3 doped TiO_2 compositions were also prepared by the same procedure (Figure 5).

2.2.1.3 *Synthesis of CeO_2-doped TiO_2 Sol*

Cerium nitrate hexahydrate [$Ce(NO_3)_3.6H_2O$] was purified by filtration and made up to 5% aqueous solution. The solid content was accurately measured by gravimetric method. For preparing 1% CeO_2-doped TiO_2, stoichiometric quantity of cerium nitrate solution (0.53 ml) was added dropwise to the partially hydrolysed titanium tetraisopropoxide solution prepared as discussed in section 2.2.1.1 after 1h stirring. Stirring continued for 2 more hours to ensure the homogeneity of the mixture. Separately, 0.1, 0.5, 2.0 and 5.0 wt. % of CeO_2 were also prepared by the same procedure (Figure 5).

2.2.1.4 *Synthesis of SiO_2 Sol*

Tetraethylorthosilicate was used as received. In case of silica, the lower reactivity of Si^{4+} moiety little demands the presence of stabilizing agent compared to Ti^{4+} moiety. [193] However, anhydrous isopropanol was used as a solvent to make the polar water and non-polar alkoxide compatible in the

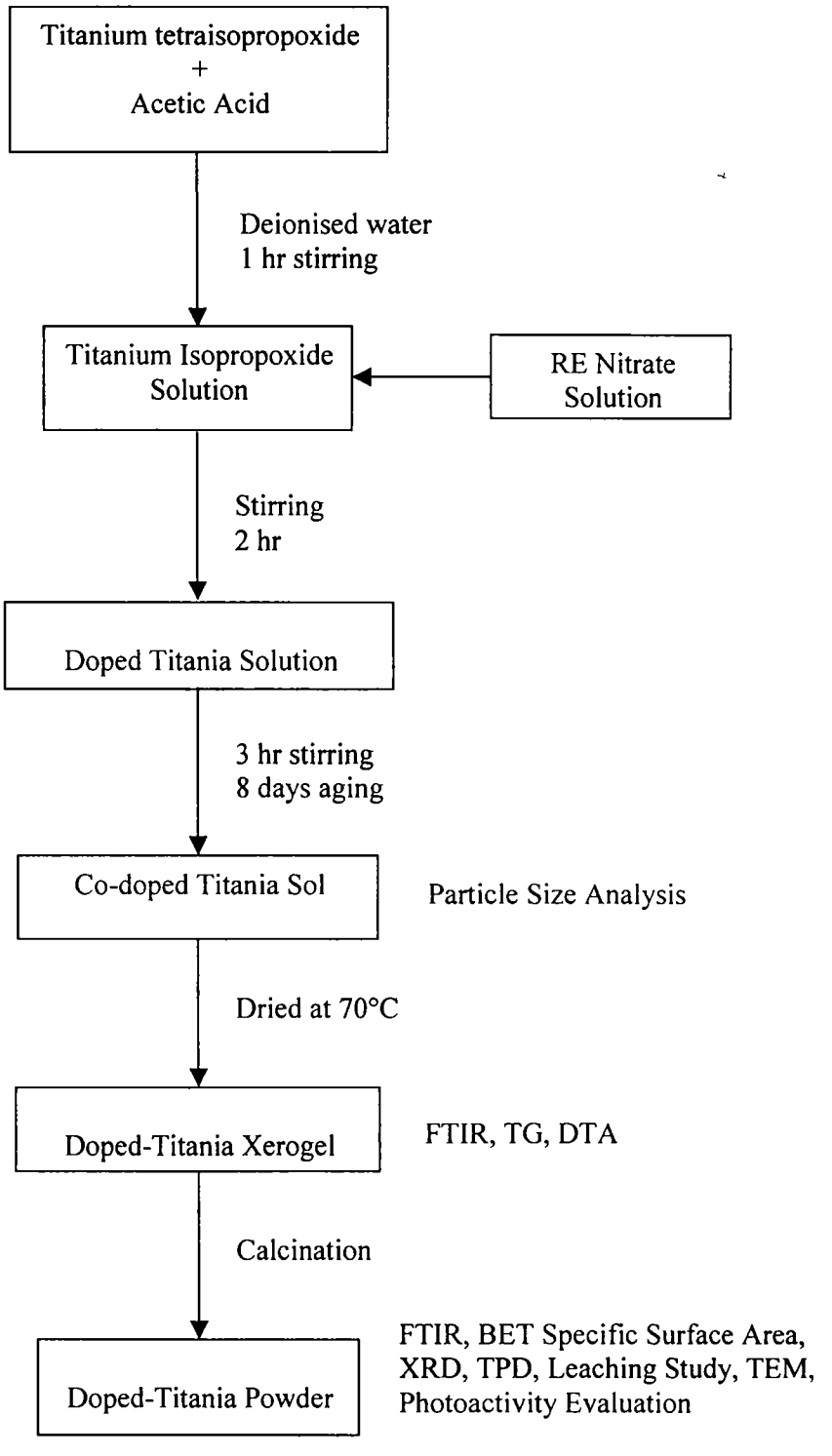

Figure 5: Flow chart for the preparation of doped TiO_2 powder

system. [194] Isopropanol was distilled to remove the water content adsorbed to it. Alkoxide-isopropanol-water ratio was fixed as 1:4:16 in all the synthesis procedures of silica in the present work. In a typical experiment, tetraethylorthosilicate (3.45g) dissolved in anhydrous isopropanol (5.08 ml) was hydrolysed by the dropwise addition of 0.001N-deionized water (4.77 ml). Stirring for a period of 3 h ensured homogeneity of the sol.

2.2.1.5 Synthesis of SiO_2-La_2O_3/CeO_2 Co-doped TiO_2 Sol

Dropwise addition of the stoichiometric quantity of silica sol, prepared as per section 2.2.1.5, to the La_2O_3 doped TiO_2 sol (Section 2.2.1.2) accomplished the formulation of co-doped composition. A ratio of 94:1:5 percentage TiO_2:La_2O_3/CeO_2:SiO_2 (wt %) was selected as the catalyst composition. The homogeneous distribution of the SiO_2 phase in the La_2O_3 doped TiO_2 sol was ensured by appropriate stirring. Repeated particle size measurements at various intervals of stirring were carried out to see the distribution of sol particles.

2.2.1.6 Synthesis of Al_2O_3 Sol / Suspension

The finer fraction of alumina was separated after suspending it in deionized water. pH of the suspension was adjusted to be 3.5 till a stable colloid is obtained. The average particle size of the sol was measured to be 275

2.2.1.7 Synthesis of Al_2O_3-La_2O_3 Co-doped TiO_2 Sol

The mixed sol was prepared by adding calculated volume of the Al_2O_3 suspension (corresponding to 10 wt % of the total mixed oxide concentration) to the 1% La_2O_3-doped TiO_2 sol, synthesised as per section 2.2.1.2, after 1 h

stirring and the mixture was stirred further for a period of 5 hrs. The coating precursor sols were prepared by the addition of 0.5 % PVA and 0.1% glycerol to the above sol. This was labelled as TLA10.

Aging for a period of 8 days followed by concentrating over a steam bath and subsequent drying at 70°C in an air oven produced the doped titania xerogel. Annealing of the xerogels at different temperatures ranging from 100-1100°C, and soaking for a period of 3 hours have been carried out in an ambient pressure and normal oxygen atmosphere. Heat treatment was done in a stepwise manner, i.e., RT to 200°C (2°C/min), 200 to 500°C (3°C/min) and 500 to higher temperature (5°C/min). The xerogels were characterized by various methods. The detailed description is provided in the following section.

2.2.2 Leaching Process

5% aqueous NaOH solution was used for leaching. 2 g 5% SiO_2-1% La_2O_3-doped TiO_2 powder calcined at 700°C was dropped into 30 ml NaOH solution. It is then heated to about 70°C. Stirring the mixture for 1h in this stature accomplished the leaching. The sodium silicate formed as slag was removed by decanting and the slurry was subsequently washed several times (20 times) to remove the sodium impurity. The complete removal of NaOH was primarily confirmed by pH measurement (washed till the pH becomes ≤ 7). The leached samples were dried in an air oven at 70° C and subsequently heat treated at 300° C to remove any residual precipitates formed due to the action of NaOH.

A list of total samples prepared for the study is provided in Table 4. Apart from these samples, the ones incorporated with silica are used for leaching.

Table 4: List of samples prepared for the study

TiO_2	La_2O_3	CeO_2	SiO_2
100	--	--	--
99	1	--	--
99	--	1	--
99	--	--	1
95	--	--	5
94	1	--	5
94	--	1	5

All the compositions are in weight percentage
All the silica-incorporated samples were undertaken leaching

2.2.3 Fabrication of Nano Titania Coatings by Dip Coating

The film fabrication was carried out on pre-treated glass slides obtained from micro slides corp. Dip coating was employed for the fabrication of films from precursor sols such as titania, doped titania and co-doped titania samples. The precursor sols were again modified with the addition of 0.5% PEG and/or 0.5% glycerol to study their effect on the film formation and also to compare with the optimized compositions employed in this work. The coated glass slides were subsequently dried at room temperature for 1 h followed by heating in an electric air oven at 70°C for another 1 h. The samples were annealed to

400° C at a heating rate of 1°C/min. and soaked further for 3 h. The detailed film fabrication procedure is provided below.

Pre-treatment of Glass Slides: The micro slides (size: 75 mm long x 25 mm wide x 1.35 mm thick) were obtained from Polar Industrial Corporation, Mumbai. The pre-treatment of the slides was necessary to remove the Na impurity and to make the glass perfectly wetting. The glass slides were first boiled in Conc. H_2SO_4 for 1 h followed by thorough washing with distilled water to remove the acid completely. H_2SO_4 will selectively extract the free-Na ions embedded in the glass slides (sheet glass) and convert it into soluble sodium sulphate. The glass slides were then ultrasonicated in a 80:1 water-isopropanol mixture for 10 minutes and subsequently dried in an oven at 100°C followed by heat treatment at 400°C to remove the organic impurities on the surface if any. The glass slides were kept in the oven at 100°C till the time of coating. The coatings were carried out using dip coating as well as spin coating technique.

Dip Coating Technique: KSV Dip coater [KSV Dip coater D, Model 1000IUD, KSV Instruments Ltd., Finland] as well as the one fabricated locally was used for dip coating. Dip coating was carried out using the pre-treated glass slides kept at 100°C by a dipping-withdrawing process. Coating was done with different withdrawal speeds such as 0.6, 1.8, 3.0, 4.2 and 6.6 cm/min with a view to study its effect on the film thickness of coatings. The dip coating using the locally fabricated equipment was carried out by keeping the glass

slides in the glass vessel containing the sol and allowing the sol to drain out in a slow controlled manner through the bore drilled at the bottom of the vessel. The speed of coating (withdrawal speed) was measured manually using a scale and stopwatch. The schematic diagram of the coating equipment is provided in Figure 6.

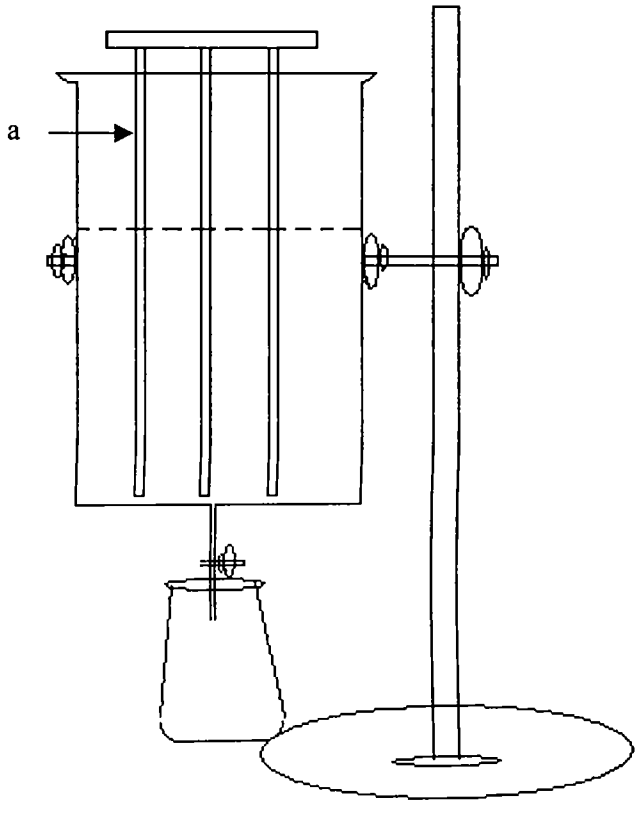

a – Glass slide

Figure 6: Schematic representation of the dip-coating unit fabricated.

The coating formulations used in the present study are given in Table 5. All the compositions are in wt % only (if not stated otherwise).

Table 5: List of coating formulations used in the present research

TiO_2	La_2O_3	CeO_2	SiO_2	GLY*	PEG**
99	1	--	--	--	--
99	1	--	--	0.5	--
99	1	--	--	--	0.5
99	--	1	--	--	--
99	--	1	--	0.5	--
99	--	1	--	--	0.5
94	1	--	5	--	--
94	1	--	5	--	0.5
94	1	--	5	--	1

* GLY – Glycerol; **PEG – Poly (ethylene glycol)

The coating formulations were restricted to the above compositions for clarity of discussion and interpretation, even though more compositions have been attempted on a trial and error basis.

2.2.4 Fabrication of Nano Titania Coatings by Spin Coating

A drop-spin coating technique was employed for the film fabrication. Pretreated glass discs were mounted on the rotating disk and the precursor sols were dropped into it at a rotation speed of 2000 RPM. The speed was increased to 4000 RPM and kept for 1 minute for evaporation of the solvent. The coated discs were dried in an air oven at 70°C for 1h and subsequently annealed to 400°C at a heating rate of 1°C/min. and soaked further for 3h. The 1°C heating

rate was selected after trial and error method since this rate and soaking at 400°C for 3 h gave almost similar film characteristics with the ones obtained for bulk powders heat treated at 700-800°C with a heating rate of RT to 200°C (2°C/min), 200 to 500°C (3°C/min) and 500 to 800°C (5°C/min).

Leaching of coated glass slides was performed by the immersion of coated glass substrates in 5% NaOH aqueous solution for a period of 1 h at 70°C. The glass slides were taken out and washed several times with deionized water to remove the sodium impurity. 1, 2, 5 and 10% NaOH solutions were used for leaching study and the 5% NaOH solution was selected for the detailed analysis.

2.2.5 Photoactivity Evaluation

Methylene blue (MB) degradation experiments were done in presence of UV light (360 nm) in a Rayonet Photoreactor (The Netherlands). The photoreactor is made up of 24 UV lambs of 360 nm wavelength arranged in concentric circular fashion. The solution/mixture can be stirred using the magnetic stirrers provided in the platform and also the base can be rotated to make sure that the solution is exposed to maximum light throughout the irradiation. A mixture of aqueous solutions of 15 ml MB (0.16 mg/100ml) and 10 ml TiO_2 (0.32 mg/100 ml) were kept in the photoreactor for UV irradiation. The mixture was exposed to UV light for a period of 5 hrs. UV-Vis spectra were recorded at regular time intervals of irradiation such as after 5 min, 15

min, 30 min, 1 h, 2h, 3h and 5 h. Similarly, photodegradation was done under sunlight as well.

The photoactivity of coated samples was also evaluated by similar experiments. Photoactivity evaluation of the coatings was done by UV light exposure of the Titania coated glass slides immersed in the methylene blue solution (2μl). The degradation profiles were drawn by plotting the maximum absorbance of the main intensity peak (664 nm) of methylene blue at regular intervals of UV exposure. In fact all the samples are calcined at 400°C at a heating rate of 1°C/min and soaked for a period of 3 h.

The flow chart for the preparation of the co-doped TiO_2 powder is provided in Figure 7 and those for the co-doped TiO_2 coatings are provided as Figures 8 and 9. The total samples prepared for the present study are labelled as provided in Table 6 and these codes are used for further discussions.

Table 6: Total samples prepared for the study and their abbreviations

Sample	Abbreviation
TiO_2-1% La_2O_3	TL-1
TiO_2- 1% La_2O_3-1% PEG	TL-PEG1
TiO_2- 1% La_2O_3-0.5% PEG	TL-PEG0.5
TiO_2-1% La_2O_3-1% GLY	TL-GLY1
TiO_2-1% CeO_2	TC-1
TiO_2-1% CeO_2-1% PEG	TC-PEG1
TiO_2-1% CeO_2-1% GLY	TC-GLY1
TiO_2-1% SiO_2	TS-1
TiO_2-5% SiO_2	TS-5
Chemically leached- TiO_2-5% SiO_2	TSN
TiO_2-1% La_2O_3-5% SiO_2	TLS
TiO_2-1% CeO_2-5% SiO_2	TCS
TiO_2-1% La_2O_3-5% SiO_2-1%PEG	TLS- PEG1
TiO_2-1% La_2O_3-5% SiO_2-1%PEG	TLS- PEG0.5
Chemically leached- TiO_2-1% La_2O_3-5% SiO_2	TLSN

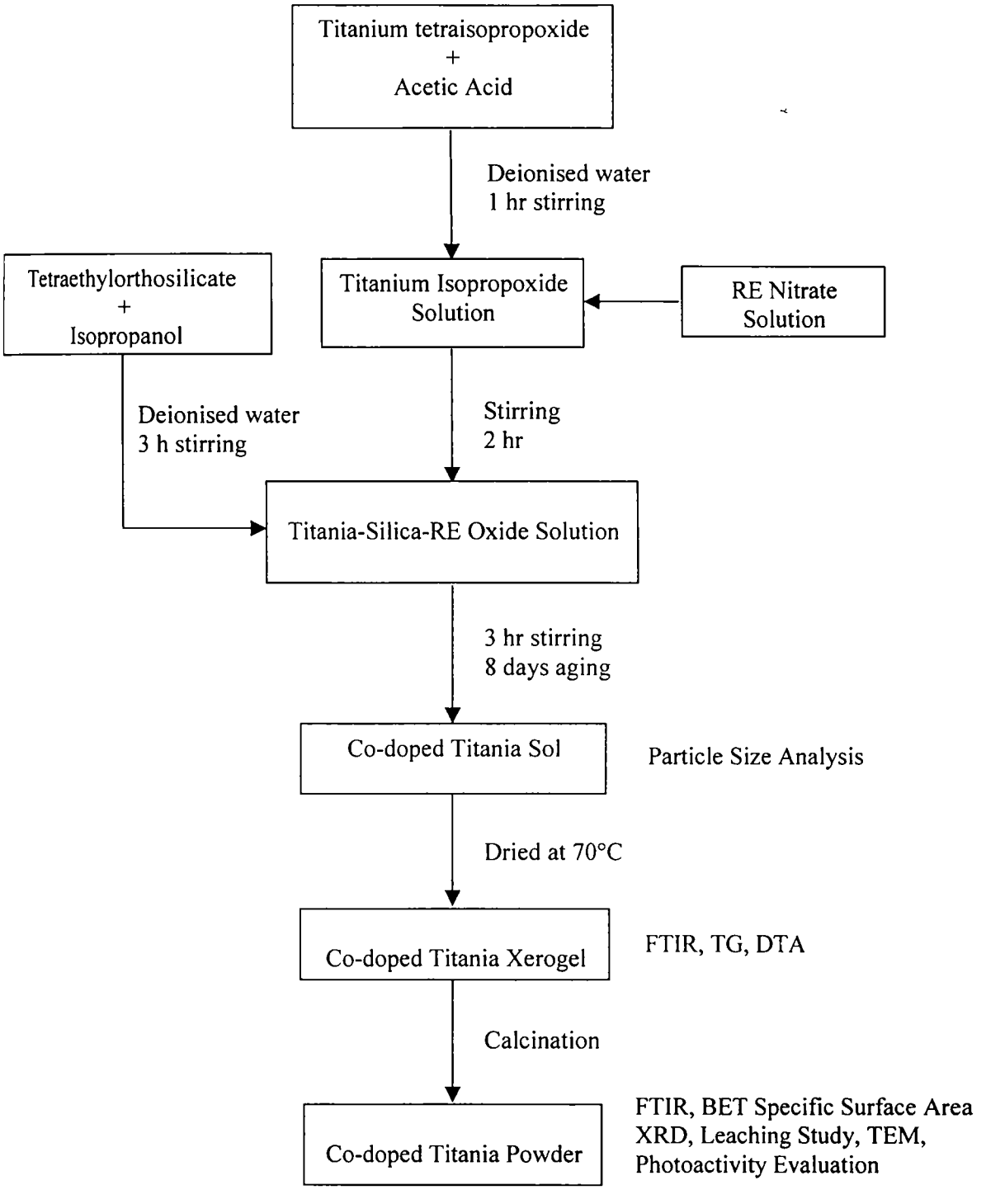

Figure 7: Flow chart for the preparation of co-doped TiO_2 powder

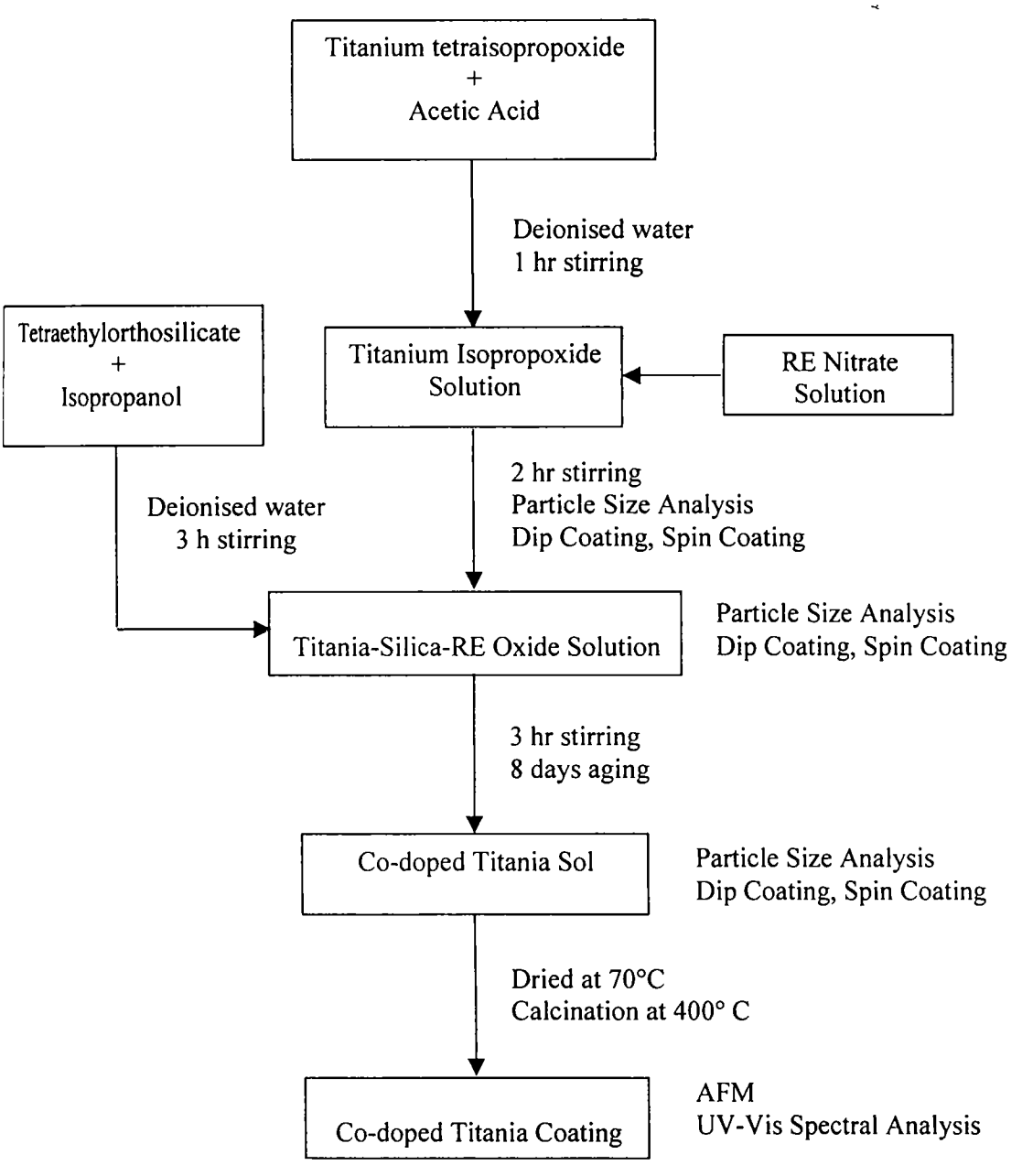

Figure 8: Flow chart for the preparation of co-doped TiO_2 coating

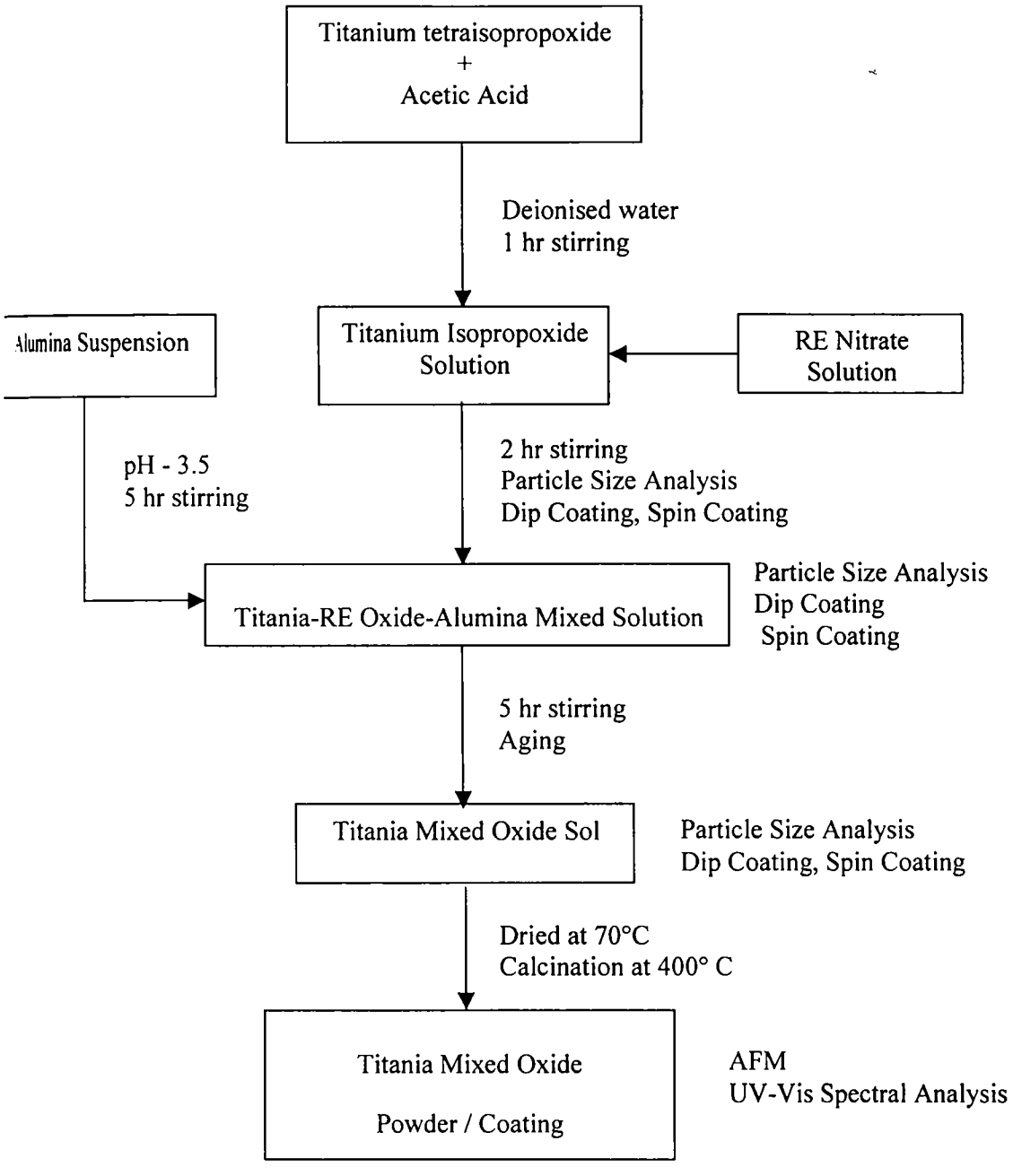

Figure 9: Flow chart for the preparation of Al_2O_3-La_2O_3 co-doped TiO_2 powder and coating

2.3 Characterization Techniques

2.3.1 Particle Size Analysis

The technique of dynamic light scattering (DLS) is ideally suited for the determination of the size of particles in the nanometre size range. The Malvern Zetasizer, Malvern Instruments Ltd, Malvern UK uses patented optics that provides exceptional levels of sensitivity and allows the determination of the size of samples that contain very small particles and/or particles that are present at very low concentrations. In addition, the backscatter optics allows for the measurement of samples at much higher concentrations than is possible using conventional DLS instruments using a 90° detection angle. Since the samples are stable sols, no deflocculant is added to the sample in the present case. Instead the measurement is done as such.

2.3.2 Fourier Transform Infrared Spectroscopy (FTIR)

The Fourier transform infrared spectra of gels and calcined samples were recorded in Nicolet Magna-560-IR Spectrometer (USA) to study the dehydroxylation and bonding characteristics of the gels and calcined powders. The disc samples were prepared using KBr.

2.3.3 Thermogravimetry (TG)

Thermogravimetry is a technique whereby a sample is continuously weighed as it is heated at a constant, preferably linear rate. The decomposition

features of the gel samples were characterized using the Shimadzu-TGA 50H in nitrogen atmosphere at a rate of 10°C/min upto 1000°C.

2.3.4 Differential Thermal Analysis (DTA)

In differential thermal analysis, the sample temperature is continuously compared with a reference material temperature, the difference in temperature being recorded as a function of furnace temperature as the sample is heated or cooled at a uniform rate. The gel samples were characterized using the Shimadzu-50H DTA in nitrogen atmosphere at a heating rate of 10°C/min.

2.3.5 X-ray Diffraction (XRD)

The X-ray powder diffraction patterns of the calcined samples were recorded in Philips Diffractometer (PW1710), The Netherlands, using Ni filtered Cu Kα radiation. The samples for XRD were prepared by smearing the powder on a clean glass plate coated with silicon grease and the smeared powder on the glass plated was pressed using another glass plate to get a plane surface. Most of the samples prepared for this study are scanned between 20 to 60° 2θ values with a step speed of 2.4°/min.

The percentage of rutile (X) in the samples was estimated from the respective integrated peak intensities using the equation.

$$X = (1+ 0.8\ I_A / I_R)^{-1}$$

Where I_A and I_R are the X-ray intensities of the anatase and (101) and rutile (110) peaks respectively. Crystallite sizes were calculated from the peak widths using the Scherrer equation. [488]

$$\Phi = k\lambda / (\beta\cos\theta)$$

Where Φ is the crystallite size, k the shape factor (a value of 0.9 was used in this study) λ- the X-ray radiation wavelength (1.540 A° for CuKα) and β is the full line width at half-maximum height of the main intensity peak after subtraction of the equipment broadening.

2.3.6 Nitrogen Sorption Studies (BET Specific Surface Area Analysis)

The phenomenon of higher concentration of any molecular species at the surface than in the bulk of a solid (or a liquid) is known as adsorption. The solid that takes up a gas or vapour or a solute from a solution is called the adsorbent while the gas or the solute, which is held to the surface of the solid is called the adsorbate. The variation of adsorption with pressure at a given constant temperature is generally expressed graphically and is known as adsorption isotherm.

Adsorption isotherms

The relationship between the magnitude of adsorption and pressure can be expressed mathematically by an empirical equation known as Freundlich adsorption isotherm, $a = Kp^n$, where 'a' is the amount of the gas adsorbed per gram of the adsorbent at pressure 'p', 'K' and 'n' are constants depending upon the nature of the gas and the adsorbent. It is possible to divide the adsorption isotherms into major five different types (Figure 10).

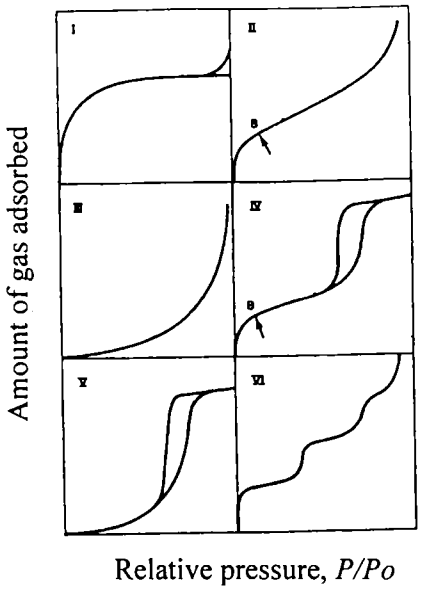

Figure 10: Types of adsorption isotherms, Brunauer, Deming, Deming, and Teller classification together with stepped isotherm

(1) Type I corresponds to unimolecular adsorption. The volume of the gas adsorbed approaches a limiting value; just enough to complete a unimolecular layer even when the gas pressure is very high. Microporous solids also show similar behaviour.

(2) Type II and Type III isotherms, the amount of adsorption keeps on rising in each case with increase in pressure. This is attributed to the formation of additional layers of physically adsorbed gas molecules.

(3) Type IV and Type V have been observed in cases where there is a possibility of condensation of gases in the minute capillary pores of the adsorbent at pressures even below the saturation pressure, 'Po' of the gas. There is not only the formation of multimolecular adsorbed layers of gas molecules but also condensation of some of the gas molecules within the

narrow capillary pores of the adsorbent known as capillary condensation of the gas.

(4) Type III and Type V are special isotherms showing by gases having less interaction with solids. Type VI is a stepped isotherm not included in the classical classification

Nitrogen sorption studies of the samples were carried out using Micromeritics BET surface area analyzer (Gemini Model, 2360). The calcined samples were preheated in a flow of nitrogen for about 3 hours at around 200°C to remove all the volatiles and chemically adsorbed water from the surface. Adsorption studies were carried out at liquid nitrogen temperature.

Determination of Specific Surface Area

The specific surface area is usually determined using the BET equation. The Langmuir theory of adsorption is restricted to the formation of a monomolecular layer of gas molecules, on the solid surface and disregards the possibility for multilayer adsorption. But in the BET theory it is assumed that multilayer adsorption can take place since the solid surface possesses uniform localized sites.

The BET equation is $$\frac{P/Po}{V(1-P/Po)} = \frac{1}{V_mC} + \frac{C-1}{V_mC}(P/Po)$$

Where, V = volume of the gas adsorbed at the pressure 'P'

V_m = volume adsorbed when the surface of the solid is completely covered with a monolayer of adsorbed gas molecules.

C = a constant depending upon the nature of the gas.

Since 'C' and 'V_m' are constant for a given gas solid system, a plot of P/V(Po – P) against (P/Po) should give a straight line. So V_m can be calculated.

The total surface area of the sample can be calculated using the equation. Surface area, S = V_mNA/M, Where, N = Avogadro number, A = cross sectional area of a single molecule of the adsorbate, M = Molecular weight of the adsorbate.

Determination of Total Pore Volume

The liquid equivalent of the designated volume adsorbed is the total pore volume (cc/g), V_{tot} = (Va) x (D), Where Va = volume adsorbed at P/Po 0.99,

D = density conversion factor.

Average Pore Size

Assuming the pores are of cylindrical shape and open at both ends, the average pore size of a given sample is calculated using the equation,

Average pore size = $4Vp/S_{BET}$

Vp = pore volume, S_{BET} = BET multipoint surface area.

Pore Size Distribution Curves

Pore size distribution curves are determined from adsorption/desorption isotherms making use of Kelvin equation, which relates the equilibrium vapour pressure of a curved surface, such as that of a liquid in a capillary or pore, to the equilibrium pressure of the same liquid on a plane surface.

$\ln\frac{P}{P_0} = -\frac{2\gamma\overline{V}}{rRT}\cos\theta$, where 'P' is the equilibrium vapour pressure of the liquid contained in a narrow pressure of radius 'r' and 'P_0' is the equilibrium pressure of the same liquid in a plane surface. The terms 'γ' and '$\overline{V}$' are the surface tension and molar volume of the liquid respectively, and 'θ' is the contact angle of the liquid. When nitrogen is used as the adsorbate at its boiling point of 77 K, the Kelvin equation can be written as,

$$r_k = \frac{4.15}{\log(P\%/P)} \text{ (Å)}$$

'r_k' is the radius obtained from Kelvin equation, which differs from actual pore size since condensation occurs to a core of pore that was already covered by an adsorbed layer. The thickness of the adsorbed layer can be obtained by comparing the absorption layer with a nonporous one. However, 't', the statistical thickness, can also be determined by Halsey equation, which for nitrogen can be written as,

$$t = 3.54\left\{\frac{5}{2.303\log(P_0/P)}\right\}^{1/3}$$

A procedure involving only the wall area and based on the cylindrical pore model put forward by Pierce and modified by Orr and Dall Valle was used for the determination of pore size determination. [489] The additional area of multilayer exposed during each step of desorption is calculated from the volume and radius from a cylindrical model. For the speedy calculation a

computer programme was written using Visual Basic and used for all the analysis of the isotherms.

2.3.7 Temperature Programmed Desorption of Ammonia (TPD)

Ammonia TPD is a method for identifying the strength of acidic sites of the sample. [490] A known weight of NH_3 is adsorbed at room temperature on the sample taken in the reactor. The NH_3 desorbed at different temperatures is determined by titrimetry. About 0.5 g of the sample was loaded into a microcatalytic reactor and degassed in a stream of nitrogen at a temperature of 300°C for 30 minutes. The reactor was then cooled to room temperature and 20 ml NH_3 was injected through the sample. The gases emerging from the reactor outlet was scrubbed into known quantity of standard sulphuric acid for 15 minutes and the eluted ammonia was estimated volumetrically using the equation:

Amount of ammonia desorbed = $(N_{NaOH} \times \Delta V) \times 17/(w \times 1000)$ (mmol/g)

Where, w = weight of the catalyst in mg/g

The experiment was repeated similarly at different temperatures 100,200,300,400,500,600 and 700°C. The desorption of ammonia at relatively lower temperatures 100 - 250°C was considered as occurring from weak Brönsted acid sites, while that occurring at high temperatures 250-650°C was considered as occurring from Lewis acid sites. The schematic representation of the locally fabricated TPD set up was provided in Figure 11.

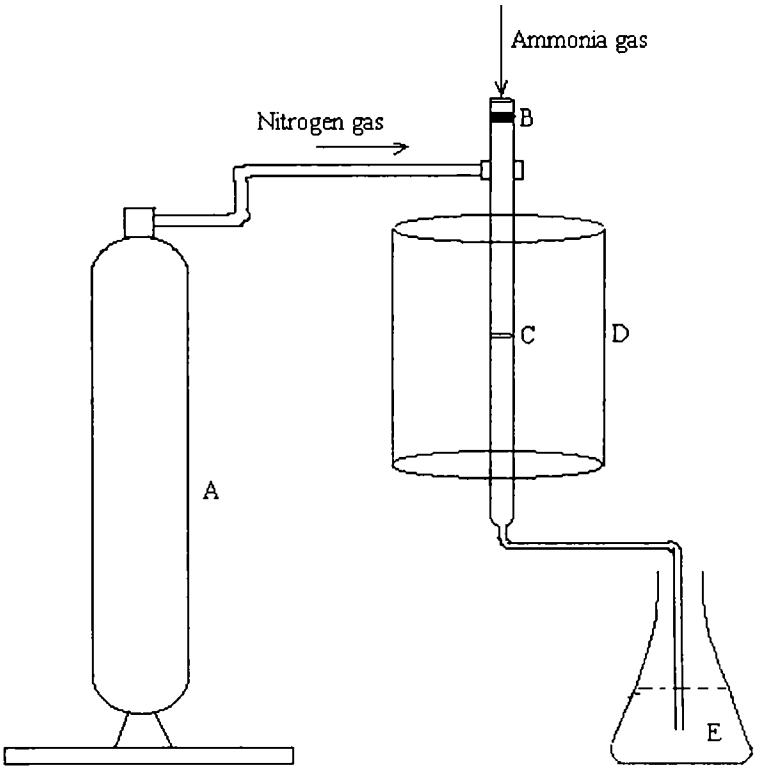

A = Cylinder

C = Sample as pellet

D = Furnace

E = Standard sulfuric acid

Figure 11: Schematic representation of TPD set up

2.3.8 Transmission Electron Microscopy (TEM)

TEM has become the primary tool for the observation of crystal defects, second phase precipitates, elucidation of the crucial role of intrinsic and extrinsic dislocations, grain boundaries, interfaces, line and planar defects. Surface morphology on a nanometer scale is obtained from TEM.

When high-energy electron beam passes through the thin specimen, the transmitted beam is ejected on the fluorescent screen. This transmitted beam gives structural information of the specimen. [490] The TEM gives very high resolution (in the order of 1A°) and very high magnification (~1 million times). However, this is obtainable for thin specimens only (~100A°). The bulk specimen need necessary thinning by various techniques like ion milling, electropolishing etc. depending on the nature of the material. The powder specimen is suspended in water or any other medium generally in the ratio 1:100 or 1:1000. Ultrasonic stirring is necessary for agglomerated samples. A drop of the suspension is placed on the grid supported by carbon or plastic films. The suspensions form a hemispherical drop on the grid. With time the liquid is evaporated and the powder is adhered to the supporting film. The grid is dried and ready for observation under TEM.

TEM of selected samples in the present work were taken in JEOL 3000EX with acceleration voltage 300kV and a resolution of less than 0.2nm. Diffraction patterns have a camera length of 80 cm. The powder was dissolved in ethanol, and homogenized in ultrasonic bath for 5 min. Then the 3mm carbon-coated Cu-grid for TEM-observation was dipped into this dispersion, so that the powder particles were stacked on the grid. Since they are so small, they are translucent for the electron beam. The upper limit for this critical thickness would be about 250 nm. Dr. Wilfried Wunderlich of Nagoya Institute of Technology, Nagoya, Japan did the TEM analysis for the present work.

2.3.9 UV-Vis Absorption/Transmission Spectroscopy

The photodegradation capacity of titania samples were measured by taking absorption spectra of the UV exposed titania-methylene blue mixture solutions. The solution was centrifuged and the solution is taken for the measurement to avoid scattering of light due to titania particles. In case of coated films, transmission spectra were recorded in the transmission mode. The UV-Vis absorption/transmission spectra of the titania-methylene blue mixture solutions were recorded using Shimadzu UV 2401 PC UV-Vis spectrophotometer.

2.3.10 Atomic Force Microscopy (AFM)

The surface morphology of the spin coated glass surface was determined by AFM imaging. A Multimode head with a Nanoscope IV controller from Digital Instruments (Santa Barbara) was used in contact mode for all imaging, Repeat scans were used to confirm that the scanning was not affecting the surface. For non-symmetrical features, two sets of orthogonal scans were used to confirm that the observed features are real and not due to the scanning direction of the tip. Prof. Frank J. Berry and Dr. Sharon Moore of Open University, UK, did the AFM analysis for the present thesis work.

Chapter III

Nanocrystalline Catalytic Titania Powders

Abstract

High surface area, nanocrystalline titania prepared through a modified sol-gel route has been further investigated and the results are presented. The sols were characterized for their particle size using Malvern Particle Size Analyzer. Resultant gel precursors were characterized by thermal analysis and IR spectroscopy. The precursor gels were further annealed at various temperatures and then were subjected to measurement of BET Specific Surface Area, Powder X-ray Diffraction, Transmission Electron Microscopy, UV-Vis Spectrophotometric Analysis, Temperature Programmed Desorption (TPD) technique and Photoactivity. Correlation between the properties of the nano oxide and the preparative route as well as experimental parameters has been attempted. The FTIR spectra indicated the formation of Ti-O-RE (RE = La and Ce) bonds. The structural modifications taken place as a result of doping in the gel structure was reflected as a four step weight loss pattern in the thermogram, wherein the undoped TiO_2 appeared to be undergoing a three step weight loss pattern. DTA also corroborates with the corresponding changes. Considerable increase in specific surface area was shown by lanthana-doped TiO_2 samples at

all temperature ranges. CeO_2 doped samples have also shown an increase in surface area but less compared to La_2O_3-doped TiO_2 samples. Powder X-ray diffraction and TEM analyses point toward the formation of nanocrystalline TiO_2. The effect of annealing on the crystallite growth and phase transformation was assessed using XRD. A decrease in crystallite size and corresponding enhancement in phase transformation temperature was established with the increasing concentrations of the dopants (both La_2O_3 and CeO_2). However, La_2O_3 was found to be more effective than CeO_2. The anatase to rutile transformation temperature increased to ~940°C in presence of 1% La_2O_3 from that of undoped TiO_2 at 670°C. The crystallite size of titania ranged between 5-70 nm and the 'critical size limit' was established to be between '39-47' nm in the present work. The photoactivity evaluation with respect to methylene blue degradation experiments established 1% La_2O_3-doped TiO_2 annealed at 700°C to be the better catalyst. The activity was found to be comparable to or even higher than that of commercial TiO_2 samples such as Degussa P-25 and Hombikat UV 100. The corresponding textural features were determined to be 52 m^2g^{-1} BET specific surface area and 0.0961 ccg^{-1} pore volume. The surface area of undoped TiO_2 was measured to be ~1 m^2g^{-1} at the same calcination temperature. Moreover, 1% La_2O_3-doped TiO_2 retained about 37% of the total pore volume at 300°C, even after calcination to 700°C. Similarly, doping with 1% CeO_2 produced a surface area of 42 m^2g^{-1} at 700°C. The influence of La_2O_3 on the enhancement of surface acidity was also established by temperature programmed desorption technique. Further, the

procedure was modified for the preparation of high surface area mesoporous doped titania. The controlled mesoporosity is achieved through a doping-leaching process; wherein silica is first added to the La_2O_3-doped TiO_2 sol precursor and allowed to form a homogeneous sol. Subsequent to gelation, drying and heat treatment, the amorphous silica phase was leached out preferentially using 5% NaOH solution. The resultant mesoporous texture, with fully crystalline matrix and pore walls has got an enormous potential in the application fields such as high surface area battery electrodes, sensors, optoelectronic devices, photoactive self-cleaning surfaces and as catalysts.

3.1 Results

3.1.1 Particle Size Analysis

Particle size distribution curves of undoped as well as lanthana and /or ceria doped titania sols are provided in Figure 12. The sol precursors are prepared through a polymeric sol-gel route and the particle size depends largely on the experimental conditions and presence of dopants. Figures 12A-12F show the typical particle size distribution curves, which indicate the presence of nanosize titania and doped titania particles. As is obvious, the final properties of the material depend on the solution chemistry and the consequent structural formation in sol-gel derived materials. The undoped titania sol showed a uniform distribution of particles with an average size ~25 nm. When

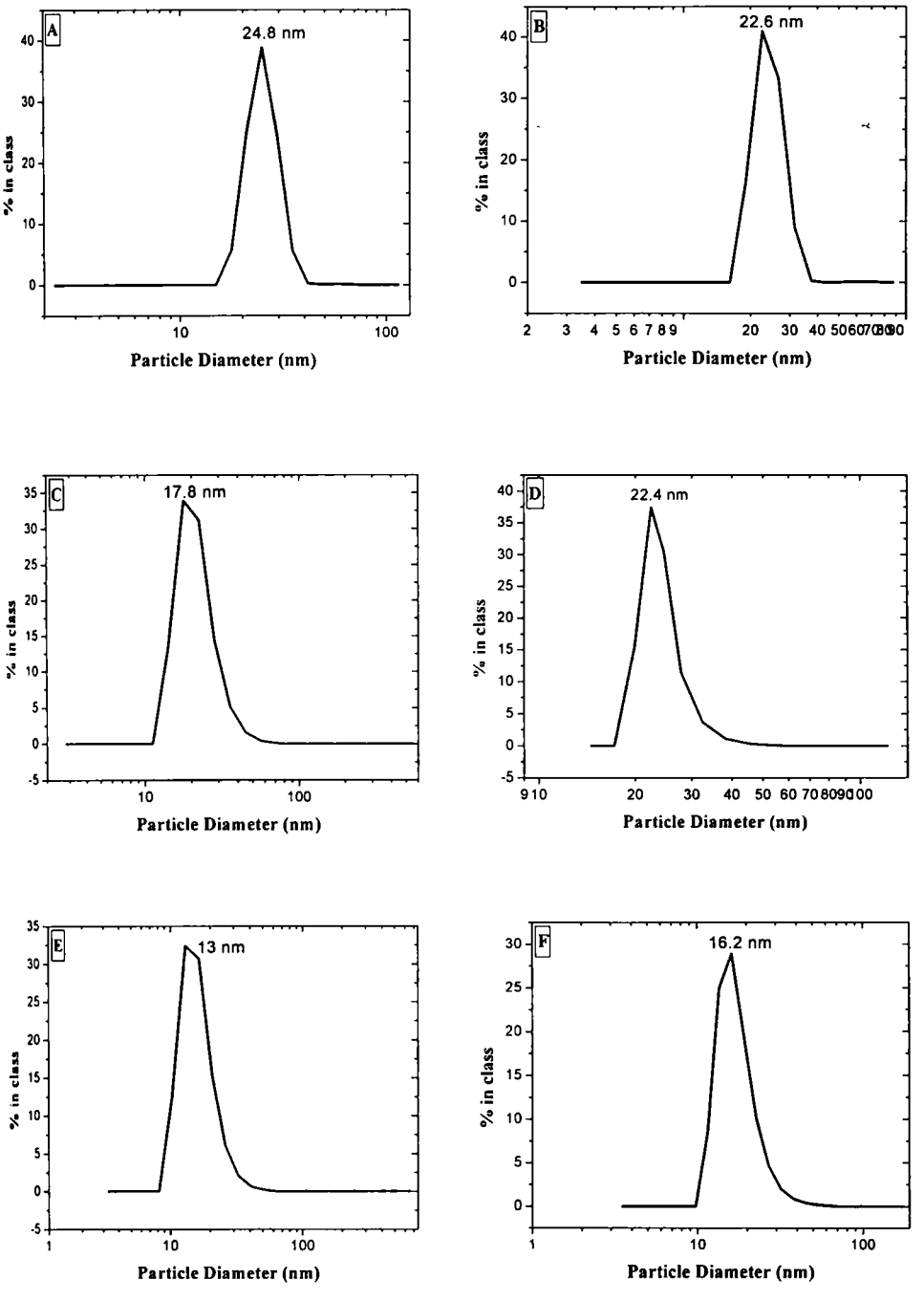

Figure 12: Particle size distribution of different titania sols. (A) TU; (B) TS-5; (C) TL-1; (D) TC-1; (E) TLS and (F) TCS

it is doped with lanthanum nitrate solution corresponding to 1% by wt. La_2O_3, the particle size got reduced to ~18 nm. In case of 1 % CeO_2-doped TiO_2 the average particle size reduces to ~22 nm. This reduction in particle sizes could be attributed to the possible capping taking place on addition of RE nitrate solutions, which will be discussed in detail later on in this chapter. The TLS and TCS sols on the other hand show particle sizes in the range ~14 and ~16 nm respectively after 8 days of aging.

3.1.2 FTIR Spectral Analysis

FTIR spectra of undoped, doped and co-doped sol-gel titania samples obtained through the acetic acid stabilized / catalyzed hydrolysis - polycondensation reactions of titanium tetraisopropoxide (TTIP) and heat treated at different temperatures were recorded and presented in this section. In the present route, acetic acid is used as a stabilizing agent for TTIP, which can either chelate to the same titanium atom or form bridges between two titanium atoms with its bidentate chelating functionalities. [491-493] Modification of the Ti^{4+} coordination sphere will be the result in both the cases, wherein the coordination sphere of titanium is increased from four to six and an effective stabilization of the isopropoxide moiety against hydrolysis is resulted. [192-193] In the present attempt, i.e., sol-gel process, TiO_2 sol was prepared by the addition of deionized water to the stabilized TTIP - acetic acid complex, and subsequent aging and drying produced the xerogel. FTIR should, therefore, establish the type of acetate ligand bonding such as chelating, bridging etc. and also the

presence of specific functional groups associated with the system. Hence, a systematic analyses of both undoped and doped titania xerogels with respect to different annealing temperatures were carried out with a view to demonstrate the effect of chelating / stabilizing agent on the crystallization of TiO_2, if any. Further, the role of acetic acid as well as the dopants on the chemical sequences of the system was also evaluated.

Figure 13 shows the FTIR spectra of undoped TiO_2 samples calcined at different temperatures. Bands corresponding to stretching and bending vibrations of hydroxyl groups as well as loosely bonded H_2O molecules (at ~3400 cm^{-1} and 1640 cm^{-1} respectively) can be clearly observed in the spectra. [494] The symmetric and asymmetric stretching vibrations of acetate ligands arise as a doublet centred at 1417 cm^{-1} and 1517 cm^{-1} respectively. The frequency separation ($\Delta\nu$ - 100 cm^{-1}) that exists between the ν_{sym} (COO) and the ν_{asym} (COO) bands is consistent with the bridging bidentate acetate ligands with a percent of chelating ones. [491,495] The band due to the presence of Ti-O-Ti network appears as a broad band below 1000 cm^{-1} probably due to the presence of an amorphous phase. [192,496-498] *The undoped titania calcined at 500°C shows* a peak centred at 466 cm^{-1}, which could be attributed to the anatase Ti-O bond vibrations. [499] The sample calcined at 700°C shows a peak at 519 and a shoulder at ~413 cm^{-1}, corresponding to the rutile and anatase Ti-O bond vibrations respectively. [492,500] Also, with the increase in calcination temperature, the bands corresponding to –OH species and those due to the

organic functionalities are vanishing, with the sharpening of the peak centred at ~450-525 cm^{-1}. The intensified peak corresponding to the vibration[232]

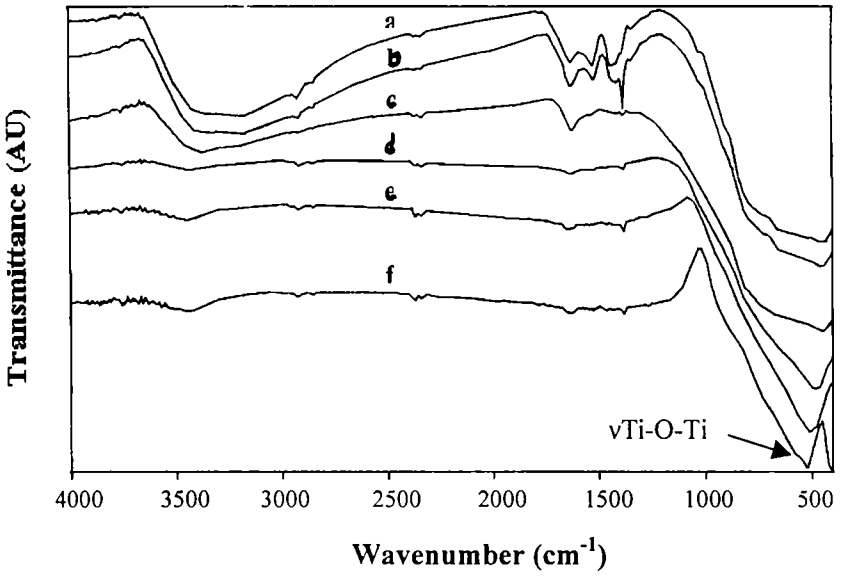

Figure 13: FTIR spectra of TU samples calcined at different temperatures. (a) 80°C; (b) 300°C; (c) 500°C; (d) 700°C; (e) 800°C and (f) 900°C

indicates the formation of extended Ti-O-Ti network with highly crystallinity. Further, a gradual shift towards the higher frequency region is also occurring for the peak corresponding to the vTi-O-Ti vibration on calcination, consistent with the crystallite growth.

Figure 14 shows the FTIR spectra of 1% lanthana doped titania heat-treated at different temperatures such as 70°C, 700°C and 900°C. The regular bonds for stretching and bending modes of vibrations of water molecules show a decrease in the intensity with temperature. Further, the band below 1000 cm^{-1} show increased peak intensity with increasing calcination temperature. However, all the other bands undergo a gradual decrease in the peak intensity.

Furthermore, for the 900°C calcined sample, the bands due to the stretching and bending modes of vibrations of water molecules are also diminished. Though, the dehydroxylation is complete at this temperature, as inferred by the TG analysis, the chances of adsorption of OH moieties to the surface is very much probable and is generally characteristic of ceramic metal oxides. A high frequency separation ($\Delta\nu$- 110 cm^{-1}) that exists between the ν_{sym} (COO, at 1417 cm^{-1}, and the ν_{asym} (COO), at 1527 cm^{-1}, bands of lanthana doped titania is consistent with the presence of more bridging bidentate acetate ligands compared to the undoped titania gels. [501-502] This enhanced bridge formation can be between titanium and lanthanum species based on the HSAB principle.

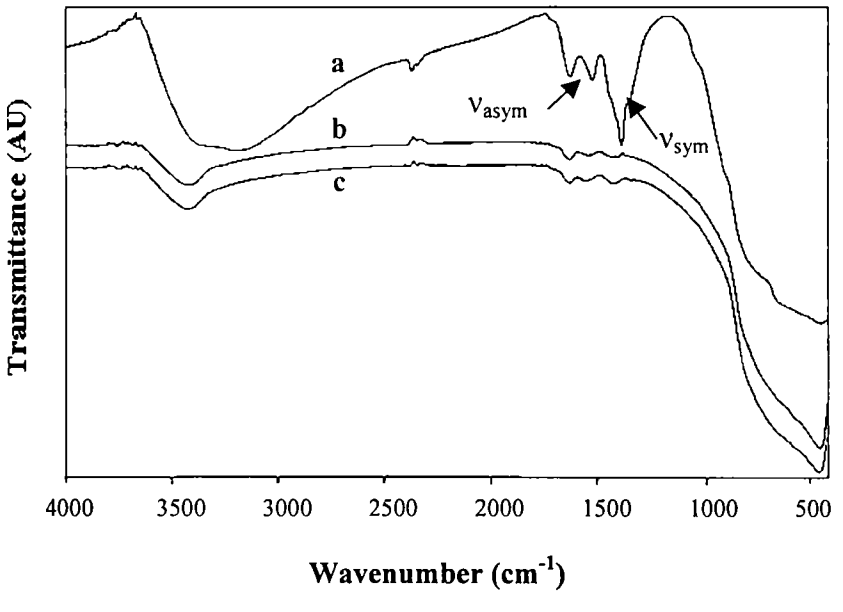

Figure 14: FTIR spectra of TL-1 samples calcined at different temperatures. (a) 80°C; (b) 700°C and (c) 900°C

Furthermore, all the samples show a shoulder at 1029 cm^{-1}. This is attributed to the anatase Ti-O bond vibration, which may have nucleated at the sol synthesis stage itself. According to Djaoued *et al*, [499] the anatase and rutile phases can also be established from FTIR spectra. In the spectra, while the 500°C calcined sample shows a peak centered at 448 cm^{-1}, the 900°C calcined sample shows a splitting of the band to ~ 512 cm^{-1} and 448 cm^{-1}. The peak at 448 cm^{-1} could be attributed to the quantum confinement effect of anatase titania particles and the one at 512 cm^{-1} is due to the presence of rutile phase. [232]

The FTIR spectra of different percentages of La_2O_3-doped TiO_2 samples (0.1, 0.5, 1, 2 and 5 %) calcined at 700°C are presented in Figure 15. All the spectra show broad bands below 1000 cm^{-1} that are centered at ~450-480 cm^{-1}. This is attributed to the phonon confinement effect of Ti-O-Ti network, as was discussed by Doeuff *et al.* [232] The formation of Ti-O-La bond is reflected in the FTIR spectra as a broad shoulder like peak in the range 680-890 cm^{-1}. [503] Further, the bands characteristic of the stretching and bending modes of vibrations of –OH functionalities show a slight increase with the increase of lanthana concentration.

Figure 16 represents the FTIR spectra of 1% CeO_2-doped TiO_2 (TC-1) samples heat-treated to different temperatures such as 70°C, 700°C and 900°C. All the peaks are almost similar as that of TL-1 samples. A high frequency separation ($\Delta\nu$- 110 cm^{-1}) that exists between the ν_{sym} (COO, at 1417 cm^{-1}, and the ν_{asym} (COO), at 1527 cm^{-1}, bands of ceria doped titania is consistent with

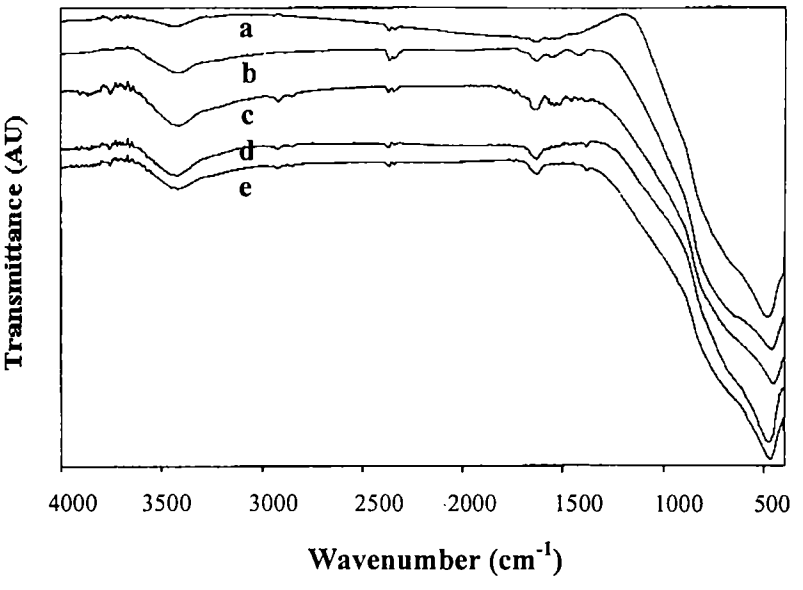

Figure 15: FTIR spectra of different concentrations of lanthana doped titania samples calcined at 700°C. (a) TL-0.1; (b) TL-0.2; (c) TL-1; (d) TL-2 and (e) TL-5

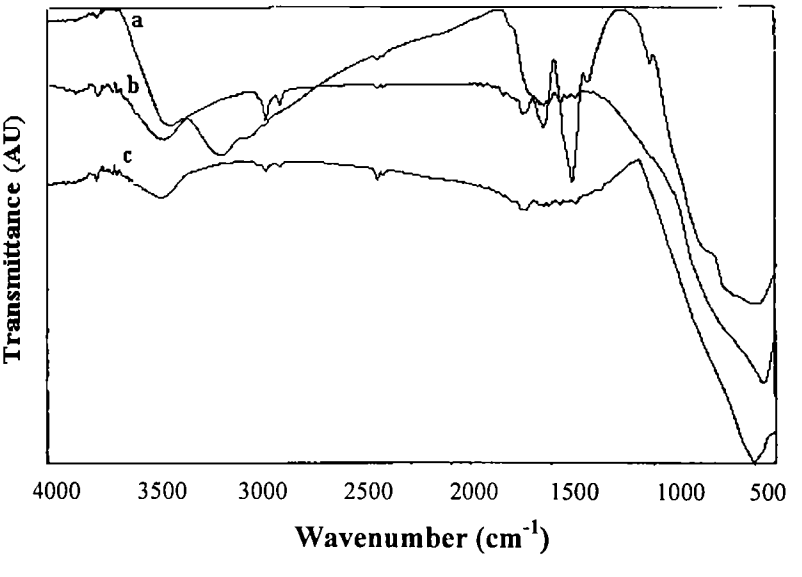

Figure 16: FTIR spectra of TC-1 samples calcined at different temperatures. (a) 80°C; (b) 700°C and (c) 900°C

the presence of more bridging bidentate acetate ligands compared to the undoped titania gels. [269,491-492,501-502] This enhanced bridge formation can be

between titanium and cerium species based on the HSAB principle, [504-505] which will be discussed later in this chapter. Furthermore, all the samples show a shoulder at 1029 cm^{-1} attributed to the anatase Ti-O bond vibration. [500]

Figure 17 presents the FTIR spectra of undoped titania (TU), TL-I, TC-1, TS-1 and TS-5 samples calcined at 700°C. The spectra clearly show a blue shift (~ 512 cm^{-1}) of vTi-O-Ti peak maxima for undoped titania, attributed to the rutile phase formation. Instead, all the doped titania samples show their respective vTi-O-Ti bands centered at ~460 cm^{-1}. Further, both the silica doped titania samples show shoulder bands (overlapped) in the region 940-1100 cm^{-1}.

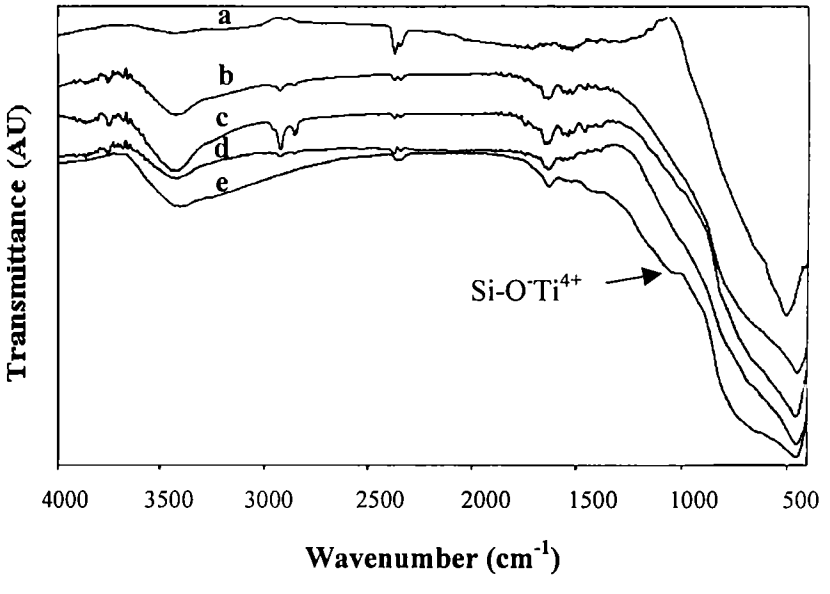

Figure 17: FTIR spectra of undoped and doped titania samples calcined at 700°C. (a) TU; (b) TL-1; (c) TC-1; (d) TS-1 and (e) TS-5

This can arise from the presence of a number of possible vibrations such as Si-O^{-} stretching vibrations in sequences involving tetrahedrally coordinated

Ti^{4+} ions (~940 cm^{-1}) [494,506,507] together with Si-O vibrations in Si-OH groups at approximately the same frequency; Si-O-Si stretching peak (1039-1073 cm^{-1}) formed due to the progressive condensation, [508] and Si-O-Ti groups obtained by the hetero-condensation. It can also be noticed that the silica doping enhances the amount of surface hydroxyl groups, [166] which can be clearly understood from the presence of a broad band, ranging from 2500 – 3700 cm^{-1} for the silica doped titania samples. The peak broadening as a result of silica addition indicates the enhancement of hydrogen bonding.

In general the FTIR spectra show the presence of acetate bridges with Ti and rare earth species, which is stable upto ~350°C, while the undoped titania shows more chelating acetate ligands.

3.1.3 Thermal Analysis

The thermal decomposition features were followed using differential thermal analysis as well as thermogravimetric analysis. Figure 18 shows the differential thermogram of undoped alkoxide derived sol-gel titania and those doped with different percentages of lanthana and ceria such as 1, 2 and 5 percentage (by wt). The undoped titania shows an endothermic peak at ~ 90°C and an exothermic peak at ~345°C. The endothermic peak [509] corresponds to the removal of loosely adsorbed water molecules present in the gel network and the exothermic peak is due to the removal of organic residues incorporated in the matrix, essentially acetic acid and residual isopropanol. [300,510] The removal of acetic acid is an exothermic process since it decomposes in the course of

heat treatment and expels as a more stable CO_2 form. [510] The other physico-chemical changes taking place in the course of heat treatment are condensation reactions leading to the formation of stronger Ti-O-Ti network and also an irreversible phase transformation from metastable anatase phase to thermodynamically stable rutile form. However, these changes do not reflect in the DTA pattern since the phase transformation is a process occurring over a range of temperature. The A→R transformation is mainly a nucleation-growth process, which is not confined to a particular temperature. [321] Once the rutile phase is nucleated, after a saturation point called 'critical nucleation limit', the sites grow in size by a dissolution-reprecipitation process at the expense of smaller particles. [320] The crystallization and phase transformation are primarily exothermic processes but due to the above limitations, will not reflect in the differential thermogram. In the present synthesis method, the anatase phase nucleation takes place in the sol preparation stage itself, [510] which will further be discussed in detail in this chapter.

On addition of lanthana as lanthanum nitrate in the solution stage, it is incorporated as La^{3+} ions surrounded by H_2O molecules as primary coordination sphere and nitrate ions as secondary coordination sphere. As lanthanum/cerium ions are hard Lewis acids they will have a tendency to coordinate with more electronegative, hard Lewis bases like CH_3COO^- ions [505] present in the acetic acid stabilized TTIP solution. Consequently, the acetate ligands coordinate with the La^{3+}/Ce^{3+} ions and act as bridges between titanium and lanthanum ions. This will stabilize the acetate ligands in the gel network,

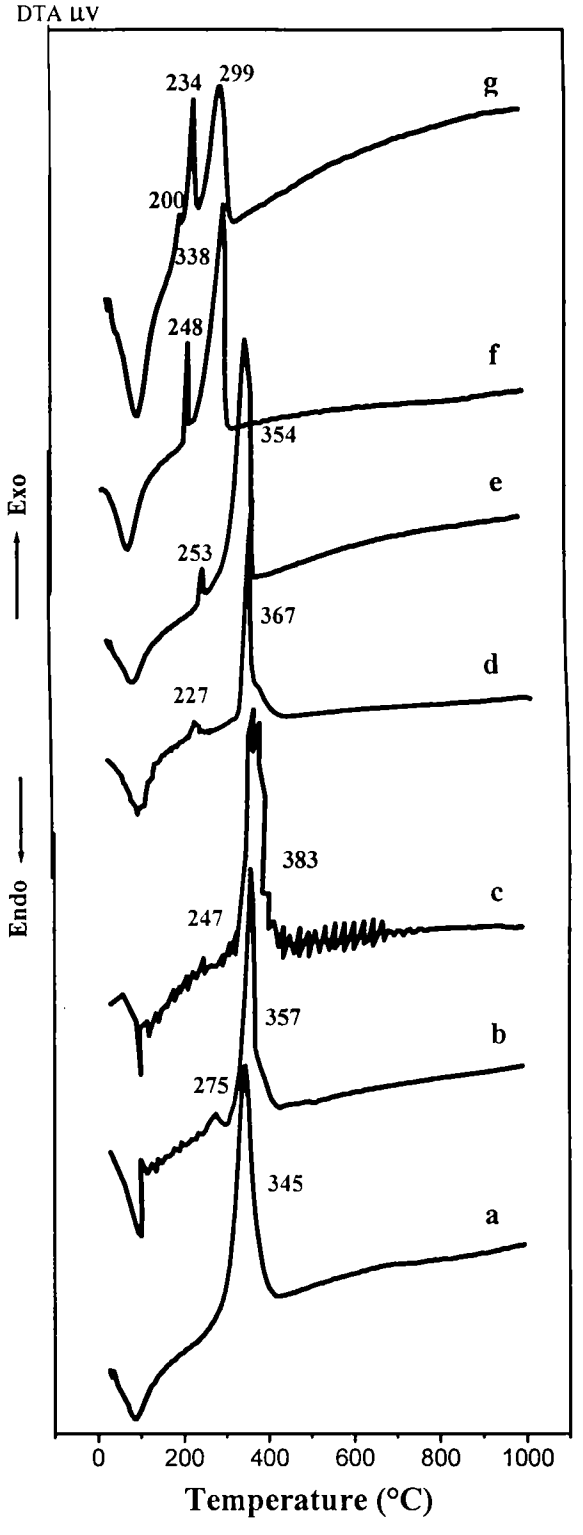

Figure 18: DTA curves of undoped and different percentages of La_2O_3 as well as CeO_2 doped titania samples. (a) TU; (b) TL-1; (c) TL-2; (d) TL-5; (e) TC-1; (f) TC-2 and (g) TC-5

which is reflected as a shift of the exothermic peak in 1% lanthana doped titania to 357°C from that of 345°C for undoped titania in the differential thermogram. For higher concentration of lanthana, (2%), the peak occurs as a doublet centred at 369°C and 383°C. The peak at 383°C could be attributed to the enhancement of bridging between titanium and lanthanum by acetate ligands, which stabilize it to exist at higher temperatures. The exothermic peak at 369°C may be due to the removal of metal-complexed NO_3^- ligands as nitrogen gas. [511]

Figure 19 shows the thermogram of undoped and different percentages of lanthana as well as ceria doped titania samples. Titania undergoes a three-step weight loss on heat treatment. The first step ranging from 29° – 100°C corresponds to the removal of physisorbed water. [300] The second gradual weight loss, ranges from 100 – 315°C, may be due to the combined removal of hydroxyls, structural water and organic residues like acetate groups, isopropanol etc., associated with the solid network. [300] The gel matrix will be strengthened by condensation reactions leading to the formation of Ti-O-Ti network right from the beginning of hydrolysis to the whole range of heat treatment temperatures. [193,300] The third weight loss step, that ranges from 315° - 400°C could be mainly due to the removal of acetate moiety incorporated in the gel network, in addition to the continued dehydroxylation process, which substantiates the occurrence of exothermic peak in the DTA. [251] Above this temperature, the thermogram shows almost little change in the sample weight but in the DTA shows a broad exothermic kind of curve at higher temperature.

This may be due to the A→R phase transformation, taking place in the course of heat treatment. [512]

On addition of 1 % lanthana as lanthanum nitrate, the thermogram changes to a four-step weight loss pattern. The first step ranging from 30° - 70°C is due to the removal of loosely adsorbed water. The second step ranging from 70° - 245°C is due to the combined effect of dehydroxylation and removal of organic residues. [513] The third weight loss step from 245° - 330°C may be due to the expulsion of gaseous nitrogen originated from the lanthanum nitrate solution, which is being associated with the metal ions as a bidentate complex ligand. The fourth weight loss step ranges from 330 – 433°C and could be attributed to the expulsion of CO_2 gas produced as a consequence of acetate decomposition. [509-510] All the four weight loss steps occurring in the thermogram corroborate with the peaks in the corresponding DTA, which substantiates the discussed sequential processes taking place on heat treatment of the xerogel.

The thermal decomposition features of CeO_2-doped TiO_2 xerogels (1, 2 and 5 percentage by wt.) are also presented in Figure 19. On addition of 1 % ceria as cerium nitrate, the thermogram changes to a four-step weight loss pattern. The first weight loss step, which ranges from 32 - 100°C is due to the removal of loosely bonded water. The second step ranging from 100 - 240°C could be due to the combined effect of dehydroxylation and removal of organic residues. The third weight loss step from 240 - 270°C may be due to the expulsion of gaseous nitrogen originated from the cerium nitrate solution,

which is being associated with the metal ions as bidentate complex ligands. The fourth weight loss step is from 270 – 380°C and this could be attributed to

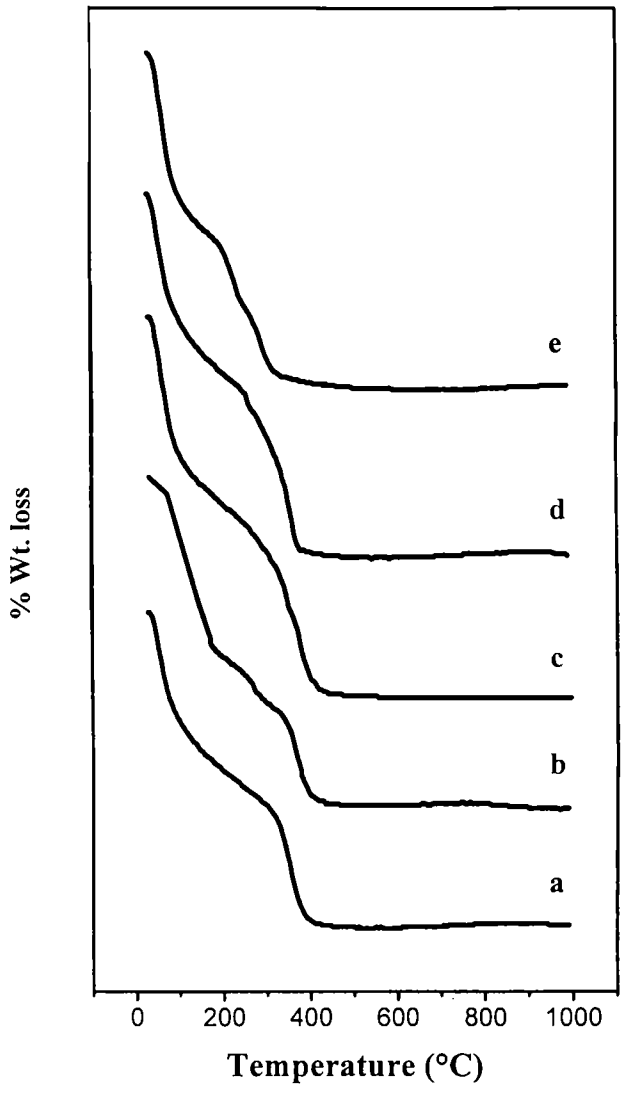

Figure 19: Thermogravimetric curves of undoped and different percentages of La_2O_3 as well as CeO_2 doped titania samples. (a) TU; (b) TL-1; (c) TL-5; (d) TC-1 and (e) TC-5

the expulsion of CO_2 gas produced as a consequence of acetate decomposition. [300] All the four weight loss steps occurring in the thermogram correspond to peaks in the respective DTA plots, which substantiate the sequential processes

taking place on heat treatment of the xerogel. In order to distinguish each of weight loss, the derivatives are also presented along with the respective thermogram.

In cerium nitrate aqueous solution, ceria is in the +3 oxidation state surrounded by $6H_2O$ molecules as primary coordination sphere and 3 nitrate molecules as secondary coordination sphere. [514] Ce(III) being highly oxophilic and/or hard Lewis acid [505] has a tendency to coordinate with those oxygen species produced as a result of hydrolysis of acetate ligands chelated with titanium ions. This produces the bridging between titanium and cerium ions.

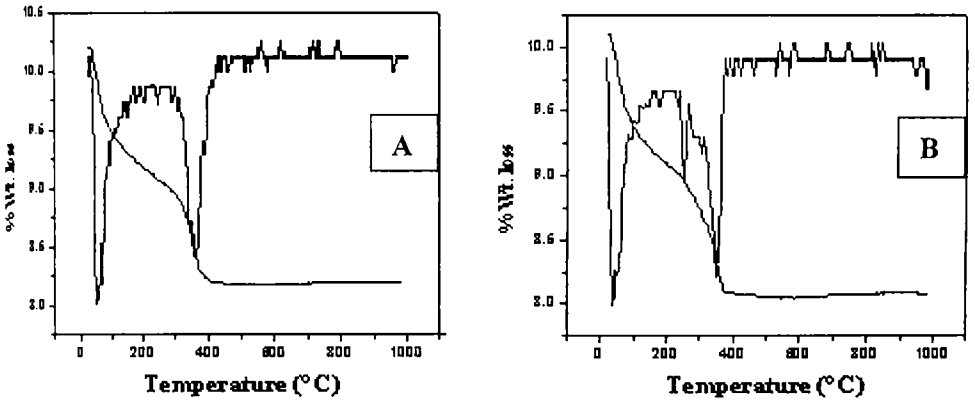

Figure 20: Thermogravimetric curves and their derivatives of (A) TU and (B) TC-1

This will stabilize the acetate ligands in the gel network, which is reflected as a shift of the exothermic peak in 1% CeO_2-doped TiO_2 to 354°C from that of 345°C in case of undoped titania in the differential thermogram. In addition, there occurs a small exothermic peak at ~253°C, which could be attributed to the removal of nitrates. Further, the intensity of this peak increases with the

concentration of cerium nitrate addition. However, for higher concentrations of ceria, the acetate peak is being shifted to lower temperature (338°C) and the nitrate peak also shows a shift to 248°C (2 %). The 5 % CeO_2-doped TiO_2 shows exothermic peaks at 299°C and 234°C. An additional small exothermic peak at 200°C is seen in case of the 5 % ceria doped sample, which is due to the cerium oxide crystallization. [515]

3.1.4 Powder X-ray Diffraction

The powder X-ray diffraction patterns of different samples calcined at different temperatures are provided and the results are discussed in the following paragraphs. The dopants such as lanthana and ceria increase the anatase to rutile phase transformation temperature and also inhibit the grain growth. The nucleation of anatase phase in the present procedure is supposed to be occurring at the time of hydrolysis-condensation stage itself as confirmed by the XRD data. According to Song and Pratsinis, [175] the presence of solvents like isopropanol prevents the anatase phase nucleation upto a certain elevated temperature. In the present case we have adopted an alcohol-free sol-gel process. The presence of hydrous anatase phase at 80°C can, therefore, be attributed to the specific preparative route adopted in the present case.

The XRD patterns of the as gelled xerogels (80°C), presented in Figure 21 show the presence of hydrous anatase crystals, which occurs as a broad peak with less intensity. The presence of amorphous phase is reflected as broad noises without any distinct peaks.[516] The undoped titania has the smallest

crystallite size compared to the doped titania samples. Particles start growing as the heat treatment temperature increases. However, undoped titania grows faster with temperature and exhibits the anatase to rutile transformation at a lower calcination temperature compared to the doped samples. In other words, the dopants inhibit the grain growth of anatase crystallites by providing a diffusion barrier by either segregating at the grain boundaries or by stabilizing the Ti-O bonds by forming Ti-O-RE (RE = La, Ce) bonds. The electropositive

RE ions provide its electron density to the oxygen, which in turn is being utilized for the stabilization of the Ti-O bonds. Therefore, the bond formation inhibits the Ti-O bond breakage towards higher heat treatment temperature, which in turn retards the oxygen diffusion needed for the structural rearrangement. The anatase to rutile transformation involves a structural rearrangement, wherein two of the Ti-O bonds break and reorient to form the rutile phase. [517] The stabilization of Ti-O bonds in turn retards the anatase to rutile phase transformation.

The formation of Ti-O-La bonds also terminates the Ti-O-Ti network formation and the RE species are located at the grain boundaries. This can be explained by a capping mechanism attributed to the HSAB principle, [504-505] assisted by the acetate ligands. Another explanation for retardation of anatase to rutile phase transformation is the locking of the Ti-O bonds by the Ti-O bonds at the interface. This assumption also corroborates with the report by Bard *et al.* [394] Bard *et al* have demonstrated the inhibition of phase

transformation and grain growth in the TiO_2-SiO_2 system by the formation of Ti-O-Si bonds, which locks the Ti-O bonds at the interface.

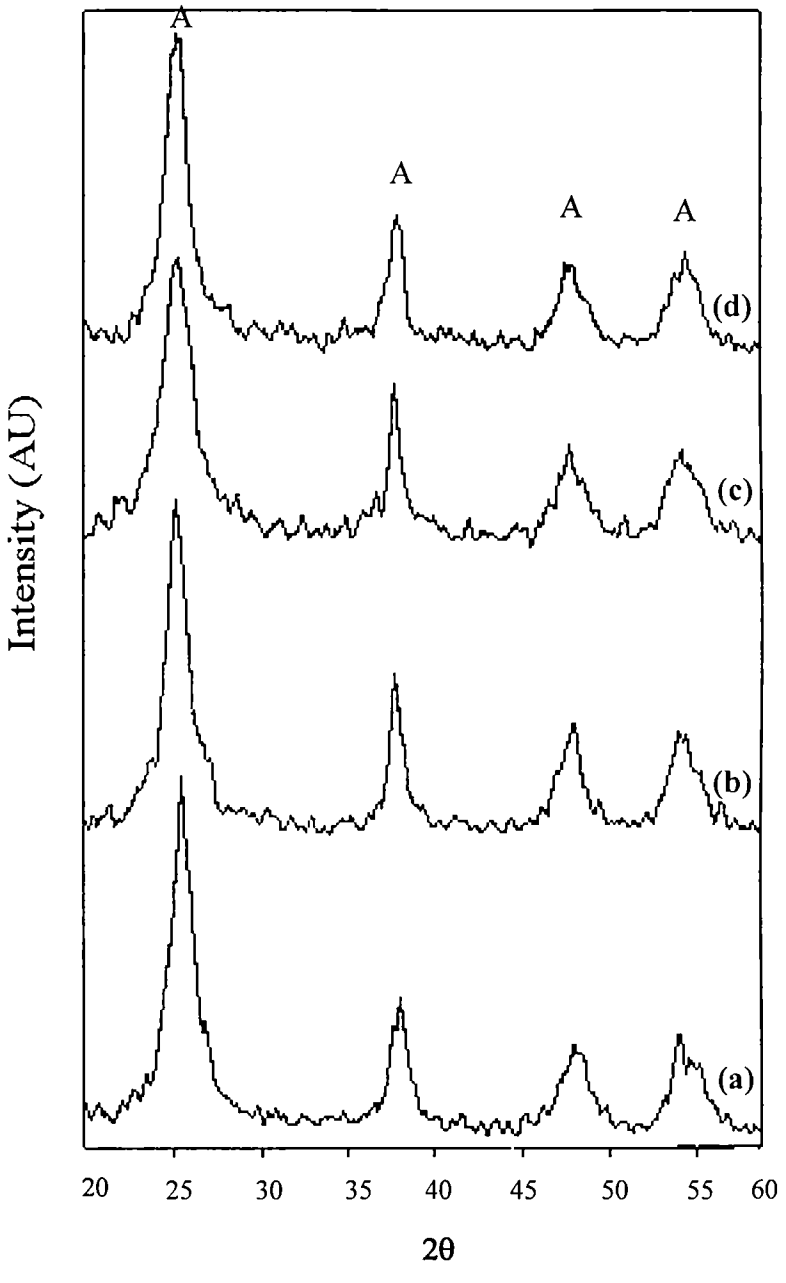

Figure 21: Powder X-ray diffraction patterns of as gelled xerogels (80°C). (a) TU; (b) TC-1; (c) TL-1 and (d) TS-5

Table 7 presents the crystallite size and phase compositions of undoped and doped titania samples heat-treated at different temperatures ranging from 80-1100°C. The effect of dopants on the inhibition of grain growth and phase transition can be clearly understood from the result. The XRD patterns indicate the presence of highly crystalline titania crystallites at 700°C, which appear as sharp intense peaks. The nanocrystallinity of titania is enhanced by the addition of both La_2O_3 and CeO_2. At 700°C, 1% La_2O_3-doped TiO_2 shows a crystallite size ~16.81 nm and 1% CeO_2-doped TiO_2 has ~18.91 nm and 1% SiO_2-doped TiO_2 sample, 23.62 nm. While rutile phase nucleation occurs at a temperature of ~670°C in undoped titania, the nucleation is delayed to ~910°C in case of 1% CeO_2 and ~940°C in case of 1% La_2O_3 doping. Furthermore, the phase transformation temperature shifts to even higher values with the increase in dopant concentration. However, the XRD patterns of the 5% lanthana and / or ceria doped samples indicated the formation of traces of La_2O_3 / CeO_2 phases in their respective patterns. Therefore, the studies were limited to less than 5 % addition of dopants. In general, La_2O_3 is found to be the most effective in the inhibition of both grain growth and phase transformation.

In Figures 22 and 23, the XRD patterns of 1 % La_2O_3 and CeO_2-doped TiO_2 powders show the presence of tetragonal titania phases. No La_2O_3 or CeO_2 crystals with XRD detectable size were formed in these powders. Identification of the exact state of the dopants in nanostructured powders is rather difficult. Even though, the TEM observation had shown (will be discussed later on) that most of the La_2O_3 and CeO_2 atoms are distributed like

Table 7: Crystallite size (nm) and phase compositions of undoped and doped titania samples heat-treated at different temperatures

Sample	Crystallite size (nm) and phase assemblages at different calcination temperatures											
	80°C	500°C	600°C	700°C		800°C		900°C		950°C		1000°C
	A	A	A	A	R	A	R	A	R	A	R	R
TU	4.67	11.72	33.74	39.09	65.44 (33.31%)	0%	70.36	0%	79.08	--	--	--
TL-1	5.25	9.59	15.28	16.81	0%	31.26	0%	37.34	0%	42.84	51.34 (8.51%)	54.82
TC-1	5.60	11.84	--	18.91	0%	35.28	0%	41.06	0%	46.87	56.49 (69.22%)	60.76

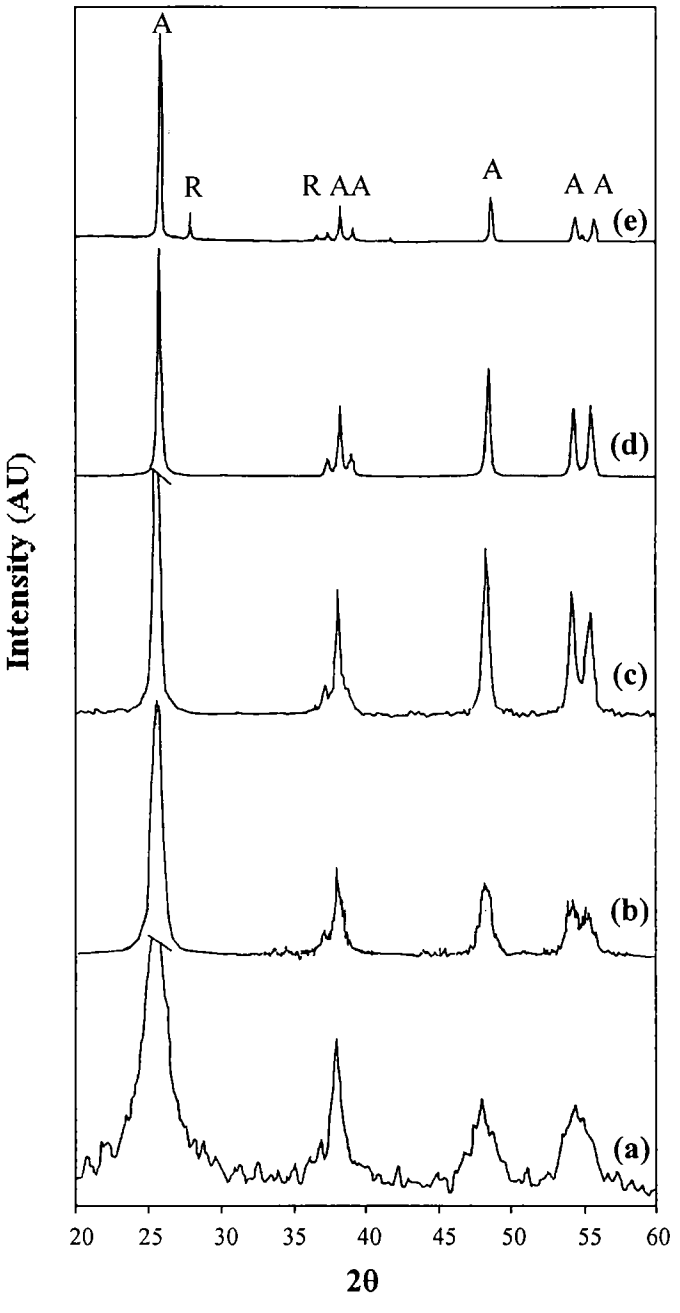

Figure 22: Powder X-ray diffraction patterns of TL-1 samples calcined at different temperatures. (a) 80°C; (b) 500°C; (c) 700°C; (d) 800°C and (e) 950°C

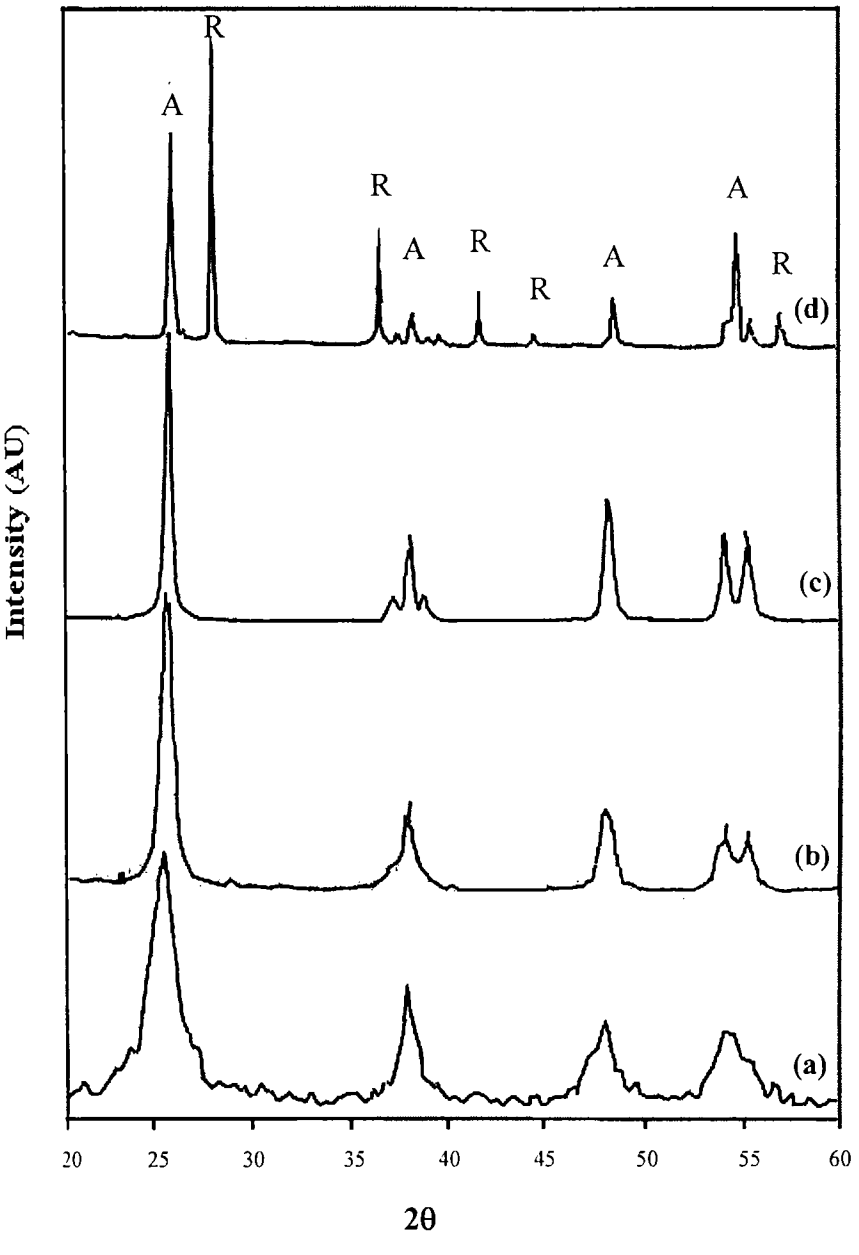

Figure 23: Powder X-ray diffraction patterns of TC-1 samples calcined at different temperatures. (a) 80°C; (b) 500°C; (c) 800°C and (d) 950°C

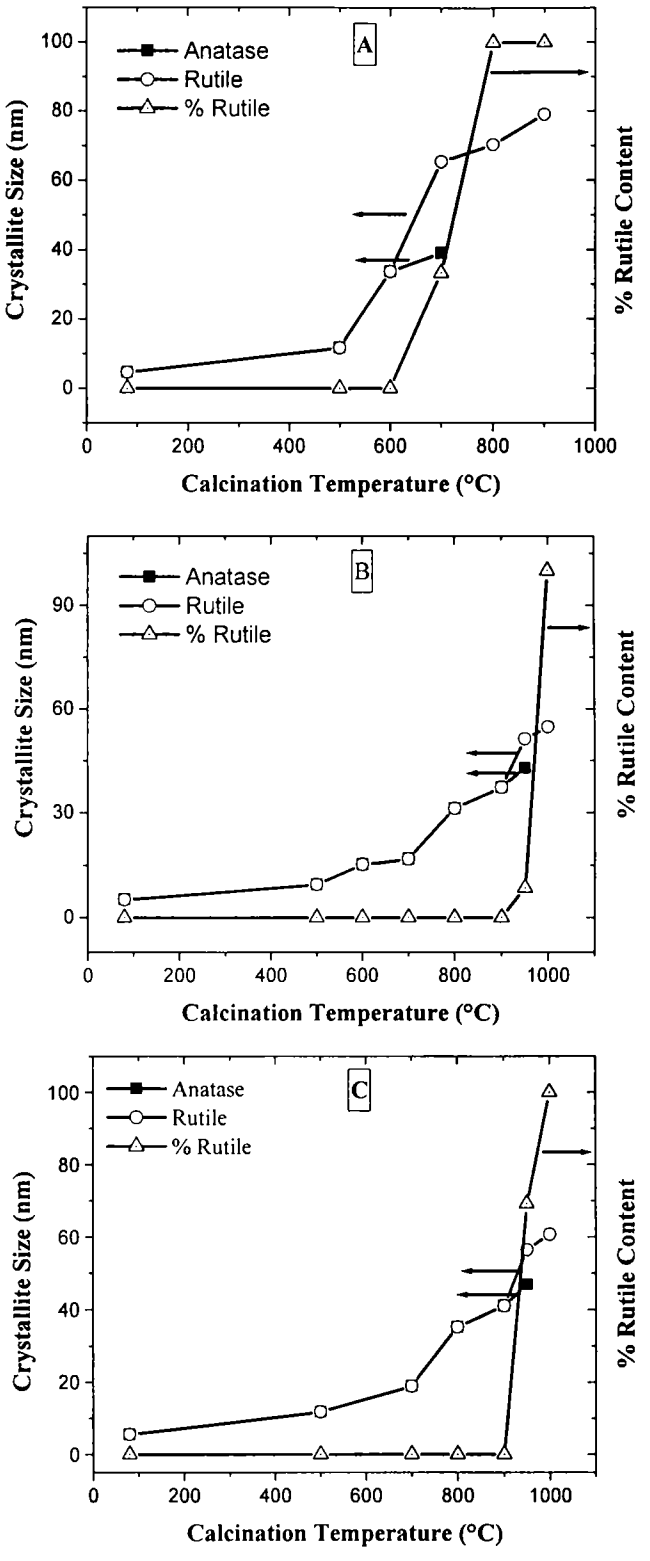

Figure 24: Anatase and rutile crystallite sizes as well as the % rutile content vs calcination temperature of (A) TU; (B) TL-1 and (C) TC-1

in amorphous material than located on definite crystallographic positions in the grain boundary core.

Figures 24A, 24B and 24C show the anatase and rutile crystallite sizes as well as the % rutile content as a function of calcination temperature for undoped 1% La_2O_3-doped and 1% CeO_2-doped TiO_2 powders. The crystallite size of undoped titania increases rapidly with increasing temperature. On the other hand, the doped titania powders show a rather slow growth of anatase crystallites upto 950°C. At 900°C, the crystallite size of undoped titania is ~79.08 nm, while the crystallite sizes of TiO_2 doped with 1% La_2O_3 and 1% CeO_2 are only 37.34 and 41.06 nm respectively. However, all the doped titania samples show higher crystallite growth above 950°C by phase transformation and sintering. [311,518-520] From table 6 we can understand that the stable rutile phase has a larger grain size (>40 nm) than that of the metastable anatase phase as indicated by sharper peaks in XRD patterns (Figure 22). In general, both anatase and rutile grain sizes of doped titania are smaller than those of undoped titania processed at the same temperature.

3.1.5 BET Specific Surface Area Analysis

Table 8 shows the BET specific surface area (SSA) and pore volume of undoped and lanthana as well as ceria doped TiO_2 powders obtained at different calcination temperatures. All the powders show a decrease of SSA with increasing calcination temperature by phase transformation and sintering. The results indicate the effect of dopants on the retention of surface area at

higher temperatures owing to their influence on the retention of porosity. The influence of the dopants are in the order lanthana > ceria > silica.

Table 8: BET specific surface area (SSA) and pore volume of undoped and doped TiO_2 powders calcined at different temperatures

Sample	**Surface area (m^2g^{-1})**	**Pore volume (ccg^{-1})**
TU (300°C)	120.54	0.1688
TU (500°C)	75.59	0.1262
TU (700°C)	0.0879	0.0021
TL-1 (300°C)	160.52	0.2573
TL-1 (500°C)	111.02	0.219
TL-1 (700°C)	51.97	0.0961
TL-2 (300°C)	260.18	0.2863
TL-2 (700°C)	134.06	0.1707
TL-5 (300°C)	244.22	0.2542
TL-5 (700°C)	113.30	0.1657
TC-1 (300°C)	157.33	0.2667
TC-1 (500°C)	113.27	0.2118
TC-1 (700°C)	42.11	0.0779
TC-2 (500°C)	157.44	0.2106
TC-5 (500°C)	182.68	0.2145

Figure 25 shows the SSA of undoped and lanthana as well as ceria doped TiO_2 powders as a function of calcination temperature. In general, all the undoped as well as doped TiO_2 samples show a decrease in SSA with increase in calcination temperature. However, lanthana is found to be the most effective among the dopants in the inhibition of both SSA and porosity reduction. The effect of ceria, on the other hand, is less compared to that of lanthana.

At 700°C, TL-1 shows a SSA of 52 m^2g^{-1} and TC-1 has ~42 m^2g^{-1} compared to the undoped TiO_2, which has a SSA of ~1 m^2g^{-1}. Titania produced in the absence of dopant have the lowest SSA at all temperatures. The SSA decreases with increasing calcination temperature by phase transformation and sintering (crystallite growth). [520] For a constant dopant concentration, there is a certain calcination temperature, which results in a sharp decrease in SSA. For undoped titania, this occurs at ~670°C, while for the doped titanias, from 900-1000°C. As a result of this, detailed investigation was carried out with 1% dopant concentrations and compared the results with XRD data. This drastic decrease in the surface area is accompanied by the transformation from anatase to rutile. [106] Generally, the phase transformation results in a dramatic pore structure change, compared to sintering (crystallite growth). [521] The variation in SSA as a function of dopant concentration is provided in Figure 26. The SSA of La_2O_3-doped TiO_2 increases on doping upto a level of 2 wt % La_2O_3 and then decreases on increasing the lanthanum concentration further. On doping with 5% La_2O_3, the SSA decreases in case of both 300° and 700°C calcined samples (The SSA of 500°C calcined samples has not been taken). In order to analyze this trend further, the pore size distribution of the samples were obtained from the multilayer condensation region of the type IV isotherm, using Kelvin

equation. The pore size distribution curves provided in Figure 27 show a slight increase in porosity in the microporous region for the TL-2 compared to TL-5. The decrease in porosity for the TL-5 could be attributed to the preferential agglomeration of La_2O_3 particles in the pores above the optimum dopant concentration, which reduces the microporosity. [522]

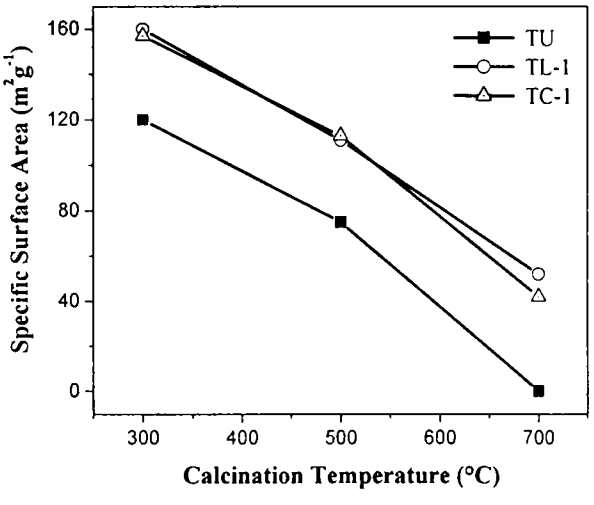

Figure 25: SSA of undoped and doped TiO_2 powders as a function of calcination temperature

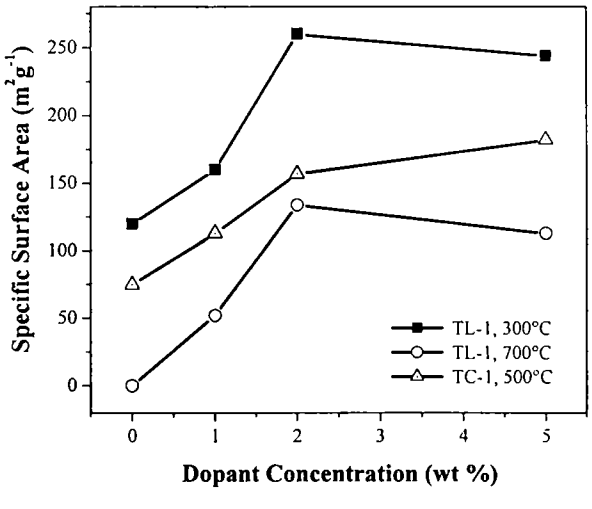

Figure 26: Variation in specific surface area (SSA) for doped TiO_2 samples as a function of dopant concentration

Figures 27 A, B and C show the pore size distribution of TU, TL-1 and TC-1 samples respectively, measured at calcination temperatures 300, 500 and 700°C. The corresponding adsorption isotherms are also provided in the inset as a point of ready reference. Undoped TiO_2 (Figure 27A) shows almost a bimodal type distribution curve at 300°C. The curve shows a shoulder type deflection, which is indicative of the bimodal distribution. On heat treatment to 500°C, the graph is converted to a skew type distribution curve, with maximum distribution at ~14 nm. In addition, as is obvious, the total porosity is lowered by the high temperature heat treatment. The SSA for the undoped TiO_2 measured at 700°C was as low as ~1m^2g^{-1} with almost non-porous characteristic. Therefore, adsorption isotherm as well as the pore size distribution curve could not be obtained for undoped TiO_2 at 700°C.

In case of 1% La_2O_3-doped TiO_2 (Figure 27B), a gradual decrease in porosity can be observed on heat treatment to higher temperatures, from the distribution curves. The 300°C heat-treated sample shows almost a continuous distribution curve. On heat treatment towards higher temperatures as 500 and 700°C, the pore sizes take a skew type distribution. The maximum distribution is in the microporous region for the high temperature heat-treated samples. This is due to the commencement of sintering.

Figure 27C shows the pore size distribution curves of 1% CeO_2-doped TiO_2 powders heat treated at 300, 500 and 700°C. In general, all the samples show almost the skew type distribution. However, the powder heat treated at 300°C shows a predominant Microporous region (~14 nm) and two more

mesoporous regions centered at, 28 and 34 nm. On heat treatment to higher temperatures, the porosity assumes a skew type distribution. Nevertheless, the 500°C heat-treated powder indicates a small pore size distribution at ~38 nm. This is due to the pore coarsening occurring because of calcination. However, the 700°C calcined sample shows a perfect skew type distribution, wherein the maximum pore size distribution is at ~14 nm. This indirectly refers to the possible commencement of sintering below 700°C. Due to sintering, the larger pores get nearly closed and a continuous distribution of micropores resulted at 700°C. The pore size distribution curves give an obvious idea on the evolution of porosity of samples on heat treatment. In the sintering process, the micropores eliminate first by pore coarsening followed by densification. [523] This will be a continuous process and the total porosity as well as the micro and meso porosity could be seen reduced for the high temperature heat-treated gels. So we can assume that on heat treatment, the densification is much more pronounced in undoped titania compared to the ceria doped titania. This inhibition of densification in CeO_2-doped TiO_2 could be due to the presence of more amount of intra as well as inter-granular pores produced due to ceria doping.

From the above results, it is clear that the presence of dopants such as La_2O_3 and CeO_2 retarded the crystallite growth and phase transformation of TiO_2 and thereby improved the textural properties at high temperatures. The extent of this retarding effect increased with the increasing dopant oxide

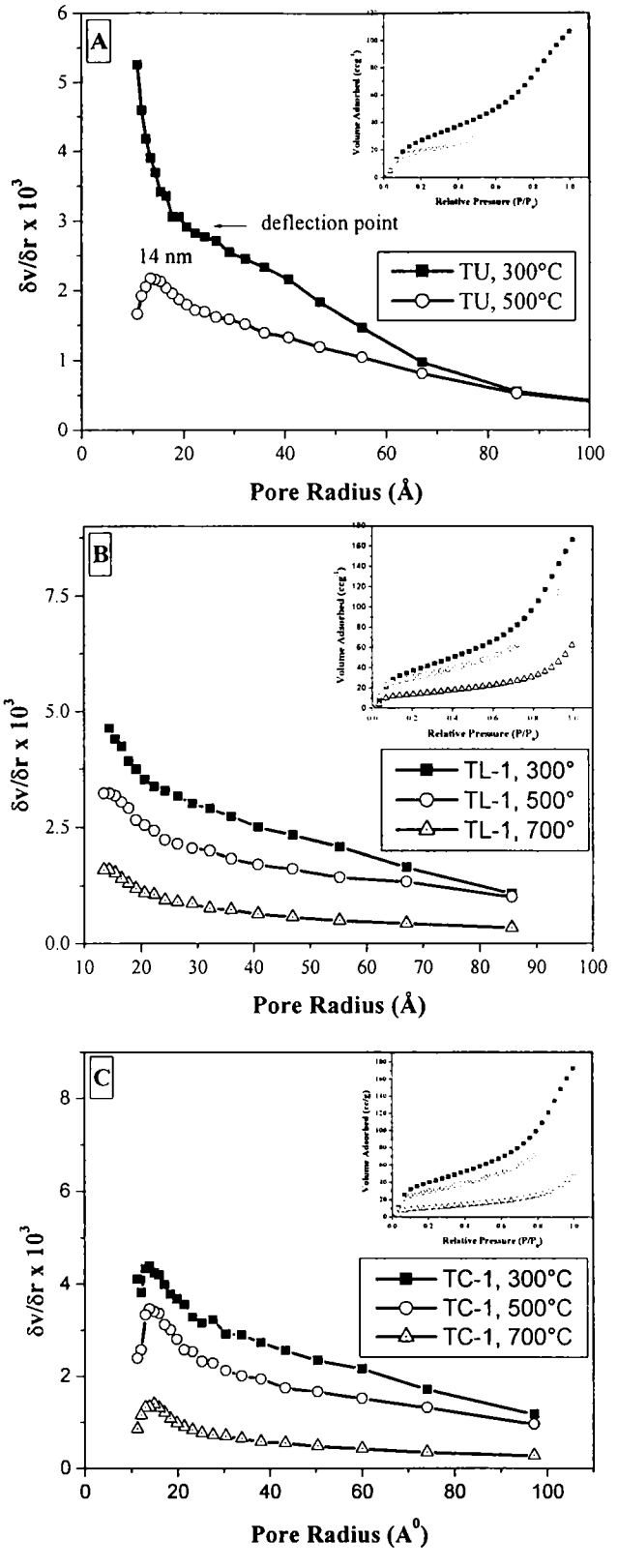

Figure 27: Pore size distribution curves of (A) TU; (B) TL-1 and (C) TC-1 powders calcined at 300, 500 and 700°C

concentration. These results are in agreement with a few other dopants such as alumina, zirconia and silica reported by Yang *et al.* [481-482]

In case of the 300°C calcined samples, SSA of titania is increased by 33 % in presence of La_2O_3 from that of undoped titania (Table 8). Further, there is a remarkable improvement in the high temperature stability of pores with both La_2O_3 and CeO_2 doping. However, La_2O_3 was found to be the most effective among the dopants stabilizing the SSA as well as porosity at high temperatures. This is in agreement with the observation reported by Kumar *et al* [93] and Gopalan *et al.* [349] However, the textural stability values observed in the present case are higher than those reported previously due to a better interaction between TiO_2 and La_2O_3 surfaces achieved through the present preparative procedure. 1% La_2O_3 doped titania, after heat treatment at 700° C shows a SSA of 52 m^2g^{-1}, while that of undoped titania under identical conditions has only ~1 m^2g^{-1} (Table 8).

With increasing calcination temperature, the pore volume of undoped and doped titania decreases continuously (Figure 27). The La_2O_3-doped TiO_2 shows the highest pore volume indicating that it has got the highest porosity among the doped samples. TL-1 retained about 37 % of its initial pore volume even after calcination to 700°C, compared to the 300°C calcined powder. At this temperature undoped titania has as low as ~1 % of its pore volume compared to that of 300°C calcined sample, due to the phase transformation and sintering. This retention of porosity is attributed to the presence of lanthanum and cerium oxide distributed uniformly in the titania gel matrix. In

addition to the effective surface coverage of lanthana on the titania particles reported based on earlier studies, [349] factors related to the presence of Ti-O-RE bonds also have some effect as is seen from the shift of titania peak to a lower energy region in the FTIR spectra and the presence of shoulder peak in the range 680-890 cm^{-1}. [503] In the present process, a molecular level mixing of the reactants is very much possible, which explains the enhanced properties.

1% CeO_2-doped TiO_2, on the other hand, retains 29 % of its pore volume on heat treatment to 700°C compared to that of 300°C calcined sample. Further, on increasing the CeO_2 concentration, the SSA values increases considerably. At 500°C, while the 1% CeO_2-doped TiO_2 shows a SSA 113 m^2g^{-1}, 2% and 5% CeO_2-doped TiO_2 samples show SSAs as 157 and 182 m^2g^{-1} respectively. However, the total pore volumes of both 2% and 5% CeO_2-doped TiO_2 are almost similar, i.e., 0.2106 and 0.2145ccg^{-1} respectively. This indirectly indicates the presence of more micropores in the 5% CeO_2-doped TiO_2, whose evolution can be attributed to the effect of particular concentration of CeO_2 in the TiO_2 matrix. The evolution of porosity with respect to the addition of dopants will be discussed later on in this chapter. The pore size distribution curves, provided in Figure 27, obtained from the corresponding BET surface area results corroborates with this assumption. 5% CeO_2-doped TiO_2 shows an increased amount of micropores compared to the 2% CeO_2-doped TiO_2 samples, which is consistent with the increased surface area.

Figure 28 shows the adsorption isotherms of undoped and doped titania powders calcined at temperatures 300, 500 and 700°C. All the powders show

isotherms of type IV behaviour. This indicates that the powders contain mesopores (2-50 nm). [489] From the figure, we can see that the porosity is distributed in a bimodal fashion with small amount of microporosity and an extended mesoporosity. The trend of the dopants on the inhibition of specific surface area and porosity reduction can be clearly observed from the figure.

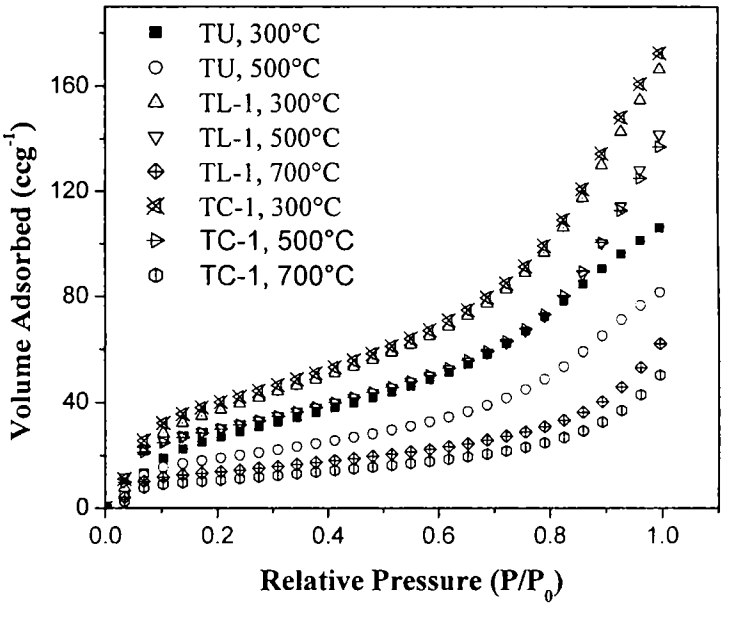

Figure 28: Adsorption isotherms of undoped and doped titania powders calcined at temperatures 300, 500 and 700°C

At 700°C, the smaller crystallite size of titania obtained by lanthana / ceria doping obviously causes an enhancement in surface area (Table 8), which is in accordance with the large surface to volume ratio possessed by the nanomaterials. [524] The enhancement in surface area could also be attributed to the stability of micropores at higher temperatures by doping. According to Hague and Mayo [525] the presence of inter-agglomerate pores prevents the anatase grain growth. In our results the same trend is observed and this shows

the formation of inter-agglomerate pores in presence of ceria and the stabilization of the same at higher temperatures. The isotherms obtained from nitrogen adsorption studies on the samples also indicate the high temperature pore stabilizing effect of ceria. All the isotherms are type IV, which indicates the presence of a mesoporous structure and also the total porosity as well as the microporosity decreases linearly with increase in temperature, irrespective of all the samples. On calcination to 700°C, about 29% of the total porosity (Table 8) is retained in case of 1 % CeO_2-doped TiO_2 compared to undoped titania, while in pure titania the powder becomes almost non porous. Moreover, the surface area decreases to ~1 m^2g^{-1}n case of undoped titania. This retention of porosity as well as the surface area is attributed to the effective homogeneous distribution of ceria particles in the titania matrix. 1% ceria doping induces 157 % increase in pore volume from that of undoped titania. This could be explained using the Hard and Soft Acids and Bases (HSAB) principle. Ceria being a hard Lewis acid can hold the excess acetate ligands present in the reaction system. This stabilizes the acetate ligands during aging, drying and subsequent heat treatment stages.

3.1.6 Transmission Electron Microscopy (TEM)

Transmission electron microscopic observations [527-529] of typical samples of undoped titania and that doped with La_2O_3 as well as CeO_2 indicate the nanocrystalline nature of particles. In general, undoped titania specimens show the highest grain size at all the calcination temperatures. The addition of dopants decreases the grain size considerably, and the increase in dopant

concentration further decreases the grain size of titania. Lanthana doped titania specimens exhibit the smallest grain sizes among the doped titania samples at all the temperature range. The extensive homogeneous distribution of La_2O_3 as well as CeO_2 particles achieved by the sol-gel process could be the reason for the enhanced nanocrystallinity of TL and TC compositions, which was further supported by FTIR results. The distribution of RE oxides in titania may be more or less at the inter-granular region and increases the diffusion barrier at the anatase-anatase grain contact. The evidence for Ti-O-RE linkages from FTIR data discussed earlier further supports this observation.

In order to have an understanding of the effect of dopants on the crystallinity of the specimens, the nature of the specimens concerning the sharpness of the diffraction pattern in reciprocal space have been appraised. The TEM images as well as the selected area electron diffraction patterns of undoped, lanthana-doped and ceria-doped samples calcined at different temperatures are provided in Figures 29-34.

TEM bright field images of undoped titania sample calcined at 500°C and 800°C and each soaked for periods of 3 hours are given in Figures 29A and 29B. Figure 29A indicates the presence of evenly distributed 5 nm fine-crystalline anatase titania crystallites, which are agglomerated to form the secondary particles of ~ 300 nm in size. Figure 29B, the TEM of 800°C calcined specimen, point towards the crystallite growth occurring as a result of heat treatment. The presence of coarse-crystalline secondary particles of 500 nm size in which the primary crystallites are of the order 50 nm can be well

understood from the figure. The origin of 'crystallinity' of the specimens is attributed to the specific preparative route adopted in the present case. According to literature, the particulate, hydrolytic route produces amorphous phase at room temperature. But the present procedure yields hydrous anatase crystals at similar ambient conditions, which is also supported by the XRD data of the xerogel.

Figures 30 A, B and C are the HRTEM, TEM and SAED pattern of 1% lanthana doped titania powder calcined at 400°C for 3 h. The TEM micrographs indicate the presence of ~7 nm anatase crystallites agglomerated to form particles of about 300 nm. The presence of amorphous phases can also be observed at the grain boundaries. [527] The SAED pattern of the fine crystalline anatase titania particles (Figure 30C) indicates a random arrangement of anatase crystals in the specimen. The presence of amorphous phase is reflected as the diffuse diffraction rings in the SAED pattern. [516]

Figure 31 presents the HRTEM, TEM and SAED pattern of TL-5 specimens (A, B and C respectively) calcined at 400°C. Lattice imaging using HRTEM revealed undisturbed lattice fringes running from one end of the grain to the other. Presence of amorphous phase can also be observed as white patches, marked by arrows, in the micrograph. It can also be observed that the grains in 5 % lanthana doped titania are stacked in a more organized way compared to the 1 % lanthana doped titania. The grain boundaries are

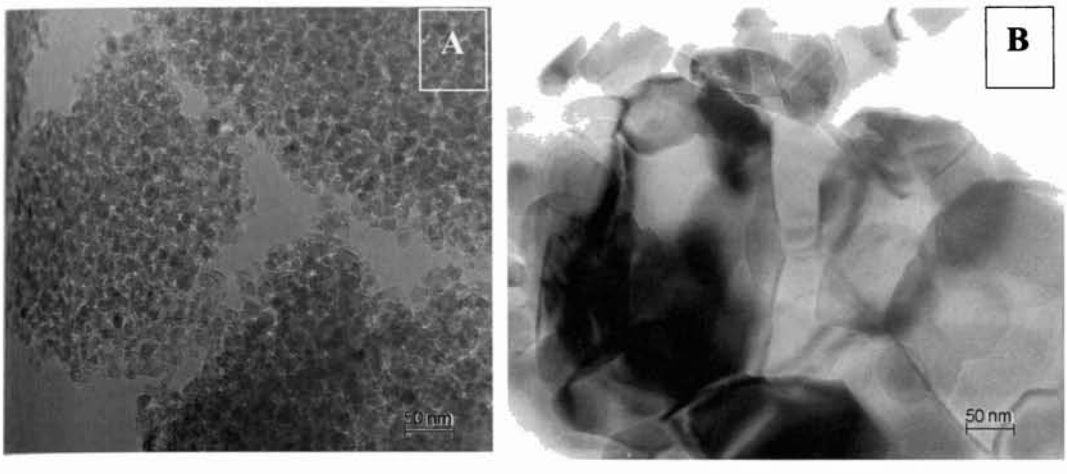

Figure 29: TEM images of (A) - undoped TiO_2 calcined at 500°C/3h. 5 nm crystallite size and 300 nm particle size, fine-crystalline and (B) - Calcined at 900°C/3h. 50 nm crystallite size and 500 nm particle size, coarse-crystalline

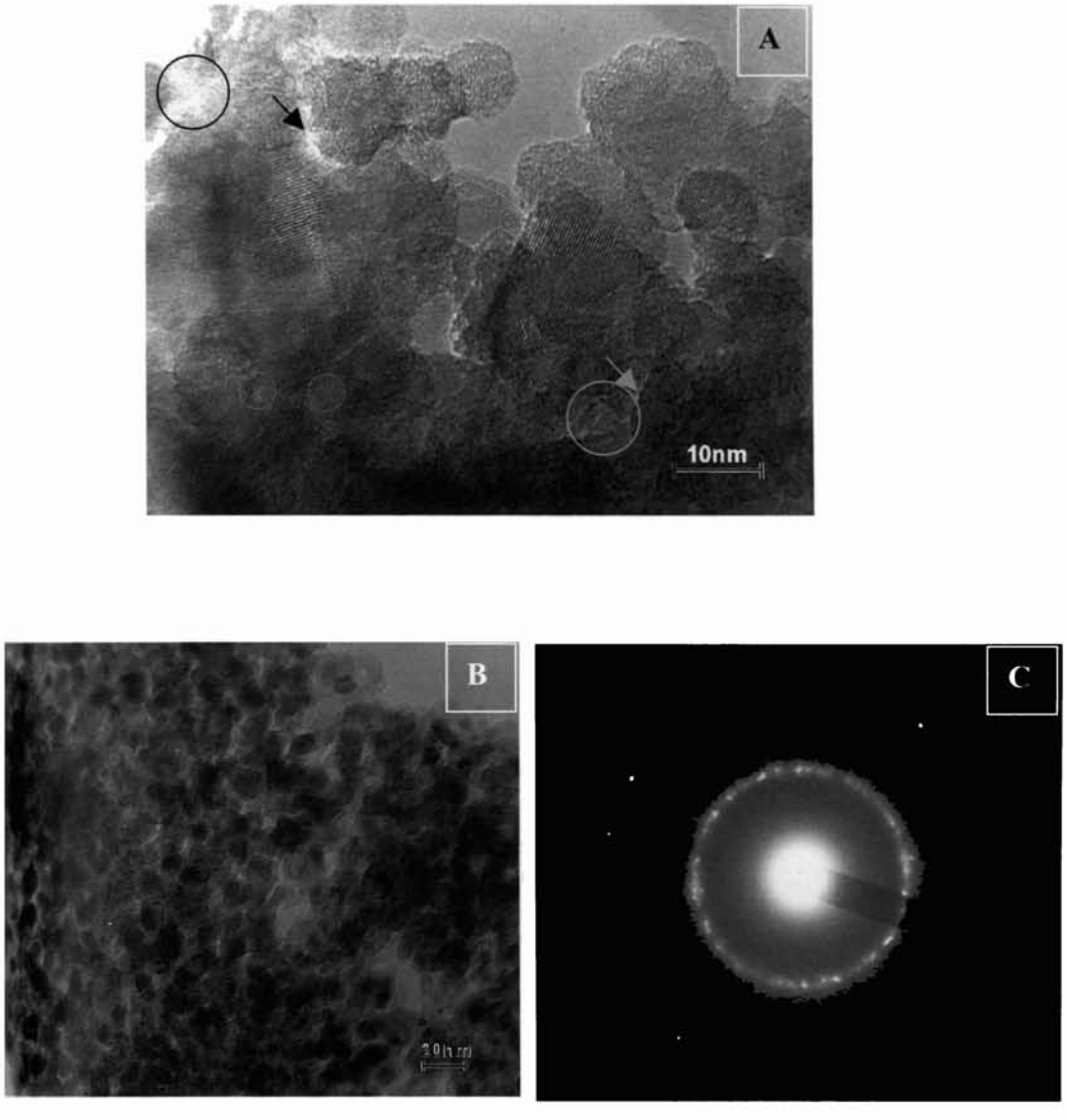

Figure 30: HRTEM (A), TEM bright field image (B) and SAED pattern (C) of TiO_2 powder calcined at 400°C for 3 h. Labelled circular portion is amorphous phase and arrow shows the pores.

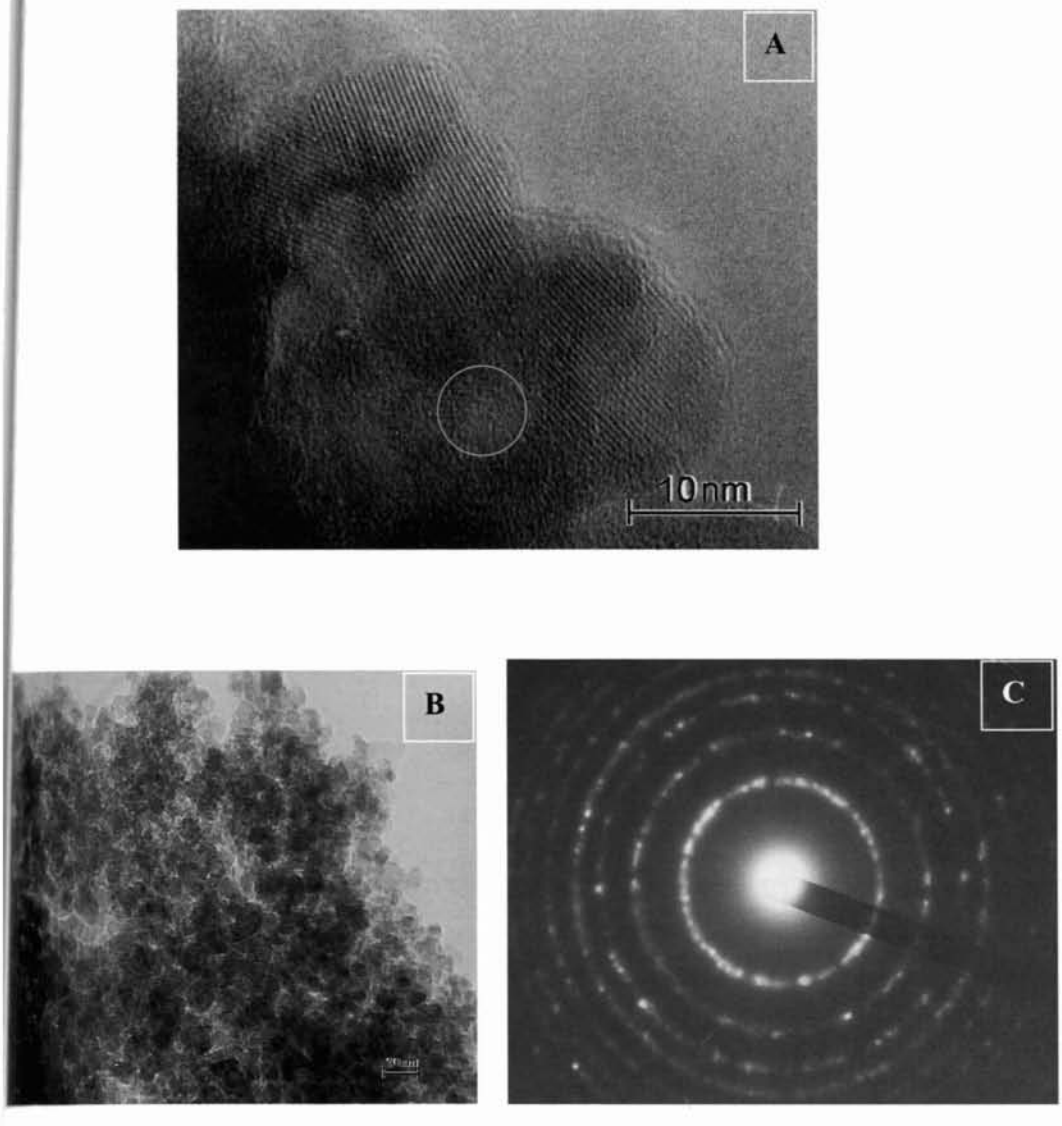

Figure 31: HRTEM (A), TEM bright field image (B) and SAED pattern (C) of TL-5 specimen calcined at 400°C. Labelled circular portion is amorphous phase.

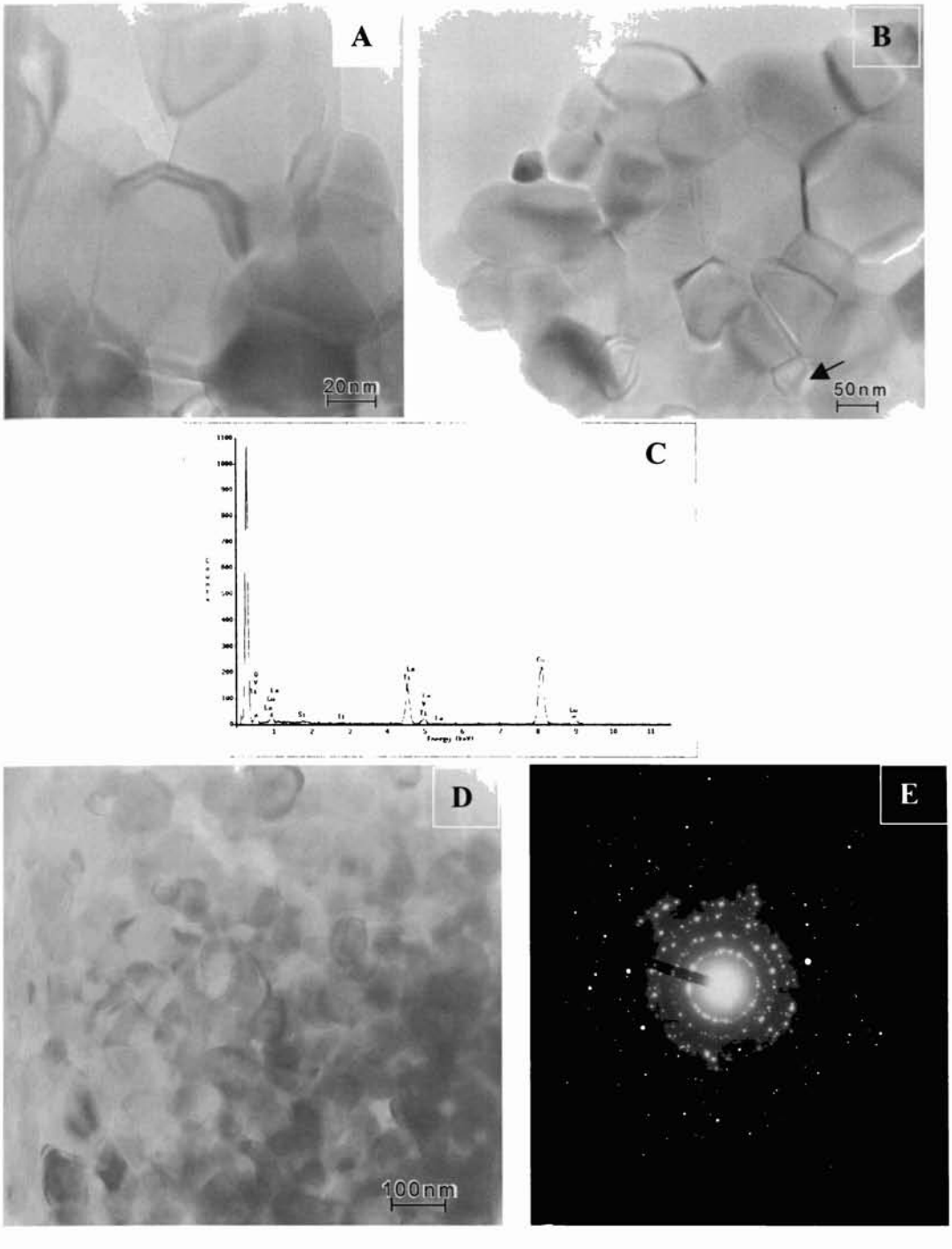

Figure 32: TEM bright field images (A, B and D); EDS (C) and SAED pattern (E) of TL-1 specimens calcined at 800°C. [Arrow indicates the pore]

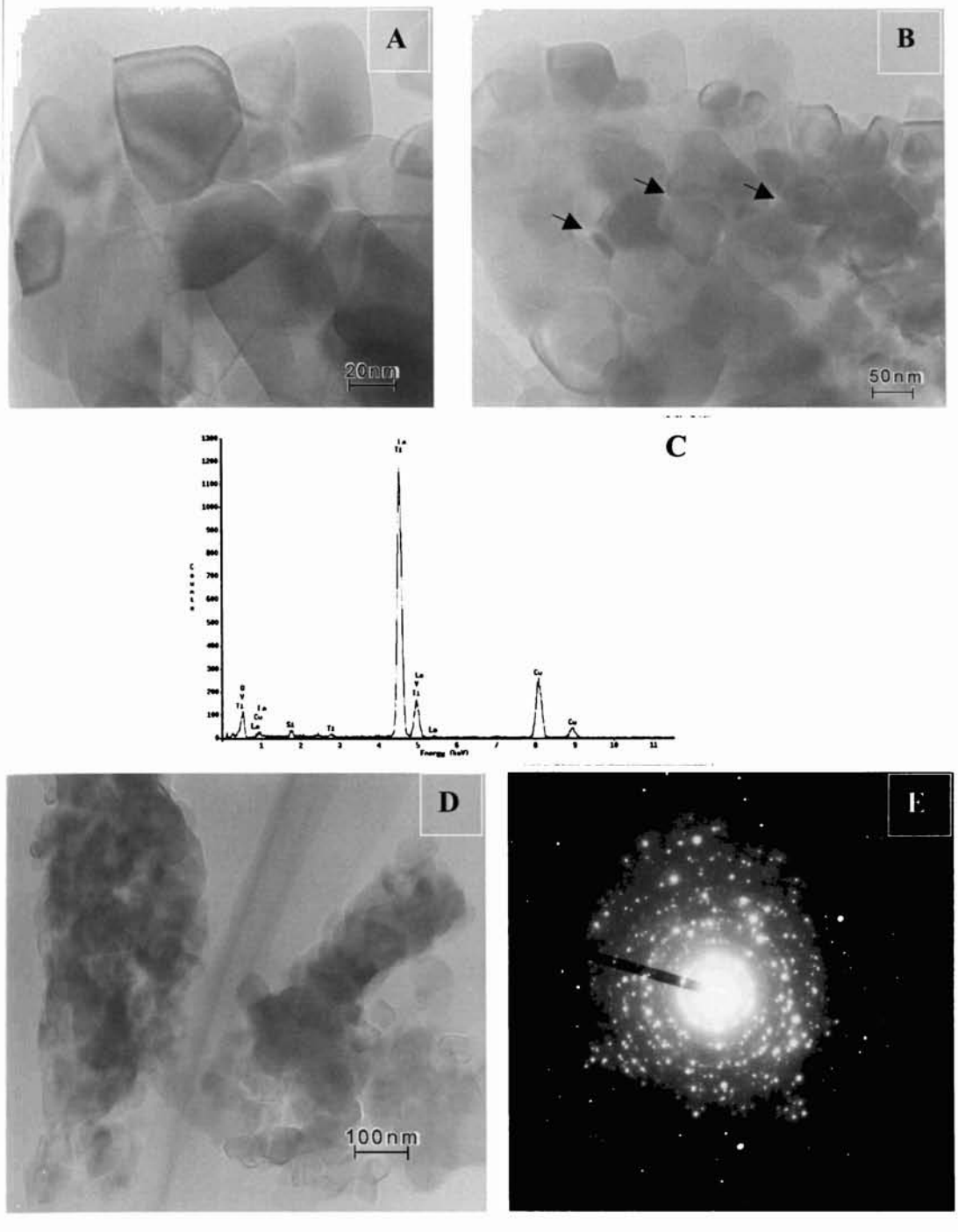

Figure 33: TEM bright field images (A, B and D); EDS (C) and SAED pattern (E) of TL-2 specimens calcined at 800°C. [Arrows indicate the pores]

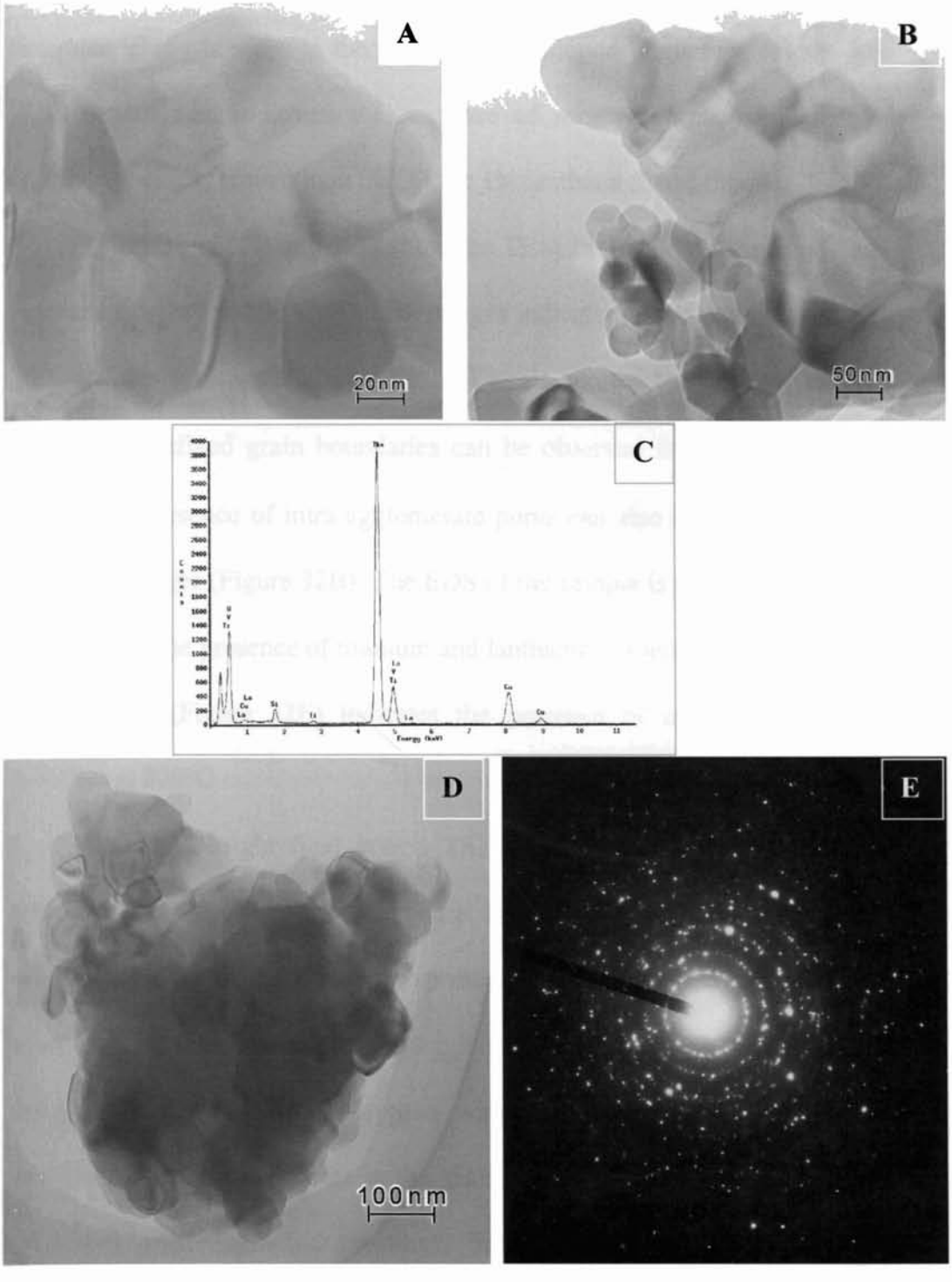

Figure 34: TEM bright field images (A, B and D); EDS (C) and SAED pattern (E) of TC-1 specimens calcined at 800°C

appearing as hairline cracks between the grains. However, the presence of amorphous phase is more in the 10% lanthana doped titania specimens. The SAED pattern also indicates the presence of more amorphous phase and smaller crystallites (grains) than that of the 1% lanthana doped titania.

Figures 32A, 32B and 32D show the TEM bright field images of TL-1 specimens calcined at 800°C. The BF images indicate the presence of ~10-100 nm crystallites (average diameter 50 nm) agglomerated to form particles of ~1 μm. Well-defined grain boundaries can be observed from the figures. In addition, the presence of intra-agglomerate pores can also be observed in the bright field images (Figure 32B). The EDS of the sample is provided as Figure 32C. It shows the presence of titanium and lanthanum atoms in the lattice. The SAED pattern (Figure 32E) indicates the presence of larger sized titania crystallites at 800°C.

The TEM bright field images (A, B and D), EDS (C) and SAED pattern (E) of TL-2 specimens calcined at 800°C are presented in Figure 33. The bright field images show the presence of ~10-90 nm size primary crystallites (average diameter 45 nm) agglomerated to form ~500 nm particles. The grain boundaries do not appear with a clear contrast in the TEM micrographs, because the atoms in the grain boundary core are not sitting on the defined crystallographic positions, but are distributed rather like in amorphous material. The higher amount of lanthana restricts the crystallite growth of titania by providing a higher diffusion barrier for the anatase-anatase grain contact. The presence of intra-agglomerate pores can also be observed in

the micrograph (marked by arrows in Figure 33B). The occurrence of intra-agglomerate pores causes the retention of surface area at higher temperatures. The EDS analysis shows that small amount of lanthanum ions have entered into the lattice. The SAED pattern provided as Figure 33E indicates the presence of highly crystalline, randomly oriented titania crystallites at 800°C.

The TEM bright field images of TC-1 specimens calcined at 800°C are provided in Figures 34A, B and D. Figure 34E shows the SAED pattern of the specimen. The grain boundaries do not appear with a clear contrast in the TEM micrographs in this image too, because the atoms in the grain boundary core are not sitting on the defined crystallographic positions, but are distributed rather like in amorphous material. The presence of ~10-100 nm size primary crystallites (average diameter 50 nm) agglomerated to form 500 nm secondary particles can be observed from the micrographs (Figure 34D). The absence of clear contrast between the grain boundaries indicates the possible commencement of sintering in the ceria doped titania samples at or below 800°C. The reduction in specific surface area for the 700°C calcined sample compared to lanthana doped titania also substantiates this conclusion. The SAED pattern (Figure 34E) indicates the presence of more or less randomly oriented highly crystalline titania crystallites. The EDS analysis shows the presence of both titanium and cerium atoms in the lattice.

3.1.7 Temperature Programmed Desorption (TPD)

The TPD of ammonia [530-531] was used to characterize the acid site distribution and furthermore to obtain the quantitative amounts of acid sites in

the specified temperature range. The distribution pattern can be classified into weak (desorption at 100-200° C), medium (300° C) and strong (400-700° C) acid sites. From the TPD result, all the lanthana doped compositions show an increased amount of total acidic sites compared to the undoped titania sample heated at 300° C (Table 9). This shows the increase in availability of adsorption sites in doped samples, making them more efficient -atalysts. Further, with increasing concentration of dopants, the amount of reactive acidic sites increases. The extent of weak as well as strong acidic sites increases with increasing calcination temperature. La^{3+} ions, if substituted in the tetrahedral Ti^{4+} site, will have a net positive charge/hole and so can accommodate a lone pair of electrons [33]. The increased amount of acidic sites of lanthana doped titania is due to the influence of substituted La^{3+} ions in the titania matrix.

Table 9: TPD results showing the amount of weak and strong Lewis acid sites

Sample	Weak site ($mmolg^{-1}$)	Medium site ($mmolg^{-1}$)	Strong site ($mmolg^{-1}$)
TU, 300°C	0.58	0.16	0.55
TU, 700°C	3.23	0.63	1.2
TL-1, 300°C	1.3	0.56	1.3
TL-1, 700°C	2.91	0.82	2.90
TL-2, 700°C	3.62	1.70	3.95

La_2O_3 doped titania has a relatively high thermal stability and contains more of strong acid sites, while undoped titania has more of weak acid sites. Generally, all the samples show an increase in the total - acidic sites with calcination temperature. This may be due to the fact that at higher temperature the physically adsorbed water and residual organics are removed, increasing the accessible surface area.

3.1.8 Photoactivity Evaluation

Photoactivity evaluation was carried out for the samples calcined at temperatures ranging from 80°C to 1100°C. Degradation of methylene blue [532] was taken as the measure of photoactivity. The detailed experimental technique is provided in Section 2.2.5. The decolourisation time was noted for each sample. Table 10 presents the time taken for the decolourisation of methylene blue for each sample (qualitative) under UV light and Table 11 under sunlight. Monitoring the maximum absorbance of the UV exposed titania-methylene blue solution at regular time intervals using UV-Vis spectrophotometer accomplished the quantitative photodegradation analysis. The qualitative analysis indicates TL-1 calcined at 700°C as the best photocatalyst among the samples, which is showing the fastest decolourisation of methylene blue. TC-1 sample calcined at 600°C was found to be showing the next highest activity. 500°C calcined TU shows the highest activity among the undoped samples. Figures 35a-c show the methylene blue photodegradation curves of TU, TL-1 and TC-1 calcined at 700°C. The graphs provided in the right hand side show the maximum absorbance of methylene blue as a function of time of exposure.

Table 10: Photoactivity evaluation results of different titania samples with respect to the decolourisation of methylene blue on exposure to UV light

Sample	Degradation time in ***minutes*** under UV light at different temperatures							
	RT	300°C	500°C	600°C	700°C	800°C	900°C	1000°C
TU	80	45	10	120	>180	--	--	--
TL-1	85	40	25	15	5	40	60	>180
TL-2	85	40	30	20	15	50	55	>180
TL-5	80	45	30	25	20	50	55	>180
TC-1	90	50	30	10	25	70	150	>180
TC-2	90	55	35	15	35	70	160	>180
TC-5	90	55	35	20	35	60	165	>180
TS-1	85	50	40	25	45	75	170	>180
TS-5	90	50	40	25	20	55	160	>180
Degussa P25					20			
Hombikat UV 100					30			

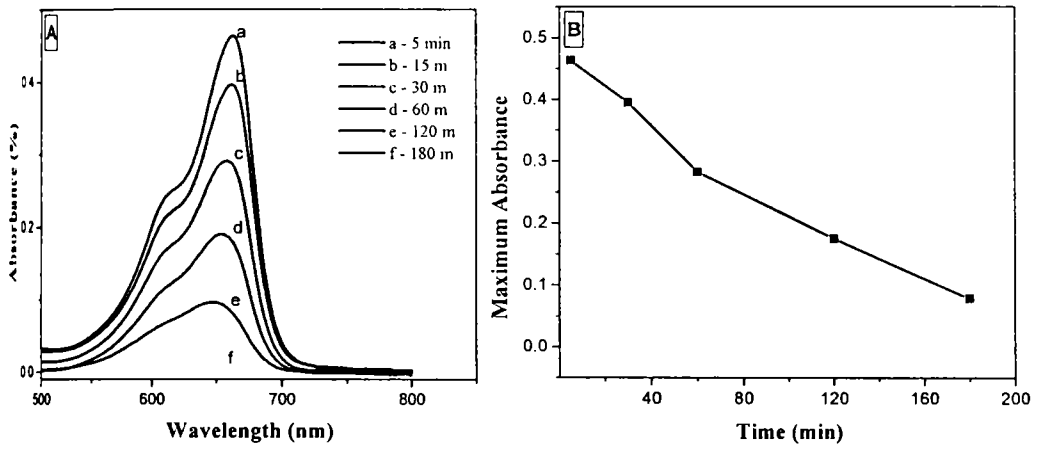

Figure 35a: A - Optical absorbance spectra of TU calcined at 700°C showing the degradation of methylene blue. The spectra were recorded at regular intervals of UV light irradiation; and B – The degradation profile showing the absorbance maximum plotted against time of exposure

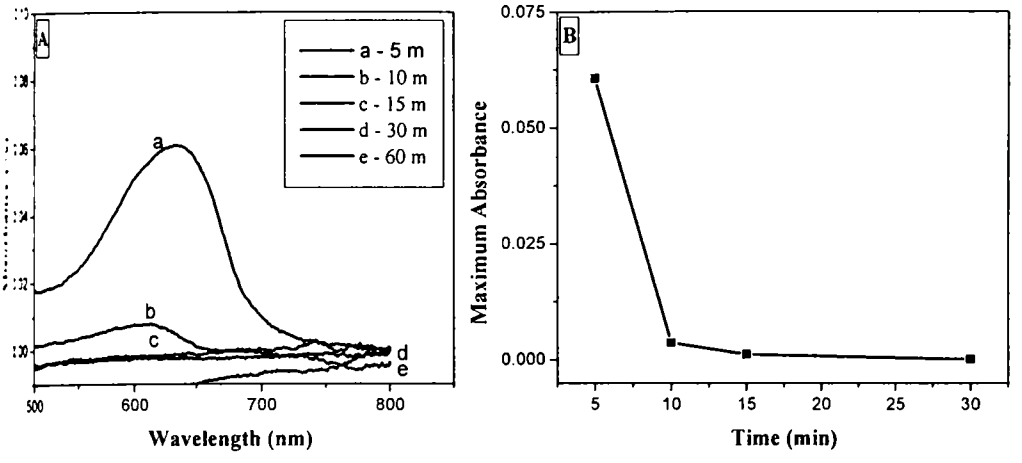

Figure 35b: A - Optical absorbance spectra of TL-1 calcined at 700°C showing the degradation of methylene blue. The spectra were recorded at regular intervals of UV light irradiation; and B – The degradation profile showing the absorbance maximum plotted against time of exposure

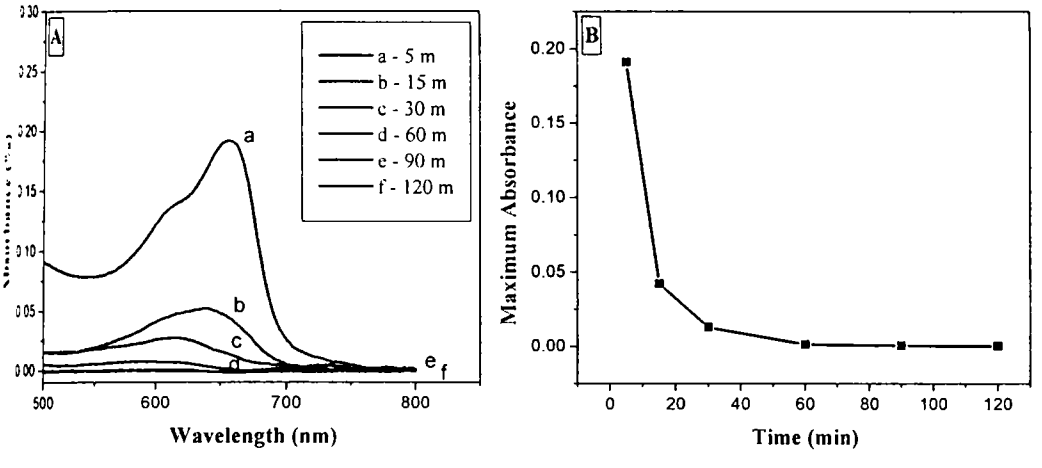

Figure 35c: A - Optical absorbance spectra of TC-1 calcined at 700°C showing the degradation of methylene blue. The spectra were recorded at regular intervals of UV light irradiation; and B – The degradation profile showing the absorbance maximum plotted against time of exposure

Table 11: Photoactivity evaluation results of different titania samples with respect to the decolourisation of methylene blue on exposure to sunlight

Sample	Degradation time in ***minutes*** under sunlight at different temperatures							
	RT	300°C	500°C	600°C	700°C	800°C	900°C	1000°C
TU	75	45	10	80	>180	--	--	--
TL-1	80	40	30	25	10	30	50	>180
TC-1	95	55	30	15	35	50	120	>180
TS-5	100	55	40	30	30	35	120	>180

3.2 *Discussion*

Sol-gel process, obviously, is a means to produce homogeneous materials of specific end uses. However, the tuning of the product characteristics necessitates an exquisite control over the preparative parameters. [193] In the present case, TTIP is highly reactive towards water and hence needs additional control against hydrolysis. Acetic acid is a suitable stabilizer, which effectively stabilizes the titanium isopropoxide moiety by either modifying its coordination sphere or by ester formation. [533] In the present work, an excess acetic acid than the calculated stoichiometry was employed to act as a stabilizing agent and an acid catalyst as well.

The formation of Ti-O-RE bonds was established by FTIR spectra. A possible capping mechanism on doping with lanthana and / or ceria as their respective nitrates can be assumed as responsible for the Ti-O-RE bond formation. The larger $\Delta\nu$ between the symmetric and asymmetric vibrations of

(COO-) is a direct indication of the heterodentating effect of acetate groups, [491,495] which holds the Ti and La / Ce atoms intact throughout much of the sol-gel process. The whole sequential chemical processes are supported by the HSAB (Hard and Soft Acids and Bases) principle, [504-505] wherein the hard Lewis acids such as Ti^{4+}, La^{3+} and Ce^{3+} (highly oxophilic) are bonded with the hard Lewis base; acetic acid. The particle size reduction occurring due to capping is also evidenced from the particle size analysis results, where the lanthana and ceria doped sols are showing a smaller sol particle size compared to the undoped sol measured after fixed aging period.

In the sol-gel process, the preparative processes and parameters have direct influence on the final structural and textural properties. The acidic hydrolysis conditions, by adding excess acetic acid, adopted in the present process leads to the formation of chain like Ti-O-Ti linkages rather than a random network formation [193] consistent with the base hydrolysis systems. However, the incorporation of lanthana and / or ceria as their respective nitrates leads to a capping mechanism, which is supposed to be responsible for the enhancement of properties in the present process.

In the molecular level sol preparation process, i.e., the hydrolysis-polycondensation process, basically the reactions occurring can be written as follows

$$Ti(OR)_4 + H_2O \longrightarrow Ti(OR)_3OH + ROH \quad (1)$$

$$Ti(OR)_4 + Ti(OR)_3OH \longrightarrow Ti_2O(OR)_6 + ROH \quad (2)$$

$$Ti(OR)_3OH + Ti(OR)_3OH \longrightarrow Ti_2O(OR)_6 + H_2O \quad (3)$$

Reactions 2 and 3 are called alcolation and oxolation reactions, respectively. Both reactions are believed to take place by an associative nucleophilic substitution, which makes electronegativity and size of the alkoxy groups a rate-determining factor. According to Sanchez *et al*, [534] the hydrolysis rate has been controlled by using either large branched alkoxy groups, or using solvents as well as stabilizing agents. The dependence of hydrolysis rate on pH of the solution has also been reported. [208] In this work, the experiments were carried out using TTIP as precursor. The stabilization of TTIP was done with the addition of acetic acid, which is reported to be a good chelating agent by many researchers. [192-193, 491-493] In fact, a calculated excess amount of acetic acid than the stoichiometry was employed to act as a stabilizing agent and as an acid catalyst as well. The excess acetic acid, in presence of excess water (350 mole %) at equilibrium, will exist as ionized acetate and H^+ ions and as solvated acetic acid monomers along with the chelated acetate moieties. These H^+ ions are being adsorbed on the chelated acetate oxygen. The partial reduction in electron density thus developed on oxygen will be subsequently compensated by the cleavage of the Ti-O (acetate) bond. The chemical sequences taking place in the process are presented in scheme 1.

In the present preparative procedure, RE nitrate aqueous solution is added to the acetic acid stabilized, partially hydrolyzed titanium isopropoxide solution after 1 h of hydrolysis. At this point of time the tentative structure of the sol will be, with titanium ions having a six-coordinated sphere (sol-gel chemistry). According to Livage *et al*, [232] during hydrolysis, the OPr^i groups

are preferentially hydrolyzed leaving the chelating / bridging acetate ligands remain bonded to titanium throughout much of the condensation process. Therefore, in the subsequent hydrolysis-condensation process in presence of lanthanum and/or cerium ions, there could be a selective hydrolysis of acetate ligands and the cleaved acetate oxygen will in turn coordinate with the lanthanum ions (hard Lewis acid) and / or highly oxophilic Ce^{3+} ions. This bridge formation will effectively hold the Ti^{4+} and La^{3+}/Ce^{3+} moieties through much of the reaction sequences that finally lead to the Ti-O-RE bond formation (Scheme I).

In the sol-gel process, the formation of nanoparticles depends essentially on the preparative methods and experimental conditions adopted for the particular process. In order to analyse the effect of RE dopants on the enhancement of nanocrystalline nature of titania, crystallite sizes of the titania powders heat treated at different temperatures were calculated from the line broadening of powder X-ray diffraction data using Scherrer equation. The results indicate a decrease in crystallite size with respect to the dopant addition. The undoped titania while shows an anatase-rutile mixture with anatase crystallite size ~39.09 nm and rutile crystallite size ~65.44 nm at a calcination temperature of 700°C, doping with 1% La_2O_3 resulted in the reduction of crystallite size to ~16.81 nm and 1% CeO_2 to ~18.91 nm. This could be attributed to the capping effect of the La^{3+}/Ce^{3+} ions in the solution stage, which probably terminates the particle growth of Ti-O-Ti network in the sol

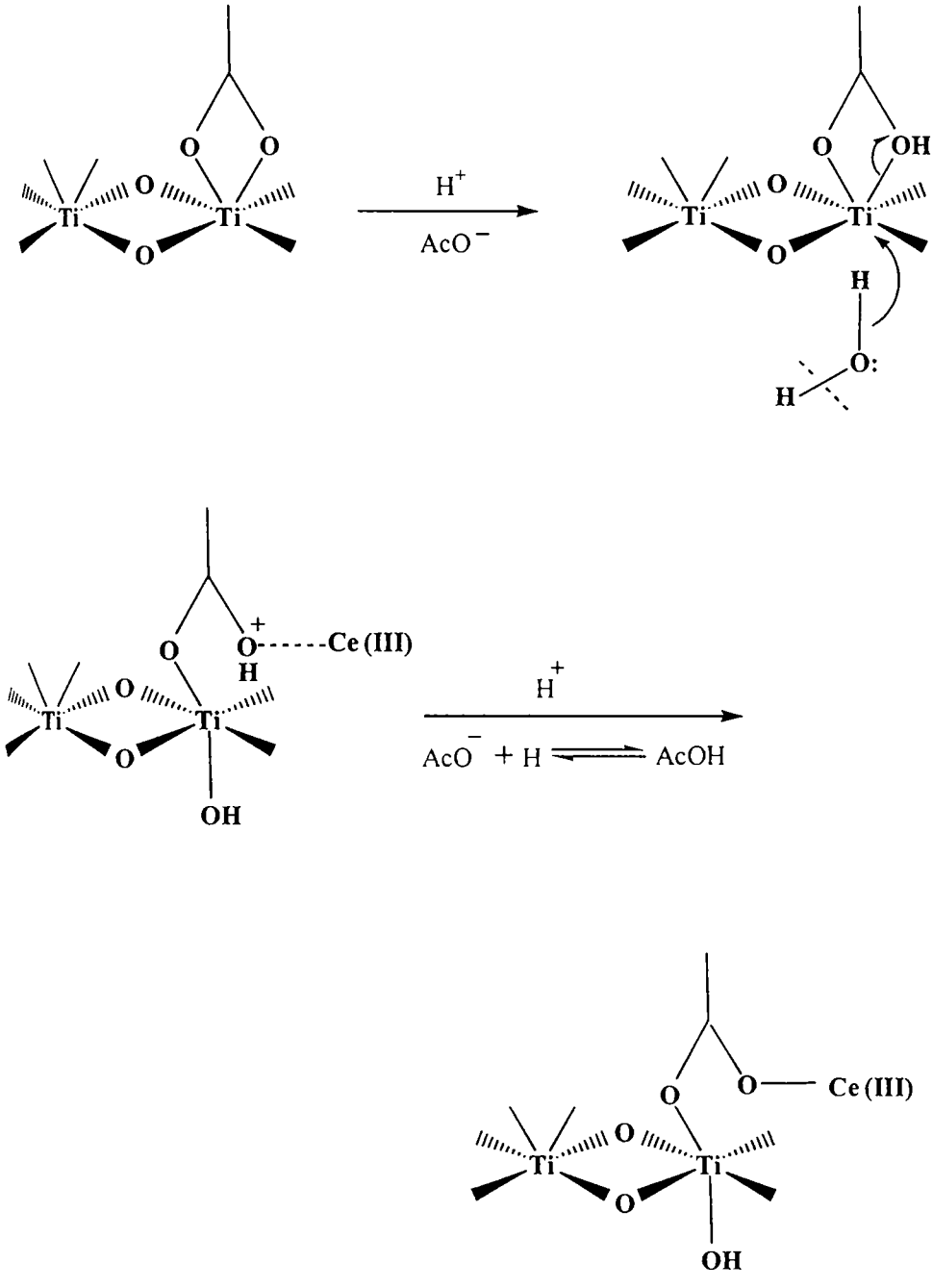

Scheme I

stage (capping), which in turn results in the reduction of crystallite size at higher temperatures by either forming Ti-O-RE bonds or segregation of lanthana and/or ceria ions at the grain boundaries. Here, we propose the heterodentate ligand formation by acetic acid molecules as a cause for the accomplishment of Ti-O-RE bond formation.

As is already discussed, the structural and textural evolution influenced by the dopants indicates a stabilization of the anatase phase towards higher temperatures. This is associated with an inhibition of crystallite growth as well as the retention of porosity at higher temperature, which also corroborates with some earlier reports. [347-349] Hague and Mayo [525] proposed the formation of intra as well as inter-granular pores as the reason for the high temperature textural stability. Our results also indicate the formation of more amount of intra as well as inter-granular pores on doping and subsequent stabilization of the same at higher temperatures.

Many researchers have extensively studied the anatase phase stability and different arguments have been offered. The major studies have carried out by Zhang and Banfield, [315,320-321] Shannon and Pask [286,313] and by Gribb and Banfield. [302] According to them, the major factors influencing the anatase – rutile transformation are presence of impurity atoms and the dependence of particle size on the rutile phase nucleation. The degree of particle packing also was reported to be one of the factors that influences the anatase to rutile transformation, of course only to some extent, by Xia *et al* [535] and by Mackenzie. [197] The present result also corroborates with these earlier

observations and this indicates the suitable structural modifications occurred as a result of doping with lanthana and/or ceria.

The sol particle size analysis results obtained in the present study indicate the reduction of particle size as well as the formation of particles with narrow size distribution on doping. The powder X-ray diffractograms indicated the formation of smaller size hydrous anatase crystallites for undoped TiO_2 samples compared to the doped titania compositions at 80°C, and this leads to the faster crystallite growth and corresponding low temperature anatase to rutile phase transformation for the undoped sol-gel titania samples prepared through the present preparative procedure. However, the dependence of particle size on the phase transformation observed in our study does not corroborate with the earlier reports by Banfield *et al* [302,321] as well as by Hirano *et al*, [536] where the critical size limit was 14 nm and 70 nm respectively for anatase to rutile transformation. The 'critical size limits' observed for our samples were ~39 nm for TU, ~47 nm for TC-1 and ~42 nm for TL-1. The difference in critical size limit for the transformation is supposed to depend on the nature of metastable anatase e.g., contained impurities, the nature and the amount of dopant, crystallinity, surrounding phases and so on. The phase transformation from metastable anatase to stable rutile phase can occur when the thermal energy is high enough to overcome the nucleation energy, which has been proposed for the similar case of phase transformation from metastable tetragonal ZrO_2 to stable monoclinic form by Behrens *et al* [537] and Yoshimura. [538] The larger grained microstructure may have had a smaller nucleation barrier

for transformation because of the increase in microstructural defects- e.g., dislocations and residual stresses generated locally by the thermal expansion anisotropy within the grain, as insisted in the case of metastable tetragonal ZrO_2 by Chen *et al* [539] and Becher *et al.* [540] In the present study, the enhancement of the stabilization of the anatase phase is due to the existence of the homogeneously distributed RE oxide particles on the grain boundaries in case of RE oxide doped TiO_2 systems; and, the surrounding amorphous silica phase through the Ti-O-Si interface as evidenced by the FTIR spectra in case of the SiO_2-doped TiO_2 system. [394] The RE oxides are distributed on the grain boundaries through the Ti-O-RE interface as evidenced by FTIR spectral studies as well as by intercalation. Further, the presence of brookite phase could not be identified from XRD and other techniques and therefore, the phase transformation may be assumed to follow through a two-step reaction.

As per XRD analyses, the anatase phase nucleation [501] is occurring at the solution stage itself, owing to the specific alcohol-free preparative route adopted in the present case. However, the required small amount of alcohol is always present in the system, primarily along with the TTIP procured and then produced as the side product of hydrolysis (alcolation). The hydrous anatase phase produced through the present sol-gel process was associated with more defects in the framework, which are titanium and oxygen vacancies. [541] Ozawa *et al* [542] as well as Ferreira *et al* reported the formation of nonstoichiometric titania through sol-gel process, mainly Ti^{3+} species, owing to the production of more hydroxyls. [543-545] These defects are responsible for promoting the anatase

-rutile transformation to a lower temperature, explaining the presence of rutile phase in undoped TiO_2 calcined at ~700°C together with the anatase phase.

The major issue involved in photocatalysis is to increase its quantum efficiency by suppressing the recombination of photogenerated charge carriers. [546] Firstly the crystallinity of titania must be improved. Earlier reports indicate that the sol-gel titania films possess good anatase crystallinity, which provides a high photocatalytic activity. [84,118,547] Addition of La_2O_3 and/or CeO_2 enhances the nanocrystallinity of TiO_2 further by inhibiting the temperature dependent crystallite growth and also stabilizes the anatase phase towards higher temperatures. In typical photocatalytic reactions, reduction and oxidation concurrently take place at adjacent reaction sites, which in turn gives raise to unique products. [548] In addition, the excited electrons must be separated spatially from holes, because the characteristic time required for the reduction (μs) is generally much greater than that for oxidation (~100μs). [549] Therefore the aim is to trap the excited electrons in surface trap sites generated by the sol-gel process and especially by doping. Due to the large number of electron surface trapping states in nanocrystalline particles, electrons localize preferentially at the TiO_2 surface. [550-552] This argument is based on the report by Henglein on nanoparticles. [524] He reported that the traps for electrons and holes are the dangling bonds, adsorbed species etc. present on the surface of nanometer particles. The fate of the charge carriers generated by light absorption is strongly dependent on the existence of these traps. [524]

X-ray absorption spectroscopic studies have shown that in TiO_2 nanocrystallites are actually co-ordinatively unsaturated Ti sites that are formed upon surface re-construction of nanoparticles. [553] EPR studies have shown that the majority of photogenerated electrons are trapped on the under co-ordinated surface sites. [554] Due to the large number of electron surface trapping states introduced by the present sol-gel process, electrons localize preferentially at the TiO_2 surface. [550-552]

Trap formation

In addition to the intrinsically formed Ti^{3+} species in the present process, the other significant factor that results in the defect formation is dopants such as lanthana and/or ceria. The lanthana atoms with its larger ionic size compared to Ti atoms (0.068 pm) will have a tendency to replace the intrinsically formed Ti^{3+} ions compared to the Ti^{4+} sites, in view of its comparatively larger size. In this case the Ti^{3+} ions will be displaced to the interstitial, which in turn will be diffused to the grain boundary on heat treatment. The Ti^{3+} species on the surface of grains will enhance the activity of the material by acting as electron trapping sites and forms highly oxidizing $OH^{\cdot}$ free radicals on the surface. [29,119,120, 237,554-556] This results in the reduction of recombination of photogenerated electrons and holes, [557] and improves the photoactivity. Further, the presence of lanthana as La^{3+} in the matrix enhances the concentration of Lewis acid centers as evidenced by TPD analysis. However, the incorporation of ceria is not as effective as lanthana in the production of Lewis acid sites.

This is because Ce^{3+} species incorporated in the titania matrix will be oxidized to Ce^{4+} species on calcination of the gel. [558]

The maximum photoactivity was shown by 1% lanthana doped TiO_2 sample calcined at 800°C. This could be attributed to the presence (existence) of maximum number of Ti^{3+} ions available for reaction (surface Ti^{3+} ions) at this temperature. The proposed explanation is based on the diffusion of atoms as a function of temperature. The dehydration, organic residue removal and dehydroxylation will be completed at around 450°C as evidenced from thermogravimetric analysis. On further increase of temperature, the amorphous phase will be completely transformed to crystalline phase as evidenced by the TEM analysis. In case of undoped TiO_2, due to its smaller grain size and corresponding higher surface energy than the doped titanias at 80°C, the crystallite growth takes place rapidly and the anatase to rutile transformation also happens at a lower temperature as confirmed by XRD analysis. But in presence of dopants like lanthana and/or ceria incorporated in the matrix, the increased diffusion barrier for the grain contact of anatase crystallites that required for the phase transition will inhibit the crystallite growth and corresponding phase transformation. The anatase to rutile phase transition is associated with the rupture of two of the Ti-O bonds and subsequent structural reorientation. The Ti-O-RE bonds formed as well as those RE species distributed on the grain boundaries are responsible for the higher diffusion barrier.

A possible explanation for the inhibition of crystallite growth based on lanthana species (applicable to ceria also due to their close resemblance in properties) is as follows. The ionic radii value [559] of doped La_2O_3 is in between that of Ti^{4+} (0.068 nm) and O^{2-} (0.132 nm). Therefore, the La^{3+} (0.1016 nm) should either replace the Ti^{4+} site or go to the interstitial. From the FTIR spectral analysis we found that some of the La^{3+} ions replace some Ti^{3+}/Ti^{4+} lattice sites. Because of the mismatch of the ionic sizes of Ti^{4+} and La^{3+} (0.068 and 0.1016 nm respectively), there is also a chance for the La^{3+} ions to go to the interstitial. The slow rate of grain growth for lanthana doped titania compared to the undoped one may also be attributed to the presence of interstitial lanthana atoms. The anatase phase is fairly stable up to 940° C in case of lanthana doped titania. On the other hand, the A→R transformation starts at as early as 670° C in case of undoped titania. The slow rate of grain growth of the former may be due to the presence of interstitial La^{3+} ions which probably have got segregated in the grain boundaries of anatase titania grains and increases the diffusion barrier at the titania-titania grain contact which is needed for the grain growth process. Also, those La^{3+} ions that have replaced the Ti^{3+}/Ti^{4+} sites will have a stabilizing effect on the Ti-O bond. Being more electropositive, La^{3+} species will render its electron density to O^{2-} so that O^{2-} can use this increased electron density to strengthen the bonding between the less electropositive Ti^{4+} ions [559] linked to it. This stabilization of Ti-O bond will in turn retard the A→R transformation temperature because the A→R transformation needs the breakage of Ti-O bonds and in this case it is difficult

to break the Ti-O bond due to the increased bond strength rendered by the La^{3+} ions. In case of undoped titania, the atomic mobility with respect to temperature will be higher compared to the lanthana and/or ceria-doped titania because of the higher probability of Ti-O bond breakage. The diffusions of atoms also will be higher due to the same reason, which could increase the grain growth rate. [306,519,521] It is interesting to note that the addition of even 1 % lanthana could bring out this considerable improvement in properties, which is attributed to the specific synthesis route followed.

The amorphous phase, which is detrimental to the photoactivity by acting as possible recombination sites, will be converted to crystalline phase on heat treatment. [315,518] However, the undoped TiO_2 due to its low diffusion barrier will be crystallized and subsequently transformed to rutile phase at a faster rate. As already mentioned, the A→R transformation occurs by the diffusion of atoms mainly through the grain boundaries of nanograins. Sol-gel process is reported to be effective in producing large amount of local defects, like grain boundaries owing to its capability to produce large amount of hydroxyls. The hydroxyls will stabilize the Ti^{3+} species, which is responsible for the high activity. An oxygen vacancy will be generated for each of the two Ti^{3+} species formation for charge balance. In the case of sol-gel titania, Ti^{3+} ions are also formed during calcination as a result of the reduction of Ti^{4+} to Ti^{3+} by organic residues [237,556] such as alcohol and unhydrolyzed alkoxide group. Organic residuals draw oxygen atoms from surrounding TiO_2 network.

Ti^{3+} ions on the surface may trap the photogenerated electrons, which are transferred from Ti^{3+} surface states to O_2 adsorbed on active sites of Ti^{3+}. This results in the reduction of recombination of photogenerated electrons and holes. The formation of a larger amount of Ti^{3+} ions contributes largely to the enhancement of the photoactivity of the TiO_2 films.

When La^{3+} replaces the Ti^{3+} species, the number of oxygen vacancies will be unchanged, but the formation of active Ti^{3+} species on the surface of the grains will be enhanced, which in turn enhances the activity. Further, the highest activity is exhibited by TL-1. The proposed explanation for this is provided in the following discussion. The concentration of intrinsic defects (Ti^{3+} ions) formed by the present sol-gel process may be in the order corresponding to the amount of 1% La_2O_3 introduced into the matrix. As the concentration of La_2O_3 increases, there will not be any improvement in the amount of Ti^{3+} species at the grain boundaries since all of the Ti^{3+} species have already been replaced by the 1 % La^{3+} species (approaximately). This also confirms the principal effect of surface trap sites, which is introduced by doping, on the photoactivity. Also the highest activity is exhibited by the 700°C calcined 1% La_2O_3 doped-TiO_2 sample and 600°C calcined 1% CeO_2 doped-TiO_2 sample. As the temperature increases further, activity shows a subsequent decrease. This indicates that 700°C as the optimum temperature at which all of the Ti^{3+} species are located at the surface through diffusion. Further increase in temperature initiates the oxidation of Ti^{3+} species to Ti^{4+} species, that decreases

the electron trapping sites and hence the activity shows a gradual decrease. In addition, above 700°C the sintering of titania grains commences as is evidenced from both TEM and BET specific surface area analysis, which also decreases the activity.

CeO_2-doped TiO_2 sample on the other hand shows a different mechanism. The calcination temperature shows remarkable effect on the solid-state reaction and phase transformation. Since the precursor of ceria is $Ce(NO_3)_3$. $6H_2O$, during the synthesis and calcination in air, Ce^{3+} ions can easily be oxidized to Ce^{4+} ions. [558,561]

$$Ce^{3+} \longrightarrow Ce^{4+} + e^-$$

This electron can reduce a Ti^{4+} species to Ti^{3+} species, which in turn increases the surface trap sites at higher temperatures and consequent high temperature photoactivity. However, the sintering of CeO_2-doped TiO_2 commences at a lower temperature than La_2O_3-doped TiO_2, which indirectly indicates its effect on the inhibition of crystallite growth and surface area reduction as well as the enhancement of photo activity compared to the latter. The effect was found to be in the order $La_2O_3 > CeO_2$.

The retardation of A→R transformation rate by lanthana and/or ceria addition can be explained in view of the structural imperfections occurring as a consequence of their addition to the titania matrix. The hydrous anatase phase produced through the present sol-gel process was associated with more defects

in the framework, which are titanium and oxygen vacancies. [543-544] The formation of nonstoichiometric titania through sol-gel process, mainly Ti^{3+} species, owing to the production of more hydroxyls was also reported by Bokhimi *et al* [545] as well as Ferreira *et al.* [211] These defects are responsible for promoting the A→R transformation at a lower temperature, explaining the presence of rutile phase in undoped TiO_2 calcined at ~700°C together with the anatase phase. On doping with lanthana and/or ceria, the anatase crystallite growth is inhibited and at higher temperatures such as 700 - 900°C, titania exists in the nanocrystalline anatase form with little amorphous phase. The high surface to volume ratio enhances the diffusion of charge carriers, which increases the concentration of surface active sites at these specific temperatures depending on the extent of influence of particular dopant. The enhanced accessible reactive surface sites, as evidenced also by TPD, favour a higher activity at these temperature ranges. The highest photoactivities obtained for the doped samples at these temperature ranges are consistent with the above results and hence corroborates with our conclusion.

On comparing with some of the earlier reports (Table 12), we can see that our compositions are superior to those studies. The present process could produce highly active nano titania with the addition of only 1% by wt of lanthana and/or ceria, which is attributed to the specific preparative route adopted.

When lanthana or ceria is added as dopants they terminate the Ti-O-Ti network formation by forming Ti-O-RE bonds. So the grain boundaries

have the abundance of RE species, which is distributed as an amorphous phase rather than being in specific crystallographic places as confirmed by TEM analysis. The presence of RE species in the grain boundary inhibits the temperature dependent grain growth. In general, nanosize titania particles show higher photocatalytic activities than the bulk, due to their large surface area per unit mass and volume and facilitate the diffusion of excited electrons and holes toward the surface before their recombination. [562] Among the crystalline phases of titania, anatase is reported to exhibit the highest activity. [84,118,547] Our results also corroborate with these earlier reports. The highly crystalline La_2O_3-doped anatase TiO_2 obtained by calcination to 700°C shows the highest activity and it is also comparable with the commercial titania samples.

Table 12: Available literature on lanthana and/or ceria doped titania systems and their comparison with the present results

Reference	System	Surface area (m^2g^{-1})	Crystallite size (nm)
LeDuc *et al* [387]	5 wt% La_2O_3-doped TiO_2 (450°C)/25 days (Degussa P25)	50	25
Gopalan and Lin [349]	16.5 wt% La_2O_3-doped TiO_2 (450°C)/3 h	184	9
Present study	1 wt% La_2O_3-doped TiO_2 (700°C/3 h)	52	16.81

3.3 *High Surface Area Titania Through Co-doping-Leaching Process*

High surface area and controlled porosity in the required (micro / meso) range is the primary requirement for an efficient catalyst / photocatalyst. The tuning and/or tailoring of porosity is a skillful task in the preparation of catalysts. The unsupported catalysts having considerably high surface area with controlled ordered porosity have been accomplished recently by templating methods, [262-266] where applying thermal energy has eliminated the templates. However, this requires a critical control over the heat treatment procedure wherein the creation of carbon impurities is very much involved. Even though, the template approach is very much appreciated in application fields like energy storage and site specific selective catalysis, particular systems with specific end uses may like to circumvent the carbon impurities, which could be detrimental to its activity. It has been illustrated that the photocatalytic activity of the amorphous titania was negligible, [442] thus mesoporous titania prepared by templating approach with amorphous framework is not suitable to be used as high efficiency photocatalyst. The same drawback is relevant for supported catalyst surfaces as well. In view of this, in the present work, silica is employed as an alternative to the organic templates and after gelation and heat treatment is selectively eliminated from the parent doped titania matrix. This preparative route has produced a very high surface area titania with meso porous texture even at a higher temperature, 700°C. Highly crystalline, thermally stable

anatase phase was retained at this temperature, where the pore walls and matrices were found to be highly crystalline. Furthermore, the anatase phase in the co-doped system was found to be stable upto 1050°C, which indirectly shows the possible retention (inhibition of surface area reduction) of surface area upto this temperature. This is because, surface area reduction occurs primarily by phase transformation assisted sintering.

The template [262-266] method-derived titania systems, however, retain its amorphous phase to much higher temperatures compared to the other titania systems, owing to the interfering residual carbons. A possible structural collapse and resultant surface area reduction could be the consequence at high temperatures. There are several reports on mesoporous titania that has comparable surface area and pore size distribution. [175,210,217,267] The thermal and chemical stability of such high surface area materials will be low owing to their high surface reactivity. [564] This will restrict the material application at high temperatures. High surface area titania has also been synthesized by many methods by many researchers. Kasuga *et al* [392,564] indicated the synthesis of titania-silica mixtures involving a leaching process and obtained specific surface area of 150 m^2g^{-1} at 600°C. Also Sang *et al* [393] reported the preparation of mesoporous titania photocatalyst by selective dissolving of titania-silica binary oxide using NaOH solution. They obtained a high surface area of 339 m^2g^{-1} at 500°C by this process with a microporous texture. Here, the selective chemical leaching has been effectively utilized for the tailoring of mesoporous texture in the titania framework. The influence of lanthana on the enhancement

of the structural as well as textural properties and also on the enhancement of photoactivty was exploited for the preparation of thermally stable active titania. In the present work, co-doping with silica has also produced high surface area La_2O_3-doped TiO_2 xerogel. The amorphous silica was leached out from the precursor using 5% NaOH solution. The results are presented and reasonable correlations and conclusions are discussed.

The Brunauer-Emmet-Teller specific surface area (SSA) and pore volume of undoped, doped, co-doped and co-doped-leached titania samples are presented in Table 13. A three-fold increase in SSA was observed after leaching. The co-doped sample without leaching showed a SSA of 79 m^2g^{-1} at 700°C. Leaching with 5% NaOH aqueous solution enhanced the SSA to 231 m^2g^{-1}. The total pore volume was increased from 0.1045 ccg^{-1} to 0.234 ccg^{-1} by leaching. The 5% silica doped titania, on the other hand shows a SSA ~55m^2g^{-1} and pore volume 0.0773 ccg^{-1}. On leaching the SSA increased to 247 m^2g^{-1} and total pore volume to 0.2093 ccg^{-1}. The increase in SSA of SiO_2-doped TiO_2 is more than that of SiO_2-La_2O_3 co-doped TiO_2. This is because the silica introduces more micropores into the system. But in presence of lanthana, the distribution of silica is tailored such that a mesoporous texture is obtained. This shows the influence of lanthana on the mesoporosity development in the present process.

The porosity features of the as calcined and leached samples were analyzed using BET N_2-adsorption method as well as pore size analysis technique. [489] The results clearly indicate the formation of mesoporous texture

n leaching. This was achieved by the preferential selective removal of morphous silica phases from the solid network. The adsorption isotherms of unleached and leached titania powders are given in Figure 36. In general, all the isotherms show type IV behaviour. As is obvious from the literature, SiO_2-doped TiO_2 has the maximum microporosity among the doped titania samples. [399]

Table 13: Specific surface area and pore volume of doped and undoped TiO_2 powders obtained using the Brunauer-Emmet-Teller N_2 adsorption technique

Sample	Specific surface area (m^2g^{-1})	Pore volume (ccg^{-1})
TU	0.0879	0.0021
TL-1	51.97	0.0961
TS-5	54.96	0.0773
TSN	247.73	0.2093
TLS	79.05	0.1045
TLSN	231.0032	0.234

Compositions are based on % by wt. calculation

Doping with La_2O_3 also provides microporosity to the titania framework. However, the effect is less than that of silica. But, the co-doping increases the total porosity of the framework as well as the mesoporosity, as is obvious from the adsorption isotherms. This shows the influence of La_2O_3 on the preferential distribution of SiO_2 phase in the titania matrix. Further, leaching enhances the porosity of titania framework. The leached samples

show more mesoporous character compared to the unleached samples. Among the leached samples, 5% SiO_2-1% La_2O_3 co-doped TiO_2 sample exhibits the highest mesoporosity.

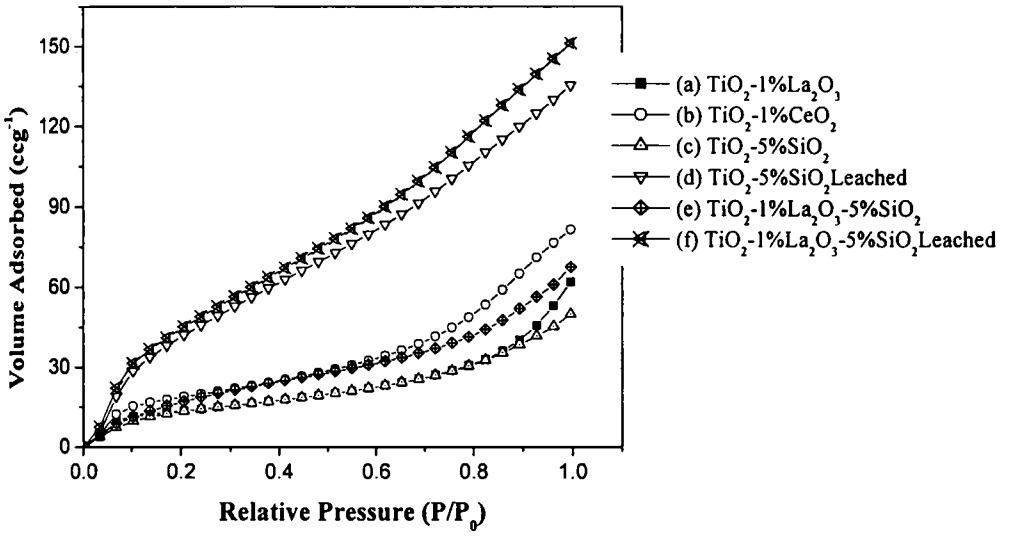

Figure 36: Adsorption isotherms of unleached and leached titania samples calcined at 700°C.

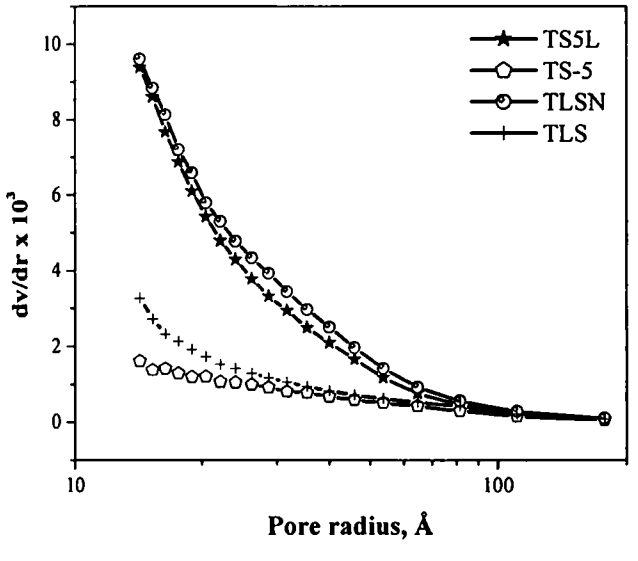

Figure 37: Pore size distribution curves of leached and unleached titania samples

Figure 37 presents the pore size distribution curves of unleached and leached TS-5 and TLS samples. The leached samples show an enhanced pore size distribution at all the porosity regions. However, the co-doped titania shows an enhanced mesopore distribution compared to the silica doped titania. This also refers to the influence of lanthana on the distribution of silica in the titania matrix.

The powder X-ray diffraction patterns of TLS and TCS samples calcined at different temperatures are presented in Figures 38 and 39 respectively. The patterns show the influence of co-doping on the retardation of titania crystallite growth towards higher temperatures. The anatase to rutile phase transformation is also retarded as a result of co-doping. In the co-doped sample, rutile phase nucleation commences only at ~1050°C, whereas the rutile nucleation started at ~940°C in the lanthana doped titania.

Figure 40 shows the XRD patterns of unleached and leached TLS specimens calcined at 500 and 700°C. The XRD was recorded mainly to know whether the chemical leaching destructs the structure of titania. Patterns indicate the retention of titania crystal structure even after chemical leaching. The crystallite sizes of the unleached and leached TLS samples calcined at 500°C are 9.55 nm and 9.89 nm respectively, and those calcined at 700°C are 10.82 nm and 10.82 nm respectively (Table 14). The slight increase in the crystallite size of the leached 500°C calcined sample can be attributed to the possible error factor that can occur in the crystallite size calculation using Scherrer equation. Further, the sharp peaks with high intensity show the

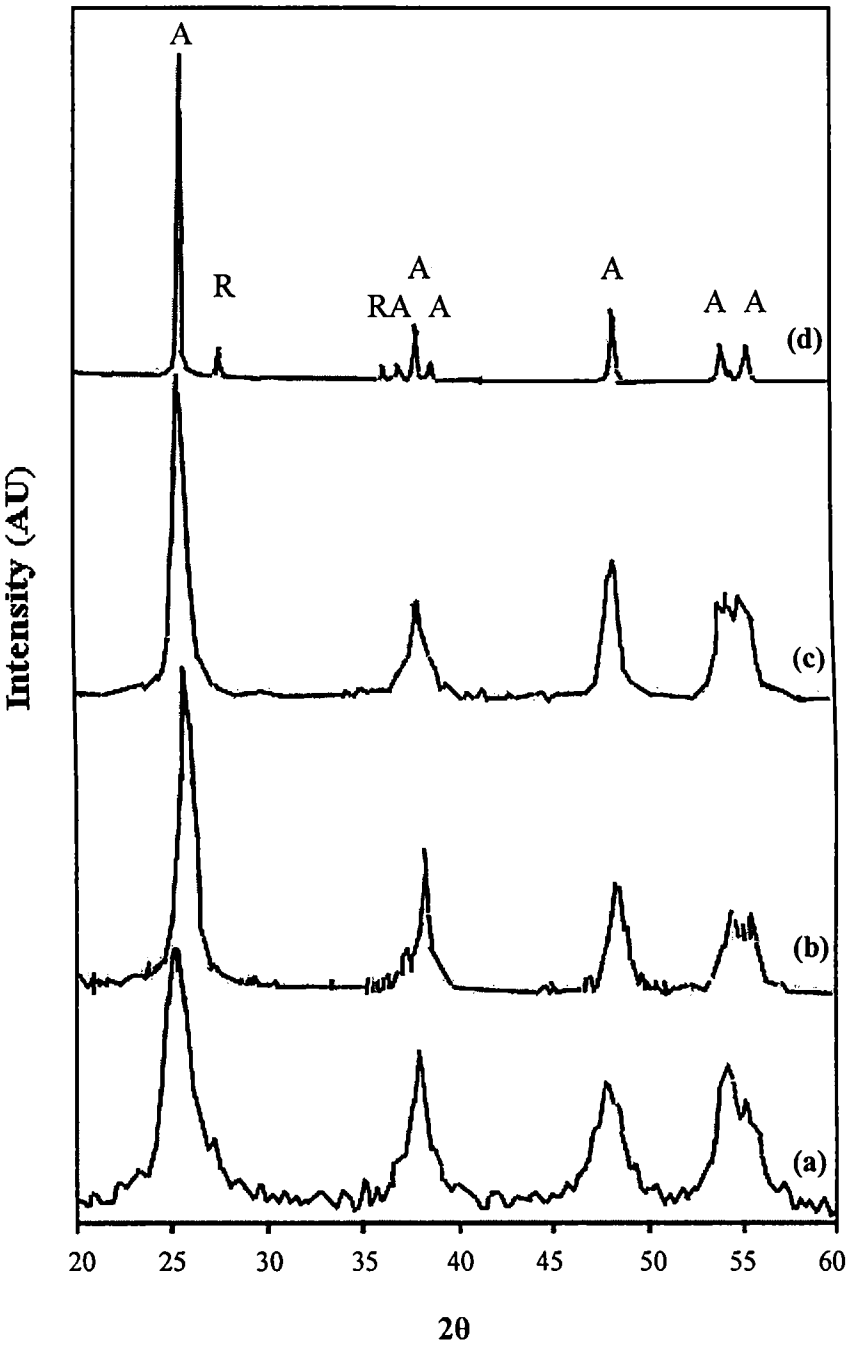

Figure 38: Powder X-ray diffraction patterns of TLS samples calcined at different temperature (a) 80°C; (b) 500°C; (c) 800°C and (d) 1050°C

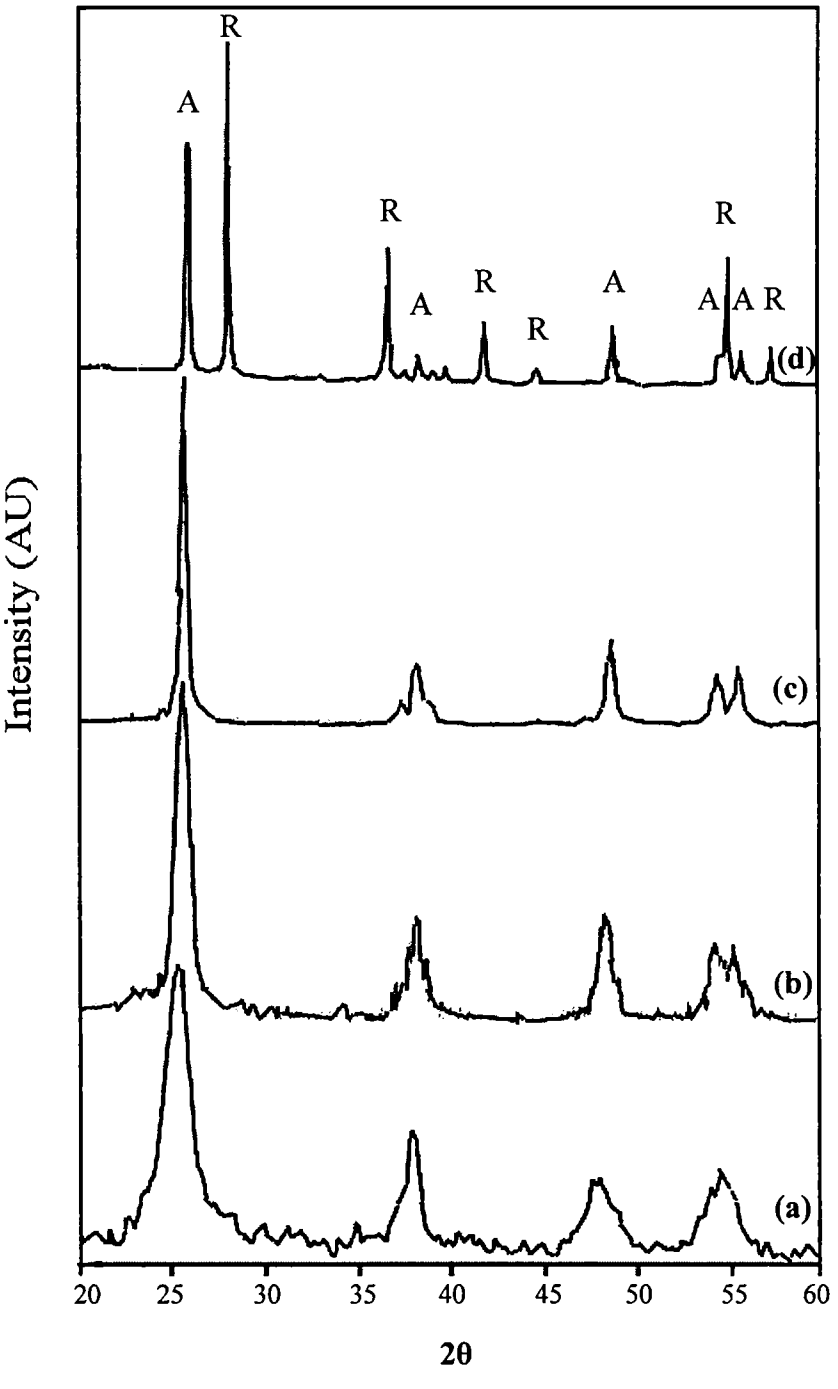

Figure 39: Powder X-ray diffraction patterns of TCS samples calcined at different temperatures. (a) 80°C; (b) 500°C; (c) 800°C and (d) 1050°C

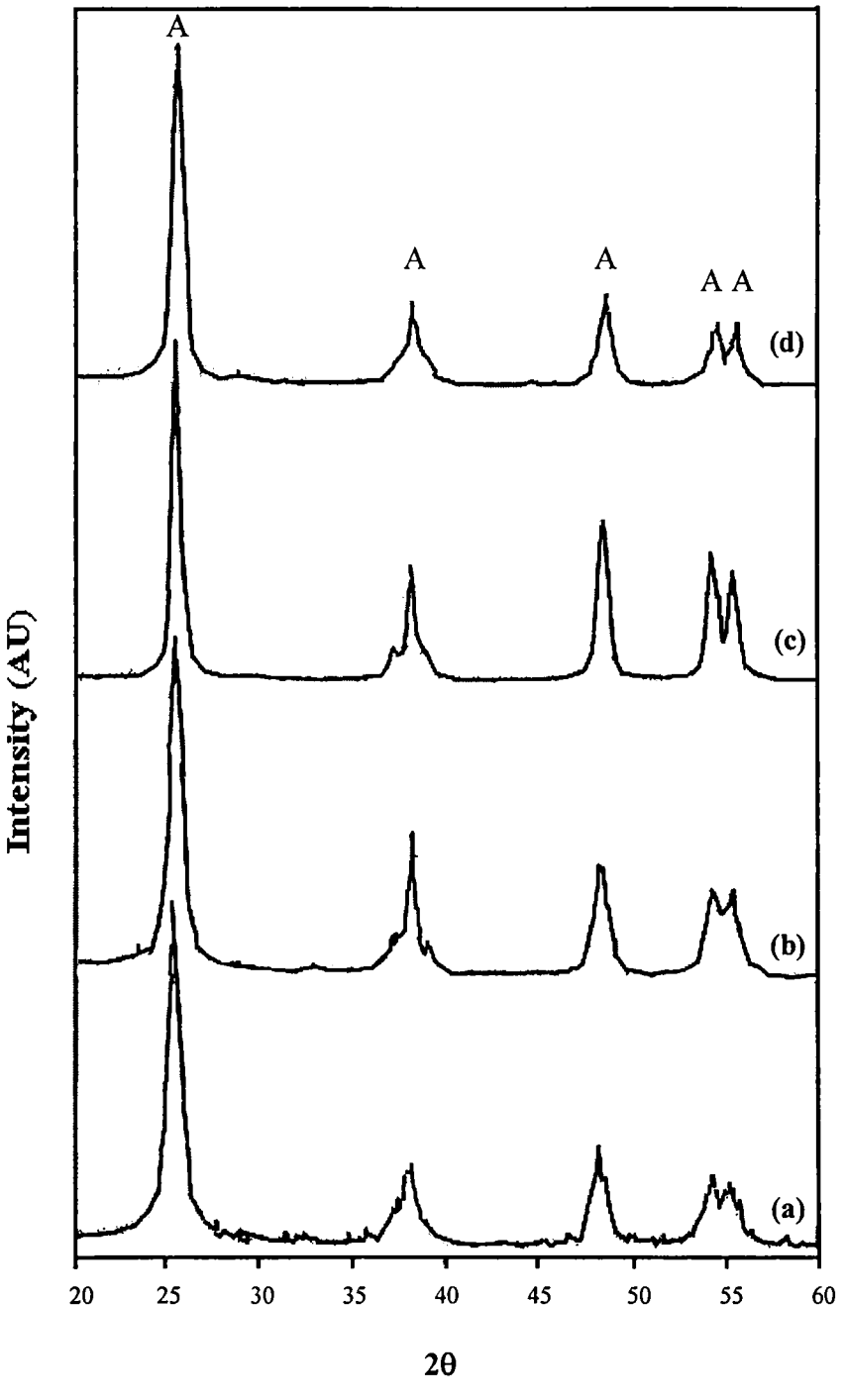

Figure 40: Powder X-ray diffraction patterns of 700°C calcined, co-doped and co-doped-leached TiO_2 samples. (a) TLS, 500°C; (b) TLSN, 500°C; (c) TLS, 700°C and (d) TLSN, 700°C

presence of highly crystalline anatase titania, which is necessary for the high activity. Therefore, it can be concluded that by chemical leaching we can obtain highly crystalline anatase phase without destructing the crystal structure of titania.

Table 14: Crystallite size (nm) of anatase titania before and after chemical leaching, calculated using the Scherrer equation

Sample	Crystallite size (nm) at different calcination temperatures			
	500°C		700°C	
	Before leaching	After leaching	Before leaching	After leaching
TLS	9.55	9.89	10.82	10.82

In order to study the effect of chemical leaching on the structural features in detail, FTIR spectra of both unleached and leached samples calcined at 700°C were taken and compared. Figure 41 presents the FTIR spectra of unleached and leached TS-5 and TLS samples as well as the undoped titania sample. All the samples show bands characteristic of the stretching and bending (1626 cm^{-1}) modes of vibrations of –OH functionalities, except undoped titania sample, which showed only a less intense band in the range 3300-3500 cm^{-1} corresponding to the stretching mode of vibration of loosely adsorbed water molecules. The spectra of the unleached samples (b and d) show shoulder peaks (overlapped) in the range 940-1100 cm^{-1}, indicative of the presence of Si-O^-, Si-O-Si and Si-O-Ti bonds. On the other hand, the shoulder peaks are almost vanished in case of the leached samples (c and e). This could

be attributed to the removal of silica phase from the titania framework. However, broad shoulder like peaks in the range 680-890 cm^{-1} can be seen in all the samples except the undoped titania sample, consistent with the presence of Ti-O-La bonds. This indicates the selective removal of silica phase from the titania structural framework. Further, all the samples show the characteristic νTi-O-Ti bands in the range 450-480 cm^{-1} compared to the undoped titania having the peak maximum at ~512 cm^{-1}, consistent with the rutile phase formation.

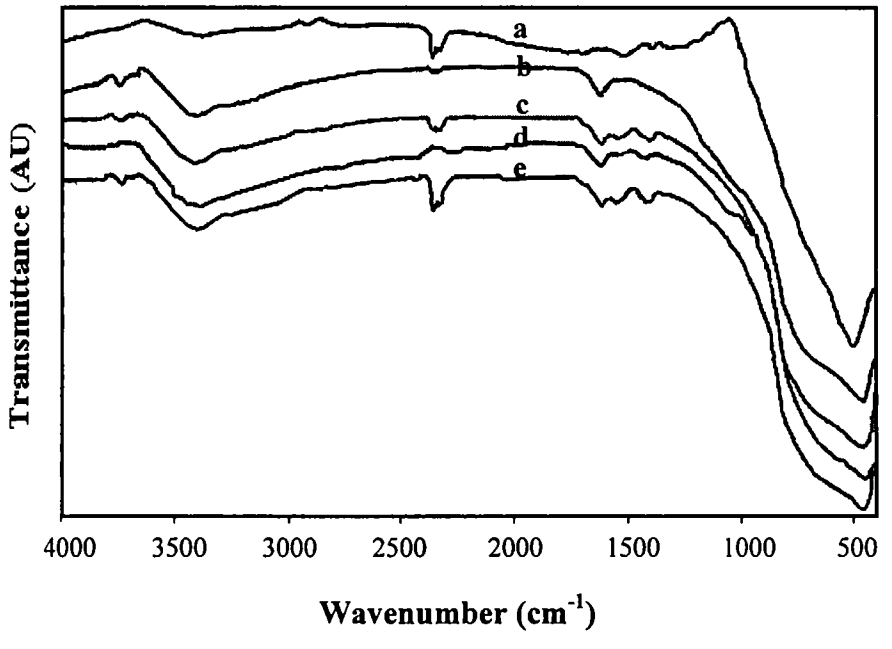

Figure 41: FTIR spectra of unleached and leached titania samples calcined at 700°C. (a) TU; (b) TS-5; (c) TS-5N; (d) TLS and (e) TLSN

The TEM bright field images of TLS calcined at 800°C are provided in Figure 42A, 42B and 42C. The effect of co-doping of lanthana and silica on the structural and textural properties of titania can very clearly be understood from

the micrographs. Compared to the earlier images of lanthana and/or ceria doped titania specimens in Section 3.1.6, the TLS specimen gives a hazy image with ~10-60 nm sized anatase crystallites (average diameter 30 nm). The haziness is due to the presence of amorphous silica phase segregated around the titania grain boundaries. The particles are not closely packed and the presence of more amount of pores can be observed. However, the cluster formation is more pronounced in co-doped specimens as can be observed from Figure 42C, which shows the presence of ~0.8-1 μm size secondary agglomerates at 800°C. Even though the primary crystallite sizes are reduced by co-doping, the silica addition enhances the particle agglomeration / clustering. As has been the cases before, the SAED pattern (Figure 42D) indicates the presence of randomly oriented highly crystalline anatase titania particles. The EDS analysis provided in the inset of Figure 42A shows the presence of titanium and lanthanum atoms in the lattice.

The TEM micrographs of TCS calcined at 800°C are provided in Figures 43A, 43B and 43C. Images A and B indicate the absence of well-defined grain boundaries in the co-doped samples. The enhancement in particle agglomeration on co-doping can be confirmed from Figure 43C. The highly crystalline nature of the titania particles can be observed from the SAED (Figure 43D) and the EDS analysis shows the presence of silicon and ceria atoms in the specimen. Even though the chemical leaching enhanced the SSA of the co-doped titania sample, it was essential to confirm the structural stability of the system, since structural collapse can drastically reduce the

activity of material. The XRD as well as TEM analyses confirmed the retention of crystal structure after chemical leaching.

Figure 44 presents the TEM bright field images as well as HRTEM images of 700°C calcined TS-5 and TLS specimens after chemical leaching. As was already mentioned, leaching was performed with a view to selectively remove the amorphous silica phase and create an ordered mesoporous texture. The TEM images look very clear compared to the unleached titania samples. Furthermore, the agglomerate size got reduced to ~300 nm on chemical leaching. The co-doped sample has a much higher amount of inter-granular porosity of mesoporous texture, which is consistent with the low SSA value compared to the leached 5% SiO_2-doped TiO_2 (TS-5) sample calcined at 700°C.

A low magnification TEM micrograph of TLS specimen is presented in Figure 45. This clearly indicates the effect of chemical leaching on the tailoring of regular mesoporous texture. Further, the order is seemed to extend upto a dimension of ~ 0.5 μ diameter. We can also see corresponding enhancement in activity for this sample with respect to the degradation of methylene blue, [565] which will be discussed in the following section.

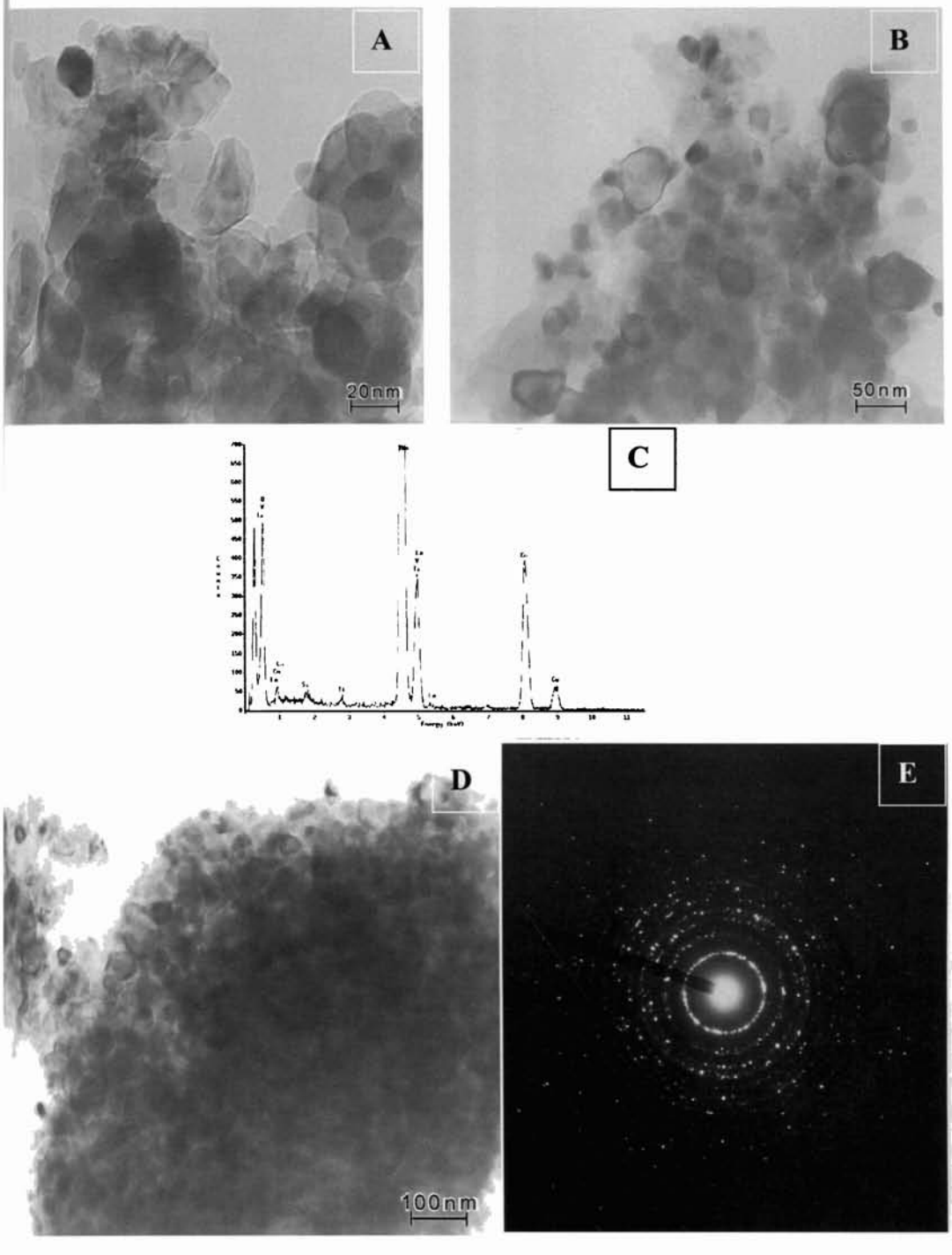

Figure 42: TEM bright field images (A, B and D); EDS (C) and SAED (E) of TLS specimens calcined at 800°C

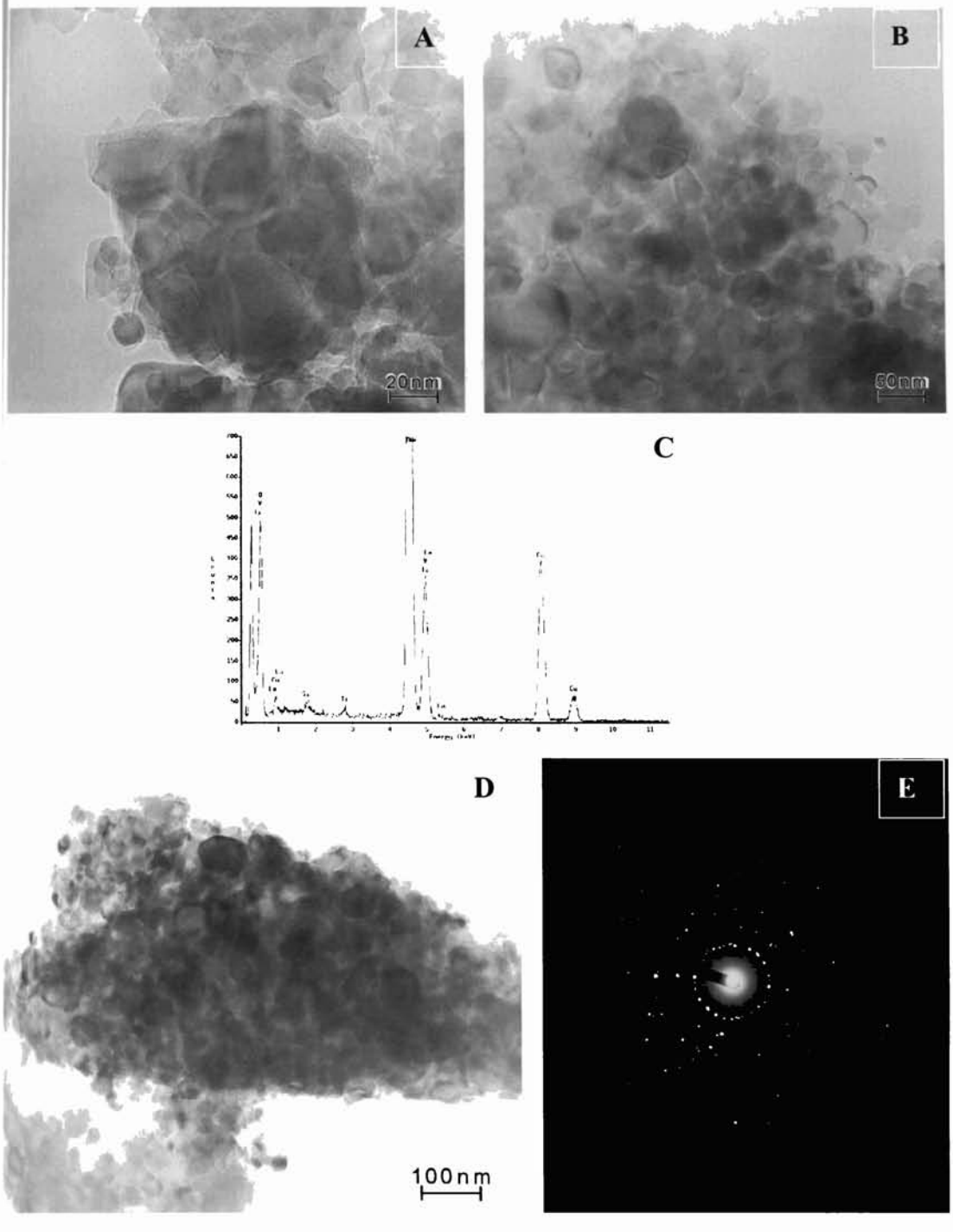

Figure 43: TEM bright field images (A, B and D); EDS (C) and SAED (E) of TCS specimens calcined at 800°C

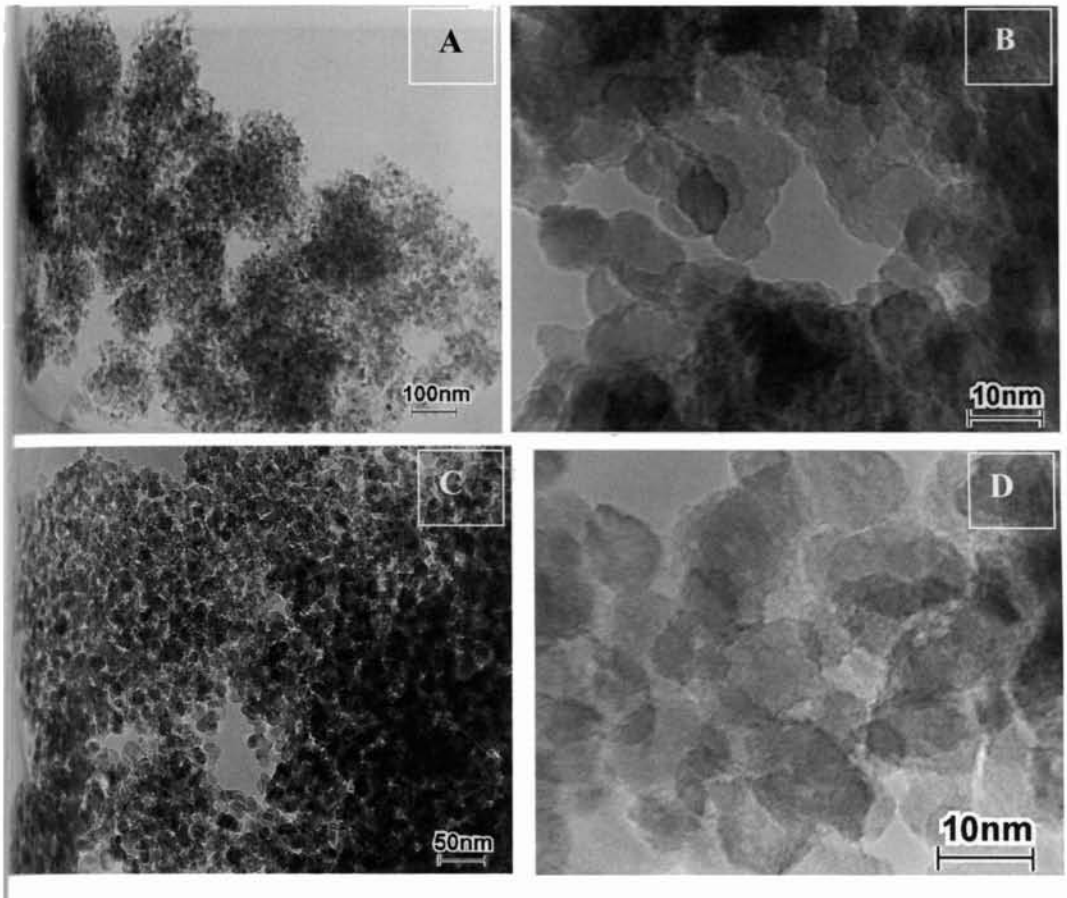

Figure 44: TEM image of (A) TS-5N calcined at 700°C; (B) HRTEM image of TS-5N calcined at 700°C; (C) TEM image of TLSN calcined at 700°C and (D) HRTEM of TLSN calcined at 700°C (All leached samples)

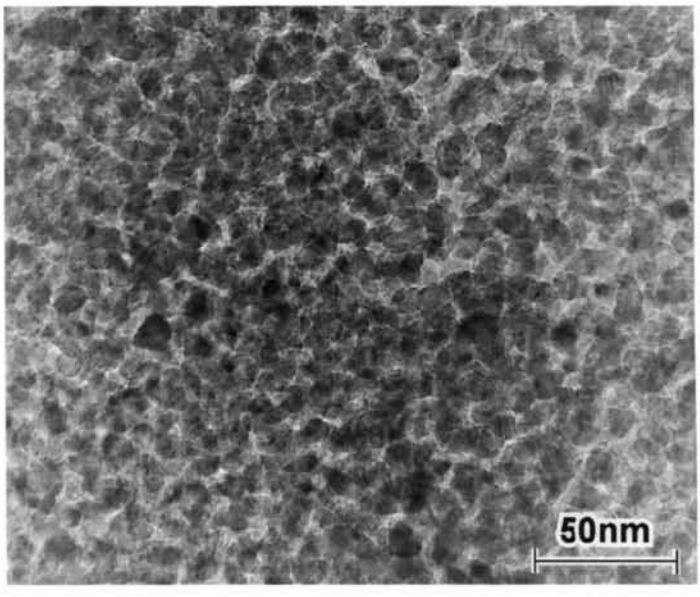

Figure 45: TEM image of TLS calcined at 700°C (low magnification) showing the effect of leaching on the tailoring of regular mesoporous texture.

3.3.1 *Photoactivity Evaluation*

Tables 15 and 16 show the methylene blue decolourisation times for different titania samples calcined at different temperatures ranging from 80°C to 1100°C. Table 15 shows the activity under UV light and Table 16 shows the activity under sunlight. The results illustrate that an enhancement in activity is observed at higher temperatures after chemical leaching. The samples showed better activity in sunlight as well. The plots of degradation profiles under UV light and sunlight are also provided in Figures 46A and 46B respectively. A photograph showing different titania-methylene blue mixtures before and after exposure to UV light is provided in Figure 47. Also in order to show the activity of titania with respect to the degradation of a common staining agent - lipstick, in presence of sunlight, photograph of the decolourisation of lipstick before and after sunlight exposure is presented in Figure 48. Lipstick films mixed with titania before sunlight exposure and after exposure are provided as A and B respectively.

Table 15: Photoactivity evaluation results of co-doped and co-doped-leached samples with respect to the decolourisation of methylene blue under UV light irradiation

Sample	Degradation time in ***minutes*** under UV light of doped TiO_2 calcined at different temperatures (°C)								
	RT	300	500	700	800	900	950	1000	1100
TS-5	90	50	40	20	25	55	160	>180	
TSN	90	50	35	25	15	45	140	>180	
TLS	90	55	40	35	30	25	35	85	>180
TLSN	90	50	30	25	20	10	5	30	150

Table 16: Photoactivity evaluation results of co-doped and co-doped-leached samples with respect to the decolourisation of methylene blue on exposure to sunlight

Sample	Degradation time in ***minutes*** under sunlight doped TiO_2 calcined at different temperatures (°C)								
	RT	300	500	700	800	900	950	1000	1100
TLS	90	55	45	40	30	20	15	15	85
TLSN	90	50	30	30	20	10	5	5	70

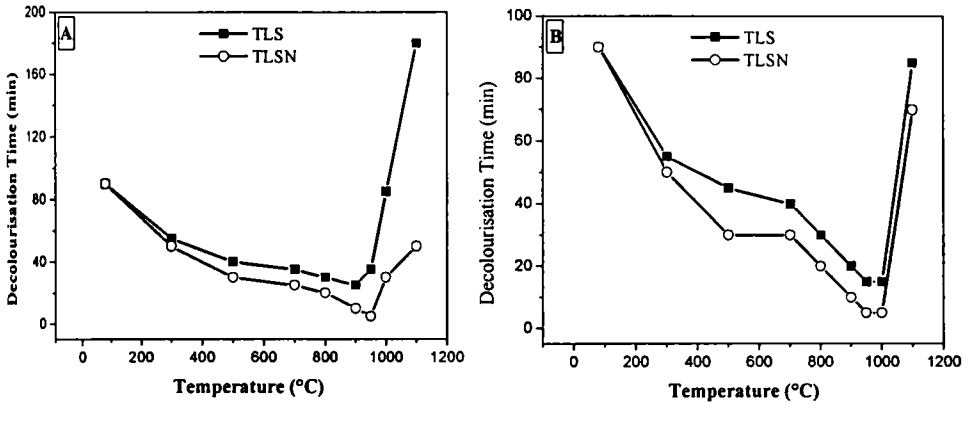

Figure 46: Methylene blue degradation profiles of TLS and TLSN samples against calcination temperature. (A) under UV light and (B) under sunlight

Finally abstracted result is presented in Table 17, which shows the major titania compositions and the temperature for optimum activity, methylene blue decolourisation time, the specific surface area at the temperature of optimum activity and phase assemblage.

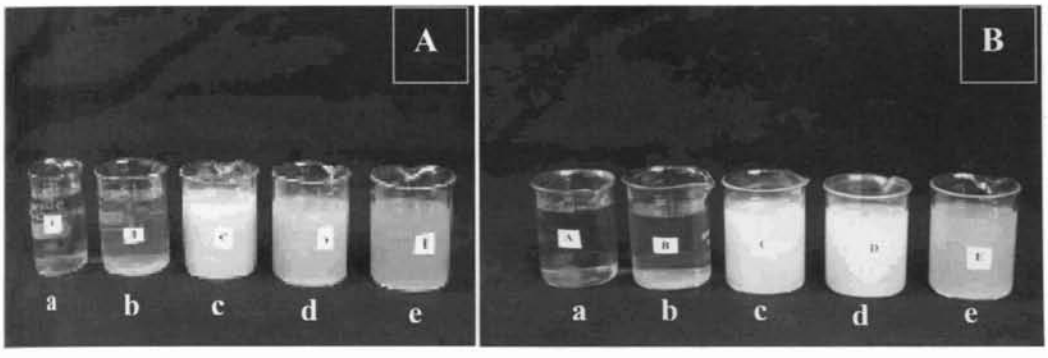

Figure 47: Methylene blue (MB) decolourisation under UV light. (A) before exposure and (B) after exposure. Beakers contain titania-methylene blue suspensions. (a) aqueous MB solution (blank); (b) MB + TU, 900°C; (c) MB + TL-1, 700°C; (d) MB + TC-1, 600°C and (e) MB + alumina suspension. Samples were exposed for a period of 30 minutes

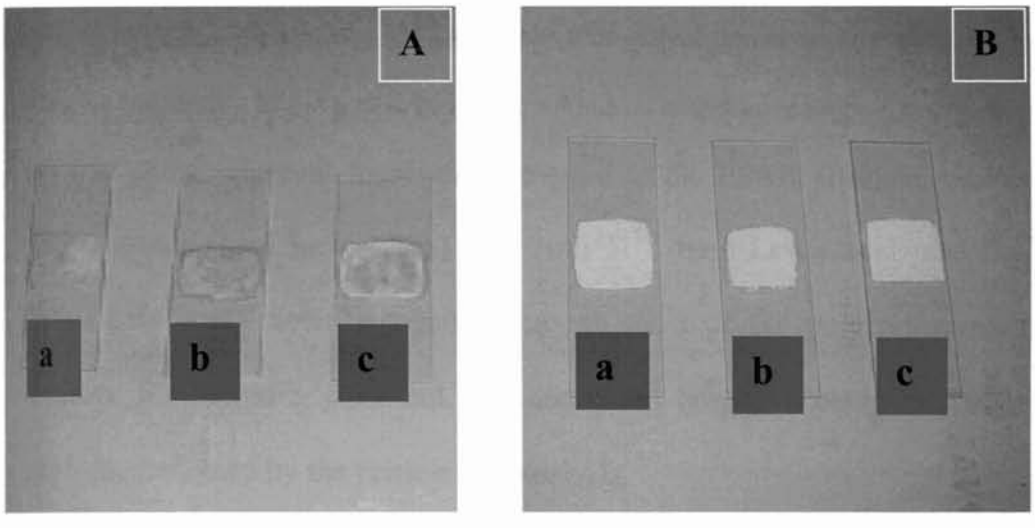

Figure 48: Degradation of stain (lipstick) under sunlight irradiation. (A) before irradiation and (B) after irradiation. (a) 1% TL-1, 700°C; (b) TC-1, 600°C and (c) alumina slurry. Samples were exposed for a period of 30 minutes

Table 17: Major results evolved from the study

Sample	Optimum calcination temperature for the highest activity	Photoactivity Decolourisation time (minutes)	Specific surface area (m^2g^{-1})	Phase assemblage
TU	500	10	120	A
TL-1	700	5	52	A
TC-1	600	10	42	A
TS-5	700	20	54	A
TLS	900	25	11	A
TLSN	950	5	43	A

3.4 Discussion

High surface area titanium oxides have also been synthesized through other methods as well. However, the sol - gel derived co-doped titania xerogel obtained by the aging and drying of the titania precursor sol has an added advantage in terms of its regularity of the structural framework, attributed to the HSAB principle, wherein acetate ligands (hard Lewis base) hold both Ti^{4+} (hard Lewis acid) and La^{3+} (hard Lewis acid) moieties together through most of the polycondensation reactions. Furthermore, silica sol also distributes homogeneously in the sol matrix as confirmed by the particle size analysis.

Sol-gel process, obviously, is a means to produce homogeneous materials of specific end uses. However, the tuning of the product characteristics necessitates an exquisite control over the preparative parameters.[193] Hydrolysis of two metal alkoxides needs separate control owing to the differing electropositivity of the metal atoms. [193] TTIP is highly reactive

towards water compared to tetraethylorthosilicate (TEOS) and hence needs additional control against hydrolysis. Acetic acid is a suitable stabilizer, which can effectively stabilize the titanium isopropoxide moiety by either modifying its coordination sphere or by trans-ester formation. [233-234] Hence, in the present work, the calculated amount of an excess acetic acid than was employed to act as an acid catalyst as well. Controlled addition of calculated amount of deionised water resulted in a stable titania sol. Separately; silica sol was prepared, using anhydrous isopropanol as the solvent and through the addition of calculated amount of water. The catalysis / photocatalysis activities of TiO_2-SiO_2 systems are reported by many researchers, including sol-gel. However, as we could observe, in the previous cases the selection of the dopants has been based on properties such as ionic radii, electrophilicity etc. Attempts on control of hydrolysis by means of the exploitation of the reactant properties were worth noting in this regard. Lanthanum ions, being hard Lewis acids, can be used with titanium ions, which are also known to be hard Lewis acids. In fact, being a hard Lewis base, acetic acid had a major role in the present sol-gel process. The modified titania xerogel is, hence, synthesized by adding the dopant precursors in the sequential order wherein lanthanum nitrate is added to the titanium isopropoxide solution first and then after 1 hr of stirring the silica precursor sol.

The mesoporous texture formation was again confirmed with powder TEM analyses (Figure 45). The crystalline nature as well as the phase composition of the material was determined from the powder XRD data. For

that, xerogels were heat treated in a stepwise manner at a range of temperatures such as 300 – 1100°C (e.g. RT to 200°C – 2°C / min; 200 to 500 – 3°C / min and 500 to 700 – 5°C / min), and soaking was carried out for a period of 3 hours in an ambient pressure and normal oxygen atmosphere. TEM images of 700°C calcined samples such as TU, (TLS), TS-5, *TS-5N* (leached) and TLSN (leached) clearly reveal the effect of co-doping as well as leaching on the structural and textural features.

The TEM analysis shows higher amount on inter-granular porosity for the TLSN sample compared to the TS-5N sample. Furthermore, the TS-5N sample shows some sinter-necking between the crystallites compared to TLSN samples, which demonstrates the structural stability of TLSN samples. The ED diffraction analyses indicate the presence of anatase phase in both the samples. The EDS analyses show the homogeneity of the structural units; wherein TS-5N sample shows Ti, Si-peaks and observes little difference between the average composition and a single grain, as confirmed by measuring five different grains. Similar experiment on TLSN sample also shows the compositional homogeneity with Ti, Si and La peaks. Furthermore, the occurrence of lattice fringes indicates the high degree of crystallinity of the materials. As a whole, the versatility of this technique offers advantages over existing routes for the production of mesoporous materials, which are limited to highly amorphous, opaque coatings and therefore do not offer the possibility of producing *thermally stable anatase structures*. Importantly, leaching is done only after the calcination step, which makes the material thermally stable. The

structural stability of the material was also confirmed by techniques such as XRD and TEM.

There are several reports on mesoporous titania that has comparable surface area and pore size distribution. The thermal and chemical stability of such high surface area materials will be low owing to their high surface reactivity. [362]

Sol-gel process, obviously, is a means to produce homogeneous materials of specific end uses. However, the tuning of the product characteristics necessitates an exquisite control over the preparative parameters. Hydrolysis of titania and silica needed separate control against hydrolysis owing to the differing electropositivity of the metal atoms. [193] Acetic acid is a suitable stabilizer, which effectively stabilizes the TTIP moiety by modifying its coordination sphere. [232-234] Hence, in the present work, the calculated amount of excess acetic acid was employed to act as an acid catalyst as well. Moreover, the selection criterion of dopant as well as control of hydrolysis – polycondensation reaction according to the HSAB principle is novel. In fact, being a hard Lewis base, acetic acid bonded to titanium ions is used to hold lanthanum ions (hard Lewis acid) throughout the sol-gel process. The co-doped titania xerogel is, hence, synthesized by adding the dopant precursors in the sequential order wherein lanthanum nitrate solution is added to the partially hydrolysed titanium isopropoxide solution first and then after 2 hr of stirring, the silica precursor sol.

The photodegradation results indicate the dependence of various factors, which are responsible for the enhanced photoactivity. They are crystallinity of the material, crystallite size, amorphous phase content, amount of defects, the optimum diffusion temperature that makes the surface saturated with the active sites and/or trap sites, phase assemblage, suitable doping and optimum dopant concentration. All are equally important and the order does not mean any hierarchy of their importance. Even though lanthanum and cerium being rare earth elements and also having almost similar physical constants, lanthanum is showing the higher performance as a dopant for titania with respect to the improvement of almost all the parameters as structural and textural characteristics and also the photoactivity. The highest activity for the La_2O_3-doped TiO_2 may be due to the maximum number of Lewis acid sites generated as a result of lanthana doping. On the other hand, the comparatively lesser activity of ceria may be due to its isovalent nature at higher temperature with titania. The Ce^{3+} ions present at lower temperature will be transformed (oxidized) to Ce^{4+} species on high temperature heat treatment, which reduces the number of Lewis acid sites in the titania matrix.

The highest activity is consistent with the smaller crystallite size and also the high crystallinity of titania. The effect of crystallinity on the photoactivity can be very well understood from the results. At lower temperatures the activity was lower and on increasing the temperature further, the activity increases, reaches maximum and then decreases drastically. As the temperature increases, the amorphous to crystalline transition takes place and

further increase of temperature results in phase transition. The amorphous phase is reported to be detrimental to photoactivity, which acts as photoexcited charge carrier recombination centers.

3.5 *Conclusion*

RE oxide-doped nanocrystalline titania was prepared in presence of acetic acid by modified solution-sol-gel route. Photocatalytic activity was evaluated by the photo-assisted degradation of methylene blue in presence of UV light as well as sunlight. The structural and textural properties of the undoped as well as doped titania compositions were evaluated. Undoped titania underwent a drastic surface area loss on calcination and possessed only ~1 m^2/g surface area after calcination to 700° C. La_2O_3 doping (1%) effectively inhibited the surface area loss and possessed about 52 m^2g^{-1} surface area and 1% CeO_2-doped TiO_2 retained 42 m^2g^{-1}. Incorporation of 1% La_2O_3 enhanced the high temperature anatase phase stability if titania and shifted the transformation temperature to ~940°C. Doping with ceria also showed an enhancement of A→R transformation temperature (addition of 1% ceria shifted the transformation temperature to ~910°C) compared to the undoped counterpart, which showed the phase transformation at ~670°C. Doping with both 1% lanthana as well as 1% ceria inhibited the anatase crystallite growth and showed crystallite sizes such as 16.81 nm and 18.91 nm respectively at 700°C compared to the undoped titania having 39.09 nm. Furthermore, there is considerable increase in the surface acidity for the La_2O_3-doped TiO_2

indicating its possibility to be used as solid acid catalysts. The photoactivity of the undoped and doped titania obtained by the degradation of methylene blue solution established that 1% La_2O_3-doped TiO_2 annealed at 700°C to be the better catalyst. The activity was found to be comparable to that of commercial TiO_2 samples such as Degussa P-25 and Hombikat UV 100. The enhanced properties of titania are due to the excellent dopant distribution in titania matrix, the presence of Ti-O-RE linkage as well as the increased surface acidity and nanocrystalline nature. Hard and Soft Acids and Bases principle was found to be responsible for the formation of Ti-O-RE bond formation, which effectively distributes the dopants such as lanthana and/or ceria in the sol preparation process. Further, the procedure is modified for the preparation of high surface area, mesoporous doped titania. The controlled mesoporosity is achieved through a doping-followed by chemical leaching process, which resulted a huge increase in surface area. 5% SiO_2-1% La_2O_3 co-doped TiO_2 after leaching showed a specific surface area of ~231 m^2g^{-1} compared to the unleached sample having 79 m^2g^{-1}. The co-doped-leached titania showed the fastest dye decolourisation time at the highest calcination temperature (i.e., 5 minutes at 900°C) in presence of UV light. The calcination temperature corresponding to the highest activity (5 min) was shifted to 950°C in presence of sunlight. This is attributed to the maximum accessibility of the small percentage (5%) of UV light associated with the sunlight acquired by the highly crystalline reactive surface sites achieved on leaching, which effectively utilizes the UV light.

Chapter IV

Sol-Gel Nanocrystalline Titania Functional Coatings

Abstract

In continuation to chapter III on the photoactive TiO_2 powder synthesis and characterization, herein, a systematic study of the preparation and characterization of photoactive TiO_2 films has been presented. The films were fabricated with both dip coating as well as spin coating techniques. The optical characterization of the coatings was carried out using UV-Visible spectroscopy and AFM technique did the morphological analysis. The parameters such as effect of dopants, effect of addition of poly(ethylene glycol), effect of withdrawal speed and effect of multi-layer coatings on the optical properties were studied. The precursor sol compositions optimised for obtaining highly photoactive, high surface area TiO_2 have been used for the coating purpose.

4.1 Introduction

The sol-gel chemistry is an important method for preparing chemically homogeneous coatings and powders with a wide variety of useful applications, as evidenced by the many conference and symposia devoted to the topic. [561-563] Sol-gel processes usually involve various metal alkoxide molecules that are

hydrolysed under controlled conditions and then subsequently reacted to condense with each other to form metal-oxygen-metal bridging units. Sol-gel coating technique is being widely used for the fabrication of passive coatings, such as protective coatings, [8-11,564] antireflective films, [565] and inorganic ultrafiltration membranes [90-95] as well as active surfaces as photoactive coatings, [83-85] bio and gas sensors, [40-42] optoelectronics, [22] and in solar energy applications. The interest in the use of sol-gel method is due to its several advantages: good homogeneity, ease of composition control, low processing temperature, large area coatings, low equipment cost and good optical properties. [193] In particular, the sol-gel process is efficient in producing thin, transparent, multi component oxide layers of many compositions on various substrates, including glass. [331] Sol-gel coatings are easily anchored on supports of complicated shapes.

Sol-gel dip-coating process is one of the best ways for preparing vitreous or polycrystalline films of excellent homogeneity, purity and uniformity on any types of substrates. [566] It consists of immersing the substrate and then withdrawing the sample at a constant rate from a container with the sol-gel solution. [193] The main factors that control the sol-gel process are pH, catalyst, alkoxide/water ratio, temperature, and dilution. A few papers have reported the preparation of TiO_2 photocatalytic coatings and thin films from alkoxide solutions via dip coating, spin coating or spray deposition, the former being the most widely used. [254,258,328,370]

Kim *et al* [564] prepared TiO_2 thin films by sol-gel dip coating and their

structural and optical properties were examined at various calcination temperatures. The X-ray diffraction (XRD) results showed that TiO_2 thin film calcined at 300 °C was amorphous, and transformed into the anatase phase at 400 °C, and further into rutile phase at 1000 °C. Since the properties of these films have direct dependence on the nature of the surfaces such as amorphous, crystalline, dense and porous; the tailoring of these properties is essential in the production of different films with different end uses. Negishi *et al* [567] reported the preparation of TiO_2 thin film for the elimination of air pollutants by the dip coating process from titanium alkoxide precursor sol containing PEG. The variation of surface structure with respect to the change in PEG size was also investigated using AFM technique.

The hardness for protective coatings, optimum refractive index and crystallinity for the antireflective coatings and suitable structural and textural features of active coatings have usually been arrived by introducing dopants as well as the use of composite mixed oxides. There are several reports on porous but non-ordered silica-titania mixed metal oxide films, [17,568-572] several on mesostructured porous silica films and a few on mesostructured porous titania films. [110,111,573] Recently, Ogawa *et al* [574] reported the preparation of a mesostructured porous silica-titania mixed metal oxide film with a Si-Ti ratio of 5:1. Kozuka *et al* [575] reported the effect of poly (vinyl pyrrolidone) for the fabrication of 1mm thick crack-free $BaTiO_3$ films. Kajihara *et al* [576] extensively studied the effects of molecular weight, dipping temperature, heat treatment temperature and chemical additives on the macroporous morphology of titania

films prepared by sol-gel dip-coating method from the system containing poly (ethylene glycol).

The existing techniques to produce porous titania films have disadvantages and limitations. One of these limitations for both nanocomposites and porous films is that a high temperature process is required to form anatase nanocrystals. [397] In the preparation of titania porous films, the particles also have a tendency to aggregate in the sol and the resultant films usually become opaque. The techniques used to form transparent anatase nanocomposite films on various substrates at low temperature are essential to the synthesis of titania photocatalyst for pollutant decomposing, self-cleaning, and hydrophilic surface systems. [577--580] Matsuda *et al* [578] successfully prepared transparent anatase nanocomposite films on various types of substrates, including organic polymers, using the sol-gel method at temperatures <100°C and at ambient pressure. The authors emphasized the role of PEG in the evolution of the nanostructure, i.e., the formation of anatase crystallites and nanosized pores in the films. The report proposes PEG addition, not only for the crack-free film formation and as sintering retardant but also for the low temperature anatase crystal formation, which is necessary for the substrates like glass and organic polymers. Minami and co-workers [581] studied the physical and chemical properties of titania-silica films derived from Poly(ethylene glycol) containing gels.

In the previous works, it has been reported that some factors, such as the morphology and crystal structure of TiO_2 coatings obviously affect the

photocatalytic activity for photocatalytic decomposition of organic wastes. [273] Paz and co-workers investigated photooxidatively self-cleaning titanium dioxide films on soda lime glass and the deleterious effect of sodium contamination and its prevention. [84,582] Fujishima and Narasinga [29] have prepared TiO_2 thin films on different substrates, such as quartz, soda lime glass (SLG) and SiO_2-precoated SLG substrates via the spray pyrolysis method, and showed that the TiO_2 coated on SiO_2/SLG had much higher catalytic activity than that of TiO_2 films coated on bare SLG.

In most of the cases, polymers were used for both regulating porosity and retarding sintering in the preparation of thin films. The polymer with its bulkier groups will adsorb on the particle surface and cause steric hindrance, which eventually causes pore formation at the time of polymer burnout. Further, the polymer incorporation needs optimisation of the polymer content, which affects the viscosity of the system considerably, and an exquisite control over the heat treatment procedure. However, introduction of polymers into the parent gel matrix produces opaqueness, and also charring of the organic moieties while heating, are problems associated with such technique. The high surface area porous coatings produced by polymer addition/organic templating have uses in the fields of optoelectronics and site-specific catalysis. However, the retention of amorphous phase could be detrimental to the activity at a lower heat treatment temperature, which is used for substrates like glass and polymers. The excess addition of polymer can also cause phase separation. Still, the introduction of polymer was found to be inevitable in view of its

influence in the development of crack-free coatings. The fabrication of crack-free coatings without using the polymer is difficult. In view of this, we attempted the fabrication of crack-free nanocrystalline titania coatings on soda lime glass surfaces without the addition of polymer. The partially hydrolysed TEOS can act like a polymeric agent. The polymeric silica sol homogeneously distributes in the titania matrix by forming heterogeneous linkages. Silica particles also act as intermediate bonding sites to the OH moieties of glass surface on thermal consolidation. Furthermore, the presence of SiO_2 phase reduces the difference in refractive index [583] between the glass substrate and TiO_2. The incorporation of SiO_2, again, has an added advantage. The Na impurities that retain in the soda lime glass even after pre-treatment can be trapped by the SiO_2 phase [554] and thus can prevent its reaction with titanium ions, which could be detrimental to its activity. Furthermore, the modified synthesis route facilitates the nucleation of anatase phase at the sol preparation stage itself, as discussed in chapter III.

Coatings with refractive index intermediate between that of silica and titania ($n \sim 1.8$) was reported to be obtained by producing sol containing mixtures of silica and titania. [583] However, an extensive study on the preparation of photoactive titania-silica film, in which silica is incorporated into the titania matrix has not been attempted systematically till date. Instead of the organic polymer, here, silica performs as the binding agent with the glass surface primarily, and then the pore-forming agent. The fabrication of crack-free, photoactive titania films on glass surface attempted in the present work is

thus novel. Therefore, a systematic study on the fabrication of photoactive nano TiO_2 coatings on glass substrates and their characterization with respect to the degradation of methylene blue, which is a common organic dye, under UV light as well as sunlight is performed and presented in this chapter. The coatings have also been characterized for their optical properties using UV-Vis spectroscopy and morphological features using AFM. The present work also deals with the basic aspects of the fabrication of coatings, such as the effect of withdrawal speed and also the effect of polymer on the optical properties of coatings. Further alumina-lanthana co-doped titania was used for the fabrication of films using spin coating, in view of alumina's high absorptivity. The correlation between activity and the structural and morphological features of titania coatings with a view to develop a process for the fabrication of optically active, transparent nanocrystalline TiO_2 films on glass surfaces has also been made.

4.2 Studies on Titania Coatings Fabricated By Dip Coating

4.2.1 Optical Studies of Undoped and Doped Titania Coatings

Undoped and doped titania films were prepared from the sols derived from the hydrolysis-polycondensation reactions of titanium tetraisopropoxide. Effect of dopants such as lanthana and/or ceria as well as the effect of co-doping that reflected on the optical properties was studied. The effect of multi-

layer coatings as well as the effect of very large organic additives such as poly(ethylene glycol) and glycerol on the absorption properties was also evaluated. This is with a view to study the porosity-absorbance and/or transmittance correlation of the coatings. According to reports, PEG addition upto ~1% produces transparent coatings and if the concentration of PEG exceeds this limit, results in opaque coatings. The opaqueness is attributed to the scattering of light occurring from the mesopores developed as a result of high concentration of PEG.

4.2.1.1 Effect of Dopants

Figure 49 shows the optical absorption spectra of titania coatings obtained from undoped TU, TL-1 and TC-1 samples respectively. The spectra exhibit the characteristic absorption of titania. However, doped titania coatings show slight shift in the absorption onset. In the lanthana doped sample the absorption onset shows a shift to higher wavelengths and in ceria doped titania sample it is shifting to a lower wavelength. This is in line with the earlier reports and indicative of the change in band gap on doping. [584] Reports show that titania has an absorption onset at ~387 nm, which shifts to either side influenced by the preparative conditions and dopants. Sol-gel titania is reported to be associated with large number of intrinsic defects, mostly Ti^{3+}, which is a result of the larger hydroxyl formation. [543-545] The presence of Ti^{3+} moieties in the titania lattice provides n-type semiconductivity to the material owing to the availability of excess free electrons. These discrete electrons will distribute just

below the conduction band and, therefore, the apparent band gap will be reduced, which is consistent with the present observation. As per the present analysis, lanthana doping reduces the band gap of titania (2.94), but ceria doping (3.28) slightly increases the band gap from that of undoped TiO_2 (3.23). This may be attributed to the difference in valence state between La and Ce atoms, which is instrumental to the formation of more oxygen vacancies in the TL system compared to the TC system.

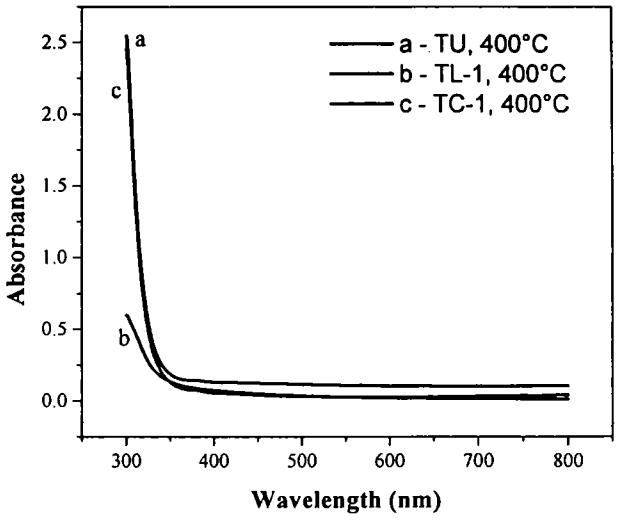

Figure 49: Optical absorption spectra of undoped and doped TiO_2 coatings

4.2.1.2 Band Gap Analysis

Band gap analysis was done using the UV-Vis absorption spectroscopy. The absorption spectra were obtained for the coated films. The absorption onset was determined by applying the sigmoidal fit, which is briefly described below. In a typical band gap measurement, as per the present technique, the absorption spectrum was fitted by sigmoidal fitting technique. The fit gives various

straight lines along the absorption curve depending on the curve profile. Tangents can be drawn on the spectrum using each straight line. We can manually select the straight line, which gives the absorption-onset wavelength. On extrapolating the tangent to the x-axis, we get the absorption onset. A typical sigmoidal fit and tangents drawn for the band gap calculation is provided in Figure 50. This wavelength is used for the band gap calculation using the equation, [584]

$$X = 1241/\lambda, \text{ Where } \lambda \text{ is the wavelength}$$

The constant 1241 is obtained by resolving the Einstein equation and de Broglie relation

The band gaps of undoped TU, TL-1 and TC-1 calculated by the above method are 3.23, 2.94 and 3.28 eV respectively. Lanthana doping induces the formation of a lower band gap to titania. This may be due to the formation of more free electrons by lanthana doping.

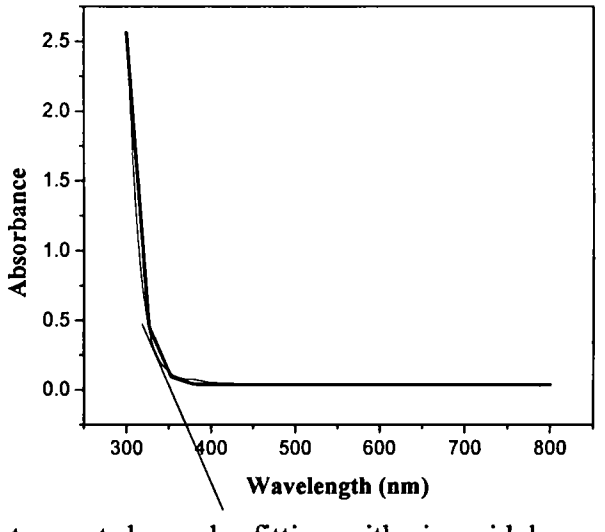

Figure 50: The tangent drawn by fitting with sigmoidal curve fit for band gap analysis

4.2.1.3 Effect of Poly(ethylene glycol)

Figures 51A and 51B show the transmittance spectra of titania coatings obtained from samples TL-1, TL-PEG1 and TL-GLY0.5, coated at two different withdrawal speeds (1.8 and 4.2 cm/min respectively) followed by calcination at 400°C. The incorporation of PEG and / or glycerol slightly decreases the absorption capacity. This may be attributed to the macroporosity generated by the addition of 1% PEG or glycerol, which scatters the light.

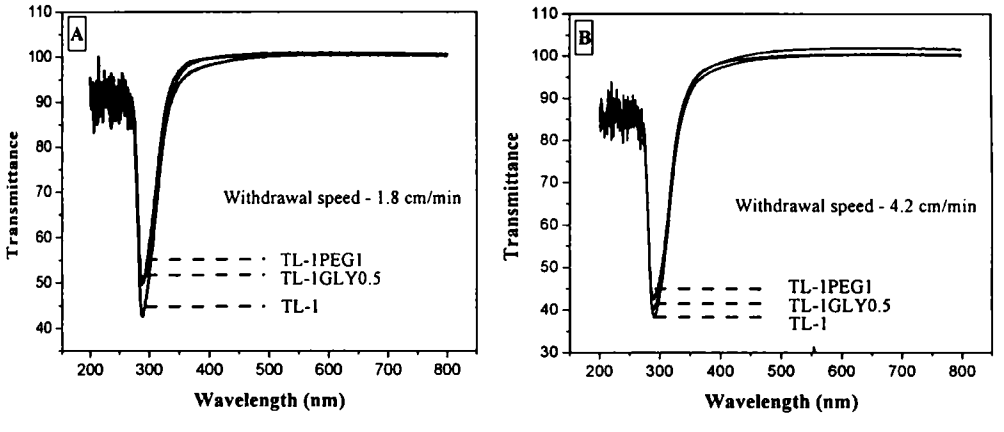

Figure 51: Optical transmission spectra of TiO_2 coatings showing the effect of addition of polymers on the absorption. Coatings have been made with withdrawal speeds such as (A) 1.8 cm/min and (B) 4.2 cm/min

Figures 52A and 52B are the absorption spectra of single layer TLS–PEG0.5 coated sample and that of three times coated sample. Incorporation of 0.5% PEG increases the absorbance of titania considerably. This is due to the formation of more micropores as a result of the addition of only 0.5% PEG, which is being eliminated from the matrix on calcination. In addition, the triply coated film shows broad absorption in the visible region. This may be

due to the retention of residual carbon, which reduces Ti^{4+} to Ti^{3+} species. [237,556] We can also conclude that 1% PEG addition is on the higher side considering the fact that the development of mesoporous texture reduces the absorption capacity of films. However, PEG was found to be more effective in the film formation properties than glycerol and hence selected as the polymeric agent for the rest of the experiments. These figures also indicate the possibility for the fabrication of films with >95% optical transmittance.

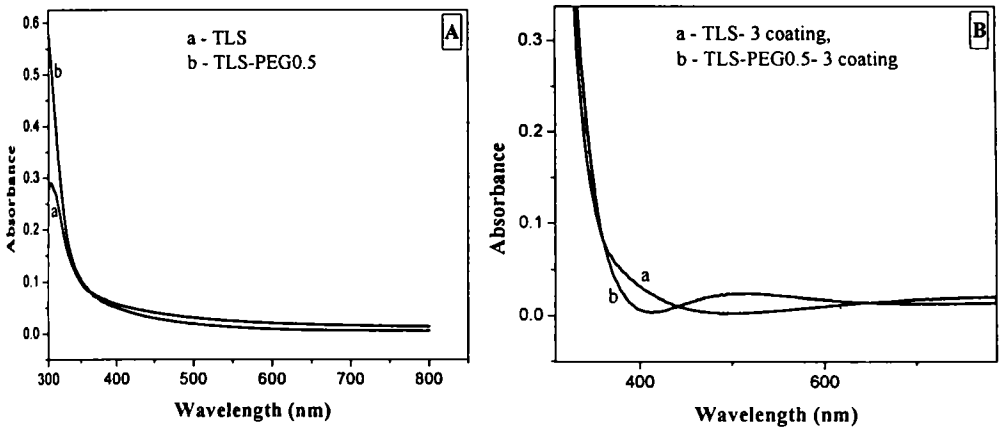

Figure 52: Optical absorption spectra of TiO_2 coatings showing the effect of addition of PEG. (A) singly coated and (B) triply coated

4.2.1.4 Effect of Withdrawal Speed

Optical absorption spectra of as dried (80°C) and 400°C calcined samples are provided in Figures 53, 54 and 55. Figure 53 shows the optical absorption spectra of as dried samples coated with different withdrawal speeds from the TL-1 sol. Figures 54 and 55 are that of 400°C calcined samples coated with TL-1 and TL-1PEG precursor sols respectively. Figures 53 and 54 clearly

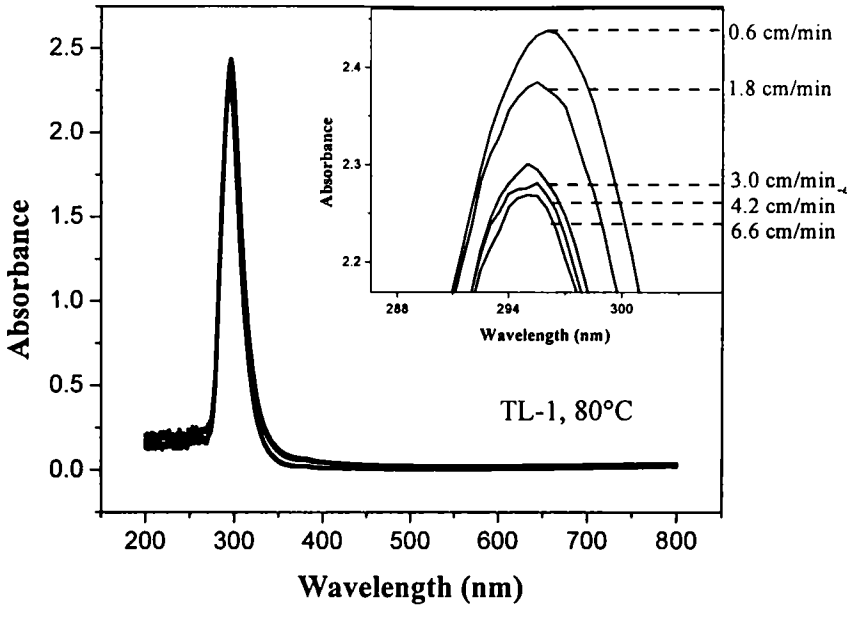

Figure 53: Optical absorption spectra of TL-1 coatings prepared with different withdrawal speeds. The coatings are calcined at 80°C

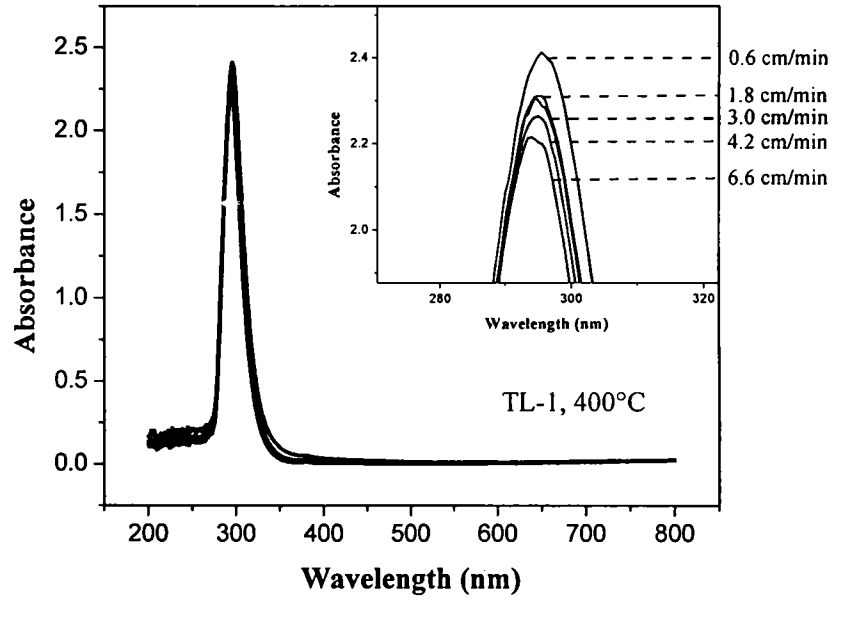

Figure 54: Optical absorption spectra of TiO_2 coatings prepared with different withdrawal speeds. The coatings are calcined at 400°C

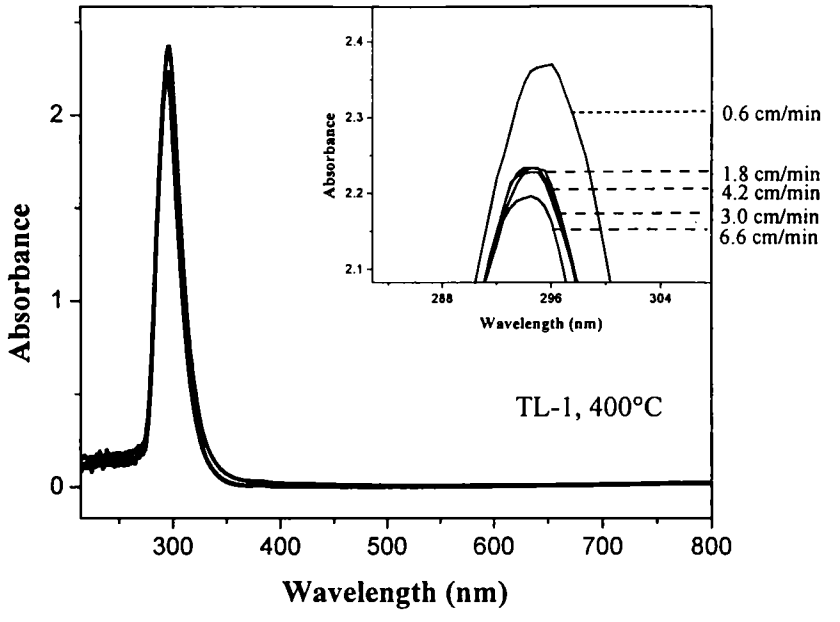

Figure 55: Optical absorption spectra of TiO_2 coatings prepared with different withdrawal speeds. The coatings are calcined at 400°C

indicate the direct relation of lifting speed with coating thickness. [585] On increasing the withdrawal speed from 0.6 to 6.6 cm/min, the optical absorbance increases and is a direct evidence of the increase in thickness of the coatings, which increases the titania content on the substrate surface. [585] Figures 54 and 55 also indicate similar trend, but a slight variation in the order can be observed. This probably points to an inhomogeneous mixing of the polymer in the coating precursor sol.

Figure 56 presents the optical transmittance spectra of 400°C calcined TLS coatings obtained with different withdrawal speeds. The percentage transmittance of the samples decreases gradually on increasing the withdrawal speed. This is a direct evidence of the increase in thickness with the increase in

withdrawal speed of coatings. [193,585] The coatings obtained with all the four withdrawal speeds were found to be non-flaky and highly adhesive. The adhesiveness was tested by scratch tape tests. The qualitative testing was also done by actual weathering followed by continuity measurement using SEM (not presented here).

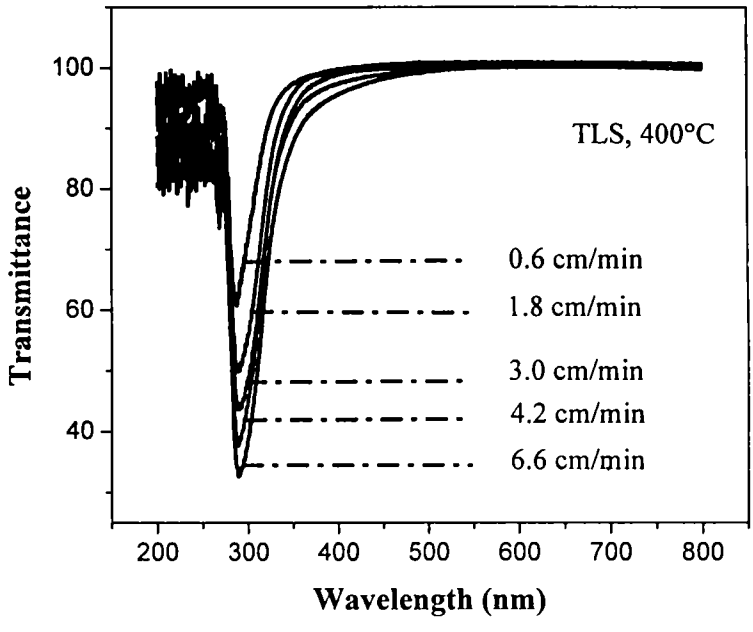

Figure 56: Optical transmission spectra of co-doped TiO_2 coatings (TLS) prepared with different withdrawal speeds. The coatings are calcined at 400°C

4.2.1.5 Effect of Multi-layer Coatings

The effect of multi-layer coatings on the optical properties was determined by optical spectral analysis. Figure 57A shows the optical absorption spectra of single and 3 times coated lanthana doped titania films. The band gap decreased from 2.94 eV to 2.43 eV on increasing the thickness of coating. This may be due to the accumulation of more discrete free electrons

(Ti^{3+} species) just below the CB due to increased lanthana content. Further, with the increase in film thickness, the absorbance also increases considerably. This is due to the increase in availability of titania particles on increasing the coating thickness. Also, as the number of coatings increases, a weak absorption at ~380 nm is occurring.

Figure 57B shows the optical absorption spectra of 0.5% PEG added TLS coated films calcined at 400°C. The absorbance increases as the number of coatings increases. Moreover, as the number of layers increases, the absorption in the visible region increases and the triply coated sample shows a broad absorption centers at ~515 nm. This absorption could be attributed to the presence of residual organics remaining at 400°C. As the number of coatings increases, the chances of retention of more organic residuals increases, which reduces Ti^{4+} to Ti^{3+} species. [237] The presence of Ti^{3+} species gives the absorption in the visible region.

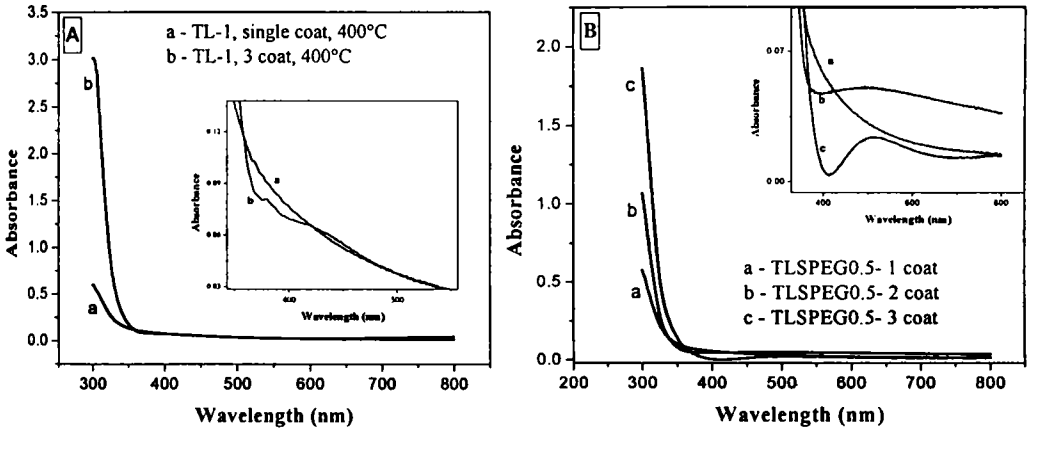

Figure 57: Optical absorption spectra showing the effect of multi-layer coatings (A) TL-1 and (A) TLS-PEG0.5 coatings calcined at 400°C

In general, dopants slightly shift the absorption onset indicative of the small change in band gap. Also, 0.5% PEG addition is found to be favourable in the development of transparent films than the mesoporous, translucent films produced in case of 1% PEG addition.

4.2.2 Morphological Studies

Morphological studies were done by mainly topography imaging as well as by RMS roughness measurements. The topography profiles, in general, indicate the change in morphology with respect to compositional changes of precursor sols. The RMS roughness values indirectly show the influence of drying and calcination on the nanocrystalline titania grains that are being coated on the substrate surface.

4.2.2.1 AFM Topography

The morphological studies of the coated samples were carried out with Atomic Force Microscopy technique. Figure 58 presents the AFM images of undoped TiO_2 coated glass slides fabricated by the dip coating method. The images indicate the formation of a thin layer of titania coating with a high roughness value (Table 18) ~50 nm. This is attributed to the co-presence of anatase and rutile phases on the surface as confirmed by the XRD data (Figure 66). The 5 μm image shows the presence of porous film with randomly packed particles over the glass substrate.

The AFM topography of the TL-1 coated slides is presented in Figure 59. The images with magnifications of 20μm as well as 5μm show almost a continuous profile in which ordered rod shaped particles are packed almost closely on the surface. The image, with a magnification of 5μm provided in the right side indicate the formation of a uniform, monodispersed regularly shaped grains with preferred orientation, which suggests the growth of an ordered nanocrystalline film. The higher order of the crystallites is attributed to the heterodentating effect of acetate ligands with both Ti^{4+} and La^{3+} species according to HSAB principle. The coating has a thickness of ~12 nm with minimum roughness value.

Figure 60 shows the AFM images of TLS coated glass slides. In contrast to the earlier figures, we can see particles with an amorphous / semi-crystalline morphology. In contrast to the rod shaped particles on the surface, the TLS sample shows poorly crystallized particles. The particles cannot be distinguished as was the case of the TL-1 coated sample. The surface is characterized by the presence of grains with rather diffused grain boundaries, which could not be observed on the TU and TL-1 films. This is attributed to the amorphous silica particles enveloping La_2O_3-doped TiO_2 particles. As a result, the thickness of the coating is increased from 12 nm to 15 nm as confirmed by the AFM analysis.

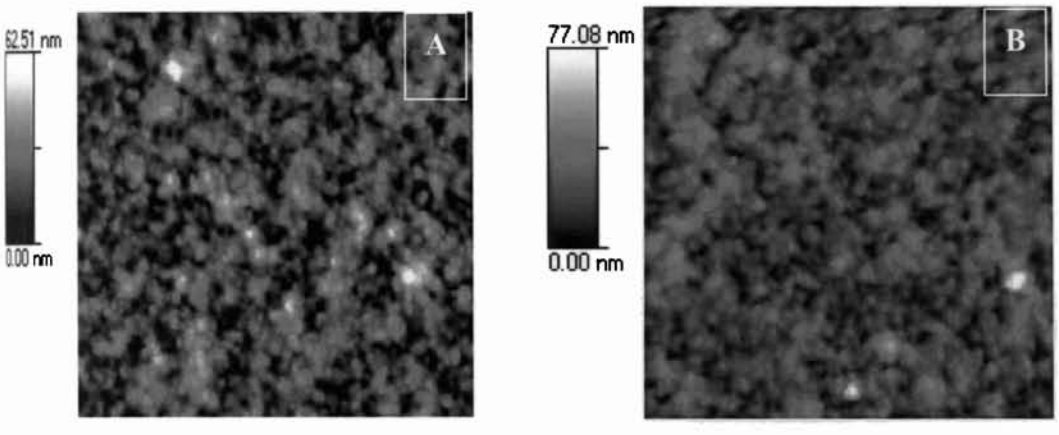

Figure 58: AFM topography (A and B) of TU coating (5µm x 5µm images)

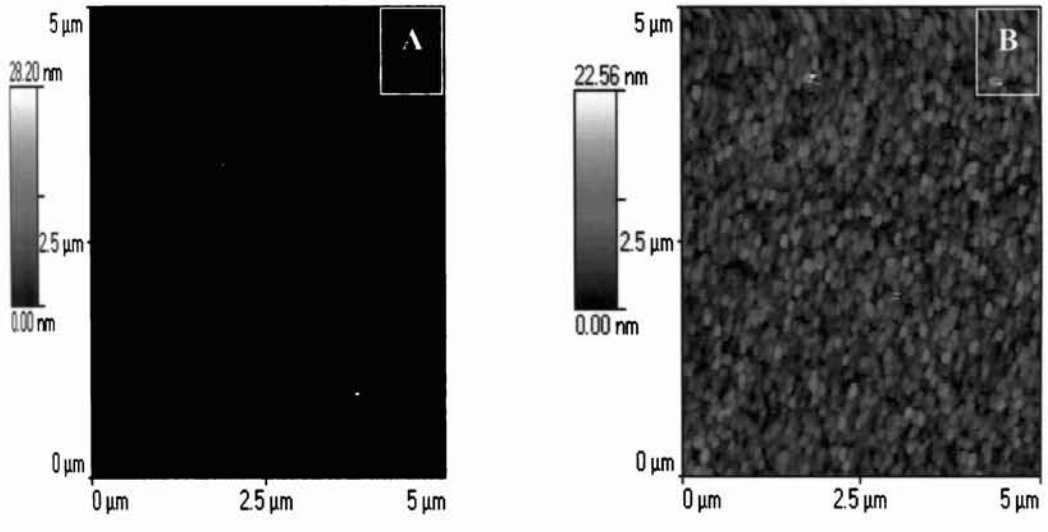

Figure 59: AFM topography (A and B) of TL-1 coating (5µm x 5µm images)

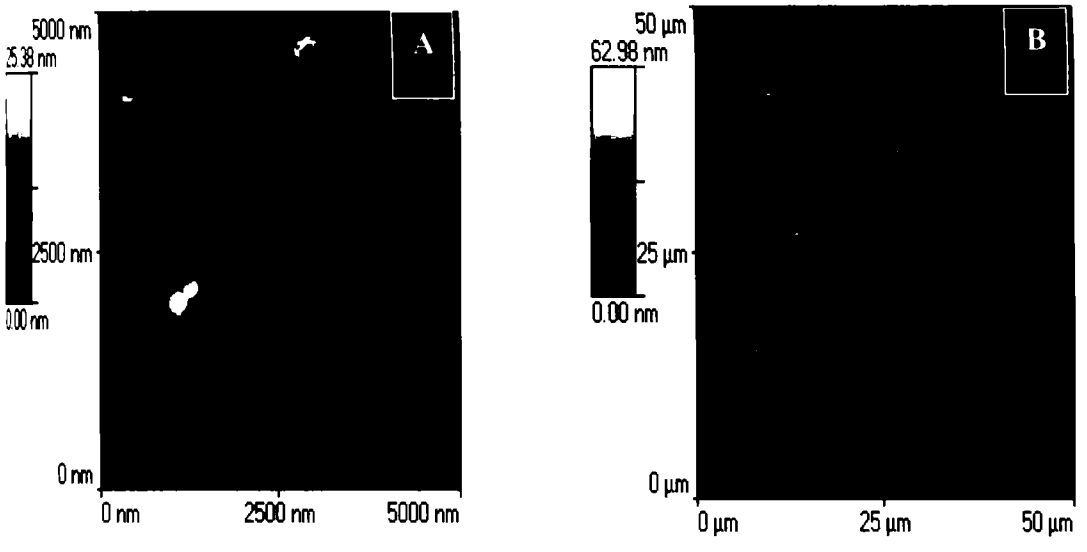

Figure 60: AFM topography (A and B) of TLS coating (different magnifications)

The surfaces of the undoped and 1% La_2O_3-doped TiO_2 films calcined at 400°C show a regular surface structure, indicating a significant degree of surface ordering on the scale of several tens of micrometers. A typical dimension of these grains is in the region 10 nm. Moreover, one can clearly see from Figure 59 that there is a preferred orientation of the regularly shaped grains, which suggests the growth of a nanocrystalline film over the glass surface. However, the TU film has a porous morphology and TL-1 film on the other hand has grains orderly arranged on the surface.

4.2.2.2 RMS Roughness Measurements

A detailed analysis of the roughness of the samples was done by RMS roughness measurements. A consolidated result of the RMS roughness measurements is provided as Table 18. Table shows that undoped TiO_2 has the highest roughness value (average RMS 20.49 nm). This is attributed to the specific polymeric sol-gel preparative route adopted in the present study. The existence of both the anatase and rutile phases at 400°C (Figure 66) explains the development of rough surface. This is also consistent with the photocatalytic properties of the powder, where the undoped titania showed a low temperature A→R phase transformation and hence a lower activity at 400°C. However, all the doped and co-doped TiO_2 coated films show smaller RMS roughness values consistent with the presence of phase pure anatase particles. This also demonstrates the effect of heat treatment on the crystallization of undoped and doped TiO_2 films. The TL-1 film shows a highly ordered morphology. The TLS film also shows some ordering, but an

amorphous / semi-crystalline nature is also observed. This indicates the influence of silica on the crystallization of titania. [394] Anatase phase nucleates at the solution stage in the present work, as confirmed by the XRD analysis. [501,510] Also, according to reports, lanthana and ceria has no influence on the amorphous to crystalline phase transition. [382-383] However, the present morphological studies point towards the influence of silica on the inhibition of atomic diffusion [394] as well as crystalline growth of titania. This is probably because of the formation of a secondary phase at the grain boundaries as evidenced from both TEM and AFM analyses. The TLSN film, obtained after chemical leaching shows a crystalline and almost a regular mesoporous texture, which is attributed to the selective removal of amorphous silica phase distributed uniformly in the films as confirmed by the TEM EDS analysis. This selective removal provides regular (surface structure) surface morphology with comparatively high roughness values, which has a higher level of OH functionality and this can enhance the hydrophilicity of surface.

TL-1 sample shows 2.35 nm average RMS roughness compared to the TLS coating with 3.99 nm and TLSN having 2.95 nm. The lowest % error of 9.18 for TL-1 sample is consistent with its ordered, closely arranged crystallite structure. The next lowest % error (9.93) is shown by TLSN sample. This is attributed to the selective removal of the amorphous silica phase leaving the lanthana doped titania on the structure. On the other hand, the TLS coating showed 17.56% error in the RMS roughness values. This indicates the homogeneous but preferential distribution of silica phase in the doped-titania matrix. The Ti-O-Si bond formation as evidenced from FTIR and the present result alongwith the TEM study leads us to the conclusion

that partially hydrolysed silica will be attached to Ti species through Ti-O-Si linkages and finally will be selectively removed from the framework leaving a small amount of silica species in the titania matrix.

Table 18: RMS roughness values of different titania coatings

	TU		**TL-1**		**TLS**		**TLSN**
5 μm images	9.2526	9.2526	2.9065	**2.5067**	3.1168	**2.91**	2.6071
	52.3631		2.1959	2.1959	5.6881	**3.8761**	2.6572
	10.8716	**10.0772**	2.1421	2.1421	4.0233	**2.8083**	3.6925
	9.4693	9.4693	2.1467	2.1467	3.117	**2.9956**	2.8253
average							
RMS	20.49	9.60	2.35	2.25	3.99	3.15	2.95
std dev	21.26	0.43	0.37	0.17	1.21	0.49	0.51
Sem	12.28	0.30	0.22	0.10	0.70	0.28	0.29
% error	59.91%	3.15%	9.18%	4.48%	17.56%	9.02%	9.93%
20 um image	11.6216	**11.2072**	2.2755	**2.0227**	6.7344	**5.9951**	4.6205
50 um image	21.0564		10.3592	**4.8632**	2.2241		3.7519

RMS data for AFM images: for each sample first column = full image data,
second column = full image (regular) + partial image data (bold)

4.2.2.3 Effect of Chemical Leaching

Figure 61 presents the AFM images of TLS precursor sol coated-400°C calcined-chemically leached glass surface. The topography shows more exposed surface with mesoporous nature, which is an indication of the effectiveness of leaching process. Also, the regular parallel packed, distinguishable particles are absent in the leached samples, which leads to the conclusion that silica inhibits the crystallization of TiO_2. Also the thickness of the film was reduced to ~12 nm after chemical leaching, which shows the effective removal of amorphous silica phase associated with the doped titania particles (Sol particle size of the TLS sol was 14 nm as can be seen from section 3.1.1, chapter III). Therefore, by chemical leaching we can develop mesoporous texture in the coated surfaces, where the matrix and pore walls of the films will be in a highly crystalline state, which open up tremendous applications in various fields such as high surface area battery electrodes, sensors, optoelectronic devices, and catalysts. However, singly coated films on leaching resulted in the production of mesoporous coatings with exposed glass surfaces. In order to avoid this shortcoming, chemical leaching was carried out on the multi-layered films. In all the multi-layered films, heat treatments (250°C) were carried out after each dipping process, which resulted in the consolidation of the films. After the final coating it was calcined at 400°C and was soaked for a period of 3 h. AFM images of the unleached as well as chemically leached bi-layer coated samples are provided in Figures 62 and 63. The chemical leaching produces almost a regular mesoporous texture to the

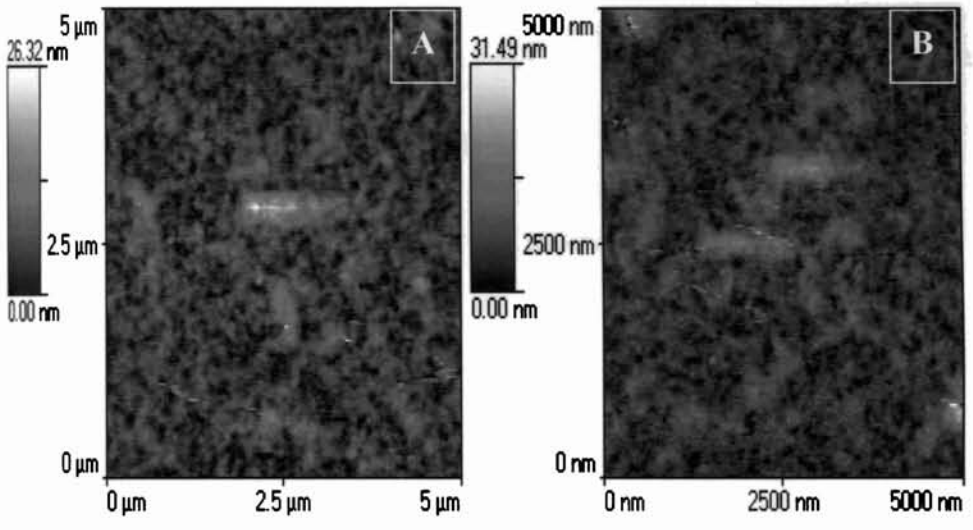

Figure 61: AFM topography (A and B) of TLS coating after chemical leaching

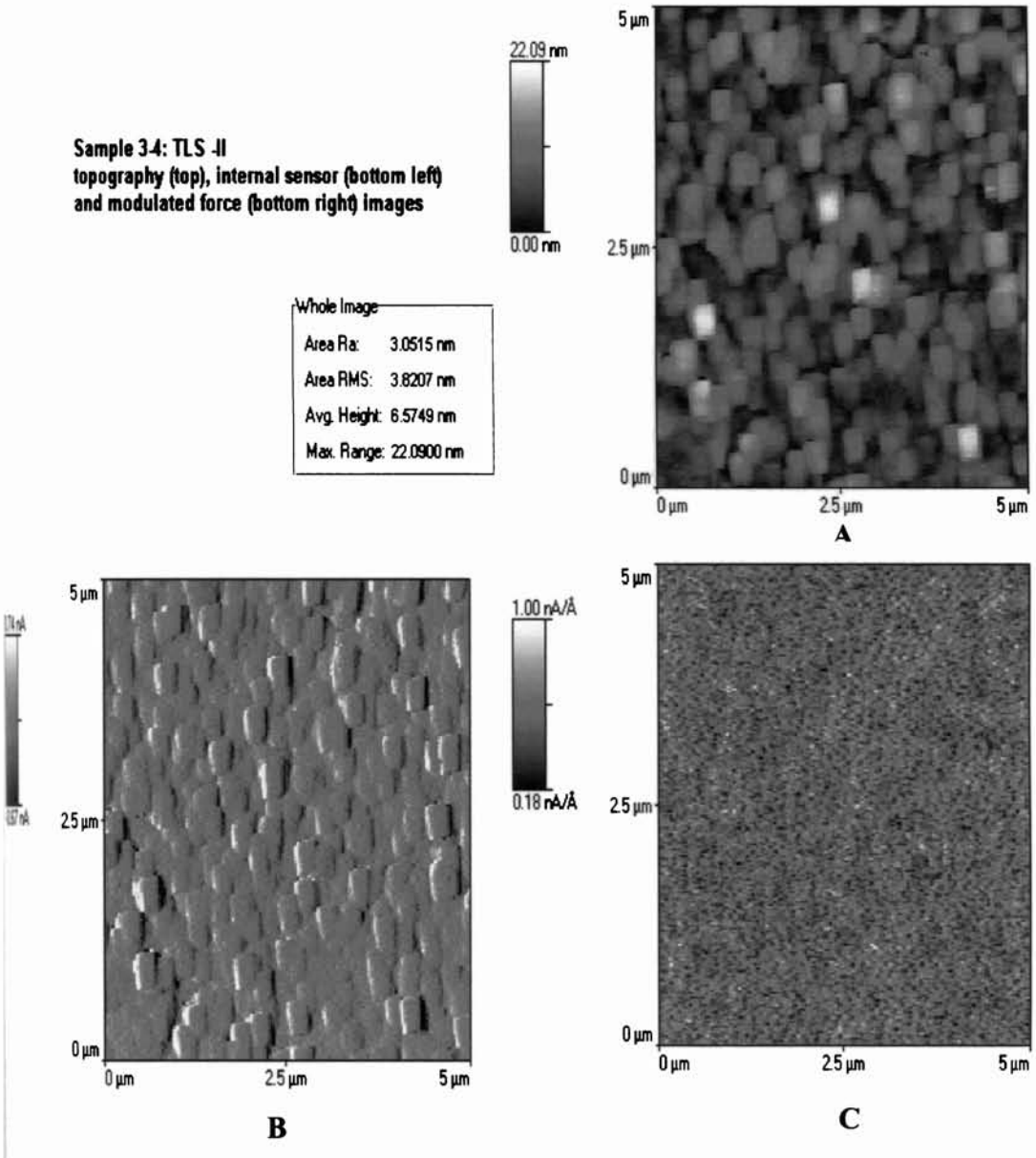

Figure 62: AFM topography (A) and internal sensor images (B and C) of 2-times coated TLS asmple before chemical leaching

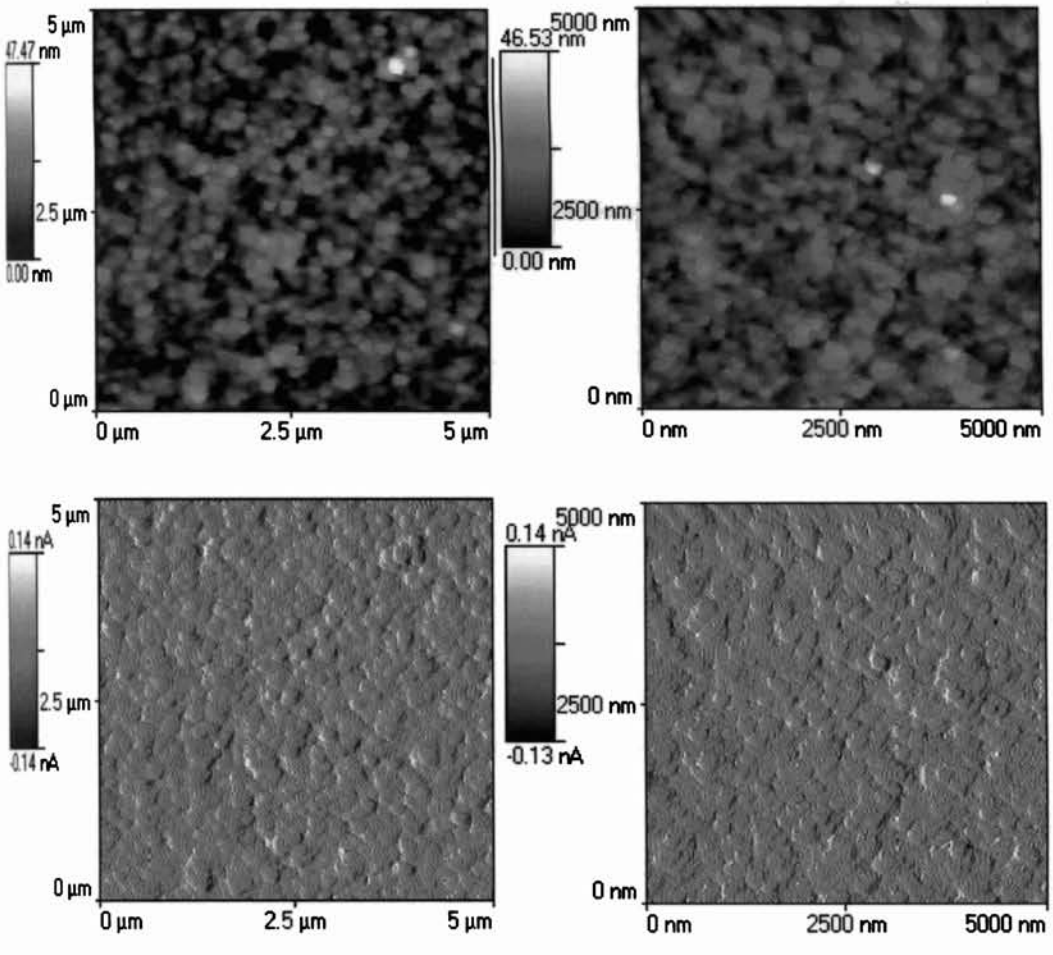

Figure 63: AFM topography (row above) and internal sensor images (row below) of 2-times coated TLS sample after chemical leaching

films. This is attributed to the homogeneous distribution of amorphous silica phase in the doped titania matrix. Unlike the singly coated films, the topography shows rectangular grains arranged in an almost parallel fashion. The internal sensor image provided as Figure 62B shows the presence of regular densely packed grains on the surface. This could be attributed to the consolidation of films by heat treatment at 250°C before the subsequent coating. The subsequently coated films can grow over the pre-consolidated titania grains and hence can attain their orientation. On chemical leaching, regular mesoporous textured morphology with homogeneously distributed grains are developed. This is attributed to the elimination of homogeneously distributed silica phase in the titania matrix, which is also confirmed from the XRD analysis. However the chemical leaching does not expose the glass surface, which is evident from the internal sensor image provided in the second row of Figure 66. Such highly irregular, high surface area films will have large number of OH functionalities and hence can act as potential hydrophilic surface. This synergic effect of hydrophilicity and photoactivity can be exploited in the field of self-cleaning surfaces.

4.2.3 Photoactivity Evaluation

Table 19 presents the decolourisation times of different titania films with respect to the degradation of methylene blue. TL-1 and TLS films calcined at 400° C at a heating rate of 1°C/min showed higher activities among the samples. However, the activity is lower than that of the corresponding

powder samples, due to their intrinsically lower surface area, which also corroborates with the results of Sopyan *et al.* [586] Nano coatings have only very low exposed surface area as well as the active surface sites that influences its activity considerably.

The graph provided in Figure 64 shows the methylene blue degradation profiles of different titania films calcined at 400°C. The TL-1 sample showed the maximum activity in presence of UV light as well as sunlight. TLSN sample showed the next highest activity. In fact, the leaching process enhanced the activity further (15-20 min less time taken for methylene blue degradation by the leached samples). Therefore the optical absorption spectra were recorded for the unleached as well as leached TLS films to see the extent of optical absorption by the two samples and also the shift of absorption onset if any, and presented as Figure 65. The spectra showed that the absorption onset little changes even on chemical leaching. The absorbance also does not show much change on leaching. This indicates the effective utilization of the available energy source (UV light) by the chemically leached titania. Normally, the enhancement in surface area should increase the absorbance of films. But in the present case, the formation of meso/macro porous surface does not show much enhancement in the absorbance. Nevertheless, the activity shows an increase on chemical leaching. This could be due to the increased accessibility of highly crystalline anatase phase achieved on chemical leaching. On the other hand, the unleached surface is associated with amorphous silica phase, which is detrimental to the activity.

Table 19: Photoactivity results of the 400°C calcined titania films with respect to the decolourisation of methylene blue in presence of UV light as well as sunlight.

Sample	Decolourisation time (minutes) on exposure to	
	UV light	Sunlight
TU	720	770
TL-1	370	370
TS-5	480	500
TLS	490	505
TSN	455	460
TLSN	440	440

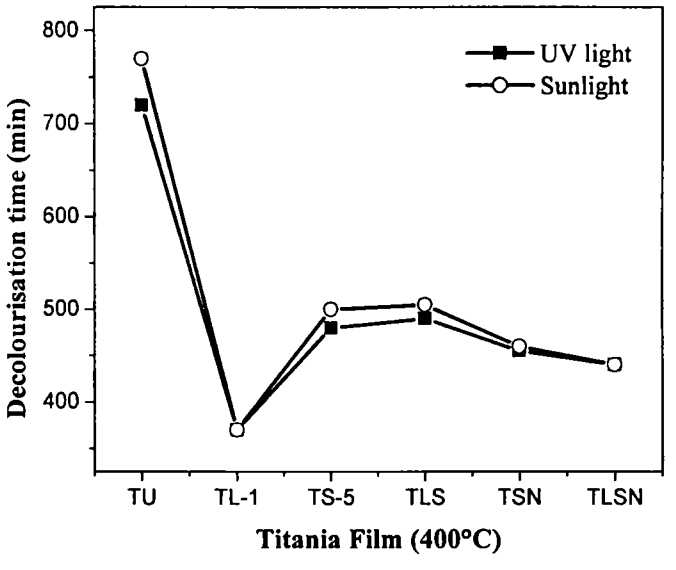

Figure 64: Methylene blue decolourisation profiles of different titania films under UV light and sunlight. The samples are calcined at 400°C

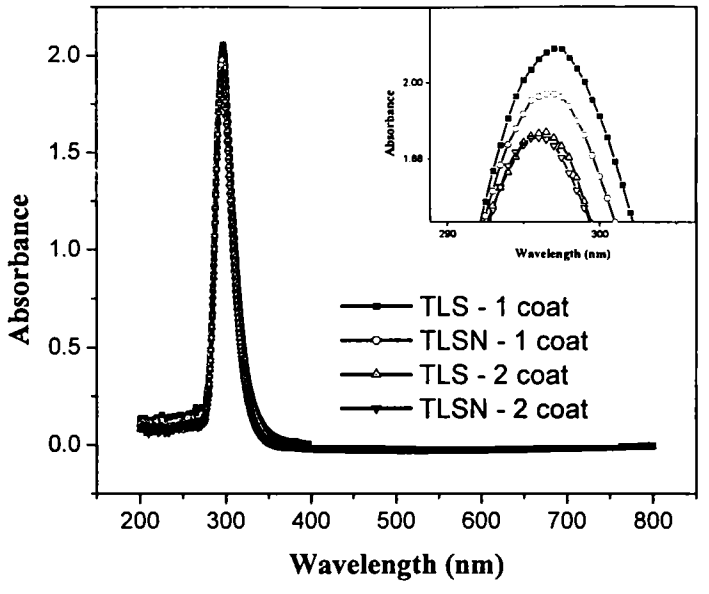

Figure 65: Optical absorption spectra of unleached and leached TLS coatings. The samples are calcined at 400°C

In order to see the phase assemblage at this temperature (400°C), X-ray diffractogram of undoped TiO_2 sample was recorded and compared with that of 700°C calcined powder. Figure 66 shows the XRD patterns of TU sample calcined to 400°C at a heating rate of 1°C/min and that of TU sample calcined to 700°C at a stepwise heating rate as indicated in Section 2.2.1. A mixture of anatase and rutile phases can be observed at this temperature. The anatase phase is ~39 nm in size and the rutile is having ~56 nm for the 400°C calcined sample and ~39 nm and 65 nm for the 700°C calcined sample. At the same temperature, the 400°C calcined doped TiO_2 sample, which has the highest activity, showed the presence of only the nanocrystalline anatase phase. This result substantiates the direct influence of nanocrystallinity as well as high

surface area on the activity of the photocatalyst. The enhancement in the properties achieved in the present study is by the use of specific dopants such as lanthana and ceria. Acetic acid, the heterodentating stabilizer, had been the key factor on the effective utilization of these dopants in the solution stage, based on the HSAB principle.

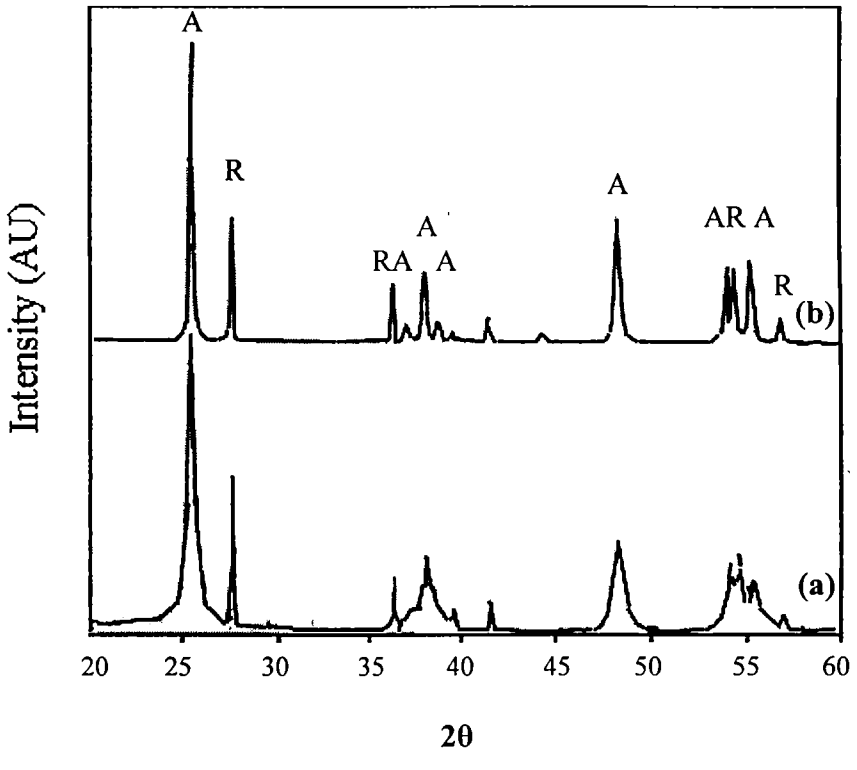

Figure 66: X-ray diffraction patterns of (a) TU specimen calcined at 400°C with a heating rate of 1°C/min. and (b) TU specimen calcined at 700°C with a stepwise heating rate (RT to 200°C, 2°C/min; 200 to 500°C, 3°C/min and 500 to 700°C, 5°C/min)

The above results also indicate towards the possibility for the development of highly active transparent, nanocrystalline anatase titania

coatings even at higher temperatures by the above composition (TLS). In the present study, however, we have investigated the activity of the compositions only on glass surfaces, which can only withstand upto the temperature 400-500°C. But the corresponding powder sample analysis results presented in chapter III indicate the possibility of fabrication of highly photoactive titania coatings on ceramic substrates that can withstand high temperatures.

4.3 Studies on Titania Coatings By Spin Coating

4.3.1 TiO_2 Xerogel Characteristics

The particle sizes of the two sols, TL-1 and TLA10 measured using laser particle size analyzer are 30 nm and 288.9 nm respectively (Figure 67). The TL-1 sol exhibited a monomodal size distribution in a narrow range. On the other hand, a bimodal distribution, wherein the individual oxides are distributed in a narrow fashion is observed for the TLA10 sol. The thermogram presented in Figure 68 indicates that the precursor gel dehydrates and further undergo dehydroxylation below 400°C, and at higher temperature, titania exists in the anatase crystalline form with practically no organic phases. The powder X-ray diffraction data indicate the presence of anatase with a crystalline size of 11 nm for sample TL-1 after calcination at 400°C and 9 nm for sample TLA10 (Table 20). The co-presence of lanthana and alumina inhibits the crystal growth and retards the anatase to rutile phase transformation in the films, which also

corroborates with some earlier results and our own results provided in Chapter III.

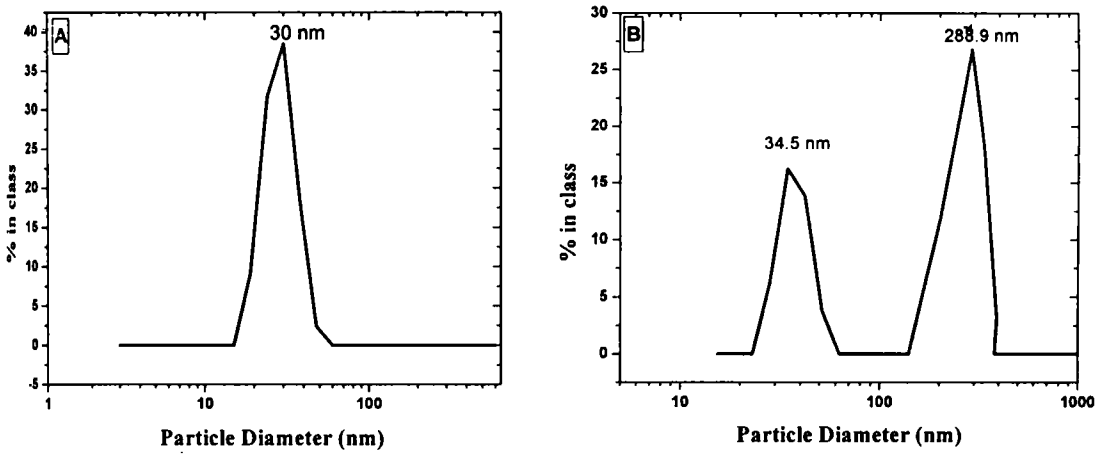

Figure 67: Particle size distribution of (A) TL-1 and (B) TLA10 precursor sols

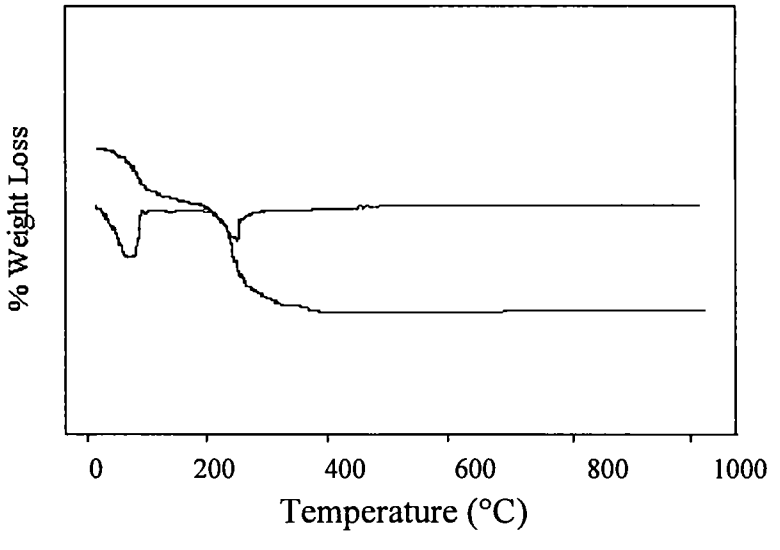

Figure 68: TG curve of TLA10 xerogel

BET specific surface area and crystallite size of TL-1 and TLA10 samples are presented in Table 20. Sample TL-1 has specific surface area

100 m^2g^{-1} and sample TLA10 has shown a much higher value 159 m^2g^{-1} at 400°C. The increase in SSA is attributed to the combined effect of co-dopants. The contribution from the porosity features could be very well understood from the BJH pore size distribution curves obtained from the desorption data (Figure 69). Sample TL-1 shows a monomodal size distribution with a peak maximum (pore diameter) at ~7.2 nm, while in case of TLA10, the peak maximum is shifted to 6.3 nm. This could be attributed to the combined effect of lanthana

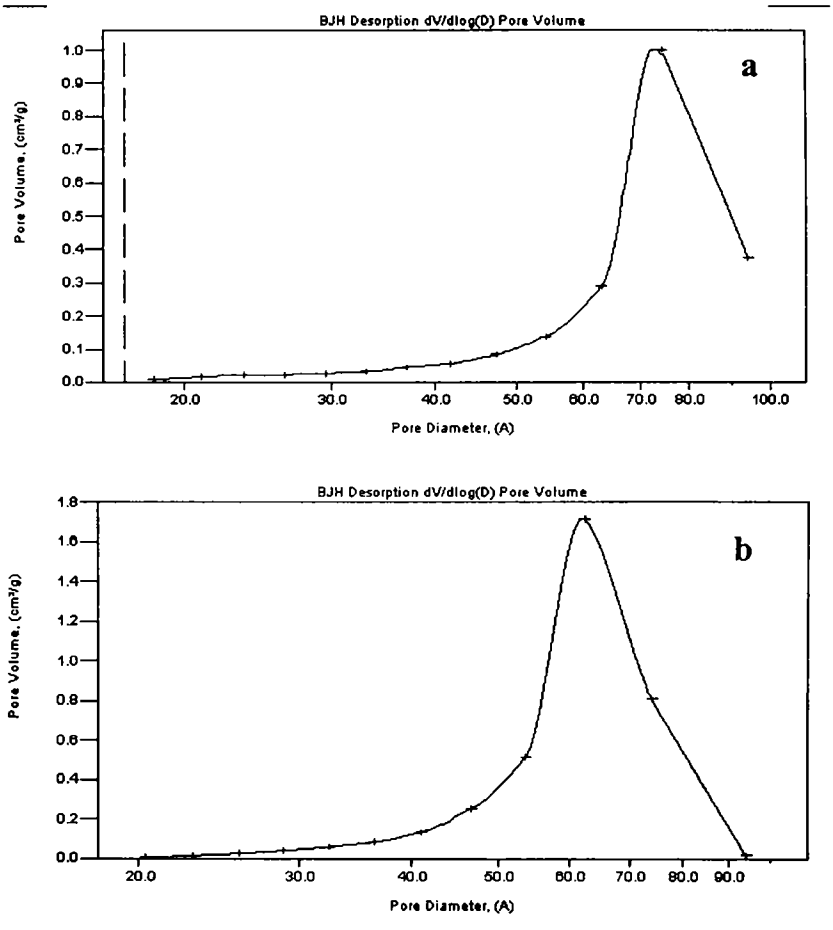

Figure 69: BJH pore size distribution of (a) TL-1 and (b) TLA10 sample calcined at 400°C

and alumina particles on the particle packing, which also leads to the possible pore structure stabilization at higher temperatures. The evolution of porosity and surface area as well as the inhibition of grain growth corroborates well with the literature data, which illustrate the selection of the co-dopants. [349]

Table 20: BET specific surface area and crystallite size of TU and TLA10 samples calcined at 400°C

Sample	Specific surface area (m^2g^{-1})	BJH cumulative pore volume (cm^3g^{-1})	Crystallite size (nm)
TU	100	0.135624	11
TLA10	159	0.187092	9

4.3.2 TiO_2 Coating Characteristics

Al_2O_3 suspension was co-doped to the La_2O_3-doped TiO_2 sol with a view to develop functional surfaces, considering the high absorptivity of alumina particles. The spin coating technique, adopted in the present investigation resulted in the formation of transparent TiO_2 films on glass substrates as confirmed by the UV-Vis transmittance spectral analysis. The transmittance of a typical co-doped titania film is presented in Figure 70. ~90%

transmittance in the visible region can be observed for the TLA10 coated samples.

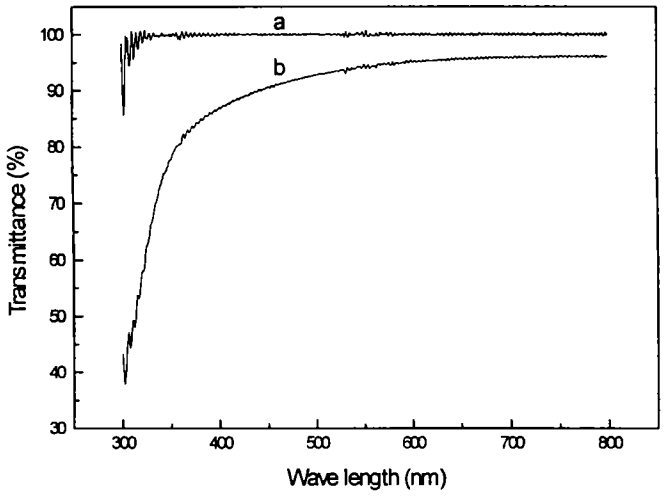

Figure 70: UV-Visible transmittance spectra of (a) glass substrate and (b) TLA10 coated glass substrate

4.3.2.1 Morphological Studies Using Atomic Force Microscope (AFM)

The AFM images of spin coated, TU film as well as TLA10 film imaged at different magnifications is presented as Figures 71a-d. The AFM topography of the films indicates the morphological difference between these coatings. While the film obtained from undoped TiO_2 precursor sol gave a teardrop shape particle distribution, the mixed oxide sol gave almost circular particles with very low thickness. The circular shape obtained in case of TLA10 could be due to the influence of second phase, alumina, on the titania matrix. Being larger in particle size and having a higher density compared to

titania, the alumina particles influence the movement of titania to some extent. The greater tangential movement of larger alumina particles compared to titania causes the teardrop shape to collapse and thus results in a thin coating. However, the alumina particles could not be observed in the AFM images of the films spin-coated with a rotation speed of 4000 RPM. The reason is the high spin rate used for coating. Therefore, the coatings were done at a rotation rate of 2000 RPM and the AFM imaging was done with the samples and the morphology is presented in Figure 72. The AFM topography shows a "bumps & valley" morphology for the TLA10 film. The role of Al_2O_3 on the morphology of TiO_2 films derived by spin coating technique indicates that the shape of TiO_2 particles are influenced by large size inclusions, while the selection of the spin speed can also be a deciding factor in such hybrid films. While La_2O_3 could improve the photoactivity of titania by enhancing the amount of Lewis acid sites, Al_2O_3 performed primarily as a thickness-regulating agent and also as a texture-enhancing agent that enhances the surface area and thus the available OH functionalities.

4.3.2.2 Thickness Measurement Using Atomic Force Microscope (AFM)

The thickness of the samples was measured using atomic force microscope by looking at the thickness of the layer as a whole. The results are provided in Table 21. The actual numbers are not really important as they can change a bit due to artifacts. The average thickness and standard deviations are provided. The analyses show more or less homogeneous thickness values.

Table 21: AFM Thickness measurement results of spin coated TiO_2 coatings

Image Size	Bottom height (nm)	Top height (nm)	Thickness	Average Thickness	Standard Deviation
	TL-1 (4000 RPM)				
10	12.708	94.11	81.402	86.92025	5.233296
5	4.567	93.351	88.784		
10	74.561	158.75	84.189		
5	66.154	159.46	93.306		
	TLA10 (4000 RPM)				
10	28.876	48.538	19.662	21.44725	6.538663
5	16.466	29.524	13.058		
10	74.254	102	27.746		
5	68.443	93.766	25.323		

The thickness of the films is found to be in the range 20-90 nm. The high thickness values of undoped TiO_2 films derived from the precursor sols having particle size ~30 nm is due to the specific drop-spin coating technique adopted in the present method. The uniformly distributed co-doped titania film was developed by adjusting the rotating speed to 2000 RPM. AFM images (Figure 72) show the formation of irregular surfaces. The presence of ~310 nm alumina particles can be observed, which are distributed in almost homogeneous fashion on the glass surface. We can also observe a thin layer in between that of the bigger particles. This can be assumed as the titania layer.

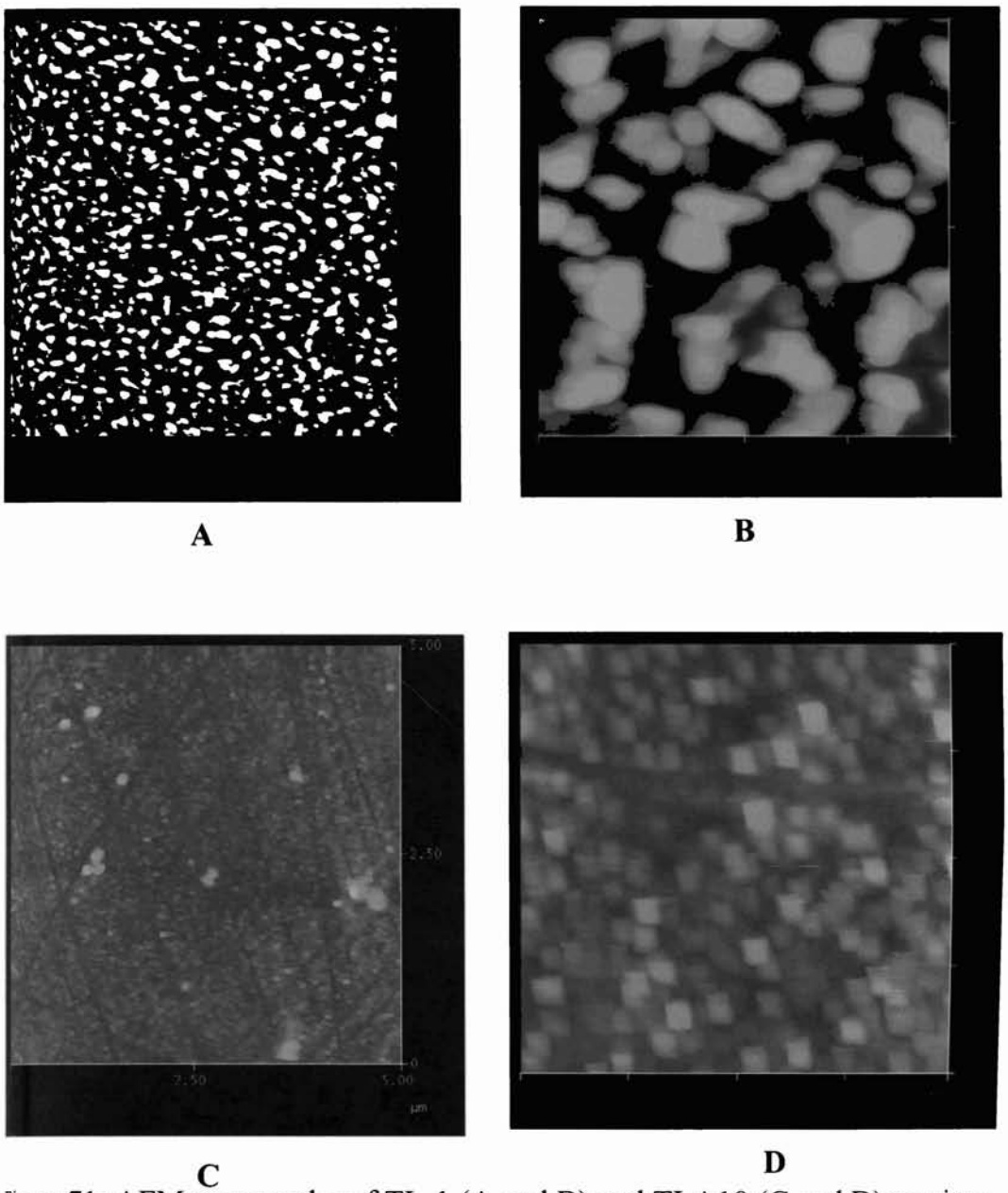

Figure 71: AFM topography of TL-1 (A and B) and TLA10 (C and D) coatings calcined at 400°C

Table 21: AFM Thickness measurement results of spin coated TiO_2 coatings

Image Size	Bottom height (nm)	Top height (nm)	Thickness	Average Thickness	Standard Deviation
	TL-1 (4000 RPM)				
10	12.708	94.11	81.402	86.92025	5.233296
5	4.567	93.351	88.784		
10	74.561	158.75	84.189		
5	66.154	159.46	93.306		
	TLA10 (4000 RPM)				
10	28.876	48.538	19.662	21.44725	6.538663
5	16.466	29.524	13.058		
10	74.254	102	27.746		
5	68.443	93.766	25.323		

The thickness of the films is found to be in the range 20-90 nm. The high thickness values of undoped TiO_2 films derived from the precursor sols having particle size ~30 nm is due to the specific drop-spin coating technique adopted in the present method. The uniformly distributed co-doped titania film was developed by adjusting the rotating speed to 2000 RPM. AFM images (Figure 72) show the formation of irregular surfaces. The presence of ~310 nm alumina particles can be observed, which are distributed in almost homogeneous fashion on the glass surface. We can also observe a thin layer in between that of the bigger particles. This can be assumed as the titania layer.

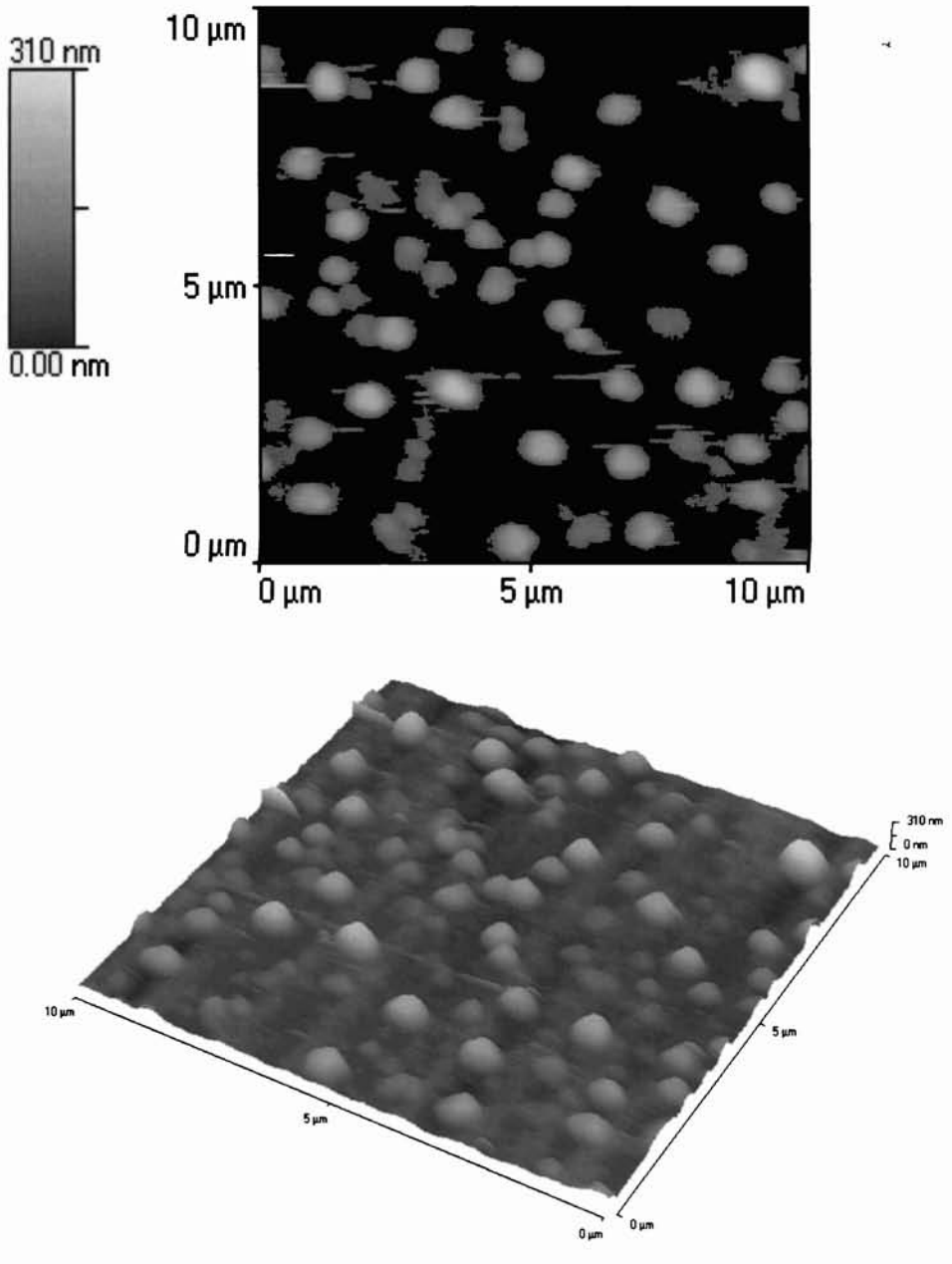

Figure 72: AFM image of TLA10 coating on glass surface

The irregularity makes the surface more hydrophilic, attributed to the increased surface area.

The photoactivity of the TLA10 coated films could not be measured as they were fabricated on 10 mm dia discs. However, the corresponding powder samples showed a higher activity for the samples.

4.4 Discussion

Coatings were made by both dip coating as well as spin coating technique. Dip coating was used for the fabrication of coatings from TLS precursor sols and spin coating from TLA10 precursor sols. The detailed characterization with respect to the optical as well as morphological features demonstrates the possibility of fabrication of highly transparent films (>95%) with the present coating formulations. The effect of withdrawal speed on the coating thickness corroborated with the earlier repots.

Coatings were carried out from the precursor sols with and without the addition of polymers. The study on the effect of polymers on the film formation as well as optical features illustrates PEG as a suitable additive among the polymers attempted. Further, the addition of 0.5% PEG was found to be enhancing the transparency as well as the absorbance of films. The absorbance decreases on increasing the polymer concentration to 1% by wt. According to reports, PEG also functions as an anatase phase nucleating agent at low temperature. However, in view of the specific alcohol-free preparative route we have adopted, the anatase formation could be achieved even at room

temperature, without the incorporation of PEG, in the present case. Further, the influence of polymers on the formation of crack-free films was a concern. However, doping 5% silica was found to be facilitating the crack-free film formation from the results. Therefore it was decided to stick to the coating formulations without the incorporation of polymers for the rest of the experiments.

The AFM analyses indicated the formation of continuous, micro crack-free films over the glass substrate when fabricated with the present coating formulation. The rate of heat treatment (1°C/min) as well as soaking period (3h) accomplished the development of highly crystalline anatase phase at 400°C, as is evident from the XRD pattern. The narrow high intensity peaks observed for the samples indicate the formation of highly crystalline anatase titania for the doped as well as co-doped compositions, while the undoped TiO_2 films showed the formation of a mixture of anatase and rutile phase. This can also be evidenced from the high roughness value for the undoped TiO_2 sample.

The presence of silica phase increases the hydrophilicity of the film. However, the presence of amorphous silica phase is detrimental to the photoactivity, owing to its possibility to act as charge carrier recombination centres. Therefore in the present work, a calcination- followed by chemical leaching is adopted to attain highly crystalline mesoporous titania framework. The films were, first, calcined at a rate of 1°C/min upto 400°C and soaked for a period of 3 h. After calcination, the films were undertaken a chemical leaching process as per the procedure given in chapter II Section 2.2.4. This was

instrumental in the 3-fold increase in specific surface area and the corresponding enhancement in activity. The highly crystalline nature of the matrix and pore walls of leached samples as confirmed by TEM demonstrates its importance in the area of active coatings.

The nanocrystalline-mesoporous-high surface area-TiO_2 film with >95 % optical transmittance obtained even after the leaching process was found to be a suitable candidate in active coatings. The high crystallinity of the mesoporous network system could be potential for applications as high surface area battery electrodes, sensors, optoelectronic devices, and catalysts as well. Furthermore, this also offers an opening in the field of solar energy utilization wherein solar cells and self-cleaning surfaces are involved.

4.5 Conclusion

Undoped, 1% La_2O_3 doped and 5% SiO_2-1% La_2O_3 co-doped TiO_2 precursor sols were prepared and films were fabricated with these sols. The films were characterized for the optical properties with UV-Vis spectroscopy and the morphological characterization was done with AFM. Band gap analysis indicated a slight change on doping with both lanthana and ceria. The band gaps of undoped TiO_2, 1% La_2O_3-doped TiO_2 (TL-1) and 1% CeO_2-doped TiO_2 (TC-1) are 3.23, 2.94 and 3.28 eV respectively. The morphological features of the films before and after chemical leaching showed the formation of transparent, homogeneous, ordered porous doped TiO_2 films on glass surface. The ordered, highly porous film formed as a result of leaching was tested to be

hydrophilic in nature. Similarly, ultrathin titania films were prepared by spin coating technique from TL-1 and TLA10 precursor sols. The lanthana doped titania sol prepared through a hydrolysis-condensation process produced teardrop shaped films. The incorporation of 10 % Al_2O_3 having larger particle size of 288.9 nm in the titania precursors influenced the morphology as well as thickness of the film considerably. Comparison with morphological features of samples prepared with different RPM established that the selection of spinning speed is also crucial in obtaining hybrid films with tailored particle distribution. The introduction of both lanthana and alumina produced a higher photoactivity and such hybrid films should form excellent self-cleaning nano coatings on glass surfaces. The tear-drop shape of the film derived from the polymeric titania sol was converted to a more or less uniform shaped ultrathin film by adding 10 % Al_2O_3 suspension (0.3μ) to the 1% La_2O_3-doped TiO_2 sol and subsequent spin coating at a rotation speed of 4000 RPM. The massy alumina particles uniformly distributed in the titania sol is found to be responsible for the formation of uniform ultra thin film. The tangential movement of alumina particles drags away the titania sol particles, which is attached to it in the sol stage. This whole process is responsible for the formation of an ultra thin film having a uniform thickness. The preliminary experiments indicate that these films are highly hydrophilic.

Chapter V

Conclusion

In the present work, synthesis of rare earth oxide doped nanocrystalline titanium oxide with appreciably high photoactivity is reported. The sol-gel titania precursor has further been used for developing self-cleaning nano coatings on glass surface. The preparative parameters for the titania such as temperature of reaction, solvent, acid concentration and water/alkoxide mole ratio were kept constant and the effect of dopants such as lanthana and ceria were studied in detail on the powder and films. The role of acetic acid on the structural and textural properties of powders as well as films was also studied. Attempt has been made to arrive at synthesis-property correlation.

Stable titania sol doped with La_2O_3 and/or CeO_2 has been prepared separately starting from TTIP through a solution-sol-gel process. Undoped titania gel after heating to 300°C has a specific surface area of 120 m^2g^{-1}, which increased to 160 m^2g^{-1} in presence of 1 % La_2O_3 and decreased considerably to 52 m^2g^{-1} on calcination to 700° C. On the other hand, undoped titania possessed only ~1 m^2g^{-1} surface area after calcination to 700° C. Further, the 1% La_2O_3 doping retained about 37% of the total pore volume at 300°C. La_2O_3 also enhanced the high temperature anatase phase stability of titania. The A→R transformation temperature increased by about 200° C in presence of

1 % La_2O_3. Doping with 1% La_2O_3 decreased the anatase crystallite size of titania to 16.81 nm at 700° C, from its undoped counterpart having 39.09 nm. Furthermore, there is considerable increase in the surface acidity for the La_2O_3-doped TiO_2 indicating its possibility to be used as solid acid catalysts. The enhanced properties of titania are due to the excellent dopant distribution in titania matrix, the presence of Ti-O-La linkage as well as the increased surface acidity and nanocrystalline nature.

Besides La_2O_3-doped TiO_2 samples, CeO_2-doped samples also have shown an increase in surface area. The addition of cerium oxide resulted in a decrease in crystallite size of titania and corresponding enhancement in phase transformation temperature, which was further increased with increasing concentration of both La_2O_3 and CeO_2. However, La_2O_3 was found to be more effective than CeO_2. The anatase to rutile transformation temperature increased to ~940°C in presence of 1% La_2O_3 from 670°C for the undoped TiO_2. The crystallite size of titania ranged between 5-70 nm and the critical size limit for A→R transformation was established to be ~'39-47' nm in the present work. The photoactivity of the undoped and doped titania obtained by the degradation experiments of methylene blue solution established that 1% La_2O_3-doped TiO_2 annealed at 700°C is the better catalyst. The activity was found to be superior to that of commercial TiO_2 samples such as Degussa P-25 and Hombikat UV 100.

The activity is depended on both the structural and textural characteristics of titania, evolved as a result of doping. Therefore, the structural

evolution of sol-gel titania was studied with the objective to understand the role of acetic acid in the ordering of Ti and La/Ce species throughout the sol-gel conversion. Lanthana and /or ceria added to sol-gel titania in the form of their respective nitrates could effectively retard the anatase to rutile phase transformation as well as the drastic reduction in surface area. The segregation of lanthana / ceria particles at the grain boundary by the formation of Ti-O-RE bonds or otherwise is demonstrated as responsible for the enhanced properties. The thrust for the Ti-O-RE bond formation is attributed to the hard Lewis basicity of acetic acid, which holds both the Ti^{4+} and La^{3+}/Ce^{3+} ions (Hard Lewis acids) by formation of heterodentate bridges that keep them intact towards much higher temperatures in the reaction sequences. The large frequency separation between the symmetric and asymmetric stretching vibrations of (COO) group in the FTIR spectra substantiates this conclusion. The understanding of the chemical sequences associated with the present procedure will provide repeatability to the material synthesis, which is a concern of the sol-gel process. The role of acetic acid in the reduction of titania sol particle size has been discussed and a possible reaction mechanism involved in the process is proposed.

Further, the procedure is modified for the preparation of high surface area, mesoporous doped titania. The controlled mesoporosity is achieved through a doping-followed by chemical leaching process; wherein silica is first added to a La_2O_3-doped TiO_2 precursor sol and allowed to form a homogeneous gel. Subsequent to gelation, drying and heat treatment, the homogeneously

distributed the amorphous silica phase is leached out preferentially using NaOH solution. The mesoporous texture, with the fully crystalline pores walls and matrix has enormous potential in the application fields such as high surface area battery electrodes, sensors, optoelectronic devices, photoactive self-cleaning surfaces and as catalysts.

The precursor sols were further used for the film fabrication and the morphological studies were carried out using the representative films. Undoped titania showed a higher RMS roughness value compared to the lanthana doped titania, which had an ordered structural morphology, while the co-doped-leached films showed almost regular mesoporous texture. The mesoporous, high surface area, transparent coatings were photoactive and hydrophilic. The major conclusions are presented below.

1. Development of photoactive doped titania compositions, which are active at higher calcination temperatures; 1% La_2O_3-doped TiO_2 at 700°C and 1% CeO_2-doped TiO_2 at 600°C. The activity was superior to the commercially available titania such as Degussa P-25 and Hombikat UV 100.
2. The role of Hard and Soft Acids and Bases principle in the structural and textural evolution of doped titania systems, which exploits the heterodentating effect of acetic acid (hard Lewis base) between titanium and lanthanum and/or cerium precursor ions (hard Lewis acids) to the fullest.

3. Synthesis of high surface area titania systems with a co-doping process (5% SiO_2-1% La_2O_3 co-doped TiO_2). Further, the chemical leaching resulted in the formation of thermally stable, extremely high surface area (240 m^2g^{-1} at 700°C) doped TiO_2 catalyst having enhanced activity with respect to the degradation of methylene blue.
4. Highly transparent (~95%), photoactive nanocrystalline titania and doped titania films were fabricated from the optimized precursor sols.
5. The chemical leaching resulted in the production of transparent, photoactive, thermally stable, mesoporous-doped titania films.

The highlight of the present work involves synthesis of nanocrystalline rare earth oxide doped and undoped titania having catalytic and photocatalytic property, through sol-gel route, synthesis of mesoporous titania having high thermal pore stability by a doping-leaching process and developing transparent photoactive, self-cleaning nano coatings. The novel synthesis method involves use of acetic acid as reactive intermediate and its role in sol synthesis stage based on HSAB principle. The role of lanthanum and cerium oxide dopants in decreasing the titania crystallite size, increase of anatase to rutile transformation temperature, enhancement of specific surface area and the enhancement of photocatalytic property have also been explained based on structural properties. The present method may have excellent applications in future developments with respect to self-cleaning nano coatings, anti-fogging and super-hydrophilic coatings and probably in solar energy related systems.

References

[1] H. Gleiter, Progress In Mater. Sci., 33 [4] 223 (1989)

[2] M. J. Mayo, International Mater. Rev., 41 [3] 85 NJ N5 (1996)

[3] K. Lu, Mater. Sci. & Eng. R16, Reports: A Rev. J., 161 (1996)

[4] C. Suryanarayana, International Mater. Rev. 40 [2] 41 (1995)

[5] M. I. Baraton and L Merhari, Nanostruct. Mater., 10 [5] 699 (1998)

[6] Third International Conference, TiO_2'93, Conference & Exhibition, September 14-15, 1993. Hyatt Regency Woodfield Hotel, Chicago, USA: Intertech Conferences, Maine, USA

[7] J. Huang, I. Ichinose, T. Kunitake and A. Nakao, Langmuir, 18 [23] 9048 (2002)

[8] M. Karches, M. Morstein, P. Vonrohr, R. L. Pozzo, J. L. Giombi and M. A. Baltanas, Catal. Today, 72 [3-4] 267 (2002)

[9] T. Ishigaki, Y. -Li Li and E. Kataoka, J. Am. Ceram. Soc., 86 [9] 1456 (2003)

[10] G. Z. Chen, D. J. Fray and T. W. Farthing, Nature, 407, 361 (2000)

[11] R. Adams, Eur. Coatings J., 6, 395 (1996)

[12] G. Buxbaum, Ed. Industrial Inorganic Pigments, VCH: Weinheim, Germany (1993)

[13] T. Rentschler, A. Reller, Eur. Coatings J., 4, 80 (1999)

[14] W. M. Burry and D. S. Keller, J. Chromatography A, 1 972 [2] 241 (2002)

[15] T. C. Patton, Pigment Handbook, Vol. 1, Properties and Economics, John Wiley 7 Sons, Inc., USA (1973)

[16] A. Shah, P. Torres, R. Tscharner, N. Wyrsch, and H. Keppner, Science, 285, 692 (1999)

[17] P. Innocenzi, G. Brusatin, M. Guglielmi, A. Martucci, G. Battaglin, S. Pelli, G. Righini, J. Non-Cryst. Solids, 220 [2-3] 202, (1997)

[18] Z. A. E. P. Vroon and C. I. M. A. Spee, J. Non-Cryst. Solids, 218, 189 (1997)

[19] X. Bokhimi, Chem. Mater., 9 [11] 2616 (1997)

[20] G. Grubert, M. Stockenhuber, O. P. Tkachenko and M. Wark, Chem. Mater., 14 [6] 2458 (2002)

[21] D. Grosso, G. J. de A. A. Soler-Illia, E. L. Crepaldi, F. Cagnol, C. Sinturel, A. Bourgeois, A. Brunet-Bruneau, H. Amenitsch, P. A. Albouy and C. Sanchez, Chem. Mater., 15 [24] 4562 (2003)

[22] C. J. Barbe, F. Arendse, P. Comte, M. Jirousek, F. Lenzmann, V. Shklover, and M. Gratzel, Am. Ceram. Soc., 80 [12] 3157 (1997)

[23] S. Matsuda and A. Kato, Appl. Catal., 8, 149 (1983)

[24] I. Arslanalaton and I. A. Balcioglu, AATCC Rev., 2 [3] 33 (2002)

[25] T. Tsumura, N. Kojitani, I. Izumi, N. Iwashita, M. Toyoda and M. Inagaki, J. Mater. Chem., 12 [5] 1391 (2002)

[26] M. A. Fox and M. T. Dulay, Chem. Rev., 93, 341 (1993)

[27] A. Fujishima and K. Honda, Nature, 238, 37 (1972)

[28] A. Fujishima and T. N. Rao, Proc. Ind. Acad. Sci. (Chem. Soc.) 109 [6] 471 (1997)

[29] A. Fujishima, T. N. Rao and D. A. Tryk, J. Photochem. Photobiol. C: Photochem. Rev., 1, 1 (2000)

[30] R. Asahi, T. Morikawa, T. Ohwaki, K. Aoki and Y. Taga, Science, 293, 269 (2001)

[31] S. Yin and T. Sato, Ind. Eng. Chem. Res., 39 [12] 4526 (2000)

[32] J. C. Yu, J. G. Yu, W. K. Ho, Z. T. Jiang and L. Z. Zhang, Chem. Mater., 14 [9] 3808 (2002)

[33] B. O'Regan and M. Gratzel, Nature, 353, 737 (1991)

[34] P. V. Kamat and N. M. Dimitrijevic, Solar Energy, 44, 83 (1990)

[35] M. K. Nazeeruddin, R. Humphry-Baker, P. Liska and M. Gratzel, J. Phys. Chem. B, Solar Cell, 107 [34] 8981 (2003)

[36] N. Kopidakis, K. D. Benkstein, J. van de Lagemaat and A. J. Frank, J. Phys. Chem. B, Solar Cells, 107 [41] 11307 (2003)

[37] S. Nakade, Y. Saito, W. Kubo, T. Kitamura, Y. Wada and S. Yanagida, J. Phys. Chem. B, Solar Cells, 107 [33] 8607 (2003)

[38] D. Y. Goswami, Engineering of the solar photocatalytic detoxification and disinfections processes, In: K.W. Boer (Ed.), Advances in Solar Energy, Vol. 10, Am. Solar Energy Soc., Boulder, CO, 165 (1995)

[39] O. Harizanov, P. Stefchev and R. Kirilov, In: Proceedings of Solar World Congress, Budapest, 357 (1993)

[40] A. Ruiz, A. Cornet, G. Sakai, K. Shimanoe, J. R. Morante and N. Yamazoe, Chem. Lett., 892 (2002)

[41] Y. –Y. Huang, B. –Y. Zhao and Y. –C. Xie, Appl. Catal. A: Gen., 171, 65 (1998)

[42] R. Kurrat, J. Prenosil and J. Ramsden, J. Coll. Interface Sci., 185, 1 (1997)

[43] M. Pang, D. E. Eakins, M. G. Norton and D. F. Bahr, Corrosion, 57 [6] 523 (2001)

[44] K. Kamada, M. Mukai and Y. Matsumoto, Electrochim. Acta, 47 [20] 3309 (2002)

[45] B. S. Richards, J. E. Cotter and C. B. Honsberg, Appl. Phys. Lett., 80 [7] 1123 (2002)

[46] L. I. Vergara, M. C. G. Passeggi and J. Ferron, Appl. Surf. Sci., 187 [3/4] 199 (2002)

[47] F. G. Bianchini, M. Gulielmi, P. Polato and G. Soraro, J. Non-Cryst. Solids, 63 [1-2] 251 (1984)

[48] S. Sakka, K. Kamiya and K. Makita, J. Mater. Sci. Lett., 2, 395 (1983)

[49] A. Duran, J. M. F. Navarro and P. Casariego and A. Joglar, J. Non-Cryst. Solids, 82 [1-3] 391 (1986)

[50] H. Dislich and E. Hussmann, Thin Solid Films, 77 [1-3] 129 (1981)

[51] Z. C. Orel, Solid State Ionics, 116 [1-2]105 (1999)

[52] J. Livage, Solid State Ionics, 86 [2] 935 (1996)

[53] B. Samuneva, V. Kozhuharov, Ch. Trapalis and R. Kranold, J. Mater. Sci., 28, 2353 (1993)

[54] J. Lee, T. Tanaka, S. Uchiyama, M. Tsuchiya and T. Kamiya, Jpn. J. Appl. Phys., Part 2, 36 [1A/B] L52 (1997)

[55] S. K. Ghosh, C. Suresh, P. Prabhakar Rao, A. K. Vasudevan, and K. G. K. Warrier, Trans. Ind. Ceram. Soc., 58 [5] 112 (1999)

[56] M. Thieme, K. P. Wieters, F. Bergner, D. Scharnweber, H. Worch, J. Ndop, T. J. Kim and W. Grill, J. Mater. Sci. Mater. In Medicine, 12 [3] 225 (2001)

[57] P. Cacciafesta, K. R. Hallam, A. C. Watkinson, G. C. Allen, M. J. Miles and K. D. Jandt, Surf. Sci., 491 [3] 405 (2001)

[58] V. Faust, F. Heidenau, J. Schmidgall, F. Stenzel, G. Lipps and G. Ziegler, Euro Ceram. VII, PT 1-3 [206-2] 1547 (2002)

[59] E. Garfunkel, E. Gusev, A. Vul (Eds.), Fundamental Aspects of Ultrathin Dielectrics on Si-based Devices, NATO Science Series, Kluwer Academic Publishers, Dordrecht (1998)

[60] S. Y. Huang, L. Kavan, I. Exnar and M. Grätzel, J. Electrochem. Soc., 142, L142 (1995)

[61] M. V. Koudriachova, N. M. Harrison and S. W. D. Leeuw, Phys. Rev. Lett., 86, 1275 (2001)

[62] T. Ohzuku and T. Hirai, Electrochim. Acta, 27, 1263 (1982)

[63] G. S. Vicente, A. Morales and M. T. Gutierrez, Thin Solid Films, 391 [1] 133 (2001)

[64] M. Grätzel, Nature, 414, 338 (2001)

[65] Z. Zou, J. Ye, K. Sayama and H. Arakawa, Nature, 414, 625 (2001)

[66] S. U. M. Khan, M. Al-Shahry, and W. B. Ingler, Jr., Science, 297, 2243 (2002)

[67] L. P. Childs and D. F. Ollis, J. Catal., 66, 383 (1980)

[68] A. L. Pruden and D. F. Ollis, J. Catal., 82, 404 (1983)

[69] I. Ait-Ichou, M. Formenti, B. Pommier and S. J. Teichner, J. Catal., 91, 193 (1985)

[70] S. A. Larson, J. A. Widegren and J. L. Falconer, J. Catal., 157, 611 (1995)

[71] J. L. Falconer and K. A. Magrini-Bair, J. Catal., 179, 171 (1998)

[72] M. D. Driessen and V. H. Grassian, J. Phys. Chem. B, 102 [8] 1418 (1998)

[73] D. Brinkley and T. Engel, J. Phys. Chem. B, 104 [42] 9836 (2000)

[74] M. C. Blount and J. L. Falconer, J. Catal., 200, 21 (2001)

[75] T. Tatsuma, S. Tachibana and A. Fujishima J. Phys. Chem. B, 105 [29] 6987 (2001)

[76] D. F. Ollis and H. Al-Ekabi, Photocatalytic Purification and Treatment of Water and Air, Elsevier, Amsterdam (1993)

[77] N. Serpone and E. Pelizzetti, Photocatalysis–Fundamentals and Applications, Wiley, New York (1989)

[78] D. –R. Park, J. Zhang, K. Ikeue, H. Yamashita and M. Anpo, J. Catal., 185 [1] 114 (1999)

[79] L. Cao, Z. Gao, S. L. Suib, T. N. Obee, S. O. Hay and J. D. Freihaut, J. Catal., 196 [2] 253 (2000)

[80] S. Ruan, F. Wu, T. Zhang, W. Gao, B. Xu and M. Zhao, Mater. Chem. and Phys., 69, 7 (2001)

[81] J. A. Navio, G. Colon, M. Macias, C. Real and M. I. Litter, Appl., Catal. A, 177, 111 (1999)

[82] K. Vinodgopal, I. Bedja and P. V. Kamat, Chem. Mater., 8 [8] 2180 (1996)

[83] V. Romeas, P. Pichat, C. Guillard, T. Chopin and C. Lehaut, Ind. Eng. Chem. Res., 38, 3878 (1999)

[84] Y. Paz, Z. Luo, L. Rabenberg and A. Heller, J. Mater. Res., 10 [11] 2842 (1995)

[85] R. Wang, K. Hashimoto, A. Fujishima, M. Chikuni, E. Kojima, A. Kitamura, M. Shimohigoshi and T. Watanabe, Adv. Mater., 10, 135 (1998)

[86] K. P. Bansal, S. Kumari (Kurinec), B. K. Das, and G. C. Jain, J. Mater. Sci., 16, 1994 (1981)

[87] G. N. Conti, N. Peyghambarian, M. Ferrari, M. Montagna, G. C. Righini, M. Brenci, M. A. Forestiere, S. Pelli and G. Ricci, Philosophical Magazine B, 82, 721 (2002)

[88] T. Ibusuki and K. Takeuchi, J. Mol. Catal., 88, 93 (1994)

[89] A. Mills, H. R. Davies and D. Worsley, Chem. Soc. Rev., 22, 417 (1993)

[90] C. Labbez, P. Fievet, A. Szymczyk, A. Vidonne, A. Foissy and J. Pagetti, J. Membr. Sci., 208 [1-2] 315 (2002)

[91] L. Shi and N. B. Wong, J. Mater. Res., 14 [9] 3599 (1999)

[92] S. Mayadevi, S. S. Kulkarni, A. J. Patil, M. H. Shinde, H. S. Potdar, S. B. Deshpande and S. K. Date, J. Mater. Sci., 35 [15] 3943 (2000)

[93] K. N. P. Kumar, K. Keizer and A.J. Burggraaf, J. Mater. Chem., 3 [11] 1141 (1993)

[94] M. A. Anderson, M. J. Giesemann and Q. Xu, J. Membr. Sci., 39, 243 (1998)

[95] D. J. Bjorkert, R. Mayappan, D. Holland, M. H. J. Lewis, J. Eur. Ceram. Soc., 19, 1847 (1999)

[96] K.I. Hadjiiivanov and D.G. Klissurski, Chem. Soc. Rev., 25 [1] 61 (1996)

[97] A. A. Azad, L. B. Younkman, S. A. Akbar and M. A. Alim, J. Am. Ceram. Soc., 77 [2] 481 (1994)

[98] F. A. Grant, Rev. Mod. Phys., 31 [3] 646 (1959)

[99] G. V. Samsonov, The Oxide Handbook, IFI/Plenum Press, New York, (1982)

[100] U. Diebold, Surf. Sci. Reports, 48 [5-8] 53 (2003)

[101] J. Yu and X. Zhao, Mater. Res. Bull., 35, 1293 (2000)

[102] B. Pal, M. Sharon and G. Nogami, Mater. Chem. Phys., 59, 254 (1999)

[103] C. Sousa and F. Illas, Phys. Rev. B (Condensed Matter), 50 [19] 3974 (1994)

[104] I. J. McColm, Ceramic science for materials technologists, Leonard Hill, Chapman and Hall, New York, (1983)

[105] S. R. Yoganarasinhan and C. N. R. Rao, Trans. Faraday Soc., 58, 1579 (1962)

[106] K. N. P. Kumar, K. Keizer, A. J. Burggraaf, T. Okubo, H. Nagamoto and S. Morooka, Nature, 358, 48 (1992)

[107] X. -Z. Ding and X. K. Liu, J. Mater. Res., 13 [9] (1998)

[108] *http://www.nl-ind.com/kronos/na/titanium3.html*cronos, inc., NL Industries, June 10 (1999)

[109] Y. K. Hwang, K. C. Lee and Y. V. Kwon, Chem. Comm., 1738 (2001)

[110] L. Kavan, J. Rathousky, M. Gratzel, V. Shklover and A. Zukal, J. Phys. Chem. B, 104 [50] 12012 (2000)

[111] D. Grosso, G. J. A. A. Soller-Illia, F. Babonneau, C. Sanchez, P. A. Albouy, A. Brunet-Bruneau and A. R. Balkenende, Adv. Mater., 13, 1085 (2001)

[112] P. C. A. Alberius, K. L. Frindell, R. C. Hayward, E. J. Kramer, G. D. Stucky and B. F. Chmelka, Chem. Mater., 14 [8] 3284 (2002)

[113] I. -S. Park, S. -R. Jang, J. S. Hong, R. Vittal and K. -J. Kim, Chem. Mater., 15 [24] 4633 (2003)

[114] A. Goossens, B. van der Zanden and J. Schoonman, Chem. Phys. Lett., 331 (2000)

[115] S. Monticone, R. Tufeu, A. V. Kanaev, E. Scolan and C. Sanchez, Appl. Surf. Sci., 162, 565 (2000)

[116] S. H. Chung, Y. Wang, L. Persi, F. Croce, S. G. Greenbaum, B. Scrosati and E. Plichta, J. Power Sources, 98, 644 (2001)

[117] J. C. Plenet, A. Brionde, E. Berstein, F. Lequevre, J. Dumas and J. Mugnier, Opt. Mater., 13, 411 (2000)

[118] N. Negishi, T. Iyoda, K. Hashimota and A. Fujishima, Chem. Lett., 841 (1995)

[119] M. R. Hoffmann, S. T. Martin, W. Choi and D. W. Bahnemann, Chem. Rev., 95, 69 (1995)

[120] A. L. Linsebigler, G. Lu and J. T. Yates, Chem. Rev., 95, 735 (1995)

[121] A. Mills and S. L. Hunte, J. Photochem. Photobiol. A: Chem., 108, 1 (1997)

[122] V. E. Henrich, G. Dresselhaus and H. J. Zeiger, Phys. Rev. Lett., 36, 1335 (1976)

[123] W. J. Lo, Y. W. Chung and G. A. Somorjai, Surf. Sci., 71, 199 (1978)

[124] H. O. Finklea, Semiconductor Electrodes, Elsevier, Amsterdam (1988)

[125] M. Radecka and M. Rekas, J. Am. Ceram. Soc., 85 [2] 346 (2002)

[126] K. L. Yeung, S. T. Yau, A. J. Maira, J. M. Coronado, J. Soria and P. L. Yue, J. Catal., 219, 107 (2003)

[127] H. Einaga, S. Futamura and T. Ibusuki, Environ. Sci. Technol., 35 [9] 1880 (2001)

[128] J. H. Schattka, D. G. Shchukin, J. Jia, M. Antonietti and R. A. Caruso, Chem. Mater., 14 [12] 5103 (2002)

[129] Y. Du and J. Rabani, J. Phys. Chem. B, 107 [43] 11970 (2003)

[130] M. E. Zorn, D. T. Tompkins, W. A. Zeltner and M. A. Anderson, Environ. Sci. Technol., 34 [24] 5206 (2000)

[131] Z. -X. Lu, L. Zhou, Z. -L. Zhang, W. -L. Shi, Z. -X. Xie, H. -Y. Xie, D. -W. Pang and P. Shen, Langmuir, 19 [21] 8765 (2003)

[132] S. Y. Chae, M. K. Park, S. K. Lee, T. Y. Kim, S. K. Kim and W. I. Lee, Chem. Mater., 15 [17] 3326 (2003)

[133] M. Schiavello, Photoelectrochemistry, photocatalysis and photoreactors, fundamentals and developments, series C: Mathematical and physical sciences Vol. 146, Reidel Publishing Company, Holland (1985)

[134] C. N. Satterfield, Heterogeneous Catalysis in Industrial Practice, 2nd ed., McGraw-Hill, New York (1991)

[135] A. Vittadini, A. Selloni, F. P. Rotzinger and M. Grätzel, Phys. Rev. Lett., 81, 2954 (1998)

[136] A. Fahmi and C. Minot, Surf. Sci., 304, 343 (1994)

[137] T. Bredow and K. Jug, Surf. Sci., 327, 398 (1995)

[138] M. Lazzeri, A. Vittadini and A. Selloni, Phys. Rev. B, 63, 155409/1 (2001).

[139] M. Lazzeri, A. Vittadini and A. Selloni, Phys. Rev. B, 65, 119901/1 (2002).

[140] U. Gesenhues and T. Rentschler, J. Solid State Chem., 143, 210 (1999)

[141] A. Kato, Y. Takeshima and Y. Katatae, M. R. S. Symp. Proc. 155, 13 (1989)

[142] K. Tanaka, Y. Murakami, T. Imai, T. Matumoto, S. Furuno, W. Sugimoto and Y. Takasu, Chem. Lett., 1280 (2001)

[143] M. K. Akhtar, S. E. Pratsinis and S. V. R. Mastrangelo, J. Am. Ceram. Soc., 75 [12] 3408 (1992)

[144] S. E. Pratsinis, W. Zhu and S. Vemury, Powder Technol., 86, 87 (1996)

[145] F. Kirkbir and H. Komiyama, Adv. Ceram. Mater., 3, 511 (1988)

[146] K. Morishige, F. Kanno, S. Ogawara and S. Sasaki, J. Phys. Chem., 89 [20] 4404 (1985)

[147] A- E. A. Barringer and H. K. Bowen, Langmuir 1, 414 (1985)

[148] J. H. Jean and T. A. Ring, Langmuir, 2, 251 (1986)

[149] L. L. Hench and J. K. West, Chem. Rev., 90, 33 (1990)

[150] T. E. Wood and H. Dislich, An abbreviated history of sol-gel technology, in Sol-Gel Science and Technology, E. J. A. Pope, S. Sakka, and L. C. Klein, (Eds.), Am. Ceram. Soc., Westerville, OH, 3 (1995)

[151] C. W. Turner, Am. Ceram. Soc. Bull., 70, 1487 (1991)

[152] X. Ding and X. Liu, Mater. Sci. & Eng. A, 224, 210 (1997)

[153] D. M. Roy and R. Roy, Am. Mineral., 39, 957 (1954)

[154] R. Roy, J. Am. Ceram. Soc., 39, 145 (1956)

[155] R. Roy, J. Am. Ceram. Soc., 52, 344 (1969)

[156] G. J. McCarthy, R. Roy and J. M. McKay, J. Am. Ceram. Soc., 54, 637 (1971)

[157] H. Schroeder, Opt. Acta, 9, 249 (1962)

[158] J. D. Mackenzie, J. Non-Cryst. Solids, 52 [1-3] 1 (1982)

[159] J. D. Mackenzie, In Ultrasonic processing of ceramics, glasses and composites; L. L. Hench and D. R. Ulrich, (Eds.), Wiley: New York, 15 (1984)

[160] J. Venzel, In Glass. Current Issues, A. F. Wright and A. F. Dupuy, (Eds.), Martinus Nijhojj: Dordrecht, Netherlands, 224 (1985)

[161] C. J. Brinker, R. Sehgal, S. L. Hietala, R. Deshpande, D. M. Smith and D. Loy, J. Membr. Sci., 94, 85 (1994)

[162] M. M. Yusuff, H. Imai and H. Hirashima, J. Non-Cryst. Solids, 285 [1-3] 90 (2001)

[163] M. M. Yusuff, H. Imai and H. Hirashima, J. Sol-Gel Sci. Technol., 25, 65 (2002)

[164] B. S. Yan, K. Miyazawa, H. Zhou, I. Honma and M. Kuwabara, Adv. Mater., 13, 1377 (2001)

[165] E. L. Crepaldi, G. J. A. A. Soller-Illia, D. Grosso and C. Sanchez, New J. Chem., 27, 9 (2003)

[166] J. Wang, S. Uma and K. J. Klabunde, Appl. Catal. B: Environ., 48 [2] 151 (2004)

[167] J. F. Hund, M. F. Bertino, G. Zhang, C. Sotiriou-Leventis, N. Leventis, A. Tokuhiro and J. Farmer, J. Phys. Chem. B, 107 [2] 465 (2003)

[168] J. J. Pietron and D. R. Rolison, J. Non-Cryst. Solids, 285 [1-3] 13 (2001)

[169] H. D. Gesser and P. C. Goswami, Chem. Rev., 89, 765 (1989)

[170] X. Z. Ding, Z. Z. Qi and Y. Z. He, J. Mater. Sci. Lett., 14, 21 (1995)

[171] F. Bosc, A. Ayral, P. –A. Albouy and C. Guizard, Chem. Mater., 15 [12] 2463 (2003)

[172] G. De, D. Ganguli and B. Karmakar, J. Non-Cryst. Solids, 272 [2-3] 119 (2000)

[173] W. Vogelsberger, A. Seidel and T. Breyer, Langmuir, 18 [8] 3027 (2002)

[174] J. Widegren and L. Bergstrom, J. Am. Ceram. Soc., 85 [3] 523 (2002)

[175] K. C. Song and S. E. Pratsinis, J. Colloid and Interface Sci., 231, 289 (2000)

[176] V. G. Courtecuisse, K. Chhor, J. F. Bocquet and C. Pommier, Ind. Eng. Chem. Res., 35 [8] 2539 (1996)

[177] J. Kim, K. C. Song and S. E. Pratsinis, J. Nanoparticle Res., 2, 419 (2000)

[178] P. Arnal, R. J. P. Corriu, D. Leclercq, P. H. Mutin, and A. Vioux, J. Mater. Chem., 6 [12] 1925 (1996)

[179] H. Zhang, M. Finnegan and J. F. Banfield, Nano Lett., 1 [2] 81 (2001)

[180] S. D. Park, Y. H. Cho, W. W. Kim and S. J. Kim, J. Solid State Chem., 146, 230 (1999)

[181] G. Cerveau, R. J. P. Corriu and E. Framery, J. Mater. Chem., 10 [7] 1617 (2000)

[182] G. Cerveau, R. J. P. Corriu and E. Framery, Chem. Comm., 20, 2081 (1999)

[183] H. Kominami, Y. Takada, H. Yamagiwa, Y. Kera, M. Inoue and T. Inui, J. Mater. Sci. Lett., 15 [3] 197 (1996)

[184] D. C. Hague and M. J. Mayo, J. Am. Ceram. Soc., 77 [7] 1957 (1994)

[185] J. L. Keddie and E. P. Giannelis, J. Am. Ceram. Soc., 74 [10] 2669 (1991)

[186] C. C. Ting and S. Y. Chen, J. Mater. Res., 16 [6] 1712 (2001)

[187] D. Larcher, G. Sudant, R. Patrice and J. –M. Terascon, Chem. Mater., 15 [18] 3543 (2003)

[188] I. Artaki, S. Sinha, A. D. Irwin and J. Jones, J. Non-Cryst. Solids, 72 [2-3] 391 (1985)

[189] A. Aelion, A. Loebel and F. Eirich, J. Am. Chem. Soc., 72, 5702 (1950)

[190] H. Schimdt, H. Scholze and A. Kaiser, J. Non-Cryst. Solids, 63 [1-2] 1 (1984)

[191] H. Schimdt, A. Kaiser, M. Rudolph and A. Lentz, In Science of ceramic chemical processing, L. L. Hench and D. R. Ulrich, (Eds.), Wiley New York, 87 (1986)

[192] J. Livage, M. Henry and C. Sanchez, Prog. Solid State Chem., 18 [4] 259 (1988)

[193] C. J. Brinker and G. W. Scherer, Sol-Gel Science, Academic Press, San Diego (1990)

[194] A. Imhof and D. J. Pine, Nature, 389, 948 (1997)

[195] D. Deffar, G. H. Teng and M. D. Soucek, Macromol. Mater. & Eng., 286 [4] 204 (2001)

[196] Q. Zhang, L. Gao and J. Guo, J. Eur. Cerm. Soc., 20, 2153 (2000)

[197] K. J. D. MacKenzie, Trans. J. Br. Ceram. Soc., 74, 29 (1975)

[198] K. J. D. MacKenzie, Trans. J. Br. Ceram. Soc., 74, 121 (1975)

[199] D. Vorkapic and T. Matsouka, J. Am. Ceram. Soc., 81 [11] 2815 (1998)

[200] X. Shi, T. Cassagneau and F. Caruso, Langmuir, 18 [3] 904 (2002)

[201] Y. Ohya, H. Saiki, T. Tanaka, and Y. Takahashi, J. Am. Ceram. Soc., 79 [4] 825 (1996)

[202] K. Terabe, K. Kato, H. Miyazaki, S. Yamaguchi, A. Imai and Y. Iguchi, J. Mater. Sci., 29, 1617 (1994)

[203] C. L. Fan, D. Ciardullo, J. Paladino and W. Huebner, J. Mater. Res., 17 [6] 1520 (2002)

[204] B. E. Yoldas, J. Mater. Sci., 21, 1087 (1986)

[205] Y. Murakami, T. Matsumoto and Y. Takasu, J. Phys. Chem. B, 103 [11] 1836 (1999)

[206] C. Suresh, V. Biju, P. Mukundan and K. G. K. Warrier, Polyhedron, 17 [18] 3131 (1998)

[207] M. Kallala, C. Sanchez, and B. Cabane, Phys. Rev. E, 48 [5] 3692 (1993)

[208] L. Shi, N. B Wong, K. C. Tin and C. Y. Chung, J. Mater. Sci. Lett., 16 [15] 1284 (1997)

[209] R. B. Zhang and L. Gao, Mater. Res. Bull., 37 [9] 1659 (2002)

[210] K. C. Song and S. E. Pratsinis, J. Mater. Res., 15 [11] 2322 (2000)

[211] J. Yang, S. Mei and J. M. F. Ferreira, J. Am. Ceram. Soc., 83 [6] 1361 (2000)

[212] B. L. Bischoff and M. Anderson, Chem. Mater., 7 [10] 1772 (1995)

[213] K. N. P. Kumar, J. Kumari and K. Keizer, J. Am. Ceram. Soc., 77 [5] 1396 (1994)

[214] F. Cot, A. Larbot, G. Nabius and L. Cot, J. Eur. Ceram. Soc., 18, 2175 (1998)

[215] A. Chemseddine and T. Moritz, Eur. J. Inorg. Chem., 235 (1999)

[216] T. Sasamoto, S. Enomoto, Z. Zhimoda and Y. Saeki, J. Ceram. Soc. Jpn., 101, 230 (1993)

[217] J. F. Quinson, M. Chatelut, C. Guizard, A. Larbot and L. Cot, J. Non-Cryst. Solids, 121 [1-3] 72 (1990)

[218] T. Y. Zeng, Y. Qiu, L. Chen and X. Song, Mater. Chem. Phys., 56 [2] 163 (1998)

[219] T. Maurer, S. P. Muller, B. Kraushaar-Czarnetzki, Ind. Eng. Chem. Res., 40 [12] 2573 (20016)

[220] S. Klein, S. Thorimbert and W. F. Maier, J. Catal., 163 [2] 476 (1996)

[221] D. Keomany, C. Poinsignon and D. Deroo, 33 [4] 429 (1994)

[222] K. Kamiya, K. Tanimoto and T. Yoko, J. Mater. Sci. Lett., 5, 402 (1986)

[223] U. S. Ozkan, M. W. Kumthekar and Y. P. Cai, Ind. Eng. Chem. Res. 33 [12] 2924 (1994)

[224] G. S. Walker, E. Williams and A. K. Bhattacharya, J. Mater. Sci., 32 [21] 5583 (1997)

[225] Y. Matsumoto, M. Murakami, T. Shono, T. Hasegawa, T. Fukumura, M. Kawasaki, P. Ahmet, T. Chikyow, S. –Y. Koshihara, and H. Koinuma, Science, 291, 854 (2001)

[226] N. Economidis, Catal. Today, 40 [1] 27 (1998)

[227] N. Y. Topsoe, Science, 265 [5176] 1217 (1994)

[228] P. V. Kamat, Chem. Rev., 93, 267 (1993)

[229] Z. V. Saponjic, Z. Rakocevic, N. M. Dimitrijevic, J. M. Nadeljkovie, V. Jokanovic and D. P. Uskokovic, Nanostrut. Mater. 10 [3] 333 (1998)

[230] Z. Yuhong, W. Ming, X. Gouxing and Y. Weishen, http://www.chemistrymag.org/cji/2000/023017pe.htm, 2 [3] 17 (2000)

[231] X. Li, X. Quan and C. Kutal, Scr. Materialia, 50 [4] 499 (2004)

[232] S. Doeuff, M. Henry, C. Sanchez and J. Livage, J. Non-Cryst. Solids, 89 [1-2] 206 (1987)

[233] D. P. Birnie and N. J. Bendzko, III, Mater. Chem. Phys., 59, 26 (1999)

[234] D. P. Birnie, III., J. Mater. Sci., 35, 367 (2000)

[235] A. Leaustic and R. E. Riman, J. Non-Cryst. Solids, 135 [2-3] 259 (1991)

[236] I. Laaziz, A. Larbot, A. Julbe, C. Guizard and L. Cot, J. Solid State Chem., 98, 393 (1992)

[237] L. Hu, T. Yoko, H. Kozuka and S. Sakka, Thin Solid Films, 219 [1-2] 18 (1992)

[238] K. Kato and A. Tsuge, K. –ichi Niihara, J. Am. Ceram. Soc., 79 [6] 1483 (1996)

[239] P. A. Venz, R. L. Frost, J. R. Bartlett, J. L. Woolfrey and J. T. Kloprogge, Thermochim. Acta, 346, 73 (2000)

[240] Q. Zhang, L. Gao and J. Guo, Appl. Catal., B: Environ., 26, 207 (2000)

[241] R. Zhang and L. Gao, Mater. Res. Bull., 36, 1957 (2001)

[242] T. Nishide and F. Mizukami, Thin Solid Films, 353 [1-2] 67 (1999)

[243] T. Nishide and F. Mizukami, J. Ceram. Soc. Jpn., 100, 1122 (1992)

[244] T. Nishide and F. Mizukami, Thin Solid Films, 298 [1-2] 89 (1997)

[245] E. Y. Kaneko, S. H. Pulcinelli, V. T. Dasilva and C. V. Santilli, Appl. Catal. A: Gen., 235 [1-2] 71 (2002)

[246] A. Makishima, M. Asami and K. Wada, J. Non-Cryst. Solids, 100 [1-3] 321 (1988)

[247] G. Yi, Z. Wu and M. Sayer, J. Appl. Phys., 64, 2717 (1988)

[248] R. A. Assink, R. W. Schwartz, Chem. Mater., 5 [4] 511 (1993)

[249] G. M. Anilkumar, A. D. Damodaran and K. G. K. Warrier, Ceram. Trans., 73 (1997)

[250] K. V. Asha, T. V. Mani, A. D Damodaran and K. G. K. Warrier, J. Mater. Sci. Lett., 14 [18] 1317 (1995)

[251] C. P. Sibu, S. Rajesh Kumar, P. Mukundan and K. G. K. Warrier, Chem. Mater., 14 [7] 2876 (2002)

[252] P. K. Nair, M. Kazuyuki, K. Yoshimichi and M. Fujio, Mater. Res. Bull., 32 [9] 1303 (1997)

[253] B. Lantelme, M. Dumon, C. Mai and J. P. Pascault, J. Non-Cryst. Solids, 194 [1-2] 63 (1996)

[254] Y. Takahashi and Y. Matsuoka. J. Mater. Sci., 23, 2259 (1988)

[255] T. Sugimoto, K. Okada and H. Itoh, J. Dispersion Sci. Technol. 19 [2-3] 143 (1998)

[256] Y. Ohya, J. Mishina, T. Matsuda, T. Ban and Y. Takahashi, J. Am. Ceram. Soc., 82 [10] 2601 (1999)

[257] P. K. Sharma and A. Ramanan, J. Mater. Sci., 31, 773 (1996)

[258] K. Kato, A. Tsuzuki, H. Taoda, Y. Torii, K. Kato, and Y. Butsugan, J. Mater. Sci., 29, 5911 (1994)

[259] M. Gotic, M. Ivanda, A. Sekuli, S. Music, S. Popovic, A. Turkovic and K. Furic, Mater. Lett., 28, 225 (1996)

[260] T. Trung, W. J. Cho and C. S. Ha. Mater. Lett., 57, 2746 (2003)

[261] T. Peng, A. Hasegawa, J. Qiu, K. Hirao, Chem. Mater., 15 [10] 2011 (2003)

[262] C. T. Kresge, M. E. Leonowicz, W. J. Roth, J. C. Vartuli and J. S. Beck, Nature, 359, 710 (1992)

[263] J. S. Beck, J. C. Vartuli, W. J. Roth, M. E. Leonowicz, C. T. Kresge, K. D. Schmitt, C. T. –W Chu, D. H. Olson, E. W. Sheppard, S. B. McCullen, J. B. Higgins and J. L. Schlenker, J. Am. Chem. Soc., 114, 10834 (1992)

[264] E. L. Crepaldi, G. J. A. A. Soller-Illia, D. Grosso, F. Cagnol, F. Ribot and C. Sanchez, J. Am. Chem. Soc., 125 [32] 9770 (2003)

[265] J. Y. Ying, C. P. Mehnert and M. S. Wong, Angew. Chem. Int. Edn., 38, 56 (1999)

[266] Y. Masuda, T. Sugiyama, W. S. Seo and K. Koumoto, Chem. Mater., 15 [12] 2469 (2003)

[267] H. Y. Zhu, J. A. Orthman, J. –Y. Li, J. –C. Zhao, G. J. Churchman and E. F. Vansant, Chem. Mater., 14 [12] 5037 (2002)

[268] C. Wang, Z. -X. Deng and Y. Li, Inorg. Chem., 40 [20] 5210 (2001)

[269] T. Ivanova and A. Harizanova, Solid State Ionics, 138 [3-4] 227 (2001)

[270] I. Moriguchi, Y. Tsujigo, Y. Teraoka and S. Kagawa, J. Phys. Chem. B, 104 [34] 8101 (2000)

[271] K. Kato and K. Niihara, Thin Solid Films, 298 [1-2] 76 (1997)

[272] S. Music, M. Gotic, M. Ivanda, S. Popovic, A. Turkovic, R. Trojko, A. Sekulic and K. Furic, J. Am. Ceram. Soc., 79 [6] 1483 (1996)

[273] K. Kato, A. Tsuzuki, A. Tsuge, Y. Torii, H. Taoda, T. Kao and Y. Butsugan, J. Mater. Sci., 30, 837 (1995)

[274] K. C. Song and S. E. Pratsinis, J. Am. Ceram. Soc., 84 [1] 92 (2001)

[275] C. A. Grimes, D. Kouzoudis, E. C. Dickey, D. Qian, M. A. Anderson, R. Shahidain, M. Lindsey and L. Green, J. Appl. Phys., 87 [9] 5341 (2000)

[276] M. Gotic', B. Grzeta, S. Music', S. Popovic', A. Tonejc, R. Trojko and A. Turkovic', In: Forth Croatian-Slovenian Crystallographic Meeting (4th Ed.), Book of Abstracts (September 28–30, 1995)

[277] D. F. Watson, A. Marton, A. M. Stux and G. J. Meyer, J. Phys. Chem. B, 107 [40] 10971 (2003)

[278] X. Liu, J. Yang, L. Wang, X. Yang, L. Lu and X. Wang, Mater. Sci. & Eng. A, 289 [1-2] 241 (2000)

[279] P. A. Venz, J. T. Kloprogge and R. L. Frost, Langmuir, 16 [11] 4962 (2000)

[280] H. Liu, W. Yang, Y. Ma, Y. Cao, J. Yao, J. Zhang and T. Hu, Langmuir, 19 [7] 3001 (2003)

[281] R. R. Bacsa and M. Gratzel, J. Am. Ceram. Soc., 79 [11] 2185 (1996)

[282] D. Vorkapic and T. Matsoukas, J. Am. Ceram. Soc., 81 [11] 2815 (1998)

[283] D. –W. Kim, T. –G. Kim and K. S. Hong, J. Am. Ceram. Soc., 81 [6] 1692 (1998)

[284] R. L. Penn and J. F. Banfield, Am. Mineral., 83, 1077 (1998)

[285] R. J. H. Clark, The Chemistry of titanium and vanadium, Elsevier Publishing Company, Amsterdam, 327 (1968)

[286] R. D. Shannon and J. A. Pask, J. Am. Ceram. Soc., 48 [8] 391 (1965)

[287] J. F. Banfield, B. L. Bischoff and M. A. Anderson, Chemical Geology, 110, 211 (1993)

[288] J. A. Gamboa and D. M., Pasquevich, J. Am. Ceram. Soc., 75 [11] 2934 (1992)

[289] H. Zhang and J.F. Banfield J. Mater. Chem., 8, 2073 (1998)

[290] H. Dislich, J. Non-Cryst. Solids, 57 [3] 371 (1983)

[291] F. D. Gnanam, Sol gel processing of advanced ceramics, Oxford & IBH Publishing Co. Pvt. Ltd. (1996).

[292] K. J. D. Mackenzie, Trans. J. Br. Ceram. Soc., 74, 77 (1975)

[293] F. C. Gennari and D. M. Pasquevich, J. Mater. Sci., 33 [6] 1571 (1998)

[294] M. Hirano, T. Joji, M. Inagaki and H. Iwata, J. Am. Ceram. Soc., 87 [1] 35 (2004)

[295] M. Hirano, C. Nakahara, K. Ota and M. Inagaki, J. Am. Ceram. Soc., 85 [5] 1333 (2002)

[296] G. Oliveri, G. Ramis, G. Busca and V. S. Escribano, J. Mater. Chem., 3, 1239 (1993)

[297] C. N. R. Rao, A. Turner and J. M. Honig, J. Phys. Chem., 11, 173 (1959)

[298] D. P. Partlow and B. E. Yoldas, Am. Ceram. Soc. Bull., 59, 640 (1980)

[299] X. –Z. Ding, X. –H. Liu and Y. –Z. He, J. Mater. Sci. Lett., 15, 1789 (1996)

[300] A. C. Pierre, Introduction to sol-gel processing, Kluwer Academic Publishers (1998)

[301] S. Hishita, I. Mutoh, K. Koumoto and H. Yanagida, Ceram. Int., 9 [2] 61 (1983)

[302] A. A. Gribb and J. F. Banfield, Am. Mineral., 82, 717 (1997)

[303] K. N. P. Kumar, Scr. Metall. Mater., 32 [6] 873 (1995)

[304] R. A. Spurr and H. Myers, Anal. Chem., 29 [5] 760 (1957)

[305] R. L. Penn and J. F. Banfield, Am. Mineral., 84, 871 (1999)

[306] X. -Z. Ding and X. -H. Liu, J. Alloys Comp., 248, 143 (1997)

[307] G. C. Fabiana and D. M. Pasquevich, J. Am. Ceram. Soc., 82 [7] 1915 (1999)

[308] R. A. Eppler, J. Am. Ceram. Soc., 700 [4], C-64- C-66 (1987)

[309] S. Vargas and R. Arroyo, J. Mat. Res., 14 [10] 3932 (1999)

[310] R. R. Talavera, S. Vargas, R. A. Murillo and R. M. Compose, J. Mat. Res., 12 [2] 860 (1994)

[311] Y. Iida and S. Ozaki, J. Am. Ceram. Soc., 44 [3] 120 (1961)

[312] K. D. Shannon, Appl. Phys., 35 [1] 3414 (1964)

[313] R. D. Shannon and J. A. Pask, Am. Mineral., 49, 1707 (1964)

[314] L. E. Depero, P. Bonzi, M. Zocchi and G. D. Michele, J. Mater. Res., 8 [10] 2709 (1993)

[315] H. Z. Zhang and J. F. Banfield, J. Phys. Chem. B, 104 [15] 3481 (2000)

[316] Y. Hwu, Y. D. Yao, N. F. Cheng, C. Y. Tung and H. M. Lin, Nanostruct. Mater., 9, 355 (1997)

[317] X. S. Ye, J. Sha, Z. K. Jiao, and L. D. Zhang, Nanostruct. Mater., 8, 919 (1997)

[318] H. Kominami, M. Kohno and Y. Kera, J. Mater. Chem., 10, 1151 (2000)

[319] Y. Zhang, C. K. Chan, J. F. Porter, and W. Guo, J. Mater. Res., 13, 2602 (1998)

[320] H. Z. Zhang and J. F. Banfield, Am. Mineral., 84, 528 (1999)

[321] H. Z. Zhang and J. F. Banfield, J. Mater. Res., 15 [2] 437 (2000)

[322] K. Okada, N. Yamamoto, Y. Kameshima, and A. Yasumori, J. Am. Ceram. Soc., 84 [7] 1591 (2001)

[323] M. Yoshinaka, K. Hirota and O. Yamaguchi, J. Am. Ceram. Soc., 80 [10] 2749 (1997)

[324] A. Zaban, S. T. Aruna, S. Tirosh, B. A. Gregg and Y. Mastai, J. Phys. Chem. B, 104 [17] 4130 (2000)

[325] P. P. Ahonen, E. I. Kauppinen, J. C. Joubert, J. L. Deschanvres and G. Van Tendeloo, J. Mater. Res., 14, 3938 (1999)

[326] P. I. Gouma and M. J. Mills, J. Am. Ceram. Soc., 84 [3] 619 (2001)

[327] M. S. P. Francisco and V. R. Mastelaro, Chem. Mater., 14 [6] 2514 (2002)

[328] K. R. Patil, S. D. Sathaye, Y. B. Khollam, S. B. Deshpande, N. R. Pawaskar and A. B. Mandale, Mater. Lett., 57 [12] 1775 (2003)

[329] Y. Ohko, D. A. Tryk, K. Hashimoto and A. Fujishima, J. Phys. Chem., 102 [15] 2699 (1998)

[330] W. Cheng, W. Y. Lin, Z. Zainal and N.E. Williams, Environ. Sci. & Technol., 28 [5] 934 (1994)

[331] N. Serpone, E. Borgarello, R. Harris, P. Cahill, M. Borgarello, and E. Pelizzetti, Sol. Energy Mater., 14, 121 (1986)

[332] S. -Z. Chu, S. Inoue, K. Wada, D. Li, H. Haneda and S. Awatsu, J. Phys. Chem. B, 107 [27] 6586 (2003)

[333] C. N. Satterfield, Heterogeneous Catalysis in Industrial Practice, 2nd Ed., McGraw-Hill, New York (1991)

[334] J. Biener, J. Wang and R. J. Madix, Surf. Sci., 442, 47 (1999)

[335] Q. Guo, S. Lee and D. W. Goodman, Surf. Sci., 437, 38 (1999)

[336] M. Sambi, G. Sangiovanni, G. Granozzi and F. Parmigiani, Phys. Rev. B, 54, 13464 (1996)

[337] Z. Zhang and V. E. Henrich, Surf. Sci., 277, 263 (1992)

[338] S. Gablenz, D. Vollzke, H. P. Abicht and J. N. Zdralek, J. Mater. Sci. Lett., 17, 537 (1998)

[339] T. Keiichi, F. V. C. Mario and H. A. Teruaki, Chem. Phys. Lett., 187, 73 (1991)

[340] G. Deo, A. M. Turek, I. E. Wachs, T. Machej, J. Haber, N. Das, H. Eckert and A. M. Hirt, Appl. Catal. A, 91, 27 (1992)

[341] R. J. Berry and M. R. Mueller, Microchem. J., 50, 28 (1994)

[342] X. Liu, C. Liang, H. Wang, X. Yang, L. Lu and X. Wang, Mater. Sci. & Eng. A, 326 [2] 235 (2002)

[343] M. Montes, F. P. Getton, M. S. W. Vong and P. A. Sermon, J. Sol-Gel Sci. Technol., 8 [1-3] 131 (1997)

[344] K. G. K. Warrier, S. Rajesh Kumar, C. P. Sibu and G. Werner, J. Porous Mater., 8 [4] 311 (2001)

[345] A. A. Ismail, I. A. Ibrahim, M. S. Ahmed, R. M. Mohamed and H. El-Shall, J. Photochem. Photobiol. A: Chemistry, 163 [3] 445 (2004)

[346] E. Pabón, J. Retuert, R. Quijada and A. Zarate, Microporous and Mesoporous Mater., 67 [2-3] 195 (2004)

[347] K. N. P. Kumar, Appl. Catal. A: Gen., 119, 163 (1994)

[348] Y. S. Lin, C. H. Chang and R. Gopalan, Ind. Eng. Chem. Res., 33, 860 (1994)

[349] R. Gopalan, and Y. S. Lin, Ind. Eng. Chem. Res., 34 [4] 1189 (1995)

[350] G. W. Koebrugge, L. Winnubst and A. J. Burggraaf, J. Mater. Chem., 3 [11] 1095 (1993)

[351] T. Ivanoa, A. Harizanova, M. Surtchev and Z. Nenova, Solar Energy Mater. & Solar Cells, 76, 591 (2003)

[352] C. B. Rodella, R. W. A. Franco, C. J. Magon, J. P. Donoso, L. A. O. Nunes, M. J. Saeki, M. A. Aegerter and A. O. Florentino, J. Sol-Gel Sci. Technol., 25, 75 (2002)

[353] V. S. Lusvardi, M. A. Barteau, and W. E. Farneth, J. Catal., 153 [1] 41 (1995)

[354] G. Sen Gupta, R. N. Chatterjee, G. C. Maity, and C. V. V. Satyanarayana, J. Colloid and Interface Sci. 170 [1] 215 (1995)

[355] D. D. Beck and R. W. Siegel, J. Mater. Res., 7, 2840 (1992)

[356] B. M. Reddy and I. Ganesh, J. Mol. Catal. A: Chemical, 169, [1-2] 207 (2001)

[357] R. B. Watson and U. S. Ozkan, J. Phys. Chem. B, 106 [27] 6930 (2002)

[358] K. E. Karakitsou and X. E. Verykios, J. Phys. Chem., 97 [6] 1184 (1993)

[359] E. Stathatos, T. Petrova, P. Lianos, Langmuir, 17 [16] 5025 (2001)

[360] N. Serpone, D. Lawless, J. Disdier and J. -M. Herrmann, Langmuir, 10 [3] 643 (1994)

[361] K. N. P. Kumar, K. Keizer and A. J. Burggraaf, J. Mater. Chem., 3 [9] 917 (1993)

[362] H. Kominami, M. Kohno, Y. Matsunaga, and Y. Kera, J. Am. Ceram. Soc., 84 [5] 1178 (2001)

[363] A. K. B. Ghosh, M. Pal, Sharon and G. Nogami, Mater. Chem. Phys., 59, 254 (1999)

[364] M. I. Litter and J. A. Navío, Chem. Phys. Lett., 108 [6] 618 (1984)

[365] J. –M. Herrmann, J. Disdier and P. Pichat, J. Photochem. Photobiol. A: Chem., 98 [3] 171 (1996)

[366] P. S. Ha, H. –J. Youn, H. S. Jung, K. S. Hong, Y. H. Park and K. H. Ko, J. Colloid Interface Sci., 223, 16 (2000)

[367] C. K. Chan, J. F. Porter, Y. G. Li, W. Guo and C. M. Chan, J. Am. Ceram. Soc., 82 [3] 566 (1999)

[368] K. R. Lee, S. J. Kim, J. S. Song, J. H. Lee, Y. J. Chung and S. D. Park, J. Am. Ceram. Soc., 85 [2] 341 (2002)

[369] H. Taoda, T. Nonami, T. Fujiwa and M. Kagotani, US Patent, 5,981,425 (1999)

[370] R. S. Sonawane, S. G. Hegde, and M. K. Dongare, Mater. Chem. Phys., 77 [3] 744 (2003)

[371] T. Watanabe, A. Kitamura, E. Kojima, C. Nakayama, K. Hashimoto and A. Fujishima, Photocatalytic purification and treatment of water and air, Elsevier Science Publishers B (1993)

[372] S. Rajeshkumar, C. Suresh, A. K. Vasudevan, N. R. Suja, P. Mukundan, K. G. K. Warrier, Mater. Lett., 38, 161 (1999)

[373] S. Rajeshkumar, C. Suresh, A. K. Vasudevan, P. Perumal, K. G. K. Warrier, Trans. Ind. Ceram. Soc., 58 [5] 118 (1999)

[374] H. Jiang and L. Gao, Mater. Chem. Phys., 77 [3] 878 (2003)

[375] J. A. Navío, J. J. Testa, P. Djedjeian, J. R. Padrón, D. Rodríguez and M. I. Litter, Appl. Catal. A: Gen., 178 [2] 191 (1999)

[376] K. Bahranowski, J. Janas, T. Machej, E. M. Serwicka and L. A. Vartikian, Clay Minerals, 32 [4] 665 (1997)

[377] L. López, J. A. Moreno, R. Gómez, X. Bokhimi, J. A. Wang, H. Yee-Madeira, G. Pecci and P. Reyes, J. Mater. Chem., 12, 714 (2002)

[378] S. T. Martin, C. L. Morrison and M. R. Hoffmann, J. Phys. Chem., 98 [51] 13695 (1994)

[379] H. Schneider, A. Baiker, V. Schar and A. Waukaun, J. Catal.. 146 [2] 545 (1994)

[380] J. Yang and J. M. F. Ferreira, Mater. Lett., 36, 320 (1998)

[381] A. K. Vasudevan, P. P. Rao, S. K. Ghosh, G. M. Anilkumar, A. D. Damodaran and K. G. K. Warrier, J. Mater. Sci. Lett., 16 [1] 8 (1997)

[382] W. Choi, A. Termin and M. R. Hoffmann, J. Phys. Chem., 98 [51] 13669 (1994)

[383] W. Choi, A. Termin and M. R. Hoffmann, Angew. Chem., 106, 1148 (1994)

[384] W. Choi, A. Termin and M. R. Hoffmann, Angew. Chem., Int. Ed. Engl., 33, 1091 (1994)

[385] T. López, J. H. Ventura, R. Gómez, F. Tzompantzi, E. Sánchez, X. Bokhimi and A. García, J. Mol. Catal. A: Chemical, 167, 101 (2001)

[386] J. Lin and J. C. Yu, J. Photochem. Photobiol. A: Chemistry, 116, 63 (1998)

[387] C. A. LeDuc, J. M. Campbell and J. A. Rossin, Ind. Eng. Chem. Res., 35, 2473 (1996)

[388] T. Yoko, A. Yuasa, K. Kamiya and S. Sakka, J. Electrochem. Soc., 138 [8] 2279 (1991)

[389] Y. H. Hsien, C. F. Chang, Y. H. Chen and S. Cheng, Appl. Catal., 31, 241 (2001)

[390] K. M. Schindler, M. Kunst, J. Phys. Chem., 94 [21] 8222 (1990)

[391] M. Ozawa, M. Kimura and A. Isogai, J. Mater. Sci. Lett., 9 [6] 709 (1990)

[392] T. Kasuga, M. Hiramatsu, M. Hirano and A. Hoson, J. Mater. Res., 12 [3] 607 (1997)

[393] Q. Sang, L. Gao and S. Zheng, Chem. Lett., 1124 (2001)

[394] C. Anderson and A. J. Bard, J. Phys. Chem. B, 101 [14] 2611 (1997)

[395] C. A. Müller, M. Schneider, T. Mallat and A. Baiker, Appl. Catal. A: Gen., 201, 253 (2000)

[396] X. Gao and I. E. Wachs, Catal. Today 51, 233 (1999)

[397] R. N. Viswanath and S. Ramasamy, Colloid Surf. A, 133 [1-2] 49 (1998)

[398] Z. Liu, J. Tabora and R. J. Davis, J. Catal., 149 [1] 117 (1994)

[399] Z. Liu and R. J. Davis, J. Phys. Chem., 98 [4] 1253 (1994)

[400] S. Klein and W. F. Maier, J. Catal., 163 [2] 489 (1996)

[401] R. Neumann and M. Levin-Elad, J. Catal., 166 [2] 206 (1997)

[402] D. C. M. Dutoit, U. Goebel, M. Schneider and A. Baiker, J. Catal., 164 [2] 433 (1996)

[403] R. Hutter, T. Mallat and A. Baiker, J. Catal., 157 [2] 665 (1995)

[404] J. Ramirez, L. R-Ramirez, L. Cedeno, V. Harle, M. Vrinat and M. Breysse, Appl. Catal. A: Gen., 93, 163 (1993)

[405] E. Olguin, M. Vrinat, L. Cedeno, J. Ramirez, M. Borque and A. L. Agudo, Appl. Catal., A: Gen., 165, 1 (1997)

[406] M. P. Borque, A. L. Agudo, E. Olguin, M. Vrinat, L. Cedeno and J. Ramirez, Appl. Catal. A: Gen., 180, 53 (1999)

[407] V. Harle, M. Vrinat, J. P. Scharff, B. Burand and J. P. Deloume, Appl. Catal. A: Gen., 196, 261 (2000)

[408] A. G. Alejandre, Langmuir, 14 [3] 630 (1998)

[409] N. Y. Topsoe, H. Topsoe and J. A. Dumesic, J. Catal., 151 [1] 226 (1995)

[410] N. Y. Topsoe, J. A. Dumesic and H Topsoe, J. Catal., 151 [1] 241 (1995)

[411] A. M. Venezia, M. Schiavello, L. Palmisano, C. Martin, I. Martin and V. Rives, J. Catal., 147 [1] 115 (1994)

[412] Y. Su, Y. Wang, J. L. Daschbach, T. A. Fryberger, M. A. Henderson, J. Janata and C. Peden, 3 [1] 63 (1998)

[413] N. V. Economidis, D. A. Peña, P. G. Smirniotisa, Appl. Catal. B: Environ., 23 [2-3] 123 (1999)

[414] S. Eibl, B. C. Gates and H. Knozinger, Langmuir, 17 [1] 107 (2001)

[415] C. Su, F. Notoya, E. Sasaoka, Ind. Eng. Chem. Res., 42 [23] 5770 (2003)

[416] M. Schneider, M. Maciejewski and S. Tschudin, J. Catalysis, 149 [2] 326 (1994)

[417] U. Scharf and M. Schneider, J. Catalysis, 149 [2] 344 (1994)

[418] M. Schneider, A. Baiker, U. Scharf and A. Wokaaun, J. Catalysis, 150 [2] 284 (1994)

[419] Y. S. Mok, D. J. Koh, K. T. Kim and I.-S. Nam, Ind. Eng. Chem. Res., 42 [13] 2960 (2003)

[420] H. Yoshitake and T. Tatsumi, Chem. Mater., 15 [8] 1695 (2003)

[421] J. B. Miller, S. T. Johnston and E. I. Ko, J. Catal., 150 [2] 311 (1994)

[422] M. Schneider, M. Wildberger, M. Maciejewski, D. G. Duff, T. Mallat and A. Baiker, J. Catalysis, 148 [2] 625 (1994)

[423] M. Schneider, D. G. Duff, T. Mallat, M. Wildberger, and A. Baiker, J. Catalysis, 147 [2] 500 (1994)

[424] M. Grätzel, J. Photochem. Photobiol. A: Chem., 164 (1-3) 2004, 3-14

[425] K. Rajeswar, J. Appl. Electrochem. 15, 1 (1985)

[426] W. Mu, J.M. Herrmann and P. Pichat Catal. Lett., 3, 73 (1989)

[427] P. -C. Maness, S. Smolinski and W. A. Jacoby, Appl. Environ. Microbiol. 65, 4094 (1999)

[428] E. J. Wolfrun, J. Huang, D. M. Blake, P. –C. Maness, Z. Huang, J. Fiest and W. A. Jacoby, Environ. Sci. Technol., 36 [15] 3412 (2002)

[429] M. Yoshikawa, S. Noguchi, N. Kato and K. Naito, Japanese Patent H10-72664 (1998)

[430] T. Domoto, Japanese Patent, H10-86258 (1998)

[431] M. Anpo and M. Takeuchi, J. Catal., 216 [1-2] 505 (2003)

[432] I. Poulios, P. Spathis and P. Tsoumparis J. Environ. Sci. Health, 34, 1455 (1999)

[433] R. Cai, K. Hashimoto, K. Itoh, Y. Kubota and A. Fujishima, Bull. Chem. Soc. Jpn., 64, 1268 (1991)

[434] A. Fujishima, R. Cai, K. Hashimoto, H. Sakai and Y. Kubota, Trace Met. Environ., 3, 193 (1993)

[435] H. Sakai, R. Baba, K. Hashimoto, Y. Kubota and A. Fujishima, Chem. Lett., 185 (1995)

[436] O. Legrini, E. Oliveros and A. M. Braun, Chem. Rev., 93, 671 (1993)

[437] D. Bahnemann, J. Cunningham, M. A. Fox, E. Pelizetti, P. Pichat and N. Serpone, Photocatalytic treatment of waters, In: G. Helz, R. Zepp, D. Crosby (Eds.), Aquatic and Surface Photochemistry, CRC Press, 261 (1994)

[438] A. Heller, Acc. Chem. Res., 28, 503 (1995)

[439] M. Gratzel, Heterogeneous photochemical electron transfer, CRC Press, Boca Raton (1989)

[440] T. Torimoto, N. Nakamura, S. Ikeda and B. Ohtani, Phys. Chem. Chem. Phys., 4, 5910 (2002)

[441] T. Ohno, K. Sarukawa, K. Tokieda and M. Matsumura, J. Catal., 203 [1] 82 (2001)

[442] B. Ohtani, Y.Ogawa, S. Nishimoto, J. Phys. Chem. B, 101 [19] 3746 (1997)

[443] J. Ovenstone and K. Yanagisawa, Chem. Mater., 11 [10] 2770 (1999)

[444] W. Ma, Z. Lu and M. Zhang, Appl. Phys. A, 66, 621 (1998)

[445] Z. Goren, I. Willner, A. J. Nelson and A. J. Frank, J. Phys. Chem., 94 [9] 3784 (1990)

[446] D. W. Bahneman, J. Phys. Chem., 98 [3] 1025 (1994)

[447] H. Lin, S. Kumon, H. Kozuka and T. Yoko, Thin Solid Films, 315 [1-2] 266 (1998)

[448] J. Lin, J. C. Yu, D. Lo and S. K. Lam J. Catal., 183, 68 (1999)

[449] K. Yoshida, K. Okamura, K. Hirano, K. Iguchi, K. Ito and M. Murabayashi, Jpn. Soc. Water Environ., 17 [5] 38 (1994)

[450] G. Dagan and M. Tomkiewiez, J. Phys. Chem., 97 [49] 12651 (1993).

[451] C. A. Martin, M. A. Baltanas, and A. E. Cassano, Catal. Today, 27 [1-2] 221 (1996)

[452] S. F. Cheng, S. J. Sai and Y. F. Lee, Catal. Today, 26 [1] 87 (1995)

[453] S. Yamashita, Y. Ichihashi, S. G. Zhang, Y. Matsumura, Y. Souma and M. A. Tatsumi, Appl. Surf. Sci., 121, 305 (1997)

[454] S. Yoshida, S. Takenaka, T. Tanaka, and T. Funabiki, J. De Physique, IV, 7 [C2] 305 (1997)

[455] G. Zhao, H. Kozuka, and T. Yoko, Thin solid films, 277 [1-2] 147 (1996).

[456] H. Yanagi, Chem. Mater., 10 [5] 1258 (1998).

[457] M. I. Litter and J. A. Navío, J. Photochem. Photobiol. A: Chem., 98 [3] 171 (1996)

[458] J. –M. Herrmann, J. Disdier and P. Pichat, Chem. Phys. Lett., 108 [6] 618 (1984)

[459] Y. R. Do, W. Lee, K. Dwight and A. Wold. J. Solid State Chem., 108, 198 (1994)

[460] K. T. Ranjit, I. Willner; S. H. Bossmann, A. M. Braun, Environ. Sci. Technol. 35, 1544 (2001)

[461] A. G. Agrios, K. A. Gray and E. Weitz, Langmuir; 19 [12] 5178 (2003)

[462] A. P. Davis and D. L. Green, Environ. Sci. Technol., 33 [4] 609 (1999)

[463] P. Sawunyama, A. Fujishima and K. Hashimoto, Langmuir; 15 [10] 3551 (1999)

[464] Y. Ohko, I. Ando, C. Niwa, T. Tatsuma, T. Yamamura, T. Nakashima, Y. Kubota and A. Fujishima, Environ. Sci. Technol., 35 [11] 2365 (2001)

[465] J. Zhang, Y. Hu, M. Matsuoka, H. Yamashita, M. Minagawa, H. Hidaka and M. Anpo, J. Phys. Chem. B., 105 [35] 8395 (2001)

[466] Y. Horie, M. Taya and S. Tone, Kagaku kogaku Ronbunshu (Japanese), 22 [5] 1241 (1996)

[467] M. Anpo, T. Shima, S. Kodama and y. Kubokawa, J. Phys. Chem., 91 [13] 4305 (1987)

[468] X. Z. Li, Liu, H. L. F. Cheng and H. J. Tong, Environ. Sci. Technol., 37 [17] 3989 (2003)

[469] T. Tatsuma, S. Saitoh, P. Ngaotrakanwiwat, Y. Ohko and A. Fujishima, Langmuir, 18 [21] 7777 (2002)

[470] D. A. Panayotov, D. K. Paul and J. T. Yates, Jr., J. Phys. Chem. B., 107 [38] 10571 (2003)

[471] C. Murata, H. Yoshida, J. Kumagai and T. Hattori, J. Phys. Chem. B., 107 [18] 4364 (2003)

[472] G. D. Lee, V. A. Tuan and J. L. Falconer, Environ. Sci. Technol., 35 [6] 1252 (2001)

[473] M. Bekboelet, Water Sci. and Technol., 95 (1996)

[474] L. Zhang, J. C. Yu, H. Y. Yip, Q. Li, K. W. Kwong, A. -W. Xu and P. K. Wong, Langmuir, 19 [24] 10372 (2003)

[475] T. S. Kim, J. D. Stiehl, C. T. Reeves, R. J. Meyer and C. B. Mullins, J. Am. Chem. Soc., 125 [8] 2018 (2003)

[476] Q. Wang, J. Biener, X. -C. Guo, E. Farfan-Arribas and R. J. Madix, J. Phys. Chem. B., 107 [42] 11709 (2003)

[477] K. Sunada, T. Watanabe and K. Hashimoto, Environ. Sci. Technol., 37 [20] 4785 (2003)

[478] H. Einaga, M. Harada, S. Futamura and T. Ibusuki, J. Phys. Chem. B., 107 [35] 9290 (2003)

[479] X. Z. Li and F. B. Li, Environ. Sci. Technol., 35 [11] 2381 (2001)

[480] R. Benedix, F. Dehn, J. Quaas and M. Orgass, Lacer, 5, (2000)

[481] J. Yang, Y. X. Huang, and J. M. F. Ferreira, J. Mater. Sci. Lett., 16 [2-3] 1933 (1997)

[482] J. Yang, and J. M. F. Ferreira, Mater. Res. Bull., 33 [3] 389 (1998)

[483] R. R. Talavera S. Vargas, R. A. Murillo, R. M. Campos and E. H. Poniatowski, J. Mater. Res., 12 [2] 439 (1997)

[484] J. Nair, P. Nair, F. Mizukami, Y. Oosawa and T. Okubo, Mater. Res. Bull., 34 [8] 1275 (1999)

[485] F. F. Lange and M. M. Hirlinger, J. Am. Ceram. Soc., 67 [3] 164 (1984)

[486] E. Sanchez, T. Lopez and R. Gomez, J. Solid state Chem., 122 [2] 309 (1996)

[487] A. M. Venezia, L. Palmisano and M. Schiavello, J. Solid State Chem., 114 [2] 364 (1995)

[488] A. K. Cheetham and P. Day, Solid state chemistry: Techniques, Oxford Science Publications, Clarendon Press (1987)

[489] S. J. Gregg and K. S. W. Sing, Adsorption, surface area and porosity, 2nd Ed., Academic Press, London (1982)

[490] F. Arena, R. Dario and A. Parmaliana, Appl. Catal. A. Gen., 170, 127 (1998)

[491] K. Nakamoto, Infrared and Raman spectra of inorganic coordination compounds, 3rd Ed. Wiley, New York (1997)

[492] G. B. Deacon and R. J. Phillips, Coord. Chem. Rev., 33 [3] 227 (1980)

[493] D. A. Edwards and R. N. Hayward, Canad J. Chem., 46, 3443 (1968)

[494] M. D. C. B. Lopez, G. Fourlaris, B. Rand and F. L. Riley, J. Am. Ceram. Soc., 82 [7] 1777 (1999)

[495] T. Rajh, D. M. Tiede and M. C. Thurnauer, J. Non-Cryst. Solids, 205 [2] 815 (1996)

[496] A. G. Gaynor, R. J. Gonzalez, R. M. Davis and R. Zallen, J. Mater. Res. 12, 1755 (1997)

[497] R. J. Gonzalez, Ph. D. Dissertation, Virginia Polytechnique Institute (1996)

[498] C. Sanchez, J. Livage, M. Henry and F. Babboneau, J. Non-Cryst. Solids, 100 [1-3] 65 (1988)

[499] Y. Djaoued, S. Badilescu, P. V. Ashrit and J. Robichaud, The Internet J. Vibrational Spectroscopy 5 [6] 1 (2003)

[500] H. W. Van der Marel and H. Beutelspacher, Atles of infrared spectroscopy of clay minerals and the admixtures, Elsevier Scientific Publishing Company, New York (1974)

[501] A. Soloviev, R. Tufeu, C. Sanchez and A. V. Kanaev, J. Phys. Chem. B, 105 [19] 4175 (2001)

[502] J. Chaibi, M. Henry, H. Zarronk, N. Gharbi and J. Livage, J. Non-Cryst. Solids, 170 [1] 1 (1994)

[503] C. M. Parler, J. A. Ritter and M. D. Amiridis, J. Non-Cryst. Solids, 279 [2-3] 119 (2001)

[504] R. D. Hancock and A. E. Martell, Chem. Rev., 89, 1875 (1989)

[505] R. G. Pearson, J. Am. Chem. Soc., 85, 3533 (1963)

[506] A. M. Seco, M. C. Goncalves, R. M. Almeida, Mater. Sci. and Eng. B, 76, 193 (2000)

[507] R. M. Almeida, J. Sol-Gel Sci. Technol., 13, 51, 1998

[508] F. L. Galeener, Phys. Rev., B19, 4292 (1979)

[509] M. L. Balmer, Y. Su, H. Xu, E. Bitten, D. McCready and A. Navrotsky, J. Am. Ceram. Soc., 84 [1] 153 (2001)

[510] H. G. Yang and H. C. Zeng, J. Phys. Chem. B, 107 [44] 12244 (2003)

[511] B. Claude, J. Michael and A. Lavelly, Catal. Today, 50 [2] 207 (1999)

[512] R. Campostrini, M. Ischia and L. Palmisano, J. Thermal Anal. & Calorimetry, 71 [3] 997 (2003)

[513] H. Xie, Q. Zhang, T. Xi, J. Wang and Y. Liu, Thermochem. Acta, 381, 45 (2002)

[514] J. C. Bailar, H. J. Emeleus, R. Nyholm and A. F. Trofman, Dickenson, Pergamon Press (1973)

[515] P. Duran, F. Capel, D. Gutierrez, J. Tartaj and E. Moure, J. Eur. Ceram. Soc., 22 [9/10] 1711 (2002)

[516] S. R. Elliot, Physics of amorphous materials, Longmen, London (1983)

[517] S. M. Owen and A. T. Brooker, A Guide to Modern Inorganic Chemistry, Elsevier, (1979)

[518] Y. U. Ahn, E. J. Kim, H. T. Kim and S. H. Hahn, Mater. Lett., 57 [30] 4660 (2003)

[519] Y. Hu, H. -L. Tsai and C. -L. Huang, Mater. Sci.& Eng. A, 344 [1-2] 209 (2003)

[520] F. Gruy and M. Pijelat, J. Am. Chem. Soc., 75 [3] 657 (1992)

[521] W. D. Kingery, H. K. Bowen and D. R. Uhlman, Introduction to Ceramics, 2nd Ed.) Wiley Inter. Sci., New York (1976)

[522] H. E. Chao, Y. U. Yun, H. U. Xingfang and A. Larbot, J. Eur. Ceram. Soc., 23 [9] 1457 (2003)

[523] J. G. Yu, J. C. Yu, M. K. P. Leung , W. K. Ho, B. Cheng, X. J. Zhao and J. C. Zhao, J. Catal., 217 [1] 69 (2003)

[524] A. Henglein, Chem. Rev., 89, 1861 (1989)

[525] D. C. Hague and M. J. Mayo, Nanostruct. Mater., 3, 61 (1993)

[526] S. L. Liao, K. D. Pae and W. E. Mayo, Nanostruct. Mater., 5 [3] 319 (1995)

[527] A. M. Tonejc , I. Djerdj and A. Tonejc, Mater. Sci. & Eng. B, 85, 55 (2001)

[528] A. M. Tonejc, A. Turkovic, M. Gotic, S. Music, M. Vukovic, R. Trojko and A. Tonejc, Mater. Lett., 31, 127 (1997)

[529] A. M. Tonejc, M. Goti, B. Grzeta, S. Music, S. Popovi, R. Trojko, A. Turkovi and I. MuSevic, Mater. Sci. & Eng. B, 40, 177 (1996)

[530] H. Suja, C. S. Deepa, K. S. Rani and S. Sugunan, Appl. Catal. A: Gen., 230 [1-2] 233 (2002)

[531] M. L. Fetterolf, H. V. Patel and J. M. Jennings, J. Chem. Eng. Data, 48 [4] 831 (2003)

[532] J. Li, L. Wu and Y. Zhang, Chem. Phys. Lett., 342, 249 (2001)

[533] P. K. Sharma, M. C. A. Fantini and A. Gorenstein, Solid state Ionics, 113-115, 457 (1998)

[534] E. Sanchez and T. Lopez, React. Kinet. Catal. Lett., 48, 295 (1992)

[535] X. Jiang, T. Herricks and Y. Xia, Adv. Mater. 15, 1205 (2003)

[536] M. Hirano, C. Nakahara, K. Ota, O. Tanaike and M. Inagaki, J. Solid State Chem., 170, 39 (2003)

[537] G. Behrens, G. W. Dransman and A. H. Heuer, J. Am. Ceram. Soc., 76 [4] 1025 (1993)

[538] M. Yoshimura, Am. Ceram. Soc. Bull., 67, 1950 (1988)

[539] I. -W. Chen and Y. -H. Chiao, Acta Metall., 33, 1827 (1985)

[540] P. F. Becher and M. V. Swain, J. Am. Ceram. Soc., 75 [3] 493 (1992)

[541] A. Templeton, X. Wang, S. J. Penn, S. J. Webb, L. F. Cohen and N. M. Alford, J. Am. Ceram. Soc., 83 [1] 95 (2000)

[542] N. Ozawa, H. Yabe and T. Yao, J. Am. Ceram. Soc., 86 [11] 1976 (2003)

[543] E. Munoz, J. L. Boldu, E. Andrade, O. Novaro, X. Bokhimi, T. Lopez and R. Gomez, J. Am. Ceram. Soc., 84 [2] 392 (2001)

[544] E. Sanchez and T. Lopez, React. Kinet. Catal. Lett., 48, 295 (1992)

[545] X. Bokhimi, A. Morales, O. Novaro, T. Lopez, E. Sanchez and R. Gomez, J. Mater. Res., 10, 2788 (1995)

[546] J. R. Bolton, Chem. Eng. News, 29 (1996)

[547] A. Hattory, K. Shimoda, H. Tada and S. Ito, Langmuir, 15, 5422, 1999

[548] A. J. Bard, Science, 207, 139, 1980

[549] C. -M. Wang, A. Heller and H. Gerischer, J. Am. Ceram. Soc., 114, 5230 (1992)

[550] T. Rajh, L. X. Chen, K. Lukas, T. Liu, M. C. Thurnauer and D. M. Tiede, J. Phys. Chem. B, 106 [41] 10543 (2002)

[551] G. Schlichthorl, S. Y. Huang, J. Sprague and A. J. Frank, J. Phys. Chem. B, 101 [41] 8141 (1997)

[552] G. Boschloo and D. Fitzmaurice, J. Phys. Chem. B, 103 [12] 2228 (1999)

[553] L. X. Chen, T. Rajh, Z. Wang, M. C. Thurnauer, J. Phys. Chem. B, 101 [50] 10688 (1997)

[554] T. Rajh, A. E. Ostafin, O. I. Micic, O. M. Tiede and M. C. Thurnauer, J. Phys. Chem. B, 100 [11] 4538 (1996)

[555] O. I. Micic, Y. Zhang, K. R. Cromack, A. D. Trifunac and M. C. Thurnauer, J. Phys. Chem., 97 [28] 7277 (1993)

[556] J. Yu, X. Zhao and Q. Zhao, Mater. Chem. Phys. 69, 25 (2001)

[557] N. Serpone, D. Lawless, R. Khairutdinov and E. Pelizzetti, J. Phys. Chem., 99 [45] 16655 (1995)

[558] J. E. Huheey, Inorganic Chemistry: Principles of structure and reactivity, 4th Ed., Harper and Row (1993)

[559] R. C. Weast and M. J. Astle, Handbook of chemistry and physics, 59th Ed., CRC Press Inc. Florida (1978)

[560] X. -Z. Ding and X. -H. Liu, J. Mater. Res., 13, 2556 (1998)

[561] C. J. Brinker, D. E. Clark, D. R. Ulrich, (Eds.), MRS Symp. Proc., 32 (1984)

[562] J. D. Mackenzie, D. R. Ulrich (Eds.), Ultrastructure processing of advanced ceramics, J. Wiley Sons, New York, (1988)

[563] C. J. Brinker and D. E. Clark and Ulrich DR (Eds.) Better ceramic through chemistry II [MRS symposium Vol. 73 (1986)] and Better ceramics through Chemistry III [MRS symposium Vol.121 (1988)] Materials Research Soc. Pittsburgh.

[564] D. J. Kim, S. H. Hahn, S. H. Oh and E. J. Kim, Mater. Lett., 57 [2] 355 (2002)

[565] S. Sanvicente, A. Morales and M. T. Gutierrez, Thin Solid Films, 403 [2-3] 335 (2002)

[566] K. A. Vorotilov, E. V. Orlova and V. I. Petrovsky, Thin Solid Films, 207 [1-2] 180 (1992)

[567] N. Negishi, K. Takeuchi and T. Ibusuki, J. Sol-Gel Sci. Technol., 13, 691 (1998)

[568] J. Zhai, L. Zhang, X. Yao and S. N. B. Hodgson, Surf. Coat. Technol., 138, 135 (2001)

[569] W. Wue, Z. Sun, Y. L. Lam, Y. C. Chan and C. H. Kam, J. Phys. D.: Appl. Phys., 34, 471 (2001)

[570] O. Martins and R. M. Almeida, J. Sol-Gel Sci. Technol., 19, 651 (2000)

[571] A. M. Seco, M. C. Goncalves and R. M. Almeida, Mater. Sci. Eng. B, B76, 193 (2000)

[572] D. Grosso, G. J. A. A. Soler-Illia, F. Babonneau, C. Sanchez, P. A. Albouy, A. Brunet-Bruneau, A. R. Balkenende, Adv. Mater., 13, 185 (2001)

[573] K. L. Frindell, M. H. Bartl, A. Popitsch, G. D. Stucky, Angew. Chem., 114, 1002 (2002)

[574] M. Ogawa, K. Ikeue and M. Anpo, Chem. Mater., 13 [9] 2900 (2001)

[575] H. Kozuka and M. Kajimura, J. Am. Ceram. Soc., 83 [5] 1056 (2000)

[576] K. Kajihara and T. Yao, J. Sol-Gel Sci. Technol., 19, 219 (2000)

[577] Y. Abe, N. Sugimmoto, Y. Nagao and T. Misono, J. Non-Cryst. Solids, 104 [2-3] 164 (1988)

[578] A. Matsuda, Y. Kotani, T. Kogure, M. Tatsumisago and T. Minami, J. Am. Ceram. Soc., 83 [1] 229 (2000)

[579] H. Imai, H. Morimoto, A. Tominaga and H. Hirashima, J. Sol-Gel Sci. Technol., 10 [1] 45 (1997)

[580] R. Wang, K. Hashimoto, A. Fujishima, M. Chikuni, E. Kojima, A. Kitamura, M. Shimohigoshi and T. Watanabe, Nature, 388 [31] 431 (1997)

[581] A. Matsuda, Y. Matsuno, S. Katayama, T. Tsuno, N. Tohge and T. Minami, J. Am. Ceram. Soc., 73 [8] 2217 (1990)

[582] Y. Paz and A. Heller, J. Mater. Res., 12 [10] 2759 (1997)

[583] L. Shi, G. -X. Zhang, J. Wang and D. Lo, J. Opt. A: Pure Appl. Opt. 5 [2] L1-L4 (2003)

[584] J. Chen, Advanced oxidation technologies. Photocatalytic treatment of wastewater, PhD Thesis (1997)

[585] I. Strawbridge and P. F. James, J. Non-Cryst. Solids, 86 [3] 381 (1986)

[586] I. Sopyan, M. Watanabe, S. Murasawa, K. Hashomoto and A. Fujishima. J. Photochem. Photobiol., A, 98, 79 (1996)